
Universidade Estadual de Campinas
Instituto de Física Gleb Wataghin

Pedro Leopoldo e Silva Lopes

# Vortex Bound States in Superconducting Topological Matter

# Estados ligados à vórtices em matéria quântica topológica

Campinas 2016

Pedro Leopoldo e Silva Lopes

# Vortex Bound States in Superconducting Topological Matter

# Estados ligados a vórtices em matéria quântica topológica

*Thesis presented to the Gleb Wataghin Institute of Physics of the University of Campinas in partial fulfillment of the requirements for the degree of Doctor in Sciences*

*Tese apresentada ao Instituto de Física Gleb Wataghin da Universidade Estadual de Campinas como parte dos requisitos exigidos para a obtenção do título de Doutor em Ciências*

*Orientador:* Amir Ordacgi Caldeira

ESTE EXEMPLAR CORRESPONDE À VERSÃO FINAL DA TESE DEFENDIDA PELO ALUNO PEDRO LEOPOLDO E SILVA LOPES, E ORIENTADA PELO PROF. DR. AMIR ORDACGI CALDEIRA

Campinas 2016

**Agência(s) de fomento e nº(s) de processo(s):** FAPESP, 2009/18336-0; FAPESP, 2012/03210-3

Ficha catalográfica
Universidade Estadual de Campinas
Biblioteca do Instituto de Física Gleb Wataghin
Lucimeire de Oliveira Silva da Rocha - CRB 8/9174

L881v

Lopes, Pedro Leopoldo e Silva, 1987-
Vortex bound states in superconducting topological matter / Pedro Leopoldo e Silva Lopes. – Campinas, SP : [s.n.], 2016.

Orientador: Amir Ordacgi Caldeira.
Tese (doutorado) – Universidade Estadual de Campinas, Instituto de Física Gleb Wataghin.

1. Topologia. 2. Supercondutividade. 3. Vórtices. I. Caldeira, Amir Ordacgi,1950-. II. Universidade Estadual de Campinas. Instituto de Física Gleb Wataghin. III. Título.

Informações para Biblioteca Digital

**Título em outro idioma:** Estados eletrônicos ligados a vórtices em matéria topológica supercondutora
**Palavras-chave em inglês:**
Topology
Superconductivity
Vortex
**Área de concentração:** Física
**Titulação:** Doutor em Ciências
**Banca examinadora:**
Amir Ordacgi Caldeira [Orientador]
Eduardo Miranda
José Antonio Brum
Eduardo Cantera Marino
Rodrigo Gonçalves Pereira
**Data de defesa:** 18-02-2016
**Programa de Pós-Graduação:** Física

MEMBROS DA COMISSÃO JULGADORA DA TESE DE DOUTORADO DE **PEDRO LEOPOLDO E SILVA LOPES – RA: 063673** APRESENTADA E APROVADA AO INSTITUTO DE FÍSICA "GLEB WATAGHIN", DA UNIVERSIDADE ESTADUAL DE CAMPINAS, EM 18/02/2016.

**COMISSÃO JULGADORA:**

- Prof. Dr. Amir Ordacgi Caldeira – (Orientador) – IFGW/UNICAMP
- Prof. Dr. Eduardo Miranda – IFGW/UNICAMP
- Prof. Dr. José Antonio Brum – IFGW/UNICAMP
- Prof. Dr. Eduardo Cantera Marino – IF/UFRJ
- Prof. Dr. Rodrigo Gonçalves Pereira – IFSC/USP

A Ata de Defesa, assinada pelos membros da Comissão Examinadora, consta no processo de vida acadêmica do aluno.

**CAMPINAS**
**2016**

# Acknowledgements

*"La filosofia è scritta in questo grandissimo libro, che continuamente ci sta aperto innanzi agli occhi (io dico l' Universo'), ma non si può intendere, se prima non il sapere a intender la lingua, e conoscer i caratteri ne quali è scritto. Egli è scritto in lingua matematica, e i caratteri son triangoli, cerchi ed altre figure geometriche, senza i quali mezzi è impossibile intenderne umanamente parola; senza questi è un aggirarsi vanamente per un oscuro labirinto."*

-Galileo Galilei, Il Saggiatore

An extensive work, both in time and body, like a PhD thesis is never done by the efforts of a single person. While signing as the author of this Thesis, I would like to dedicate some words of appreciation to all those who have helped me through this quest. While I could never live, or get here, without the support of my family, I believe that, in this particular case, I should start by thanking the support, discussions, company and camaraderie of my long-term friend and colleague, and office-mate, Victor Luiz Quito. Without our daily discussions and arguments I am pretty aware that the derivative of my learning would be much less steep; I consider our joint interactions in doing physics to have led to a real emergent phenomenon in what says respect to our developments as scientists.

That being said, I should turn to the regular and well deserved order, and thank both my father, Renato Carvalho Lopes, and mother, Christina Leopoldo e Silva, for the support and understanding of my career choice; I believe very few people in the world get the support in their lives I have gotten from my parents, and none is as proud of their family as I am. Following them, my beloved partner, Larissa Lubiana Botelho, who has been understanding and supporting for the past eight years, deserves something bigger than my appreciation and gratitude. For all her support and patience, for waiting for me through my long journeys, for helping me in the hard times, she deserves nothing less than my complete love and devotion.

I am then indebted to my colleagues from undergratuate and graduate studies, Vinícius Njaim Duarte, Udson Cabral Mendes, Pedro Vaz Duque, Priscila Ferreira Rosa, Nuno Cardoso, Thales Roque and Tiago Botari for great discussions and happy moments. I thank also my advisor Amir O. Caldeira, who has always supported me and gave me freedom to pursue my own interests from the beginning of my studies. Also, professors José Brum, Eduardo Miranda, Alberto Saa, Ricardo Doretto, Alex Antonelli, Marcus Aguiar, Kyoko Furuya, Roberto Clemente and Jorge Mujica, for great discussions, awesome classes, and many fun experiences for all these years at Unicamp.

I would like also to thank my friends from the University of Illinois at Urbana Champaign, with whom I shared some very cherished times and learnings. I would mention Vasudha Shivamoggi, Norman Tubman, Ilkka Kylänpää, Billy Passias, David ChangMo Yang, Hitesh Changlani and Wathid Assawasunthonnet, who were closest to me, but also, Xueda, Wladimir, Chang-Tse, AtMa, Anshur, Mayukh, Apoorv, Cihan, Cecilia, tom, Luis Santos, Yuxuan... I have made many friends and colleagues while in there. I would like to thank professors Taylor Hughes, Michael Stone, Philip Phillips and Eduardo Fradkin for discussions, collaborations and support and teachings. More particularly, I want to leave my deepest acknowledgments for Professors Shinsei Ryu (UIUC), Jeffrey Teo (UV) and Pouyan Ghaemi (CCNY). Without their support and teachings, I would never have gotten this far, and working with them has been, by far, one of the most important marks in my academic life, I really wish to say: thank you so much!

Still internationally, I would like to thank also my Dutch friends in the high-energy physics community, Drian van der Woude, Yvette Welling, Nick Plantz and Watse Sybesma. I hope we can keep in touch and share knowledge about physics in our different points of view!

Personally, and back in Brazil, the friendship of Tomás Mendes Martini, Lucas Mendes Martini, whom I have known since the day I was born, and Pedro Rafael Sônego Rocha, whom I have known for not much less time, were fundamental to bring me here; the bonds made as a child, after lasting for so long, are never really broken. Thanks for all! Thanks also Gabriel Queiroz Guimarães Hernandes, João Victor Chiba Vieira, Thalis Montalli, Felipe Bacurau, Rafael Scheiner, Gustavo Rahme, Gustavo Toledo, Emille Rodrigues, José Forni and Leonardo Zamariola for lots of fun memories.

From my personal circles of activities, I need to lay my acknowledgments to my friends from Niten Kobudo Kenkyusho. Arigato gozaimashita Sensei Jorge Kishikawa, Senpais Daniel Moraes, Danilo Pedroso and Leonardo Holschuh and all my other long term friends, Guilherme, Fernando, Batalha, Fusari, Ian and many others! It is impossible to mention all of whom I have exchanged swords, but the learning and experience from following the Kobudo with you will never be forgotten.

Again back in the US, I cannot miss the chance to thank all my friends of the Chambana Irish Session! Playing music with you has, literally, changed the sound of my everyday life. I also do not have words to express my full appreciation for your company and friendship, but I want to bring, particularly, the names of Dean Karres and Jake Schumacher, but as well those of Tracey Mitchell, Lisa Boucher, Dave Glenn, Laura Lynch, Jerome Colburn, John Funston, Daniel Flora; I am sorry if I missed any one of you, but I really appreciate our times together; few times in my life I felt so peacefully happy as when making music with you all! I hope I can keep visiting you, and that our reel sets never stop!

Finally, I need to thank the rest of my family and all the other friends and colleagues whose names I might have impolitely missed. I am aware that I have too many people to thank, and too little words for that, so I am very sorry if I missed mentioning anyone explicitly.

I thank the support from FAPESP under processes 2009/18336-0 and 2012/03210-3.

## Resumo

Nos focando em dois exemplos de matéria supercondutora topológica - isolantes topológicos dopados supercondutores e supercondutores topológicos invariantes por reversão temporal - nós estudamos a estrutura dos estados eletrônicos ligados a vórtices supercondutores. No contexto de isolantes topológicos dopados, nós aprofundamos o desenvolvimento da ideia de que a matéria eletrônica ligada à vórtices se comporta, efetivamente, como supercondutores topológicos do tipo onda-p unidimensionais. Nós desenvolvemos soluções, tanto analíticas quanto numéricas, para as funções de ondas deste problema e as utilizamos para estudar efeitos de movimento quântico de ponto-zero dos vórtices na densidade local de estados eletrônicos no seu interior. Nós mostramos como este problema pode ser conectado àquele de uma rede de supercondutores topológicos unidimensionais. No que diz respeito a supercondutores topológicos invariantes por reversão temporal, nós estudamos uma ação eletromagnética efetiva recentemente proposta para descrever a resposta elétrica destes sistemas. Esta ação indica que supercondutores topológicos possuem vórtices com propriedades topológicas exóticas. Nós descobrimos e digredimos sobre um paradoxo neste problema, apresentando uma possível solução para ele. Os conceitos de matéria topológica, modos-zero de Majorana, bombeamento quântico adiabático e anomalias quânticas são centrais para as nossas discussões; deste modo, nós apresentamos uma abordagem compreensiva e pedagógica para todos estes conceitos. Em particular, nós apresentamos uma discussão detalhada sobre as assinaturas de modos-zero de Majorana via tunelamento quântico macroscópico em junções Josephson.

## Summary

Focusing on two main examples of topological superconducting matter - superconducting doped topological insulators and time-reversal invariant topological superconductor - we study the structure of electronic modes bound to superconducting vortices. In the context of doped topological insulators, we further develop the understanding that the electronic matter bound to vortices behaves, effectively, as one dimensional p-wave topological superconductors. We compute approximate analytic and numerical solutions to the wavefunctions of this problem and use them to study the effects of vortex quantum zero-point motion in the local electronic density of states within the vortex core. We show how this problem can be connected to that of a network of one dimensional topological superconductors. As for the case of vortices in time reversal invariant topological superconductors, we study a recently proposed effective electromagnetic action which should describe the charge response of these systems. Non-trivial topological properties of vortices are implied by such an action. We

discover and digress about a paradox in this problem, and present a possible solution to it. Central to all the discussions throughout this work are the concepts of topological matter, Majorana zero-modes, adiabatic quantum pumps and quantum anomalies; we provide a comprehensive and pedagogical approach to all of these concepts. In particular, we provide also an in-depth discussion about signatures of Majorana zero-mode physics in macroscopic quantum tunneling.

# Contents

# Chapter 1

# Introduction

From the several branches of "modern" mathematics (the concept of "modern mathematics" is highly science-field dependent), nowadays, topology probably holds the youngest position in the rank of importance in physics. While hints about the importance of the relationship between physics and topology exist since the decade of 1960 (with the measurement of the Aharonov-Bohm effect[1]), its true value in condensed matter physics has only been recognized recently (in the last 10 years [2, 3, 4].)

Topology is a mathematical field which deals with the 'global' classification of objects. Local geometry details are not important. Instead, small sets of rules must be identified which create classes in which, apparently, different objects satisfying the same rules must fit in. The simplest example deals with the number of "handles" (holes) in surfaces of a given dimension. Such surfaces are assumed to be continuously deformable, as long as one does not "act violently" putting an extra hole in the surface. In this context, donuts are equivalent to mugs, while bottles are equivalent to spheres. The evident local differences in geometry are disregarded. Indeed, when looked at from this point of view, this idea seems rather handy to apply in classifying phases of matter, in case such a notion of topology can be properly defined in the condensed matter context.

Indeed, it can. While it is true that the usefulness of topology in the analysis of defects in solid state (and soft-) matter has been recognized since at least the seventies [5], only in 1982 the first hints of its importance in the study of electronic matter has been realized with the work of Thouless, Kohmoto, Nightingale and den Nijs (TKNN) in the integer quantum Hall effect [6]. In fact, in the past 10 years we have seen the notion of topological fermionic and bosonic states elevated to a point such as to demolish the completeness status of Landau's paradigmatic classification of the states of matter [7].

Landau's classification scheme dictates that different states of matter exist such that they are defined by a symmetry (continuous or discrete), and that accessing the different states demands the (spontaneous or explicit) breaking of some of these symmetries[8, 9]. Canonical examples are the solid-liquid transition (in which translational and rotational symmetries are broken) and, perhaps more exotically, superconductivity (in which a charge conservation - U(1) - symmetry is broken.) It turns out that other, anti-unitary, symmetries such as time-reversal and particle-hole conjugation have now been realized to 'protect' novel electronic phases in gapped systems.

We now explain what we mean by 'protecting' a novel phase. In the paradigmatic, non-interacting, classification of topological fermionic matter, a new set of ingredients is introduced. (i) Firstly, one only talks about gapped systems. (ii) Secondly, a set of discrete symmetry operations must be defined, which will define the topological classes. (iii) Thirdly, a real/momentum space dimensionality must be defined [10, 11].

Points (i)-(iii) fix classes of non-interacting electron Hamiltonians/evolution operators. The demand (i) implicitly implies that, without loss of topological information, one can exchange any arbitrary gapped Hamiltonian, and its given set of bands, with another arbitrary Hamiltonian as long as one keeps the same number of general bands and obeys the same symmetries defined by condition (ii). This process is known as "retracting" the Hamiltonian; the most convenient retraction exchanges the arbitrarily curved bands by a set of positive energy flat bands separated from a set of negative energy ones, without losing topological information. One can

retract Hamiltonians even further, considering the flattened spectrum as completely degenerate into a set of, say $k$ conduction bands and $n-k$ valence bands, for a system with a total of $n$ bands. One can associate then, each flattened Hamiltonian to its set of $n$ eigenvectors (defining a $U(n)$ matrix) modulo unitary transformations within the conduction and valence bands,

$$G_{n,k} = U(n)/U(k) \times U(n-k). \tag{1.1}$$

Each Hamiltonian defines a point in $G_{n,k}$, formally known as a Grassmanian manifold[12]. We do not want to get too technical at this point, but together with a notion of 'stable equivalence' (under addition of an arbitrary number of extra trivial bands), this Grassmanian manifold defines a "classifying space" in which a notion of equivalence can be defined. Then points (ii) and (iii) fix the final details defining the "base space" and classifying space. First, point (iii) defines the "base space", the simplest example being the Brillouin zone in a given dimensionality (typically taken as a d-torus for d dimensions.) Second, point (ii) imposes constraints in the classifying space. Due to the notion of equivalence classes of Grassmanians, maps from the base space to the classifying space have topological content, and invariant numbers accounting for this can be defined.

For example, the originally considered symmetries were anti-unitary time-reversal operations (which we represent by an operator $\Theta$) and particle-hole conjugation (represented by $\Xi$), as well as the chiral symmetry given by their product $\Pi = \Theta\Xi$. These can be thought of as reality constrains (in the complex analysis sense) in the electronic Hamiltonians. These define what are known as the Altland-Zirnbauer classes of random matrices [13].

Remarkably, the Altland-Zirnbauer analysis also fixes the critical behavior of surfaces of these gapped systems under disorder. This is understood in the sense of allowing or not for topological terms in the non-linear sigma model arising from a replica formalism[14]. As a direct consequence, insulating systems with non-trivial topological invariants are seen to have non-trivial transport properties, despite a seemingly 'boring' bulk. Notice, interestingly, that superconducting systems *also* represent a class of gapped systems - fixed by the particle-hole conjugation $\Xi$ above in the context of Bogoliubov-de Gennes Hamiltonians, as we will discuss - having their place of right in this new concept of phase too. A summary of the different topological behaviors in the 10 Altland-Zirnbauer classes is shown in Figure 1.1, where the entries $0, \pm 1$ under "Symmetry" refer to whether the Hamiltonian does *not* respect the symmetry (0 entry) or respects the symmetry such that the anti-unitary operator squares to $\pm 1$. Under $d$, the dimensionality of momentum space, 0 represent trivial phases (no topological invariant), while $\mathbb{Z}$ and $\mathbb{Z}_2$ are phases with integer and integer mod 2 invariants, respectively. For each dimension there will be always 5 topologically non-trivial phases, and as function of dimension, there is a mod 8 periodicity (Bott periodicity.) Classes A and AIII are known as "complex" while the others are "real" - as we mentioned, anti-unitary symmetries are reality constraints in the Hamiltonians.

Some examples come in hand. The first example constitutes the integer quantum Hall system. This is indeed a gapped fermionic system which has no particle-hole symmetry and time-reversal symmetry is also broken (due to the presence of an external magnetic field.) This corresponds to class A in $d = 2$, and one sees that there is an integer invariant for this phase. This integer, in fact, counts the number of chiral edge modes along the boundary of a Hall bar. This is the mentioned result of TKNN[6]. A second example is class AII in $d = 3$, which corresponds to the so-called time-reversal invariant topological insulators. Similarly, AII in $d = 2$ corresponds to the quantum spin Hall system, whose topological nature was first realized by Kane and Mele and triggered most of the subsequent development in topological systems in the literature.

Nowadays, the set of discrete symmetries in fermionic one-body Hamiltonians has been enlarged. It now contains mirror symmetries and even non-symmorphic ones (rotations plus half-lattice translations) [15, 16]. This concept of topological classification *under the protection of a symmetry* is indeed completely different from that of Landau's. In the topological reasoning, even if two gapped systems possess all the same symmetries, still, a topological invariant may be defined which can tell us that distinct phases are realizable. As discussed, physically, what distinguishes two distinct gapped phases with the same symmetries is typically a set of low-energy (gapless) boundary modes. These modes are protected by the symmetries: they develop a strong

| Symmetry | | | | $d$ | | | | | | | |
|---|---|---|---|---|---|---|---|---|---|---|---|
| AZ | $\Theta$ | $\Xi$ | $\Pi$ | 1 | 2 | 3 | 4 | 5 | 6 | 7 | 8 |
| A | 0 | 0 | 0 | 0 | $\mathbb{Z}$ | 0 | $\mathbb{Z}$ | 0 | $\mathbb{Z}$ | 0 | $\mathbb{Z}$ |
| AIII | 0 | 0 | 1 | $\mathbb{Z}$ | 0 | $\mathbb{Z}$ | 0 | $\mathbb{Z}$ | 0 | $\mathbb{Z}$ | 0 |
| AI | 1 | 0 | 0 | 0 | 0 | 0 | $\mathbb{Z}$ | 0 | $\mathbb{Z}_2$ | $\mathbb{Z}_2$ | $\mathbb{Z}$ |
| BDI | 1 | 1 | 1 | $\mathbb{Z}$ | 0 | 0 | 0 | $\mathbb{Z}$ | 0 | $\mathbb{Z}_2$ | $\mathbb{Z}_2$ |
| D | 0 | 1 | 0 | $\mathbb{Z}_2$ | $\mathbb{Z}$ | 0 | 0 | 0 | $\mathbb{Z}$ | 0 | $\mathbb{Z}_2$ |
| DIII | $-1$ | 1 | 1 | $\mathbb{Z}_2$ | $\mathbb{Z}_2$ | $\mathbb{Z}$ | 0 | 0 | 0 | $\mathbb{Z}$ | 0 |
| AII | $-1$ | 0 | 0 | 0 | $\mathbb{Z}_2$ | $\mathbb{Z}_2$ | $\mathbb{Z}$ | 0 | 0 | 0 | $\mathbb{Z}$ |
| CII | $-1$ | $-1$ | 1 | $\mathbb{Z}$ | 0 | $\mathbb{Z}_2$ | $\mathbb{Z}_2$ | $\mathbb{Z}$ | 0 | 0 | 0 |
| C | 0 | $-1$ | 0 | 0 | $\mathbb{Z}$ | 0 | $\mathbb{Z}_2$ | $\mathbb{Z}_2$ | $\mathbb{Z}$ | 0 | 0 |
| CI | 1 | $-1$ | 1 | 0 | 0 | $\mathbb{Z}$ | 0 | $\mathbb{Z}_2$ | $\mathbb{Z}_2$ | $\mathbb{Z}$ | 0 |

Figure 1.1: Periodic table of topological insulators and superconductors. Operators are $\Theta$ for time-reversal symmetry, $\Xi$ for particle-hole symmetry and $\Pi = \Theta\Xi$ for the chiral symmetry. $\pm$ entries correspond to the presence of the corresponding anti-unitary operators squaring to $\pm 1$, respectively. 0 entries mean the symmetry is absent. The "AZ" column indicates the notation of Altland and Zirnbauer for the classes. Entries $\mathbb{Z}$ mean that there is an integer number of different topological states, while $\mathbb{Z}_2$ means integer mod 2, i.e. only two distinct phases. [14, 10, 11]

anti-localization, even in the presence of disorder, as long as the disorder preserves the protecting symmetries. This is also known as the "bulk-boundary correspondence" - a topologically non-trivial bulk has robust gapless surface modes.

Recent developments in the field have been taking this topological classification idea beyond the notion of non-interacting systems [17]. Introduction of interactions have shown that the periodic table above is not complete, and several of the phases above are, nowadays, known to be more restricted (time-reversal invariant superconductors in class D in $d = 3$, for example, have their classification reduced from $\mathbb{Z}$ to $\mathbb{Z}_{16}$ due to interactions [18].) Importantly, these studies have shown that such topological matter displays intrinsically quantum behavior [7]. The classification of topological states nowadays is known to comprehend two distinct classes. The first contains the states with "true topological order". These include, for example, the fractional quantum Hall effect, in which a ground state degeneracy is associated with the real space sample topology and there may be the development of fractionalization of constituent quasiparticles. These systems are defined by developing long-range spatial entanglement in the ground state and are truly quantum (ground state cannot be deformed in a product of states localized at each site). Different entanglement patterns can lead to distinct phases in this case.

Topological matter from the context of the non-interacting classification above, falls in the second class. These are known as symmetry protected topological phases. They do not develop a topology dependent ground state degeneracy, and develop a short-range entangled ground state. Nevertheless, the presence of different symmetries still allows for the definition of different phases (like the ones described by the non-interacting periodic table), these contain ground states which cannot be deformed into the same product state *if* the protecting symmetry is not broken. Also, such classes are not relevant only to the non-interacting limit; the Haldane phase spin-1 chains (with spin 1/2 quasi-particles at the edges) comprises an example of an interacting symmetry protected topological phase in 1D [19].

Having exposed the plethora of information known to date, as well as some of the challenges in this field, we emphasize that advancing towards a complete classification of topological matter in the presence of interactions is not our goal with the present work (although we may make some comments on a particular situation in our the third chapter). Our objective *is* to study the known phases given by the periodic table beyond its standard non-interacting scheme, but from a different perspective. Our goal is to study the physics of electronic states bound to topological defects in these phases. Here defects must be understood as smooth disturbances in the single-body fermionic Hamiltonians which encapsulate, in real space, regions of singular behavior. The simplest example is the very surface of an insulator sample. It can be surrounded by a pair of points (spheres of zero-dimension $S^0$). Vortices in superconductors will be our main concern; they correspond to line-like defects, which can be surrounded by circular, $S^1$, loop surfaces. Systems with such defects are also subject to topological classification, under given sets of symmetries. The manifestation of the bulk-boundary correspondence, in this case, enforces the binding of low-energy degrees of freedom in the defects [12].

We focus on two related, yet distinct, scenarios, both related to superconductivity. Our first example lies in class AII in 3D. This is a known topological insulator under time-reversal invariance. The first material discovered to fall in this class is $Bi_2Se_3$ [20]. It turns out that, under doping (by $Cu_x$, optimal at $x = 0.12$), this insulator becomes a metal. Even more interestingly, this metal, at low temperatures, develops a superconducting phase [21, 22, 23, 24]. A simple question is, how conventional is a superconductor arising from a metallic doped topological insulator parent metal? We will explore this question from the point of view of vortex electronic matter. We touch the concept of vortex topological phase transitions [25, 26, 27] from a novel approach and will study a proposal to measure the uncommon features of these electronic vortex bound states. This proposal will further unfold into hinting for new signatures of topological superconductivity in 1D[28].

Our second point will focus on topological superconductivity itself. Among the gapped phases defined by the topological classification above, we defend that superconducting phases really play a role which deserves special attention. The topological superconducting phases (classes D, DIII, C and CI) are fixed by a particle-hole

symmetry defined when writing fermionic Hamiltonians in the so-called Bogoliubov-de Gennes doubled form

$$\begin{aligned}\mathcal{H} &= \sum_{i,j} c_i^\dagger H_{ij} c_j \\ &= \sum_{i,j} \left(c_i^\dagger, c_i\right) \begin{pmatrix} H_{ij} & \\ & -H_{ij}^T \end{pmatrix} \begin{pmatrix} c_j \\ c_j^\dagger \end{pmatrix}. \end{aligned} \tag{1.2}$$

This particle-hole symmetry reads $\Xi = \rho_x K$ or $\Xi = i\rho_y K$ (depending on whether it squares to $+1$ or $-1$, respectively), where $K$ represents complex conjugation and $\rho_i$ are Pauli matrices acting in the so-called Nambu space of $\left(c_i^\dagger, c_i\right)$. The annihilation operators $c_i$ may have a multiple band internal structure. Due to the particle-hole symmetry nature of this system, Bloch states of energy $E_{\mathbf{k}}$ and $-E_{-\mathbf{k}}$ are identified. This leads to a condition of "reality" (in the sense of complex numbers) on the states. In particular, surface (or other defects) bound states develop a Majorana character. That means that their corresponding second quantized operators are self-Hermitian, they create particles which are their own anti-particles. These particles, as being real, are neutral, and do not couple to electromagnetism. They are elusive (in the sense that their physical signatures are difficult to measure) and, sometimes as we will see, do not have a properly defined and understood description.

This thesis focus then on the unconventional physics of superconducting vortex bound states, in particular Majorana bound states on what we call topologically non-trivial contexts (as to embrace both the previously mentioned doped topological insulator *and* topological superconductor scenarios.) This leads us beyond the non-interacting classification of topological phases in several different ways: from the interplay of "regular" topological insulation and superconductivity, to the effective physics of "actual" topological superconductors in 3D, defect bound states, ground state degeneracy, and a correct classification of the different phases in the presence of interactions.

We separate our developments in three chapters. In Chapter 2, we will discuss the basic physics of the most paradigmatic topological superconductor: the Kitaev p-wave chain in 1D[29]. We will use it to pedagogically introduce and review all the ingredients necessary to understand the notion of topology in superconducting gapped systems. We will talk about the relation of bulk topological invariants and boundary gapless modes and the advent of Majorana fermions[30]. We will then talk about some standard signatures of Majorana fermions and show our own proposals for their detection in 1D systems via fractional Josephson effects in SQUIDs[31, 32]. Chapter 3 will concern the study of vortex bound states in doped topological insulators. We will describe in more detail the topological features of insulators and the $\mathbb{Z}_2$ invariant in 3D [33]. We connect, from our own point of view, the physics of vortex bound states to the case described in the first chapter, discussing how vortices in this unconventional superconductor behave effectively as Kitaev p-wave one-dimensional chains [26, 27, 25, 28]. We show how the physics of these may be unveiled by scanning tunneling microscopy measurements of the local density of states of vortex cores. Finally, Chapter 4 is devoted to the study of actual topological superconductors. We discuss the effective electromagnetism of this phase, discussing the Maxwell action which gets modified by an axion-type term[34]. We show how such an action can lead to paradoxical results, with incurable quantum anomalies at superconducting vortices. We show a possible way out of this problem in terms of a Cooper-pair adiabatic quantum pump and degeneracy of ground state multiplets; this then connects the problem to that of the classification of the topological phases and can be mapped into a novel type of fractional Josephson effect [35], tying, again, back to the concepts introduced in Chapter 1. We finish with a chapter of conclusions. We emphasize there are works published during the development of this Doctoral thesis which are not studied in this present body of work.

# Chapter 2

# Topological superconductivity in 1D

## 2.1 Introduction

The main theme of this thesis is not topological superconductivity, but rather vortex electronic bound states in superconducting topological matter. By superconducting topological matter we mean two different kinds of systems: (i) superconducting systems whose metallic phase carries topological information from the underlying band structure (ii) actual topological superconductors. Yet, both of these systems will be seen to share several common physical properties and, as such, it will prove pedagogical to introduce the diverse phenomenological and technical aspects of topological superconductivity in its simplest setting. This way, all the basic concepts can be carried further into the following Chapters as they will be properly contextualized. We thus devote this Chapter to a thorough introduction to the subject of topological superconductivity, choosing the basic 1D setting for such pedagogical reasons. We will also make use of this chance to further explore the physics of topological superconducting systems in 1D, demonstrating some proposals of our own to verify signatures of such phases in the context of macroscopic quantum tunneling [36, 37].

## 2.2 Kitaev Chains

We will start our exposition on the relationship between superconducting vortices, vortex bound states and topological matter, by considering a paradigm which summarizes the main remarkable phenomena that arise when one joins superconductivity, topology and localized states.

We will talk about the simplest model of the so-called topological superconductivity. Topology is a branch of mathematics which relies on the classification of quantities, typically surfaces in a broad sense, by a global analysis of the given quantities properties, as opposed to geometry which analyses surfaces locally. We will postpone a more in-depth discussion about the mathematical details of topological classification of gapped systems to the next chapter, where our initial discussion of topological insulators should settle down the mathematics with some (physicist) details. For now, we will just consider the so called "Kitaev model"[29] explicitly, describing its properties and trying to get a flavor of these notions of topology in the context of gapped (Bloch) Hamiltonians. We follow the details from [30], with some of our own insights.

The Kitaev model describes a set of non-interacting fermions along a chain within the tight-binding approximation, under the influence of a p-wave superconducting pairing, in the mean-field approximation. The Hamiltonian reads

$$\mathcal{H}_{Kit} = -\mu \sum_x c_x^\dagger c_x - \frac{1}{2} \sum_x \left( t c_x^\dagger c_{x+1} + \Delta e^{i\phi} c_x c_{x+1} + h.c. \right), \tag{2.1}$$

where $x$ is summed over $N$ sites. Here, $\mu$ is a chemical potential, $t$ a hopping amplitude and $\Delta$ represents a p-wave (notice that it connects neighboring sites) type of superconducting pairing (with phase $\phi$). Several attempts were made in order to realize this model experimentally, with some remarkable advances and successes (as well as failures and drawbacks. Check [38, 39] for a pair of relevant examples). Taking a unit lattice parameter, one

can define a new set of fermionic operators $c_k$, through the Fourier transform

$$c_x = \frac{1}{\sqrt{N}} \sum_k e^{ikx} c_k, \tag{2.2}$$

obtaining

$$\mathcal{H}_{Kit} = \sum_k c_k^\dagger \underbrace{(-\mu - t\cos k)}_{\epsilon(k)=\epsilon(-k)} c_k + \frac{\Delta}{2} \sum_k \left( e^{i\phi} e^{ik} c_k c_{-k} + e^{-i\phi} e^{-ik} c_{-k}^\dagger c_k^\dagger \right). \tag{2.3}$$

While the diagonalization of this second quantized Hamiltonian can be achieved by a Bogoliubov transformation, the standard practice when talking about topology is slightly different - altbeit equivalent. First, using the fermionic canonical anti-commutation relations

$$\left\{ c_k, c_{k'}^\dagger \right\} = \delta_{kk'}; \{c_k, c_{k'}\} = \left\{ c_k^\dagger, c_{k'}^\dagger \right\} = 0, \tag{2.4}$$

one rewrites the two terms in parenthesis above as

$$\sum_k \epsilon(k) c_k^\dagger c_k = \underbrace{\frac{1}{2} \sum_k \epsilon(k)}_{E_0} + \frac{1}{2} \sum_k \epsilon(k) \left( c_k^\dagger c_k - c_k c_k^\dagger \right) \tag{2.5}$$

and

$$\sum_k e^{i\phi} e^{ik} c_k c_{-k} + e^{-i\phi} e^{-ik} c_{-k}^\dagger c_k^\dagger = \sum_k i \sin k \left( e^{-i\phi} c_k^\dagger c_{-k}^\dagger - e^{i\phi} c_{-k} c_k \right). \tag{2.6}$$

Now one introduces the so-called Nambu spinors $C_k^\dagger = \begin{pmatrix} c_k^\dagger & c_{-k} \end{pmatrix}^T$ generating the Bogoliubov-de Gennes (BdG) version of Kitaev's Hamiltonian in momentum space, which up to an unimportant constant $E_0$, can be written as

$$\mathcal{H}_{Kit} = \frac{1}{2} \sum_{k \in ZB} C_k^\dagger H_k^{BdG} C_k, \tag{2.7}$$

$$H_k^{BdG} = \begin{pmatrix} \epsilon_k & \tilde{\Delta}_k^* \\ \tilde{\Delta}_k & -\epsilon_k \end{pmatrix} \tag{2.8}$$

$$= \rho_z \epsilon_k + Re\tilde{\Delta}_k \rho_x + Im\tilde{\Delta}_k \rho_y. \tag{2.9}$$

Here, $\tilde{\Delta}_k = -i\Delta e^{i\phi} \sin k$ exposes explicitly the p-wave nature of the superconducting pairing of this model and the Pauli matrices $\rho_i$ act in the Nambu space.

For future reference, let us consider the Hamiltonian above for small momentum,

$$H_{\delta k}^{BdG} \approx \rho_z \left( -\mu - t + \frac{t}{2} \delta k^2 \right) - \rho_y \Delta e^{i\phi\rho_z} \delta k. \tag{2.10}$$

Notice that this is a Dirac-like Hamiltonian in 1D for small enough $\delta k$ (actually the superconducting phase here can be interpreted in terms of geometric deformations in standard Dirac fermions in 1D, a subject which we will actually not approach.) This type of Hamiltonian will appear many other times along the development of this thesis, and it condenses most of the simple structure and notation which we will use. For now, however, let us not focus on it, rather just keeping it in the back of our minds.

Back to the second quantized Hamiltonian, notice that $C_k$ and $C_k^\dagger$ are ***not*** independent operators now. Indeed, they are related by

$$\left( C_k^\dagger \right)^T = \rho_x C_{-k}. \tag{2.11}$$

Accordingly, the first quantized Hamiltonian obeys an anti-unitary symmetry described by $\Xi = \rho_x K$, where $K$ is the complex conjugation operator . This is a particle-hole symmetry because it transforms the single-body

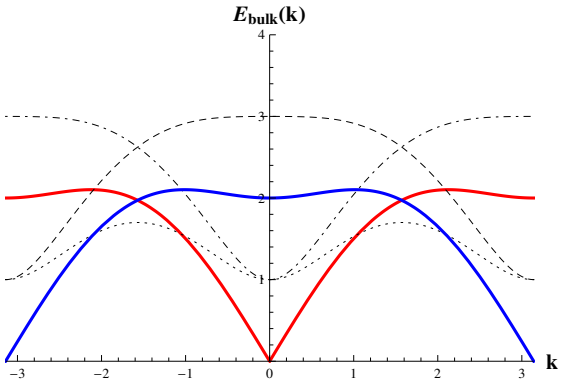


Figure 2.1: Dispersion relation for the quasi-particles in Kitaev's chain. The parameters used are $t = 1$ and $\Delta = 1.7$. Then we have, respectively, point-dashed ($\mu = -2$), full red ($\mu = -1$), dotted ($\mu = 0$), full blue ($\mu = 1$) and dashed ($\mu = 2$) curves. Notice that the system is gapless at $\mu = \pm 1$, which define the topological phase transition.

Hamiltonian as

$$\rho_x H_{-k}^{BdG*} \rho_x = -H_k^{BdG}, \tag{2.12}$$

that is, it implies that the spectrum is symmetric with respect to $E_k \to -E_{-k}$. This is known also as a Nambu constraint. We show how this works out explicitly in Section 2.4.1.

The BdG form of a superconductor Hamiltonian can be written for any pairing symmetry and dimensionality and is convenient because of a few of reasons. Firstly, diagonalization is achieved by a standard unitary transformation in $H_k^{BdG}$. The extra, artificial, negative energy bands can be discarded by normal ordering the new Hamiltonian with respect to a completely filled Fermi sea of negative energy modes. Secondly, the introduction of artificial negative energy bands allows one to look at the problem as in an insulator, with a valence and conduction bands; this opens space to treating superconducting Hamiltonians topologically in the same way as done for regular insulators (other reasons exist which we will not explore right now, like rewriting the Hamiltonian in a convenient form for functional integration, for example).

The application the Nambu constraint to the wavefunctions and operators recovers the standard result of the Bogoliubov transformation with new Fermions,

$$a_k = u_k c_k + v_k c_{-k}^\dagger \tag{2.13}$$

in terms of which the Hamiltonian simply reads

$$H = \sum_k E_{bulk}(k)\, a_k^\dagger a_k, \tag{2.14}$$

where

$$u_k = \frac{\tilde{\Delta}_k}{\left|\tilde{\Delta}_k\right|} \frac{\sqrt{E_{bulk}(k) + \epsilon_k}}{\sqrt{2E_{bulk}(k)}};\ v_k = \left(\frac{E_{bulk}(k) - \epsilon_k}{\tilde{\Delta}_k}\right) u_k \tag{2.15}$$

and the single-particle spectrum reads

$$E_{bulk}(k) = \sqrt{\epsilon_k^2 + \left|\tilde{\Delta}_k\right|^2}, \tag{2.16}$$

and is illustrated in Fig.2.1.

As long as $\mu \neq \pm t$, the spectrum of this problem is fully gapped over the whole Brillouin zone. Phases with $\mu < -t$ and $\mu > t$ are related by the particle-hole constraint and we can focus in the former case, for concreteness. Let us study then the difference in the physics between the two distinct regimes $\mu < -t$ and $|\mu| < t$.

The BCS ground state may be written

$$\begin{aligned} |g.s.\rangle &\propto \prod_{0<k<\pi} \left[1+\varphi_{C.p.}\left(k\right) c_{-k}^{\dagger} c_{k}^{\dagger}\right] |0\rangle \\ \varphi_{C.p.}\left(k\right) &= \frac{v_k}{u_k} = \left(\frac{E_{bulk}\left(k\right)-\epsilon_k}{\tilde{\Delta}_k}\right), \end{aligned} \tag{2.17}$$

where $|0\rangle$ is the empty state in Fock space. Here $\varphi_{C.p.}\left(k\right)$ can be interpreted like a "Cooper pair wavefunction". We may study it in real space by Fourier transformation. First, one writes

$$\begin{aligned} \varphi_{C.p.}\left(k\right) &= \frac{\sqrt{\epsilon_k^2+\left|\tilde{\Delta}_k\right|^2}-\epsilon\left(k\right)}{\tilde{\Delta}_k} \\ &= ie^{-i\phi}\left(\frac{\sqrt{\left(t\cos k+\mu\right)^2+\Delta^2\sin^2 k}+t\cos k+\mu}{\Delta\sin k}\right). \end{aligned} \tag{2.18}$$

Then,

$$\varphi_{C.p.}\left(x\right) = \int_{-\pi}^{\pi} dk e^{ikx} \varphi_{C.p.}\left(k\right), \tag{2.19}$$

and

$$\left|\varphi_{C.p.}\left(x\right)\right| = \int_{-\pi}^{\pi} dk \sin\left(kx\right) \underbrace{\left(\frac{\sqrt{\left(t\cos k+\mu\right)^2+\Delta^2\sin^2 k}+t\cos k+\mu}{\Delta\sin k}\right)}_{\equiv f(k)}. \tag{2.20}$$

Some details of the k-space wavefunctions follow in Fig.(2.2)

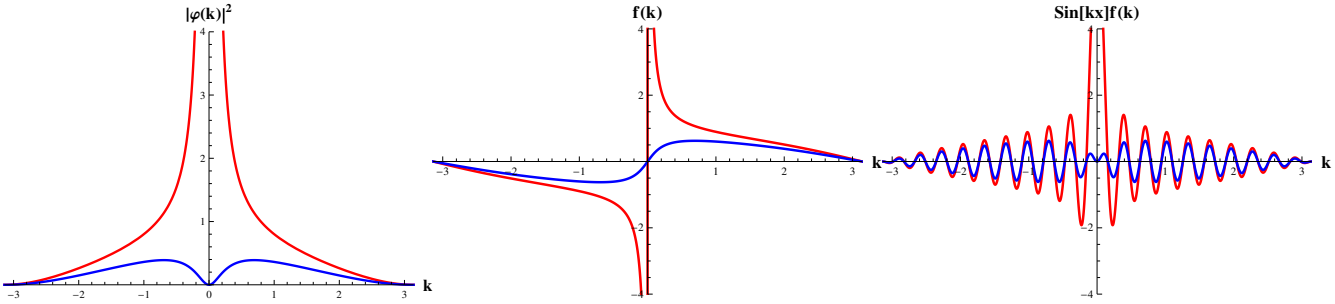


Figure 2.2: k-space wavefunction and Fourier transform details. Parameters are $\Delta = 1.7$ and $t = 1$ and (blue) $\mu = -1.3 < -t$ and (red) $|\mu = -0.7| < t$. The details explore the localization behavior of the Cooper pair "wavefunctions" in k-space, as well as the integrand of the Fourier transform. The right most figure takes large $x = 20$, showing that the integrand decays quickly to zero. This justifies enlarging the Fourier integration range from $-\pi \to \pi$ to $-\infty \to \infty$, for $x$ large with respect to some characteristic length scale $\zeta$. This is convenient for analytical calculations.

For large enough $x$, with respect to some length scale $\zeta$ (related to the superconducting coherence length), one can see that the integration range in the Fourier series can be extended to infinity. Accordingly, the integrals can be computed analytically, resulting in

$$\left|\varphi_{C.p.}\left(x\right)\right| \sim \begin{cases} e^{-|x|/\zeta}, & \mu < -t \text{ (strong pairing)} \\ const., & |\mu| < t \text{ (weak pairing)} \end{cases}. \tag{2.21}$$

The first and second integrals can be understood by approximating the momentum space wavefunctions by, respectively, $2/\left(1+k^2\right)$ (which is a good approximation for the tails but bad for the central part of the function) and a Bessel function of order zero (or a Dirac delta function). The results of the Fourier transforms are represented by the above equations. These details are illustrated in Fig.2.2

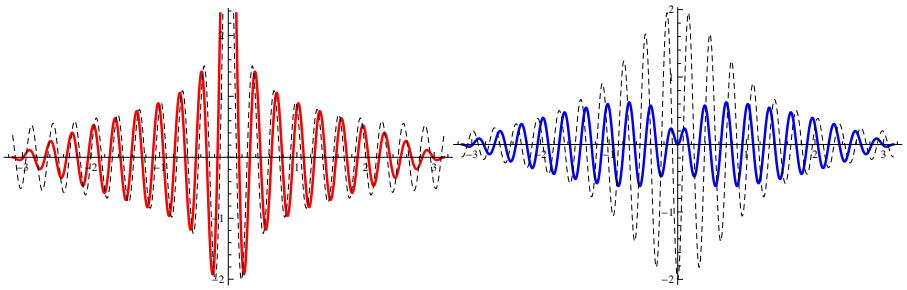

Figure 2.3: Here we compare the Cooper pair Fourier transform integrands in momentum space with the approximations described in the text; we use same parameters as in Fig.2.2 and values of the position variable $x = 20$. The good approximations show that this value of $x$ is much larger than the length scale $\zeta \sim v_F/\Delta \sim 1$. On the left, we have the weak pairing case with the integrand approximated by $5J_0(20\,k)$. For strong pairing,we use $-\cos(20\,k)\,\frac{2}{1+k^2}$. Notice that these approximations are best where the weight of the integrands are largest.

This implies two very distinct behaviors for this problem, which we will represent as saying that this system is in a $\mathbb{Z}_2$ class, that is integer modulo 2. In one case, Cooper pairs are small, with tightly bound constituents; in the other, they are extended.

Indeed, we now show that the one-body Hamiltonian carries in itself information about these two behaviors. First, notice that the BdG Hamiltonian can be written

$$H_k^{BdG} = \mathbf{h}(k) \cdot \boldsymbol{\rho}, \tag{2.22}$$

where the $\mathbf{h}(k)$ vector is written in terms of $\epsilon(k)$ and $\tilde{\Delta}(k)$. Now we apply the Nambu particle-hole constraint. It results that the following relationships must be satisfied,

$$h_{x,y}(k) = -h_{x,y}(-k)\,,\; h_z(k) = h_z(-k)\,. \tag{2.23}$$

This implies that it is enough to specify $\mathbf{h}(k)$ only in half of the Brillouin zone $0 \leq k \leq \pi$. Furthermore, the eigenvalues of the BdG Hamiltonian are$\pm|\mathbf{h}(k)|$ and, as long as $\mathbf{h}(k) \neq 0$ throughout the Brillouin zone, the system is completely gapped. One then defines the unit vector $\hat{\mathbf{h}}(k)$ which maps the Brillouin zone (here, a circle)to the unit sphere. Due to the particle-hole symmetry relations above, this map is strongly constrained at $k = 0, \pm\pi$, such that

$$\hat{\mathbf{h}}(0) = s_0\hat{\mathbf{z}},\;\; \hat{\mathbf{h}}(\pi) = s_\pi\hat{\mathbf{z}}$$

where $s_0$ and $s_\pi$ are the signs of the kinetic energy with respect to the Fermi energy at $k = 0, \pi$. This means that, as one varies $k : 0 \to \pi$, two possibilities arise. The first case would have $\hat{\mathbf{h}}(k)$ starting at a pole in the unit sphere and ending at the same pole (i.e. $s_0 = s_\pi$). The second case would have the opposite (i.e. $s_0 = -s_\pi$) behavior.

These signs $s_0$ and $s_\pi$ can be computed explicitly for the Kitaev model above, resulting in

$$s_0 = -\frac{t+\mu}{|t+\mu|} \tag{2.24}$$

$$s_\pi = \frac{t-\mu}{|t-\mu|}. \tag{2.25}$$

The different behaviors of $h_z$ are illustrated in Fig.2.4.

We can thus make explicit the topological analysis of a Hamiltonian explained in the Introduction. The reasoning above associates with the Hamiltonian $H_k^{BdG}$ an integer mod 2 number

$$\nu = s_0 s_\pi, \tag{2.26}$$

which may be used to classify the two distinct phases. In practice, $\nu = +1$ corresponds to the **strong-pairing**

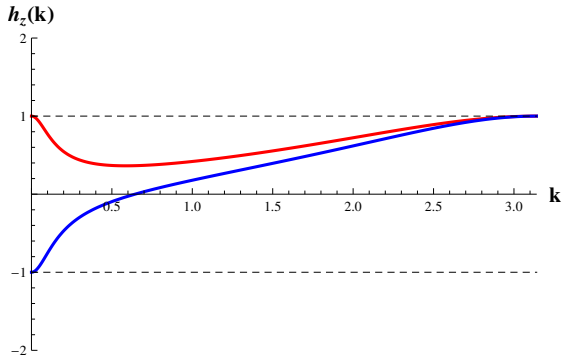


Figure 2.4: $h_z(k)$ for Kitaev's p-wave chain. (red) trivial phase (blue) topological regime.

**limit** and is known as a *topologically trivial* phase. For $\nu = -1$, we have the **weak-pairing limit** and this is known as a *topologically non-trivial* phase. This is a mathematical topological notion which classifies the ways one can map the 1D Brillouin zone (base space is a circle, $k : 0 \to 2\pi$) into the space of Hamiltonians satisfying the BdG particle-hole symmetry (classifying space.) The reason why $\nu$ defines a topological invariant in the mathematical sense is that the space of Hamiltonians can be thought of as a surface which can be smoothly deformed. The notion of smoothness here is fixed by the condition of *not closing the gap*. From a topology point of view, closing the gap in a insulating Hamiltonian is equivalent to puncturing a sphere, adding a hole to it.

This analysis above shows how convenient the BdG form of a superconducting Hamiltonian is to study this type of physics. It immediately implements the notion that superconductors are similar to insulators, in the sense of having massive quasi-particle excitations. All this discussion above is, therefore, also valid for regular insulators in 1D. The caveat is that a different anti-unitary symmetry must be used in the latter case. The one typically used to fulfill this role is the time-reversal symmetry, as we will discuss in the next chapter in the context of 3D topological insulators. As topology is not the main theme of this thesis, we will avoid dwelling further in this subject, postponing some more comments to Chapter 3. We will move now onto the different physical signatures of these two quantum regimes.

## 2.3 Majorana fermion physics

Up to now, we have realized that the physics of the simple Hamiltonian 2.1 contains, in fact, two distinct superconducting regimes. Physically, the two distinct superconducting regimes have Cooper pairs tightly or loosely bound. We have seen that, from the non-interacting Hamiltonian point of view, these two distinct behaviors are connected to a topological invariant; such a quantity that does not change as one tunes the Hamiltonian parameters, as long as the system's gap does not close. It is now our mission to discuss how could one distinguish, experimentally or by phenomenology, these two situations. In the process, we will explore the concept of bulk-boundary correspondence. We will keep on following, mostly, reference [30].

The different quantum regimes enforced by the Hamiltonian above are fixed for concreteness by

$$\begin{cases} \mu < -t & \text{, strong pairing, topologically trivial} \\ |\mu| < t & \text{, weak pairing, topologically non-trivial} \end{cases} . \tag{2.27}$$

Let us study the two extreme limits, $t = 0$ and $\mu = 0$. It is convenient to introduce a Majorana fermion operator basis, by writing

$$c_x = \frac{e^{-i\phi/2}}{2} \left(\gamma_{B,x} + i\gamma_{A,x}\right) . \tag{2.28}$$

The $\gamma_{A,B,x}$ operators are known as Majorana fermion operators. This decomposition implies that each site

containing a "complex" Fermion is equivalent to a site containing a pair of Majorana fermions. They are "real" operators, obeying,

$$\gamma^{\dagger}_{\alpha,x} = \gamma_{\alpha,x},\ \{\gamma_{\alpha,x}, \gamma_{\alpha',x'}\} = \frac{1}{2}\delta_{\alpha\alpha'}\delta_{xx'}. \tag{2.29}$$

This means that we are "breaking" each complex fermion $c_x$ in two real fermions $\gamma_{A,x}$ and $\gamma_{B,x}$ which will couple according to the Hamiltonian. We do this in real space, as it will be simple in the two limits above. The system can be thought of as a Majorana fermion chain with two atoms in the basis. A few important identities read

$$c^{\dagger}_x c_x = \frac{1}{2}\left(1 + i\gamma_{B,x}\gamma_{A,x}\right); \tag{2.30}$$

$$c^{\dagger}_x c_{x+1} + h.c. = \frac{i}{2}\left(\gamma_{B,x}\gamma_{A,x+1} - \gamma_{A,x}\gamma_{B,x+1}\right); \tag{2.31}$$

$$e^{i\phi}c_x c_{x+1} + h.c. = \frac{i}{2}\left(\gamma_{B,x}\gamma_{A,x+1} + \gamma_{A,x}\gamma_{B,x+1}\right); \tag{2.32}$$

from which the Hamiltonian yields

$$\begin{aligned}\mathcal{H}_{Kit} = & -\frac{\mu}{2}\sum_{x=1}^{N}\left(1 + i\gamma_{B,x}\gamma_{A,x}\right) \\ & -\frac{i}{4}\sum_{x=1}^{N-1}\left[\left(\Delta + t\right)\gamma_{B,x}\gamma_{A,x+1} + \left(\Delta - t\right)\gamma_{A,x}\gamma_{B,x+1}\right].\end{aligned} \tag{2.33}$$

We take $t = \Delta$ for concreteness. From this version of the Hamiltonian, the importance of the two limits above is manifest. In the topologically trivial limit, $t = 0$, the Hamiltonian becomes

$$H = -\frac{\mu}{2}\sum_{x=1}^{N}\left(1 + i\gamma_{B,x}\gamma_{A,x}\right). \tag{2.34}$$

One sees that this Hamiltonian induces hybridization between$\gamma_{A,x}$ and $\gamma_{B,x}$, which are Majorana fermions located at the same site. The ground state can be simply inferred from the Hamiltonian in the complex fermion regime. It corresponds to a state with all $c_x$ states singly occupied. The spectrum is obviously gapped as adding a spinless fermion to the ground state costs a finite energy $|\mu|$. One can now move away from the $t = \Delta$ and $\mu = 0$ regime and, as long as the gap does not close, the physics will be the same.

For the second (topological) limit, we use $t = \Delta \neq 0$ e $\mu = 0$. The Hamiltonian becomes

$$\mathcal{H}_{Kit} = -it\frac{1}{2}\sum_{x=1}^{N-1}\gamma_{B,x}\gamma_{A,x+1}, \tag{2.35}$$

which now couples real fermions of adjacent sites. By redefining new complex fermionic operators,

$$d_x = \frac{1}{2}\left(\gamma_{A,x+1} + i\gamma_{B,x}\right), \tag{2.36}$$

we can write our steps backwards again, and the Hamiltonian reads

$$\mathcal{H}_{Kit} = t\sum_{x=1}^{N-1}\left(d^{\dagger}_x d_x - \frac{1}{2}\right). \tag{2.37}$$

The ground state can be described easily once again. The system is gapped in the bulk (by $t$ now). This is consistent with the solution with periodic boundary conditions as before. On the other hand, it is clear that the fermions $\gamma_1 \equiv \gamma_{A,1}$ and $\gamma_2 \equiv \gamma_{B,N}$ do not contribute to the Hamiltonian. The analysis is very similar to the case of edge modes in the spinless Su-Schrieffer-Heegger chain [40] (some loosely think of this as a "half"

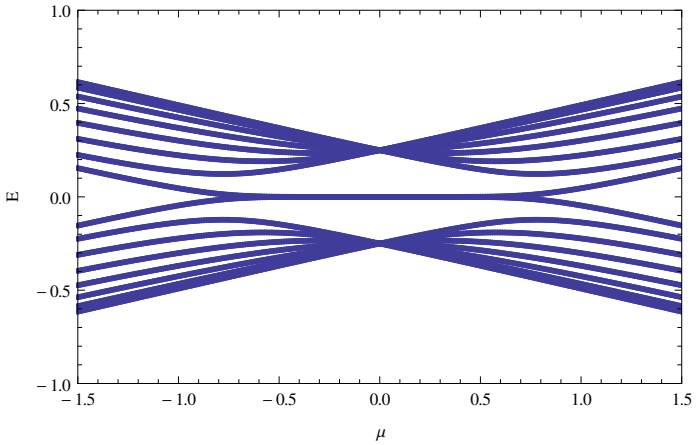


Figure 2.5: Open Kitaev chain spectrum as function of $\mu$. We use $\Delta = t = 1$. Notice the pair of degenerate zero modes for $|\mu| < 1$. In real space, they are localized at opposite edges of the chain.

spinless 1D chain). In the present case, however, the edge Majorana operators may be combined in a single, highly non-local (in the thermodynamic limit) fermion,

$$f = \frac{1}{2}(\gamma_1 + i\gamma_2) \tag{2.38}$$

whose occupation energy cost is zero. This means that the ground state is doubly degenerate. Explicitly, if $|0\rangle$ is a ground state satisfying $f|0\rangle = 0$ and $d_x|0\rangle = 0$, then $|1\rangle = f^\dagger|0\rangle$ is also a ground state. For systems with $N_0$ Majorana zero modes, the corresponding ground states are known to be $2^{N_0/2}$ degenerate. Moving away from this extreme limit by tuning $\mu \neq 0$ e $t \neq \Delta$, without closing the gap, the Majorana zero-modes $\gamma_1$ and $\gamma_2$ start mixing with the bulk states and are not uniquely determined by $\gamma_{A,1}$ and $\gamma_{B,N}$ anymore. Instead, their wavefunctions decay exponentially into the bulk. The decay length is controlled by the *bulk gap*, a point which will become important again in Chapter 3. For a finite chain, an overlap between the Majorana fermions breaks the degeneracy of the $|0\rangle$ and $|1\rangle$ ground states. The energy scale of this energy gap is controlled by $e^{-L/\xi}$, where $L$ is the chain's length and $\xi$ is the coherence length. In the thermodynamic limit, $L \gg \xi$ and the energy splitting may be neglected. The spectrum of the open Kitaev chain, as function of the chemical potential, follows in Fig. 2.5.

This is a convenient place for some final comments on the edge modes and topology. First of all, the existence of zero energy states at the edge, which separates a topologically non-trivial phase from a topologically trivial phase (the vacuum), is a manifestation of the so-called "bulk-boundary correspondence". It states that at the boundary between phases characterized by some non-trivial topological invariants, gapless modes arise. This has no formal proof, although the result follows generally from the work of Teo and Kane which characterizes the bound states and topology of fermionic phases in the presence of spatially smooth defects of different dimensions (hedgehogs, vortices, surfaces, etc)[12]. The statement is generically true for non-interacting systems and also applies in several systems where interactions are important. It may fail, however, when true topological order arises (in sum, when the ground state degeneracy depends on the sample real space topology - sphere, torus, etc. - like in fractional quantum Hall effect or Kitaev's toric code[41]). A second, also important, point, is what happens when one has mode degrees of freedom available. For example, let us allow for a spinful Kitaev chain. In this case, when in the topological $|\mu| < t$ phase, each edge posses two Majorana zero modes. By the same reasoning as before, this is equivalent to an ordinary zero-energy complex fermion at each edge. It turns out that, as long as extra symmetries are not imposed, perturbations like spin-orbit coupling may shift the states away from zero energy. Doubling the degrees of freedom trivializes the problem, which could be expected from the $\mathbb{Z}_2$ invariant characterizing this problem. Topologically, having two Majorana zero modes is equivalent to having none. As long as Kramers degeneracy is broken, one may freeze the spin degree of freedom and reduce the discussion to the spinless case. Several attempts have been made recently in the direction of trying to realize

the Kitaev p-wave chain experimentally [42, 30]. We will postpone the discussion on some of these until later; they will not be the focus of our discussion in this thesis as we will describe our own system of interest which realizes explicitly a Kitaev chain behavior in Chapter 3.

## 2.4 Signatures of Majorana zero-modes physics

While the existence of Majorana zero-modes localized at point defects (edges above) is definitely a hallmark of topological superconductivity, finding experimental evidence of their existence turns out to be quite a formidable task. To the present date, no unequivocal evidence of Majorana fermion physics has been found. The main problem with this is two-fold. First of all, sub-gap states exist in several situations, as we will see in the next chapter, and filtering the zero-mode is not easy as energy scales may not be very helpful. Also, several other effects can give rise to zero-energy states which are not Majorana fermions [43, 44, 45, 31]. A second, perhaps more fundamental problem, comes from the fact that Majorana fermions are "real" fermions. They do not carry U(1) phases and, as such, no electromagnetic charge. They are neutral and blind to electromagnetic interactions. Zero-bias peaks in tunneling experiments are then agreed to be inconclusive regarding Majorana zero-mode detection, while typical linear responses are usually not even considered (an exception goes for thermal transport, which can be thought of as computing gravitational responses, which couple to energy-momentum tensors. These have been considered, but again, experimentally isolating the Majorana contributions is far from trivial).

From some time now, the main sought-after signature of Majorana fermion physics, considered a smoking gun if verified (which it has never been, so far, for reasons to be discussed) is called the "fractional Josephson effect"[29, 31]. Let us start by reviewing the standard Josephson effect in the case of a linear Kitaev chain. This will give reproduce all the standard results in the trivial regime, but not in the topological one. We will then show how it is modified in the topological regime.

### 2.4.1 Regular Josephson effect

A Josephson junction consists of a pair of superconducting wires connected by a weak-link or insulating junction. The Josephson effect consists in the phenomenon of finding a current across this junction even at zero-voltage-bias. Such a current arises when the difference in the phase between the superconducting wires is finite. Let us show how this behaves for a junction made out of Kitaev p-wave wires.

We start with the diagonalization of the BdG Hamiltonian in detail. First we write

$$UH_k^{BdG}U^\dagger = D_k, \tag{2.39}$$

where $D_k$ is the diagonal matrix with eigenvalues $\pm E_{bulk}(k)$, $E_{bulk}(k) = \sqrt{\epsilon_k^2 + \left|\tilde{\Delta}_k\right|^2}$ and

$$U = \begin{pmatrix} u_{+,k} & v_{+,k} \\ u_{-,k} & v_{-,k} \end{pmatrix}, \tag{2.40}$$

with

$$\begin{aligned} u_{+,k} &= e^{-i\phi}\mathrm{sgn}k v_k, \qquad & v_{+,k} &= u_k \\ u_{-,k} &= -\mathrm{sgn}k e^{-i\phi} u_k \qquad & v_{-,k} &= v_k. \end{aligned} \tag{2.41}$$

and general functions $u_k$ and $v_k$ such that

$$u_k = \sqrt{\frac{1}{2}\left(1 - \frac{\epsilon}{E_{bulk}}\right)}, \; v_k = \sqrt{\frac{1}{2}\left(1 + \frac{\epsilon}{E_{bulk}}\right)}. \tag{2.42}$$

The Bogoliubov quasi-particle operators in each energy branch are written now

$$\begin{aligned} a_{+,k} &= e^{-i\phi}\mathrm{sgn}k v_k c_k + u_k c^\dagger_{-k} && (2.43)\\ a_{-,k} &= -e^{-i\phi}\mathrm{sgn}k u_k c_k + v_k c^\dagger_{-k}. && (2.44) \end{aligned}$$

These $\pm$ states are related by the Nambu particle-hole constraint and are not independent. The physical ground state is obtained by filling the negative energy modes

$$|N\rangle = \prod_{-\pi<k<\pi} a^\dagger_{-,k}\,|0\rangle \tag{2.45}$$

with respect to which, we normal order all the operators - like the Hamiltonian. This amounts to droping the $a_{-,k}$ fermions.

Analogously, one may invert the relations of the original fermions and Bogoliubov quasiparticles,

$$\begin{aligned} c_k &= e^{i\phi}\mathrm{sgn}k\left[v_k a_{+,k} - u_k a_{-,k}\right] && (2.46)\\ c^\dagger_{-k} &= u_k a_{+,k} + v_k a_{-,k}. && (2.47) \end{aligned}$$

Now, if the original operators are to be related by Hermitian conjugation (and momentum inversion), this results in

$$\begin{aligned} c_k &= -e^{i\phi}\mathrm{sgn}k u_k a_{-,k} + e^{i\phi}\mathrm{sgn}k v_k a_{+,k} && (2.48)\\ c_k &= u_k a^\dagger_{+,-k} + v_k a^\dagger_{-,-k}, && (2.49) \end{aligned}$$

which my be solved by identifying

$$a^\dagger_{-,-k} = e^{i\phi}\mathrm{sgn}k a_{+,k}. \tag{2.50}$$

In the Hamiltonian this leads to

$$\begin{aligned} \mathcal{H}_{Kit} &= \frac{1}{2}\sum_{k\in BZ} E_{bulk}\left(a^\dagger_{+,k}a_{+,k} - a^\dagger_{-,k}a_{-,k}\right)\\ &= \frac{1}{2}\sum_{k\in BZ} E_{bulk}\left(a^\dagger_{+,k}a_{+,k} - a^\dagger_{-,-k}a_{-,-k}\right)\\ &= \frac{1}{2}\sum_{k\in BZ} E_{bulk}\left(a^\dagger_{+,k}a_{+,k} - a_{+,k}a^\dagger_{+,k}\right)\\ &= \sum_{k\in BZ}\underbrace{E_{bulk}}_{\equiv E_k}\left(a^\dagger_{+,k}a_{+,k}\right) + \underbrace{\sum_{k\in BZ}\frac{E_{bulk}}{2}}_{const.}, \end{aligned} \tag{2.51}$$

which demonstrates that one effectively excludes the negative energy modes.

After dropping unphysical modes, one may similarly drop the $\pm$ label and consider the general ground state

$$a_k\,|0\rangle = 0 \tag{2.52}$$

and the physical one-body excited states with

$$|\pm q\rangle = a^\dagger_{\pm k}\,|0\rangle\,, \tag{2.53}$$

and so on. The fermionic operators then read

$$c_k = u_k a^\dagger_{-k} + v_k e^{i\phi}\mathrm{sgn}k a_k. \tag{2.54}$$

To study the Josephson junction physics in the trivial regime, we consider two bulk Kitaev superconductors which we label $L$ and $R$, coupled by a tunneling Hamiltonian. They are 1D p-wave systems with superconducting phases $\phi_R$ and $\phi_L$. As we will see, only their difference is important. The Hamiltonian reads

$$\begin{aligned} \mathcal{H} &= \mathcal{H}_{Kit_R} + \mathcal{H}_{Kit_L} + \mathcal{H}_T \\ \mathcal{H}_T &= \sum_{k,l} \left[ T_{kl} c^\dagger_{L,k} c_{R,l} + T^*_{kl} c^\dagger_{R,l} c_{L,k} \right]. \end{aligned} \tag{2.55}$$

The tunneling matrix elements obey $T_{-k,-l} = T^*_{k,l}$. The interpretation of each fermion operator is evident in the tunneling context. The ground state of $H_{S_R} + H_{S_L}$ is given by

$$|0\rangle = |0_L\rangle \, |0_R\rangle \,, \tag{2.56}$$

Considering an average number $N_{L/R}$ of Cooper pairs in the L/R superconductor,$\Delta N = N_L - N_R$ characterizes the system, as the total number of Cooper pairs $N_L + N_R$ is fixed. We are interested in studying the electron tunneling at zero bias voltage.

The Josephson effect can be read from the correction to the ground state energy of the system in the presence of the tunneling Hamiltonian, as it is characterized by the transition amplitude from a state with a fixed $\Delta N$ to tunnel into another with $\Delta N + 1$. So we compute the effective energy in the presence of tunneling to second order perturbation theory

$$E_0^{(2)} = \langle 0| \, \mathcal{H}^{(2)} \, |0\rangle = \sum_{exc} \langle 0| \, \mathcal{H}_T \frac{|exc\rangle \, \langle exc|}{E - E_{exc}} \mathcal{H}_T \, |0\rangle \,. \tag{2.57}$$

Computing the variation of the energy with respect to the superconducting phase difference between the two wires (which is conjugate to the difference of particle number) we can find the Josephson current.

First we start writing $\mathcal{H}_T$ in terms of the quasi-particle Bogoliubov operators. Out of the four arising terms, two of them actually introduce no net tunneling from one superconductor to the other. In the ground state average these contribute only with a constant energy shift and no phase dependence. We neglect these, for simplicity, as they are physically unimportant for the computation of the Josephson currents.

The remaining simplified Hamiltonian reads

$$\tilde{\mathcal{H}}_T = \sum_{k,l} T_{kl} \alpha_{k,l} a_{L,-k} a_{R,l} + \sum_{k,l} T_{kl} \beta_{k,l} a^\dagger_{L,k} a^\dagger_{R,-l}, \tag{2.58}$$

where

$$\begin{aligned} \alpha_{k,l} &= e^{i\phi_R} \mathrm{sgn}l \, (u_k v_l) + e^{i\phi_L} \mathrm{sgn}k \, (v_k u_l) \\ \beta_{k,l} &= e^{-i\phi_L} \mathrm{sgn}k \, (v_k u_l) + e^{-i\phi_R} \mathrm{sgn}l \, (v_l u_k) \end{aligned}$$

Now we are ready to take the average of the second order simplified and projected tunneling Hamiltonian in the ground state. Proper counting of quasi-particle number shows that, out of the four arising contributions, only a single one is non-vanishing

$$E_0^{(2)} = -\sum_{exc} \sum_{k,l;k',l'} \frac{T^2_{kl}}{E_{exc}} \alpha_{k,l} \beta_{k',l'} \, \langle 0| \, a_{L,-k} a_{R,l} \, |exc\rangle \, \langle exc| \, a^\dagger_{L,k'} a^\dagger_{R,-l'} \, |0\rangle \tag{2.59}$$

Notice that the product of matrix elements is non-vanishing only for $l = -l'$ and $k = -k'$. The excited intermediate state contains, necessarily, two quasi-particles - one quasi-particle in each superconductor - such

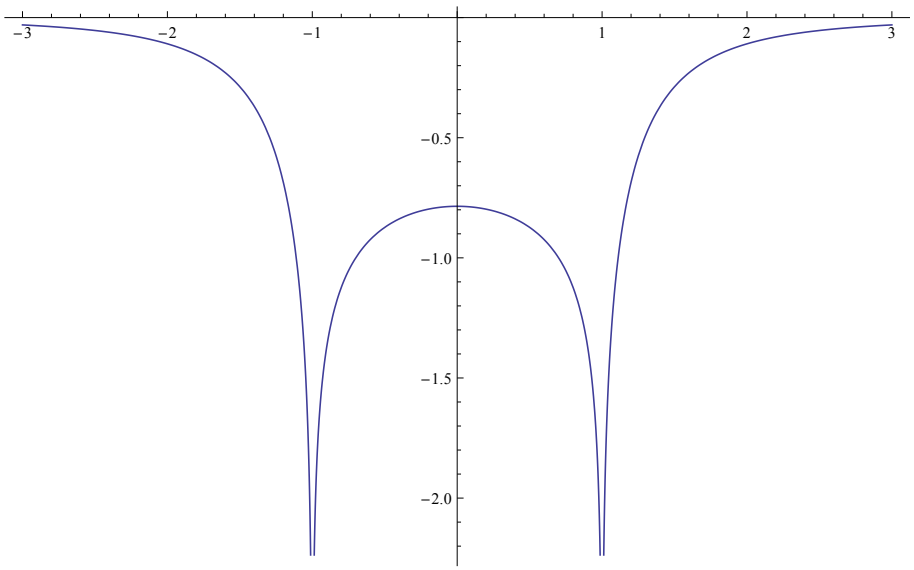


Figure 2.6: $J_0(\mu)$ in 2.64 (y axis) versus $\mu$ (x axis) for $T_{kl} = \delta_{kl}$ and $t = 1$. Notice that at $\mu = \pm 1$ the divergent behavior points the topological phase transition.

that $E_{exc} = E_p + E_q$, with $p, q$ the momenta of the states in each wire. Putting all of this together leads to

$$E_0^{(2)} = \sum_{p,q}\sum_{k,l} \frac{T_{kl}^2}{E_p + E_q} \alpha_{k,l}\beta_{-k,-l}\delta_{l,p},\delta_{-k,q} \tag{2.60}$$

$$= \sum_{k,l} \frac{T_{kl}^2}{E_l + E_{-k}} \alpha_{k,l}\beta_{-k,-l}. \tag{2.61}$$

Considering the functions $\alpha, \beta$ explicitly, setting $\Delta\phi = \phi_R - \phi_L$ and, again dropping the $\Delta\phi$ independent terms, we find

$$E^{(2)}(\phi) = J_0 \cos\Delta\phi, \tag{2.62}$$

where and

$$J_0 = -\frac{1}{2}\sum_{k,l} \mathrm{sgn}l\mathrm{sgn}k \frac{T_{kl}^2}{E_l + E_k} \sqrt{\left[1 - \left(\frac{\epsilon_k}{E_k}\right)^2\right]\left[1 - \left(\frac{\epsilon_l}{E_l}\right)^2\right]} \tag{2.63}$$

$$= -\frac{\Delta^2}{2}\sum_{k,l} \frac{T_{kl}^2}{E_l + E_k} \frac{\sin k \sin l}{E_k E_l}. \tag{2.64}$$

This is enough to demonstrate the existence of the "integer" Josephson effect. The effective Hamiltonian is $2\pi$ periodic in the superconducting phase difference between the two wires. As the superconducting phase is conjugate to the particle number, differentiating with respect to the phase leads to a current due to Cooper pairs tunneling between the two superconductors.

To further enrich the analysis, one may also study the coefficient $J_0$. This coefficient is sensitive to the chemical potential applied in the system $\mu$ (uniform through both superconductors for zero-bias voltage), and the system behaves in two very distinct ways depending on the relation $\mu/t$, namely the trivial $\mu < -t$ and topological regimes $|\mu| < t$. To compute $J_0$,we need to model $T_{kl}$. This may be tricky and would demand new microscopic calculations. Instead, let us consider a simple example, just to get a feeling of how $J_0$ may be sensitive to the topological phase transition. Any function $T_{kl}$ with well defined parity in $k$ or $l$ (or both) will give a vanishing result for $J_0$ (just make, e.g., $k \to -k$ to see that.) An interesting non-vanishing situation is such that $T_{kl} \propto \delta_{kl}$.This is a simple forward scattering between the two superconductors.

Figure 2.6 shows the result for $J_0$ in this approximation. It shows a divergence in this coefficient as the superconducting gap closes. In this case, $J_0$ is seen to be sensitive to the topological regime. For very large and

very small chemical potentials, the superconducting phase is not well established and the coefficient vanishes accordingly.

### 2.4.2 Fractional Josephson effect

It turns out that the previous analysis is not sufficient in the case of a Kitaev chain in the topological regime. The reason for that is that the presence of Majorana zero-modes at the edges allows novel single-electron tunneling effects at the weak-link between the two chains. To see this explicitly, let us return to the real space Hamiltonians and tune the Kitaev chains parameters deep into the topological regime, $\mu = 0$, $t = \Delta$. We have

$$\mathcal{H} = \sum_{a=L,R} \mathcal{H}_a + \mathcal{H}_\Gamma, \tag{2.65}$$

$$\mathcal{H}_a = -\frac{t}{2} \sum_{x=1}^{N-1} \left( c_{ax}^\dagger c_{ax+1} + e^{i\phi_a} c_{ax} c_{ax+1} + H.c. \right), \tag{2.66}$$

$$\mathcal{H}_\Gamma = -\Gamma \left( c_{LN}^\dagger c_{R1} + H.c. \right) \tag{2.67}$$

with $\mathcal{H}_\Gamma$ describing the electronic tunneling across the barrier. Let us study these in the Majorana fermion basis and show that first order perturbation theory changes in energy are finite now.

Rewriting $\mathcal{H}_0$ in terms of the Majorana operators $c_x = \frac{e^{-i\phi/2}}{2} \left( \gamma_x + i\gamma_x^{'} \right)$, we have

$$\mathcal{H} = \sum_{a=L,R} \mathcal{H}_a + \mathcal{H}_\Gamma, \tag{2.68}$$

$$\mathcal{H}_a = -\frac{it}{2} \sum_{x=1}^{N-1} \left( \gamma_{ax} \gamma_{ax+1}^{'} \right) \tag{2.69}$$

$$\begin{aligned} \mathcal{H}_\Gamma = & -\frac{i\Gamma}{2} \left( \sin\left( \frac{\phi_L - \phi_R}{2} \right) \left[ \gamma_{LN} \gamma_{R1} + \gamma_{LN}^{'} \gamma_{R1}^{'} \right] \right) \\ & -\frac{i\Gamma}{2} \cos\left( \frac{\phi_L - \phi_R}{2} \right) \left[ \gamma_{LN} \gamma_{R1}^{'} - \gamma_{LN}^{'} \gamma_{R1} \right] \end{aligned} \tag{2.70}$$

Now, for $x = 1, ..., N-1$, we apply the same trick as before and redefine the complex fermion operators as $d_x = \frac{1}{2} \left( \gamma_{x+1}^{'} + i\gamma_x \right)$ and the Hamiltonian becomes

$$\mathcal{H}_a = t \sum_{x=1}^{N-1} \left( d_{ax}^\dagger d_{ax} - \frac{1}{2} \right) \tag{2.71}$$

with the ground state of the two wires

$$d_{ax} \left| G.S. \right\rangle = 0, \ x = 1, ..., N-1, \ a = L, R \tag{2.72}$$

with total energy $-t\,(N-1)$. The main point is that this ground state is actually degenerate, due to the absence of the Majorana operators $\gamma_{a1}^{'}$ and $\gamma_{aN}$ in $\mathcal{H}_a$. As we have four Majorana fermions, there is a fourfold degeneracy of the ground state. At the weak-link between the L and R chains, we define the complex, quasi-non-local fermion

$$b = \frac{1}{2} \left( \gamma_{R1}^{'} + i\gamma_{LN} \right). \tag{2.73}$$

The effects of the superconducting phase difference across the weak-link will affect directly the occupancy of this $b$ mode. Fermion parity conservation dictates that the occupation of this $b$ state is intertwined with the occupation of the, more non-local, state $b^{'} = \frac{1}{2} \left( \gamma_{RN} + i\gamma_{L1}^{'} \right)$. Given a total fermionic parity, occupation/unoccupation of $b$ states will fix the occupation/unoccupation of the $b^{'}$ states, such that only a *doubly degenerate* sub-manifold of ground states can be accessed; the good quantum number characterizing these two degenerate ground states is the fermionic parity of, say, the $b$ states. We then write the two ground states as $|G.S.; \mu\rangle$ with

$\mu = 0, 1$ obeying

$$\begin{aligned} b\,|G.S.;0\rangle &= 0 \\ b^\dagger\,|G.S.;1\rangle &= 0 \\ |G.S.;1\rangle &= b^\dagger\,|G.S.;0\rangle\,. \end{aligned} \tag{2.74}$$

In sum, we repeat. These $b$ states are relevant due to the proximity of the end tips of the two SC at the junction. There are also other, even more non-local, $b^{'}$ states made out of $\gamma^{'}_{L1}$ and $\gamma_{RN}$. These are further separated for long chains, and their physics will not be important locally at the weak-link, where tunneling gives rise to the Josephson effect. Their existence is however important as it is necessary for tuning between the different parity states in the "weak-link fermion" $b$. This is so because total parity is conserved and the parity of the two non-local states must be exchanged if we try to flip the parity of one of them, say the weak-link mode $b$, which is exactly what will happen as a function of the superconducting phase difference, as we will see now.

Due to the absence of the end points Majorana fermions, the bulk Hamiltonian has no contribution from the $b$ fermions. As for the tunneling Hamiltonian, it becomes

$$\begin{aligned} H_\Gamma &= -i\frac{\Gamma}{2}\left(\sin\left(\frac{\phi_L-\phi_R}{2}\right)\left[i\left(b^\dagger-b\right)i\left(d^\dagger_{R1}-d_{R1}\right)+\left(d^\dagger_{LN-1}+d_{LN-1}\right)\left(b^\dagger+b\right)\right]\right) \\ &\quad -i\frac{\Gamma}{2}\left(\cos\left(\frac{\phi_L-\phi_R}{2}\right)\left[i\left(2b^\dagger b-1\right)-i\left(d^\dagger_{LN-1}+d_{LN-1}\right)\left(d^\dagger_{R1}-d_{R1}\right)\right]\right). \end{aligned} \tag{2.75}$$

Now we compute the change in the ground state energy in perturbation theory again. Since the operators $d_1$ and $d_{N-1}$ annihilate the vacuum, it is easy to take matrix elements in this basis. Taking matrix elements with $\{|G.S.;0\rangle, |G.S.;1\rangle\}$, we start with first order (degenerate) perturbation theory. As parity is conserved, the corresponding subspaces decouple,

$$\Delta E^{(1)} = -\frac{\Gamma}{2}\cos\left(\frac{\phi_L-\phi_R}{2}\right)\begin{pmatrix} 1 & 0 \\ 0 & -1 \end{pmatrix}. \tag{2.76}$$

So, after projection, the Hamiltonian is simply

$$\mathcal{H}_{eff} = \Gamma\cos\left(\frac{\Delta\phi}{2}\right)(\hat{n}_1 - 1/2)\,, \tag{2.77}$$

where $\hat{n}_1 = b^\dagger b$.

In summary (and with the benefit of the hindsight), one may start from the original operators and define the edge complex fermions

$$\begin{aligned} c_{LN} &= \frac{e^{-i\phi_L/2}}{2}\left(\gamma_1 + i\gamma_1^{'}\right) \\ c_{R1} &= \frac{e^{-i\phi_R/2}}{2}\left(\gamma_2^{'} + i\gamma_2\right). \end{aligned} \tag{2.78}$$

Low energy physics at the weak-link implies that the projection onto the zero energy subspace is equivalent to simply writing

$$c_{LN} \to \frac{1}{2}e^{-i\phi_L/2}\gamma_1,\ c_{R1} \to \frac{1}{2}e^{-i\phi_R/2}\gamma_2. \tag{2.79}$$

The tunneling Hamiltonian then gives the previous result automatically

$$\begin{aligned} \mathcal{H}_{eff} &= -\frac{\Gamma}{2}\cos\left(\frac{\Delta\phi}{2}\right)i\gamma_1\gamma_2 \\ &= -\Gamma\cos\left(\frac{\Delta\phi}{2}\right)(\hat{n}_1 - 1/2)\,. \end{aligned} \tag{2.80}$$

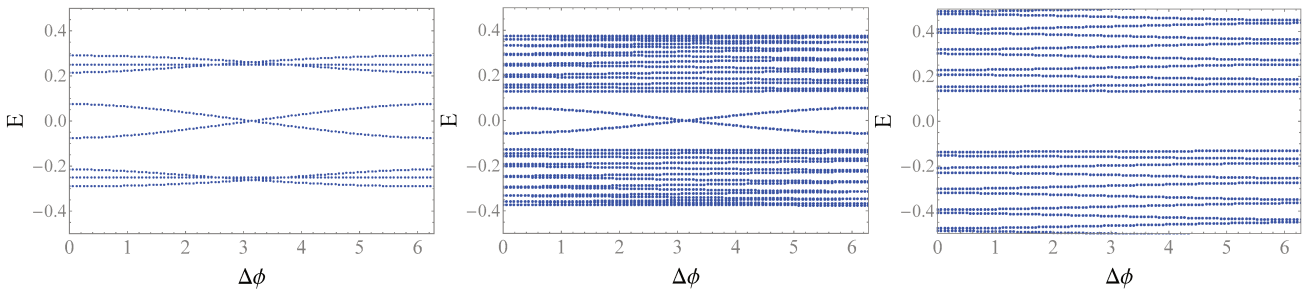


Figure 2.7: Diagonalization of two Kitaev chains with tunneling term. We fix $t = \Delta = 1$ and $\Gamma = 0.3$ and fix the different topological regimes by (left) $\mu = 0$ (center) $\mu = 0.5$ (right) $\mu = 1.5$. As long as we are inside the topological regime (left and center), the lowest Majorana modes are preserved and protected. They display a $2\pi$ periodic spectrum and two opposite parity branches. The trivial regime (right) hybridizes the Majorana modes with the other bulk states and has no protected edge modes.

If $n_1$ is conserved, starting with a system with initial value $\hat{n}_1 = n_1^i$ and varying the phase across the junction yields the Majorana-mediated current,

$$I_e = \frac{2e}{\hbar}\frac{d\langle \mathcal{H}_{eff}\rangle}{d\Delta\phi} = \frac{e\Gamma}{2\hbar}\sin\left(\frac{\Delta\phi}{2}\right)\left(2n_1^i - 1\right). \tag{2.81}$$

This corresponds to a "half" Cooper pair tunneling with $4\pi$ periodicity in $\Delta\phi$. This type of current-phase relationship defines what is known as the "fractional Josephson effect". Cooper-pair tunneling dominates the Josephson current in regular junctions because the bulk gap suppresses single electron tunneling. The existence of edge zero-modes coupled by $\mathcal{H}_\Gamma$ overcomes this suppression.

The origin of the $4\pi$ periodicity is more subtle and related to fermion parity conservation. It stems from the fact that, despite the Hamiltonian of the weak-link being $2\pi$ periodic in $\phi_{R,L}$, the states are not. To see this, consider $\Delta\phi = 0$ and $n_1^i = 1$ in (2.80), which implies a ground state with energy $E_i = -\Gamma/2$. If $\hat{n}_1$ is conserved, after evolution of $\Delta\phi$ by $2\pi$, we end up in a state with $E_f = +\Gamma/2$ and an extra finite energy quasi-particle at the junction. Total fermion parity conservation dictates that the system may decay back to the ground state only if fermions can transfer between the edge Majoranas of each given wire, which is (exponentially) forbidden by hypothesis due to the bulk wire gap. Advancing $\Delta\phi$ by $2\pi$ again restores the original state and uncovers the $4\pi$ periodicity. This phenomenon is also known as a "fermionic parity pump", as the evolution of the superconducting phase allows one to transfer the parity quantum number of the outer fermions into the weak-link ones and vice-versa; this phenomenon is a superconducting realization of the Thouless charge pump (1D insulators)[46, 47] and of the "Laughlin's argument"[48] of edge modes pumps between the edges of 2D quantum Hall systems upon the insertion of a magnetic flux in a cylinder Hall strip geometry.

These points can be easily seen by diagonalizing the Kitaev Josephson junction Hamiltonian explicitly in real space numerically. Fig. 2.7 shows the results for the spectrum as function of the phase difference different values of the chemical potential, inside and outside the topological regime. Focusing in the deep topological limit of $\mu = 0$, one clearly sees a set of in-gap modes. We omit a flat band (in $\Delta\phi$) of zero-modes corresponding to the outer edge states. The energies are clearly $2\pi$ periodic in the superconducting phase difference across the junction. The energy bands however have a crossing which is protected by parity conservation, each branch of the crossing bands has a different parity $(-1)^{b^\dagger b}$. Evolution of the phase difference by $2\pi$ does not return the Hilbert space to its original profile. A full $4\pi$ evolution is necessary for that, exchanging the two states of opposite parity twice.

Despite the success of finding a potentially interesting scenario for realizing physical effects of Majorana fermions, some subtleties arise:

1. In a real system, the single electron current $I_e$ must compete with a regular $2\pi$ periodic $I_{2e}$ current contribution. For $\Gamma \sim 1K$, we have an order of magnitude estimate $I_e \sim e\Gamma/(2\hbar) \sim 10\text{nA}$, setting the current resolution needed to see the anomalous single electron tunneling current;

2. Finite size effects will inevitably lead to coupling of the outer Majorana fermions to the weak-link ones, with characteristic energy $\delta E \propto e^{-L/\xi}$ ($L$, size of topological regions, $\xi$ topological phase coherence length). Although exponentially suppressed, this spoils conservation of $\hat{n}_1$ and restores $2\pi$ periodicity. In order to avoid this, to see the fermion parity pump, $\Delta\phi$ should cycle on a time scale short compared to $\hbar\Gamma/\delta E^2$ but long on the scale of the inverse bulk gap;

3. Inelastic processes involving stray quasi-particles (due to imperfect initialization of thermal excitations or, simply, disorder, for example), may also switch $\hat{n}_1$; this is also a relaxion process which restores $2\pi$ periodicity, if $\Delta\phi$ cycles on scales longer than the typical switching time. This is known as quasi-particle poisoning.[31]

In principle, one can proceed with a second order perturbation theory calculation in the topological regime also. Although we will omit the results, the physics is simple. It generates another, regular, Josephson junction contribution to the energy. This, as coming from second order perturbation theory, is sub-dominant to the fractional Josephson effect for a simple Kitaev wire junction. A two fluid model for the physics in such junctions seems to be reasonable from the phenomenological point of view and we will employ this idea in the next Section in order to study how the unconventional physics in this system could be measured experimentally.

## 2.5 Macroscopic quantum tunneling and Majorana fermions

The superconducting state is a macroscopic quantum system. In particular, superconducting quantum interference devices (SQUIDs) provide a standard device to study the macroscopic properties of the superconducting state. It consists of a loop closed by a Josephson junction (JJ henceforth). Magnetic fluxes in superconducting loops are quantized in units of the so called superconducting flux quantum $\Phi_0 = hc/2e \equiv \pi$. The weak-link relaxes this quantization condition and allows for tunneling of flux tubes from outside of the SQUID to its inside across the junction. This tunneling is accompanied by the appearance of a supercurrent along the device, which is a macroscopic coherent behavior of the electronic Cooper pair condensate. The superconducting phase difference across the junction, in this context, is controlled by an external flux bias through the SQUID. All of the previous results are maintained, except that the superconducting phase should now be re-interpreted as a magnetic flux through the broken-loop[49, 50, 51, 52, 36, 53].

As justified previously, a p-wave wire Josephson junction can be described by a fractional Josephson effect energy term accompanied by a, sub-dominant, regular Josephson contribution. Realizing such p-wave wires is, however highly non-trivial. The main experimental proposal for the realization of the fractional Josephson effect in SQUIDs consists of building a regular s-wave SQUID with a semi-conductor wire traversing the weak-link [38]. If the semi-conducting wire is subject to strong spin-orbit effects, an effective p-wave pairing develops, induced by the bulk s-wave SQUID superconductivity. As the effective Kitaev wire sits on top of a larger regular SQUID, the JJ should be described by a two fluid model with a regular Josephson effect dominating the fractional Majorana one. Here we provide a phenomenological approach for the physics of macroscopic quantum tunneling - described below - in such hybrid devices, in which regular and fractional Josephson effects compete[37].

We start with a brief review of regular SQUID and macroscopic quantum tunneling phenomenology[36]. The physics of a regular SQUID ring is very successfully modeled by an RLC circuit with a JJ circuit element as in Fig.2.8. This is known as the resistor-capacitor shunted junction (RCSJ) model. This model describes the interplay of the capacitive (kinetic), resistive (from leads and normal current components going around the loop), (self-)inductive and JJ current contributions to the flux going through the ring. Current conservation through the circuit and Faraday's law result in the equation of motion

$$C\ddot{\Phi} + \frac{\dot{\Phi}}{R} + I_C \sin\Delta\phi\left(\Phi\right) = \frac{\Phi_X - \Phi}{L} + \zeta\left(t\right), \tag{2.82}$$

where $C$ is the capacitance of the junction, $R$ is its resistance in the normal state, $I_C$ is the junction critical

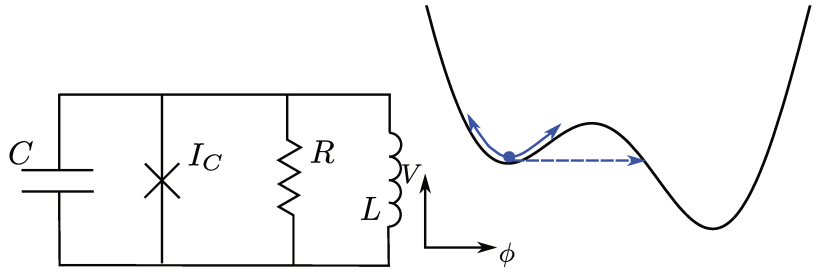


Figure 2.8: (left) Lumped circuit representation of an rf-SQUID (no-topological component here). The circuit consists of a capacitive component connected in parallel with a resistor, an inductor and a Josephson junction. (right) Potential energy (2.85) for a particle with position "$\phi$", actually the magnetic flux, according to the SQUID equations of motion.

current, and $\zeta(t)$ is a fluctuating current represented by a delta correlated thermal noise. We have also considered the possibility of adding an externally controlled flux $\Phi_X$ through the ring. The phase difference $\Delta\phi(\Phi)$ across the junction is a function of the magnetic flux in the closed geometry. The function may be fixed by the usual flux quantization rule which for a broken superconducting loop reads,

$$\Phi + \frac{\Phi_0}{2\pi}\Delta\phi = n\Phi_0, \tag{2.83}$$

as long as the SC is thicker than the London penetration depth.

In this way, the equation of motion reduces to

$$C\ddot{\Phi} + \frac{1}{R}\dot{\Phi} + U'(\Phi) = \zeta(t), \tag{2.84}$$

which is a Langevin equation of motion for a classical dissipative particle (with coordinate $\Phi$) in a conservative potential $U(\Phi)$ given by

$$U(\Phi) = U_0\left[\frac{(2\pi(\Phi - \Phi_X))^2}{2} - \beta_L\cos(2\pi\Phi)\right], \tag{2.85}$$

where $U_0 = \frac{\phi_0^2}{4\pi^2 L}$, $\beta_L = \frac{2\pi L i_0}{\phi_0}$ and with $\Phi$ (here and henceforth) measured in units of $\Phi_0 = h/2e$.

As this is a first approach, we neglect dissipation (and noise) and focus on the conservative part of the system. In this limit, a semi-classical analysis is enough. The potential is depicted in Fig.2.8 for some arbitrary values of $\beta_L$ and $\Phi_X$. As long as the Josephson energy (i.e. $\beta_L$) is comparable to the inductive energy, ripples develop in the parabolic potential, giving rise to local metastable minima.

For high enough temperatures, the flux may be thermally excited and will slip to lower minima. Each minimum defines an oscillation frequency

$$\omega_0 = \sqrt{\frac{1}{C\Phi_0^2}\frac{\partial^2 U}{\partial\Phi^2}|_{\phi=\phi_{min}}} \sim \sqrt{\frac{1}{LC}}, \tag{2.86}$$

from which a characteristic temperature may be defined as

$$T_0 \equiv \frac{\hbar\omega_0}{k_B} = 0.76\times 10^{-11} s\sqrt{\frac{1}{LC}}K. \tag{2.87}$$

Parameters like $C \sim 10^{-12}F$, $L \sim 10^{-10}H$ lead to $T_0 \sim 1K$ (these parameters also lock $I_C$ to $\sim 10^{-5}A$). If the system is set at temperatures lower than $T_0$, it may resolve the discrete energy levels within the metastable wells. In this case, even if temperatures are much lower than the barrier height, the magnetic flux may still escape to lower energy wells, now due to quantum tunneling. This is the macroscopic quantum tunneling phenomenon.

Again, our system of interest will consist of a straight wire - made of a material with strong spin-orbit coupling - on top of a regular SQUID. The wire becomes an effective Kitaev chain and we have a pair of

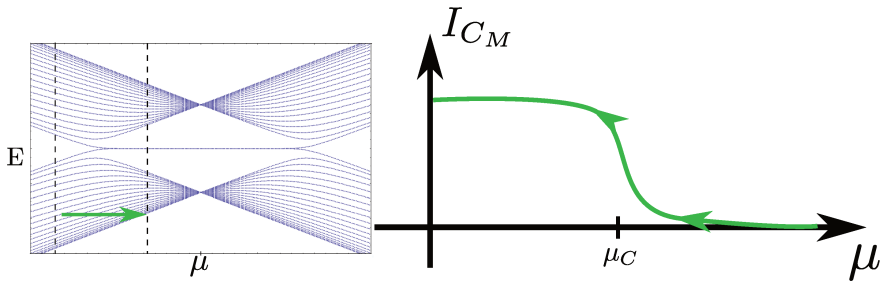


Figure 2.9: Schematic description of the behavior of the critical current ratio $\eta$. (top) Schematic energy spectrum of an open Kitaev chain at unit hopping and superconducting pairing. For low chemical potential the topological superconducting phase develops, as indicated by the midgap flat-band; (bottom) Topological contribution to the critical current as function of the chemical potential;

coupled topological and trivial junctions. To model this system, we focus on the conserved fermionic parity regime. The wire in a topological phase allows for the introduction of a topological JJ term in addition to the usual Josephson current. The wire is assumed to be much thinner than the superconducting ring, so that the capacitance and inductance of the device are predominantly defined by the corresponding values from the parent superconductor and do not depend on the chemical potential of the wire in any important way. We also assume the linear dimensions of the parent superconductor to be longer than the penetration depth in such a way that the SQUID flux "quantization" condition is not changed. Finite-size effects of the ring are not taken into account.

We now introduce the two fluid model. The full potential energy thus has $2\pi$ periodic and $4\pi$ periodic contributions which compete for making $\Phi$ (close to) an arbitrary or even-only integer. We consider then a new JJ element to the RCSJ model. The conditions of thin wire guarantee that the phase across the topological JJ is also controlled by the phase across the parent superconducting junction. The new potential energy of the problem becomes

$$U(\phi) = U_0 \left[ \frac{(2\pi(\Phi - \Phi_X))^2}{2} - \beta_L (\cos 2\pi\Phi + \eta(\mu) \cos \pi\Phi) \right]. \quad (2.88)$$

Here, $\eta(\mu)$ is a parameter given by the ratio $I_{C_M}/I_C$ between the critical currents of the parent s-wave junction and the topological one. Its magnitude is roughly controlled by the ratio between the magnitudes of the parent superconductor gap and the induced p-wave gap in the wire. It will depend on the strength of the proximity effect and on the parent superconductor 2D density of states. For high chemical potentials, the 1D wire is in a trivial superconducting phase, whereas for low chemical potentials it enters the topological regime.

A subtlety concerns the sign of $\eta$. It is determined by which parity sector the system is in, and, as we assumed the fermionic parity to be conserved, is fixed to a given value along a complete tunneling process. Taking all that in consideration, we give $\eta(\mu)$ a phenomenological treatment. Assuming that, through gating, the chemical potential may be tuned, $\eta$ changes from zero to a saturated value as the chemical potential moves from the trivial to the topological regime. This general behavior is depicted in (2.9). As the chemical potential goes from smaller to larger values, the Majorana edge modes at the link penetrate the bulk of the wire and, when in the trivial phase, hybridize and gap-out, annihilating the topological contribution. In the trivial regime the wire may give a small contribution to the $2\pi$ Josephson energy. We neglect these effects assuming that whatever $2\pi$ periodic contribution there may be, it is already included in $\beta_L$. This potential also assumes a short junction. In the long junction limit, more bound states develop at the junction and the physics becomes more complicated [31, 54, 38].

Since the wire is much thinner than the s-wave superconductor and since the p-wave pairing induced in the wire depends on the proximity coupling, it is reasonable to assume that the saturated value of $\eta$ is not very large and we will focus our quantitative discussions on this case. On the other hand, by adding to the the JJ of the parent superconductor a secondary loop , we may actually control the value of $\beta_L$ [55], and as such, of $\eta$,

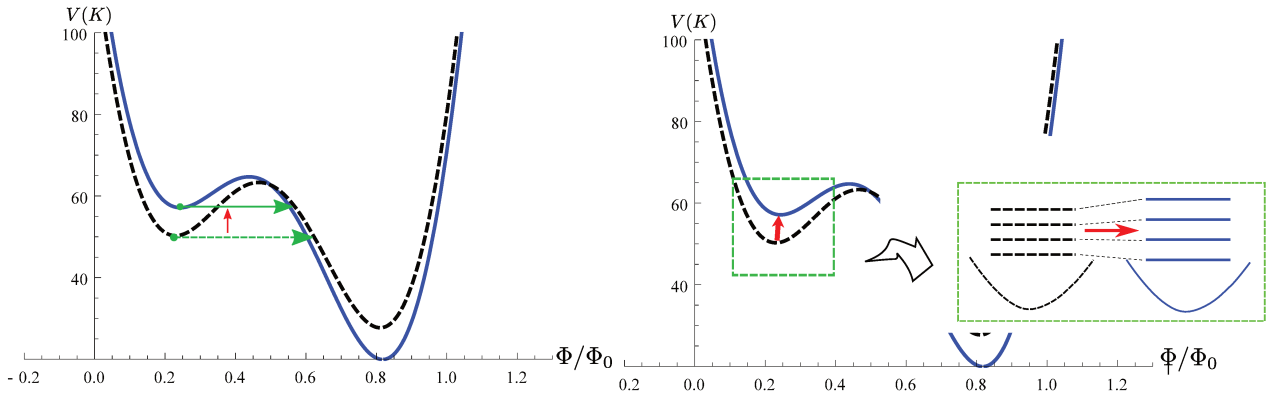


Figure 2.10: Qualitative signatures of the topological phase in the potential energy for the flux through the hybrid SQUID. Dashed black curves represent the trivial limit when $\eta = 0$, and blue curves a generic saturated (negative) value of $\eta$ in the topological regime. (left) Modification of the tunneling barrier induces a change in tunneling rates. (right) Frequency shifts due to changes in curvature lead to shifts in the discrete energy levels;

thus allowing for some of control over this parameter.

At this point we are ready to discuss qualitatively the consequences of this proposal. We look mainly at two possible signatures, namely, changes in the tunneling rates and shifts in the harmonic oscillator levels. The former might be probed in actual tunneling experiments while the latter may be studied in spectroscopy or coherent tunneling experiments[55]. Figure 2.10 illustrates the two phenomena and summarize the main ideas.

One sees how the competition between arbitrary integer and even integer flux holds. The $|\Phi \approx 0\rangle$ well becomes shallower while the $|\Phi \approx 1\rangle$ well is deepened in comparison with the trivial situation (this actually depends on the sign of $\eta$, which will be assumed negative). We may exploit many different schemes to study the consequences of the topological regime. Fig.2.11 gives some possibilities. In all cases we take a physical value of $\beta_L = 1.9$ and shift $\Phi_X$ around the symmetric value for the non-topological regime $\Phi_X = 0.5$. For clearly describing the different situations we take a value of $\eta = -0.15$. In Figs.2.11a and 2.11b we see that both enhanced and suppressed tunneling rates in the well may be achieved, just by tilting the potential changing $\Phi_X/\Phi_0$ from 0.47 to 0.53. These plots also make clear that the suppression or enhancement are actually not symmetric around $\Phi_X = 0.5$.

The last two cases of 2.11c and 2.11d present very interesting possible applications. In Fig.2.11c, we see that starting with a symmetric potential, in a Schrödinger's cat state, we may transform the qubit into a simple classical bit or tune the quantum state into a preferred value of the flux, just as a function of the chemical potential. In Fig.2.11d we see how to create an adiabatic pump from the unit flux to zero flux and back by lowering the chemical potential into the topological regime and raising it back to the trivial situation.

Now we discuss quantitatively the consequences of these ideas. In order to keep ourselves on safe physical grounds, we use real parameters and units taken from [55]. Namely, we have $C = 1.04 \times 10^{-13}F$, $L = 2.4 \times 10^{-10}H$ and keep in mind that experiments are done at temperatures of the order of $10^{-2}K$. With all these in mind, we may calculate the frequency and tunneling rate shifts as functions of $\eta$.

For the frequency we locate numerically the minima of the potential as a function of $\eta$ and evaluate equation (2.86). In Fig.2.12 we plot the corresponding results, for both positive and negative values of $\eta$ and for $\beta_L = 1.6$ (in red) and $\beta_L = 1.7$ (in blue). The results show that if we have a ratio of about 5% between the Majorana critical current and the parent SQUID critical current, we may achieve a shift of ~7GHz. Whereas it is not a very strong signature, this may be resolved with the current precision achievable in experiments.We also see that for different $\beta_L$ the curves are not simply displaced parallel to each other. It can be verified that for smaller $\beta_L$ the slope is always larger than for greater $\beta_L$.

For the tunneling rate the calculation is slightly more involved. In the non-dissipative limit it may be simply performed within the Callan and Coleman's instanton calculation scheme [56]. In summary, it resumes to a saddle point approximation in the path integral approach, considering paths in an inverted potential starting

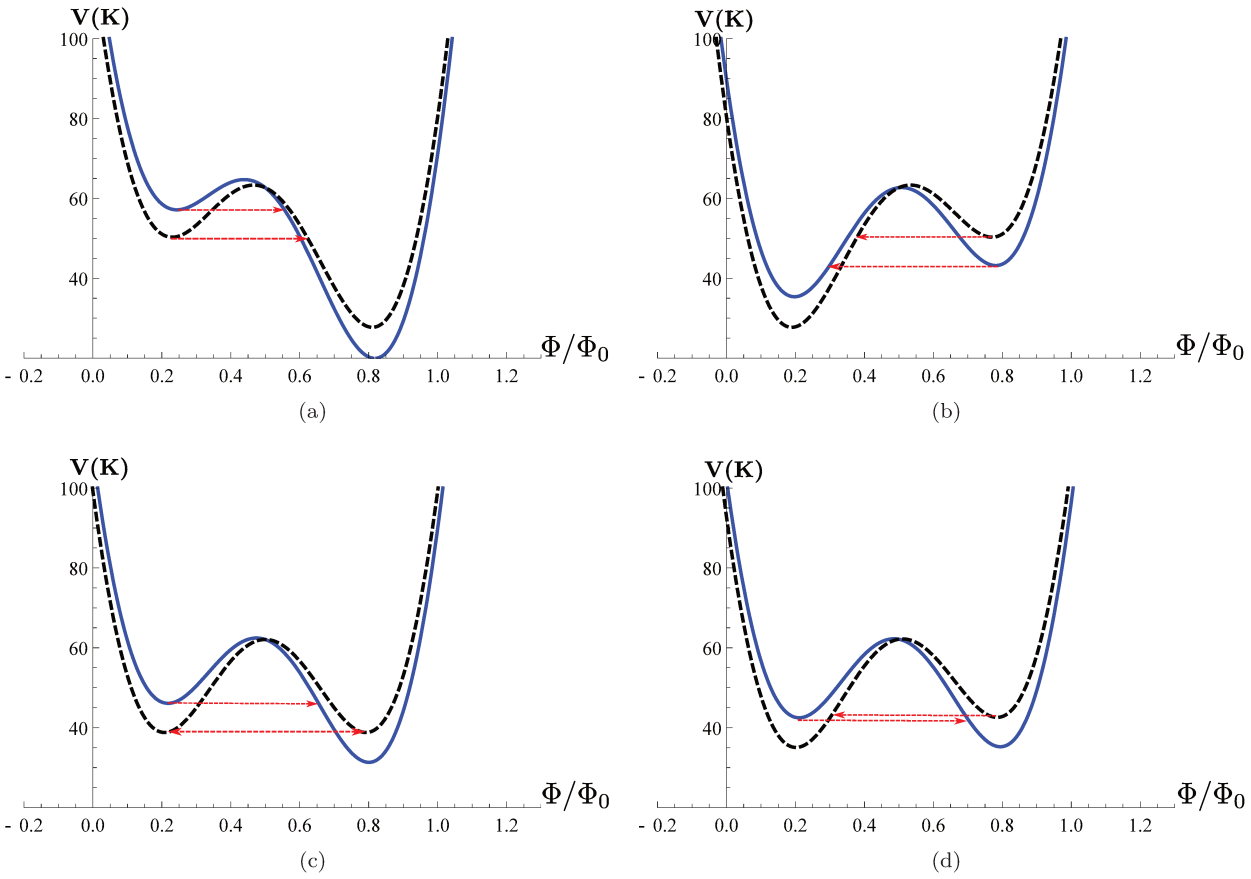


Figure 2.11: Different flux potentials for representative values of the external flux $\Phi_X/\Phi_0$. Black dashed curves represent $\eta = 0$, blue solid curves represent $\eta = -0.15$. $\beta_L = 1.9$ in all cases. (a - top left) ($\Phi_X/\Phi_0 = 0.53$) and (b - top right) ($\Phi_X/\Phi_0 = 0.47$) show the differences of tuning the external flux around the symmetric (for the trivial regime) point $\Phi_X/\Phi_0 = 0.5$. In the case of figure (a) the tunneling rate is enhanced while in (b) it is suppressed by the topological contribution. In case (c - bottom left) $\Phi_X = 0.5$ and we see how a "cat state" may be destroyed by lowering the chemical potential into the topological regime. (d - bottom right) shows how to build a pump between the flux states by tuning the chemical potential into and out of the topological regime.

at the equilibrium point of the metastable potential and ending at a return point . The result of the tunneling rate $\Gamma$ reduces to

$$\Gamma = C\sqrt{\frac{B}{2\pi\hbar}}e^{-B/\hbar}\left[1+\mathcal{O}\left(\hbar\right)\right], \tag{2.89}$$

where

$$B = \int_{-\infty}^{\infty} dt\left[\frac{C}{2}\dot{\Phi}_{Cl}^2 + U\left(\Phi_{Cl}\right)\right] \tag{2.90}$$

$$= 2\int_0^{\Phi_w} d\Phi\sqrt{2CU\left(\Phi\right)} \tag{2.91}$$

and

$$C = \sqrt{\frac{\det\left[-\partial_t^2+\omega_0^2\right]}{\det{}'\left[-\partial_t^2+\omega_0^2+U"\left(\Phi\right)\right]}}. \tag{2.92}$$

Here $\Phi_{Cl}$ is the classical "bounce" solution in the saddle point approximation and we used the equations of motion and energy conservation to write $B$ independently from the exact solution $\Phi_{Cl}$. The prime in the denominator determinant in $K$ means that zero eigenvalues should be omitted. Also, $\Phi_w$ is the width of the barrier the particle has to tunnel through and $\omega_0$ is again the small oscillations frequency around the metastable minimum. Instead of evaluating all the factors from the complicated potential (2.88), we follow

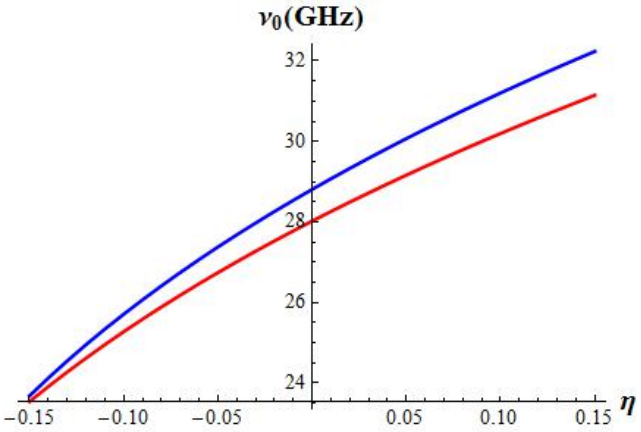


Figure 2.12: Quantitative change in the oscillator frequencies $\nu_0 = \omega_0/2\pi$ as a function of the saturation value of $\eta$ in the topological regime. We use real physical parameters for the SQUID as described in [55] and $\Phi_X/\Phi_0 = 0.52$ for concreteness. Comparing $\beta_L = 1.7$ (blue) and $\beta_L = 1.6$ (red) shows that smaller $\beta_L$ gives more expressive shifts in the frequency.

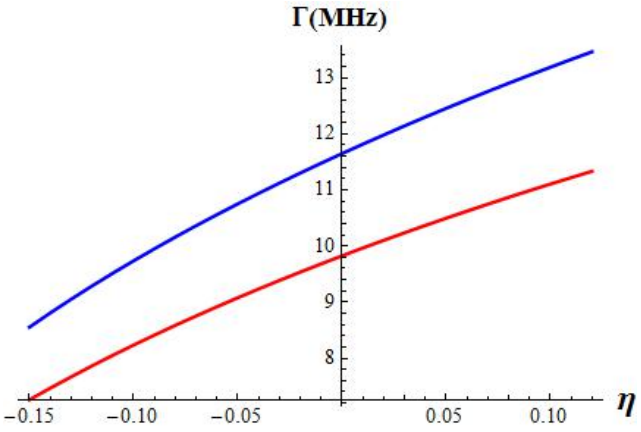


Figure 2.13: Quantitative change in the tunneling rates as a function of the maximum value of $\eta$. We use real physical parameters for the SQUID as described in [55] and $\Phi_X/\Phi_0 = 0.52$. Comparison between $\beta_L = 1.7$ (blue) and $\beta_L = 1.6$ (red). Although less clear visually, smaller $\beta_L$ is again favored given bigger changes in tunneling rates

standard procedure and adopt a "quadratic plus cubic" approximation for the potential,

$$U_{eff}\left(\Phi\right) = \frac{1}{2}C\omega_0^2\left[\Phi^2 - \frac{\Phi^3}{\Phi_w}\right]. \tag{2.93}$$

This is a very reasonable approximation [57] and allows us to write the tunneling rate in terms of dimensionless integrals as

$$B \;=\; 2C\omega_0\Phi_w^2\int_0^1 dz\sqrt{[z^2 - z^3]}. \tag{2.94}$$

The $C$ factor is dimensionless and in the non-dissipative limit that we are considering is given by $\sqrt{60} \sim 7.75$ [57, 58].

Considering these, we may calculate numerically the minima and maxima from the original potential, from which we can also extract $\Phi_w$. The results are shown in Fig.2.13. Again, for different values of $\beta_L$, the slopes of the curves change and smaller values of $\beta_L$ produce more expressive changes in tunneling rates. In particular, again for $\eta = 0.05$ (5% ratio between critical currents), the tunneling rate presents variations of $\sim$23 mHz.

Figures (2.12) and (2.13) are our main results. Although the topological effects are small, they definitely exist, and these ideas work as proof of concept. The changes in the SQUID potential well parameters and tunneling

rates are inside an experimentally accessible range, for the parameters we considered here, and one may hope that these effects can be actually observed. One positive characteristic of these ideas is that the measurements made are thermodynamic; they are equilibrium measurements and do not involve actual transport physics. This means that, following this proposal, one avoids the issue of justifying zero-bias peaks and relating them, unequivocally, to Majorana zero-modes. One negative point, which remains, is the necessity of fermionic parity conservation. Avoiding quasi-particle poisoning is nearly impossible, due to disorder effects, and the fractional Josephson effect is still very fragile. Comments regarding how the quasi-particle poisoning affects these results will be omitted, to keep the discussion short, but we note in passing that, depending on the time scales for the tunneling process (and feeding the SQUID back into the higher metastable well), such breaking of local parity conservation might actually enhance the shifts of tunneling rates and energy quantization in the topological regime (but the notion of topological regime will then be lost.)

## 2.6 Conclusions

With the discussions in this Chapter, we hope to have presented all the basics necessary to understand the relations between topology and superconductivity we will discuss throughout this work. The main concepts to be remembered are the notions of protecting symmetries, topological invariants, the bulk-boundary correspondence and topological phase transitions between gapped systems. Also the Majorana, neutral fermion, nature of gapless modes in superconducting scenarios must be remembered with due attention, as well as the phenomenon of topological fractional Josephson junctions. We have also exposed our own points of view on simple physical scenarios to verify such physics. Armed with these ideas and concepts, we now move on to higher dimensions and the main theme of this Thesis, vortices in superconducting topological matter.

# Chapter 3

# Vortex modes in superconducting doped topological insulators

## 3.1 Introduction

We have settled our knowledge of the effects of topology in superconductivity. We move now to one of our main problems, that of superconductivity in doped topological insulators. As discussed, an important signature of topological phases is the appearance of novel, low-energy, robust, edge states; one such state is the so-called Majorana bound state at the edges of topological superconductors [59]. As ubiquitous signatures, the detection of these neutral fermions has been the main trend in the characterization of particle-hole symmetric topological phases. Although evidences of Majorana fermion physics have been identified in tunneling [60] and scanning tunneling microscopy (STM) measurements[61], the interpretation of their signatures is controversial in many cases, as the imprints from the topological regime are often mixed with signals from disorder and extra undesired quasiparticles, as discussed.

While the aforementioned gapless edge states act as a signature of topologically non-trivial regimes, one can shift perspectives and worry about the signatures of the *transition* from a topologically trivial to a topological phase; these present themselves in the *bulk* by the closing and re-opening of the excitation energy gap[62, 63]. In many of the proposed systems which can be tuned through such a topological phase transition (TPT), however, the excitation gap is very small compared to experimental achievable resolutions and cannot be probed directly.

Here, we provide a discussion of these points in the context of the chemical potential induced topological phase transition in vortices of superconducting doped topological insulators. We show that quantum fluctuations in the vortex position can *shift the spectral weight* in the density of states of a given system before and after a TPT to further separated energies and, as a result, magnify the change of the spectrum resulting from this process. In this particular situation, we also demonstrate how the effects of Magnus forces on vortex dynamics[64] display a novel signature in the spectral change at this TPT, exposing the pumping of vortex modes responsible for the phase transition, as described below. Our results are general, however, and can be extended to other types of topological phase transitions. To demonstrate this, we present a way to map the 3D situation into a 1D setting in terms of wire networks which may be used to probe for the topological phase transitions of actual Kitaev chains, Su-Schrieffer-Heeger chains and other unidimensional topological chains.

To understand how quantum fluctuations affect vortices in superconducting doped topological insulators, we start by shortly discussing how vortex quantum dynamics affect electronic vortex modes in regular superconductors [65, 66]. Within the BCS theory of superconductivity, an stationary vortex affects the spectrum of the superconductor by generating in-gap modes localized around and along the vortex core [67]. The energy of these discrete bound states, known as Caroli-de Gennes-Matricon (CdG) modes, is given by $\epsilon_l = \frac{\Delta^2}{E_F}\left(l + \frac{1}{2}\right)$ where $\Delta$ is the size of the bulk superconducting gap, $E_F$ is the Fermi energy of the normal phase and $l$ is an integer. The signatures of these in-gap states have been experimentally observed by STM measurements[68, 69].

In practice, however, even though the spatial resolution of STM is well within the size of the vortex modes[70], given the small size of their so-called mini-gap, $\delta \equiv \frac{\Delta^2}{E_F}$, the energy of each single mode is hard to be resolved and usually multiple modes are observed together [68].

It is well known that the pinning of vortices is necessary for the stability of type-II superconductors. The discussion above would be the final status of the problem for pinned vortices, were they absolutely static. Although a pinned vortex has a fixed position at the sample, even at the lowest temperatures, their quantum zero point motion cannot be ignored. Interestingly, it was shown that such quantum fluctuations affect the quasiparticle spectrum, moving part of the spectral weights of the in-gap vortex modes into novel "satellite peaks" at frequencies associated with vortex fluctuations[65, 66, 71]. We then contend that exploiting this ubiquitous quantum mechanical phenomenon to probe for TPTs is a promising idea, leading to novel signatures of these transitions.

To test this approach, superconducting doped topological insulators arise as the most natural test ground. The discovery of superconductivity in doped topological insulators triggered several studies, particularly because of the suggestions that these materials might realize topological superconductivity [22, 23, 24, 21, 72]. Theoretical studies of superconductivity in the surface states of topological insulators started even before the experimental realization of bulk superconductivity in the doped case, when it was shown that, theoretically, if superconductivity is induced in their helical surface states, vortex modes will include a zero-energy Majorana bound state [73]. In the context of bulk superconducting doped topological insulators, it was later shown that the Majorana mode at the ends of a vortex line persist up to a critical value of doping in these systems as well [25, 27, 26]. At this critical doping level, the two Majorana modes at the ends of the vortex hybridize and become gapped. The presence or absence of Majorana modes at the end of the vortex line contrast two topologically distinct phases. In fact, the vortex in doped superconducting topological insulator becomes effectively equivalent to a Kitaev chain.

From the bulk-boundary correspondence, a signature of this TPT also shows up in the spectrum of the states extended along the vortex. The original mechanism lies in the CdG modes. The important property of these states is that they are gapped by the small energy scale of the mentioned mini-gap. This energy protects the surface Majorana zero modes, confining them to the surface of the sample. Because of strong spin-orbit coupling and the resulting band inversion of the insulator [74], the Fermi surface here has non-trivial topological properties which show up as a non-zero Berry connection. The CdG modes then inherit this Berry phase as a modification to their energy spectrum - which also separates in two sets due to the existence of two degenerate Fermi surfaces - which becomes $E_l^{\pm} = \frac{\Delta^2}{E_F}\left(l \mp \frac{1}{2} \pm \frac{\Phi_b(\mu)}{2\pi}\right)$. Here $\Phi_b$ is the mentioned Berry phase around the curve on the Fermi surface (this it is dependent on the chemical potential $\mu$) defined by setting the wave-vector along the vortex line equal to zero. In this case, when $\Phi_b = \pi$, $E_0^{\pm} = 0$ and the zero energy surface Majorana modes at the ends of the vortex can merge through the gapless $l = 0$ mode which is now extended along the vortex.

We will thus study in this Chapter how the problem of quantum vortex motion affects the CdG modes in doped topological superconductors and its influence on the associated topological phase transition. We proceed, firstly, by describing 3D time-reversal invariant topological insulators. Following that, we will describe the superconducting doped case and, subsequently, the vortex bound states physics and their corresponding topological phase transition. We then discuss the signatures of this transition in energy space, and discuss how the vortex zero-point motion may affect it. We show also how the physics in 3D can be transported to a, perhaps simpler, 1D scenario.

## 3.2 topological insulators in 3D

As our system of interest consists of Copper doped Bismuth Selenide, we start by describing the minimal model for such a 3D topological insulator. This way we may get more acquainted with the minimal Dirac fermion physics all so ubiquitous to the physics of topological matter, as well as with the notion of the $\mathbb{Z}_2$ topological

invariant.

Bismuth Selenide comprises the easiest-to-deal-with topological insulator [20, 33]. Its electronic properties can be described solely by focusing on a single Dirac point (a point in k-space which is well approximated by a Dirac Hamiltonian) at the $\Gamma = (0,0,0)$ point of the Brillouin zone, as we will show. A minimal tight binding model to describe its Brillouin zone is given by the following Bloch Hamiltonian (we start with no doping $\mu = 0$)

$$H_{\mathbf{k}} = \tau_x \boldsymbol{s} \cdot \mathbf{d}_{\mathbf{k}} + m_{\mathbf{k}} \tau_z \tag{3.1}$$

$$d^i_{\mathbf{k}} = 2t \sin k_i \tag{3.2}$$

$$m_{\mathbf{k}} = M + m_0 \sum_i \cos k_i. \tag{3.3}$$

This corresponds to a cubic lattice model where $\vec{\tau}$ and $\vec{s}$ Pauli matrices represent the orbital and spin degrees of freedom. Time reversal symmetry acts as $\Theta = i s_y K$ and, at the Bloch Hamiltonian level,

$$s_y H^*_{-\mathbf{k}} s_y = H_{\mathbf{k}}. \tag{3.4}$$

Of fundamental interest are the so-called time-reversal-invariant-momenta, or TRIM. In the cubic lattice, there are eight of them, namely $\Gamma_i = (\pi,0,0), ..., (\pi,\pi,0), ..., (\pi,\pi,\pi)$ and $(0,0,0)$. Also, it is very important that this Hamiltonian, as well as the $Bi_2Se_3$ composite itself, has an inversion symmetry. This is manifest as

$$H_{-\mathbf{k}} = \tau_z H_{\mathbf{k}} \tau_z. \tag{3.5}$$

The electronic spectrum corresponding to this Hamiltonian contains a pair of doubly degenerate bands and reads

$$E_{\pm} = \pm \sqrt{|\mathbf{d}_{\mathbf{k}}|^2 + m^2_{\mathbf{k}}}. \tag{3.6}$$

Whether or not this system is gapped and describes an insulator depends on the interplay between the parameters $M$ and $m_0$.

The interplay between these quantities also fix the topological regime of the system. The topological invariant is related to the number of different ways in which one may map the Brillouin zone (a 3-torus $T^3$ as each $k_i : -\pi \to \pi$) to the space of time-reversal invariant and inversion symmetric Hamiltonians which preserve the gap separating positive and negative one-particle energies. In mathematical language, we identify $T^3$ as the *base* space, while the Bloch Hamiltonian $H_{\mathbf{k}}$ (or rather its eigenvectors) fix the *classifying* space. For our specific case, the base space can be simplified in the classification scheme to a sphere $S^3$, if desired, as the "strong" topological invariants which classify the spherical base space also classify the toroidal base spaces - although there may exist further topological structure in $T^3$ which does not exist in $S^3$; these are the so called "weak" topological invariants, which we will overlook as unimportant to our present situation.

Our classifying space consists of a Hamiltonian which satisfies the time-reversal constrain (3.4) and belongs to the so-called class AII in the Altland-Zirnbauer scheme [14]. It also satisfies the inversion symmetry condition in (3.5). The corresponding "strong" topological invariant is very simple in this system. It is a $\mathbb{Z}_2$ (there are only two distinct sets of Hamiltonians in the classifying space) number and may be written as

$$(-1)^{\nu_0} = \prod_i \delta_i \tag{3.7}$$

$$\delta_i = \prod_{m=1}^{N} \xi_{2m}(\Gamma_i), \tag{3.8}$$

where we have $2N$ occupied bands ($N = 1$ for our particular case) and the product picks only a single element of each Kramers degenerate pair $\xi_{2m} = \xi_{2m-1}$. Then, $\xi_{2m}(\Gamma_i)$ is the parity eigenvalue of the $2mth$ occupied energy band at $\Gamma_i$. This is known as a "strong" topological invariant because it only depends on time-reversal symmetry. Other invariants may be defined which corresponds to subsets of multiplications of parity eigenvalues according

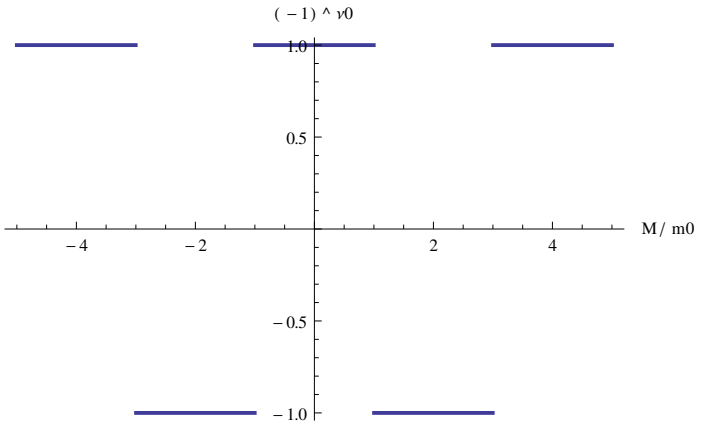


Figure 3.1: Topological regimes for inversion and time-reversal symmetric topological insulator in 3D. This shows a strong topological behavior ($\nu_0 = 1$) at $1 < |M/m_0| < 3$.

to each of the three directions in 3D. These are known as "weak" invariants as they depend on corresponding mirror symmetries - under the effects of spatial disorder the topology is broken with respect to this case, even if time-reversal is left symmetric. We will not worry about these cases.

Notice that the inversion operator for us reads $P = \tau_z$. At the TRIM, the only matrix in the Hamiltonian which is even under such inversion symmetry corresponds to the one multiplying $m_{\mathbf{k}}$, which is $P$ itself. We thus know that in the present case

$$\delta_i = -\mathrm{sgn}\left(m_{\mathbf{k}=\mathbf{\Gamma}_i}\right). \tag{3.9}$$

If we order the TRIM as before, $\Gamma_i = (\pi,0,0), ..., (\pi,\pi,0), ..., (\pi,\pi,\pi)$ and $(0,0,0)$, we have

$$\begin{aligned}
\delta_1 = \delta_2 = \delta_3 &= -\mathrm{sgn}\left(m_{\mathbf{k}=(\pi,0,0)}\right) = -\mathrm{sgn}\left(M + m_0\right) && (3.10)\\
\delta_4 = \delta_5 = \delta_6 &= -\mathrm{sgn}\left(m_{\mathbf{k}=(\pi,\pi,0)}\right) = -\mathrm{sgn}\left(M - m_0\right) && (3.11)\\
\delta_7 &= -\mathrm{sgn}\left(m_{\mathbf{k}=(\pi,\pi,\pi)}\right) = -\mathrm{sgn}\left(M - 3m_0\right) && (3.12)\\
\delta_8 &= -\mathrm{sgn}\left(m_{\mathbf{k}=(0,0,0)}\right) = -\mathrm{sgn}\left(M + 3m_0\right). && (3.13)
\end{aligned}$$

Thus,

$$\begin{aligned}
(-1)^{\nu_0} &= \mathrm{sgn}\left(M + m_0\right)\mathrm{sgn}\left(M - m_0\right)\mathrm{sgn}\left(M - 3m_0\right)\mathrm{sgn}\left(M + 3m_0\right)\\
&= \mathrm{sgn}\left(\frac{M}{m_0} + 1\right)\mathrm{sgn}\left(\frac{M}{m_0} - 1\right)\mathrm{sgn}\left(\frac{M}{m_0} - 3\right)\mathrm{sgn}\left(\frac{M}{m_0} + 3\right). && (3.14)
\end{aligned}$$

We plot this as function of $M/m_0$ in Fig. 3.1.

From the simplified structure of the topological invariant, one may come up with an easy rule to detect the strong topological regimes. As we saw, we depend on the product of the sign of $m_{\mathbf{k}}$ at the different points in the Brillouin zone. Time-reversal symmetry implies that only half of the TRIM are important to compute the topological invariant, say the $\Gamma = (0,0,0)$ point and the $(\pi,0,0), (\pi,\pi,0)$ and $(\pi,\pi,\pi)$ points. This implies that a single band inversion starting at the origin of the Brillouin zone and ending at any of its corners is enough to fix the topological invariant. Indeed, this result is actually quite general, the strong topological regime demands a band inversion when moving through the Brillouin zone from its origin along each of the base directions towards its surfaces, showing that the contributions from the corners must be the same.

The above consideration implies that an isotropic analysis is enough to fix the topological invariant, which leads us to a continuum theory close to the $\Gamma = (0,0,0)$ point. In particular, the mass term $m_{\mathbf{k}}$ becomes

$$\begin{aligned} m_{\mathbf{k}} &\approx M + m_0\left(3 - k^2/2\right) \\ &= (M + 3m_0) - m_0 k^2/2. \end{aligned} \tag{3.15}$$

This shows that if

$$M + 3m_0 < 0 \Rightarrow M/m_0 < -3, \tag{3.16}$$

$m_{\mathbf{k}}$ does not change sign as $k \equiv |\mathbf{k}| \to \infty$ while it has a single sign change if $|M/m_0| > 3$.

We may then write a continuum model for a 3D topological insulator with inversion symmetry,

$$H_{TI} = -iv_D \tau_x \boldsymbol{s}.\boldsymbol{\nabla} + \tau_z\left(m + \epsilon\nabla^2\right). \tag{3.17}$$

In this case, studying band inversion reveals the two distinct topological behaviors as

$$\begin{aligned} m\epsilon > 0 &\text{ strong topological insulator} \\ m\epsilon < 0 &\text{ trivial insulator.} \end{aligned}$$

In the absence of the $\epsilon$ term this system displays an emergent Lorentz symmetry and corresponds to Dirac fermions in 3D.

One last, but fundamental, point,which we have not yet discussed is: how does these different topological classes manifest themselves physically?

We again are supported by the bulk-boundary correspondence. The non-trivial topological regime is signaled by gapless surface states which cannot be gapped if the symmetries (in this specific case, time-reversal symmetry and U(1) electromagnetic charge conservation) are preserved. The existence of such surface states can be verified by noticing that the different topological regimes are determined by the sign of $m$. So solving for the Hamiltonian in the presence of a domain-wall in $m$ (with $\epsilon = 0$ for simplicity, this term is unimportant to compute differences in topology; it is only relevant to compute the absolute topological regime of a phase) with $m(z) > 0$ for $z > 0$ and $m(z) < 0$ for $z < 0$, then states exponentially localized (as $e^{-\int dz m(z)/v_D}$) develop at the domain-wall and one gets a projected surface Hamiltonian

$$H_{surf} = -iv_D\left(\tilde{s}_x\partial_x + \tilde{s}_y\partial_y\right), \tag{3.18}$$

where $\tilde{s}$ are Pauli matrices in the projected basis (and still describe the states spin content.) This means that at the interface of a topologically non-trivial insulator and a trivial one (such as the vacuum itself), there develops a single set of gapless relativistic fermions, also known as a Weyl fermion. Notice that the chirality (spin-momentum locking) is fixed at a single value at a given surface, the opposite material surface would develop Weyl modes with opposite chirality.

## 3.3 Doped superconducting topological insulators

We have seen that the simplest model of a topological insulator in 3D demands time-reversal and inversion symmetry and is described by a quasi-Dirac Hamiltonian. This implies, as discussed, a pair of doubly degenerate bands. Shifting the chemical potential away from the insulating gap, for example by doping, allows one to develop a finite Fermi surface and and turn this system into a metal. Now with a finite density of states at the Fermi level, such system's ground state is subject to instabilities of several sorts.

For some time now it has been known that superconducting instabilities indeed develop when doping Bismuth Selenide with Copper [22, 23, 24]. The composite $Cu_xBi_2Se_3$ can become superconducting at optimal doping fraction $x = 0.12$. Table 3.1 summarizes the main superconducting parameters for this system.

Take particular notice of the Landau factor of approximately 53, much larger than $1/\sqrt{2}$, showing a strong

| | |
|---|---|
| $T_c$ | 3.8K |
| $\Delta$ | 0.6meV |
| $\xi$ | 2000Å |
| $\kappa = \lambda/\xi$ | 53 |

Table 3.1: Physical parameters relevant to Copper doped Bismuth selenide at optimal doping. We have, from top to bottom, the critical temperature, superconducting gap, coherence length and Landau's factor (showing strong type II behavior)

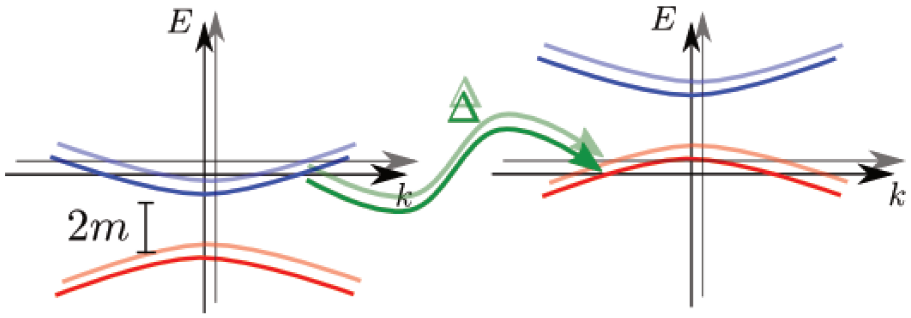


Figure 3.2: Doped topological insulator. Two degenerate (blue) bands are shifted in energy by the chemical potential. Once they cross the Fermi level, a superconducting instability develops. In a Bogoliubov-de Gennes representation, one may think of doubling the number of bands in the problem while inverting the artificial new set. The superconducting pairing couples the upper bands from the original spectrum to the lower bands of the doubled one. At weak pairing and in centrosymmetric systems, the pairing is not expected to mix the different bands.

type II behavior. The pairing symmetry is known to be of s-wave type. The Fermi energy at optimal doping leads to a Fermi momentum $k_F \sim 10^{-1}\text{Å}^{-1}$. Together with a coherence length of the order of 2000Å, this implies also that $\xi k_F \gg 1$, also setting this material in the weak-pairing limit.

The details above strongly suggest a simple mean field model for the superconducting phase of the doped topological insulator. Figure 3.2 schematizes the band couplings by the s-wave pairing. For centro-symmetric systems (with inversion symmetry, nodeless superconducting gap, non-mixed singlet and triplet Cooper pairing) the pairing is not expected to connect the orbitals of different parity. The simplest model for this phase then reads [25]

$$\begin{aligned} H_{SCTI} = & \int d^3x \psi (H_{TI} - \mu)\psi \\ & + \Delta \psi_{A\uparrow}\psi_{A\downarrow} + \Delta \psi_{B\uparrow}\psi_{B\downarrow} + H.c., \end{aligned} \tag{3.19}$$

where $\psi = (\psi_{A\uparrow}, \psi_{A\downarrow}, \psi_{B\uparrow}, \psi_{B\downarrow})$, $\uparrow\downarrow$ represent up and down z-component of spins and $A, B$ the two orbital degrees of freedom. For convenience of mathematical manipulation, this Hamiltonian may be written in the Bogoliubov-de Gennes (BdG) form as

$$\mathcal{H} = \frac{1}{2}\int d^3x \Psi^\dagger H_{BdG} \Psi \tag{3.20}$$

where

$$H_{BdG} = \begin{bmatrix} H_{TI} - \mu & \Delta(\mathbf{r}) \\ \Delta^\dagger(\mathbf{r}) & -H_{TI} + \mu \end{bmatrix}. \tag{3.21}$$

The Nambu spinor reads, in this basis, $\Psi = \left(\psi, is_y\psi^\dagger\right)^T$. One may introduce a Dirac-like notation for this also,

$$H^0_{BdG} = v_D \mathbf{\Gamma}\cdot\mathbf{P} - \mu\Sigma + \Gamma_0\left(m - \epsilon P^2\right) - \mathbf{\Lambda}\cdot\mathbf{\Delta}(\mathbf{r}), \tag{3.22}$$

where $\mathbf{P} = -i\nabla$. The matrices obey $\{\Gamma_\mu, \Gamma_\nu\} = 2\delta_{\mu\nu}$, $\{\Lambda_a, \Lambda_b\} = 2\delta_{ab}$ (Dirac algebra) and $[\Gamma_\mu, \Sigma] = \{\Lambda_a, \Sigma\} =$

0, where $\mu, \nu = 0, ..., 3$ and $a, b = 1, 2$. Notice $\Sigma$ commutes with the kinetic Hamiltonian and is not considered a "mass" term (mass terms enhance the gap and must obey the Dirac algebra.) In our basis, a choice for the representation follows

$$\mathbf{\Gamma} = \rho_z \tau_x \boldsymbol{s}, \qquad \mathbf{\Lambda} = \boldsymbol{\rho} \tau_0 s_0 \tag{3.23}$$

$$\Gamma_0 = \rho_z \tau_z s_0, \qquad \Sigma = \rho_z \tau_0 s_0, \tag{3.24}$$

where we allowed for both real and imaginary terms in the superconducting pairing. From the anti-commuting structure of the matrices, one sees that at $\mathbf{k} = 0$ the spectrum is given by

$$E^{\pm\pm}_{\mathbf{k}=0} = \pm\sqrt{|\Delta|^2 + (m \pm \mu)^2}, \tag{3.25}$$

with each sign being doubly degenerate. This way, in the absence of superconducting pairing, the chemical potential can lead to a vanishing insulating gap as long as $\mu = m$ reaching the bottom of the conduction band. If the system develops a superconducting instability it then remains gapped by the pairing strength.

This system is subject to the two anti-unitary time-reversal and particle-hole operators

$$\Theta = i\sigma_y K \tag{3.26}$$

$$\Xi = \rho_y \sigma_y K, \tag{3.27}$$

with time-reversal only respected if the superconducting order parameter phase vanishes and there are no external magnetic fields.

## 3.4 Doped superconducting topological insulators: vortex bound states

Vortices are regions in the superconducting condensate where supercurrents develop around (quantized) magnetic flux tubes [75]. Such systems act, from the point of view of the fermionic underlying system, as a string-like potential. The superconducting pairing vanishes at the vortex core (the length scale for this being fixed by the coherence length $\xi$.) As such, the gapped bulk states tend to become gapless - less energetic - as they reach closer and closer to the defect. As these are states with lower energy, the vortex is able to bind electrons to itself.

Fermionic states bound to superconducting vortices are known as Caroli-de Gennes-Matricon (CdG) modes, in the honor of their discoverers [67]. From the bulk of the system, they are inevitably gapped by a small quantity called the "mini-gap", $\delta_1 = \Delta_0^2/E_F$, where $\Delta_0$ is the modulus of the superconducting gap in the bulk and $E_F$ is the Fermi energy.

These bound states have a very unusual realization in the context of doped topological insulators. As we have seen in previous sections, the surface of topological insulators is metallic. This means that, even if the chemical potential is below the insulating gap, a topological insulator is always subject to superconducting instabilities. If the chemical potential is below the gap, only the surface is metallic and may superconduct, whereas for larger values of doping, the full bulk may also be a superconductor.

Superconducting surfaces of topological insulators consist of a very unusual electronic system. That is because, as a (semi-)metal, it consists of a single 2D Weyl cone (odd numbers of Fermi points are usually forbidden in condensed matter systems as the lattice demands that they appear in pairs, a feature known as "Fermion doubling problem" or Nielsen-Ninomiya theorem.) As discussed before, such surface modes are gapless, unless one breaks the time-reversal or electromagnetic U(1) protecting symmetries. Indeed, a superconducting instability breaks the latter, and may gap the fermions in such a surface. More interestingly, the CdG modes

spectrum at the surface may develop a zero-energy mode, which due to the Nambu particle-hole symmetry of these systems is a Majorana fermion.

The remarkable physics in this problem appears when one realizes that, for large enough chemical potential, the topological nature of the insulating bulk must become irrelevant, as the parity of the number of filled bands changes and the $\mathbb{Z}_2$ invariant looses meaning and vanishes. In this case, the Majorana modes bound to vortices in superconducting surfaces must also be unstable. As function of the chemical potential, a mechanism must develop such that the Majorana zero-energy states can annihilate (always in pairs); furthermore this mechanism must come from a bulk-condition, as the Majorana partners belong to opposite surfaces of the doped topological insulator.

In what follows we will describe these points in detail, first deriving the Majorana surface bound states in 2D, then explaining the concept of a vortex phase transition and describing the mechanism through which it occurs in terms of the 3D bulk CdG modes.

### 3.4.1 Majorana modes bound to superconducting topological insulator surfaces

Computing the wavefunctions and energies of such states is a very simple job [73]. One starts with the surface Hamiltonian with a Bogoliubov-de Gennes grading

$$h_{BdG} = -iv_F\tilde{\rho}_z\left(\tilde{s}_x\partial_x + \tilde{s}_y\partial_y\right) - \tilde{\rho}_z\mu + \mathbf{\Delta}\cdot\tilde{\mathbf{\Lambda}}, \tag{3.28}$$

where at the surface we have

$$\tilde{\mathbf{\Lambda}} = \left(\tilde{\rho}_x, \tilde{\rho}_y\right), \tag{3.29}$$

(we use tildes whenever talking about surface projected quantities). We use the basis of operators $\Psi^T = \left(\psi_\uparrow, \psi_\downarrow, \left(\psi_\uparrow^\dagger, \psi_\downarrow\right) i\sigma_y\right)$. This corresponds to a single superconducting Weyl fermion in 2D (superconducting Weyl fermions will, again, be a subject of interest in Chapter 3, then in 3D.)

When the pairing is spatially homogeneous and the system is infinite, the spectrum reads

$$E_{\mathbf{k}}^{\pm} = \pm\sqrt{\left(v_F\left|k\right| - \mu\right)^2 + \left|\Delta\right|^2}. \tag{3.30}$$

This means that the surface modes are gapped by the superconducting pairing, as it breaks the U(1) protecting symmetry. We then allow for a winding in the superconducting pairing phase, $\mathbf{\Delta} = \Delta_0\left(\cos\theta, \sin\theta\right)$. In this case,

$$\mathbf{\Delta}\cdot\tilde{\mathbf{\Lambda}} = \Delta_0\tilde{\Lambda}_1 e^{i\tilde{\rho}_z\theta}. \tag{3.31}$$

To unwind the angular dependence in the Hamiltonian, one writes

$$\psi\left(r,\theta,z\right) = e^{i\left(l - \frac{\tilde{\rho}_z + \tilde{s}_z}{2}\right)\theta}\phi\left(r\right).$$

Here, $l$ is an integer, to satisfy periodic boundary conditions and we will focus at the $\mu = 0$ limit, for concreteness (we discuss the finite $\mu$ scenario below). The Schrödinger equation reduces to

$$\begin{aligned}&\left[-iv_F\tilde{\rho}_z\left[\tilde{s}_x\partial_r + i\tilde{s}_y\frac{l - \left(\tilde{\rho}_z + \tilde{s}_z\right)/2}{r}\right] + \Delta_0\tilde{\rho}_x\right]\phi_n \\ &= E_{ln}\phi_n.\end{aligned} \tag{3.32}$$

The lowest energies exist for $l = 0$. A zero-mode $E_{0,n} = 0$ solution exists

$$\psi_0(r,\theta) = e^{-i\pi/4}\frac{e^{-\int_0^r dr'\frac{\Delta_0}{v_F}}}{\sqrt{\mathcal{N}}}e^{-i\left(\frac{\tilde{\rho}_z+\tilde{s}_z}{2}\right)\theta}\begin{pmatrix}0\\ i\\ 1\\ 0\end{pmatrix} \tag{3.33}$$

$$= e^{-i\pi/4}\frac{e^{-\int_0^r dr'\frac{\Delta_0}{v_F}}}{\sqrt{\mathcal{N}}}\begin{pmatrix}0\\ i\\ 1\\ 0\end{pmatrix}, \tag{3.34}$$

where $\mathcal{N}$ is a normalization factor and the phase $e^{-i\pi/4}$ is introduced as a simple gauge convenience.

Notice that the particle-hole operator again reads $\Xi = \tilde{\rho}_y\tilde{s}_y K$ (where $K$ is complex conjugation), and implies

$$\Xi\psi_0 = \psi_0. \tag{3.35}$$

The corresponding second quantized operator implies

$$\Psi(\mathbf{x}) = \sum_n \psi_n(x)\gamma_n$$
$$\Rightarrow \gamma_n = \int d^2x\psi_n(x)^\dagger\Psi(\mathbf{x}). \tag{3.36}$$

Substituting $\Psi$ in the equation above,

$$\gamma_0 = 2\pi e^{-i\pi/4}\int rdr\frac{e^{-\int_0^r dr'\frac{|\Delta|}{v_F}}}{\sqrt{\mathcal{N}}}\left[\psi_\downarrow + i\psi_\downarrow^\dagger\right] \tag{3.37}$$

with fixed $l = 0$ for the angular momentum quantum number; this obeys $\gamma_0^\dagger = \gamma_0$.

This shows, as promised, that surfaces of topological insulators, when superconducting, may bind Majorana fermions in vortices. Indeed, adding the chemical potential still leaves a zero-energy Majorana state, as can be solved analytically in terms of Bessel functions for some specific radial structures in the pairing function. This happens because for Majorana fermions to disappear, they must hybridize with other zero-modes. Partner zero-modes exist only on the other side of the topological insulator bulk, at the opposite surface. This means that local changes in the surface chemical potential cannot destabilize the Majorana states. It turns out that bulk changes in the chemical potential can.

### 3.4.2 Vortex (topological) phase transition

The concept of a vortex phase transition is known for a while now [25]. As discussed before, changes in the bulk system's chemical potential change may fix the binding of Majorana surface states or not. The surface zero modes must be able to tunnel through the bulk of the system as the chemical potential rises through the zero-mode binding phase transition.

The hybridization of the Majorana states at opposite surfaces is deeply connected to the physics of the CdG modes throughout the vortex. The CdG modes are extended states and are gapped by a mini-gap $\delta \sim \Delta_0^2/E_F$. The Majorana modes are exponentially localized at the surfaces and it is, in fact, the CdG mini-gap that controls the localization length of the surface states. If one can show that the CdG energy spectrum depends on the bulk doping level and, for some critical value of the latter, has a vanishing energy state, this means that Majorana surface states can dive deep into the bulk of the material, connecting to their partners at the other surface through the vortex.

This is the mechanism of the "vortex topological phase transition", and implies that the vortex in the

superconducting phase of a doped topological insulator effectively behaves as a 1D Kitaev linear p-wave system. This mechanism has been demonstrated previously both analytically, and numerically in a lattice model [25, 26, 27]. Here we develop a novel numerical model in the continuum approximation, and provide an explicit demonstration that the vortex in this system contains a channel of states which behave as if they were a Kitaev chain.

**Caroli de Gennes states in vortices of superconducting doped topological insulators** The starting point for this derivation is equation (3.22). We start with a procedure similar to as we did for the 2D surface of the topological insulator. We focus on writing $\mathbf{\Delta}(\mathbf{r}) = \Delta_0(r)(\cos\theta, \sin\theta)$ and choose an specific radial profile $\Delta_0(r) = \Delta_0 \tanh(r/\xi)$ profile, to be concrete.

The vortex runs along the $z$ direction and translation invariance allows us to consider the $k_z$ momentum; with the understanding that only $k_z = 0, \pi$ are topologically relevant, we start taking $k_z = 0$ since we are looking only for the low energy CdG modes [25]. The $z$ momentum will be reintroduced perturbatively later.We choose a cylindrical geometry.

The Hamiltonian commutes with the generalized angular momentum operator $\bar{L}_z = -i\partial_\theta - \frac{S_z+\Sigma}{2}$, where $\Gamma_x\Gamma_y = i\rho_0\tau_0 s_z \equiv iS_z$. This allows writing the solution spinors as

$$\chi_{l,n}(\mathbf{r}) = \frac{1}{\sqrt{2\pi}} e^{-i\left(l-\frac{S_z+\Sigma}{2}\right)\theta} \phi_{l,n}(r), \tag{3.38}$$

where $l$ is an integer representing the standard angular momentum and $n$ labels the many possible energies for a given $l$. At $k_z = 0$, the Hamiltonian obeys a further symmetry given by $\mathcal{M} = \rho_0\tau_z s_z$. Noticing that $\{\Xi, \mathcal{M}\} = 0$ and naturally $\{\Xi, H_{BdG}\} = 0$, we see that the eigenvalues of $\mathcal{M}$ also label particle and hole partners. This allows one to separate $\phi_{l,n}(r)$ in four-spinors $\phi^{\pm}_{l,n}(r)$, obeying corresponding Schrodinger's equations with projected Hamiltonians $H^{\pm}$[25],

$$H^{\pm}\phi^{\pm}_{l,n} = E^{\pm}_{l,n}\phi^{\pm}_{l,n}. \tag{3.39}$$

We focus on $\phi^{+}_{l,n}$, noticing that $\phi^{-}_{l,n} = \Xi\phi^{+}_{-l,n}$ with $E^{-}_{l,n} = -E^{+}_{-l,n}$. The $4\times 4$ reduced radial Hamiltonian reads

$$\begin{aligned} H^{+}_{\perp} &= \rho_z\nu_y\left[-i\partial_r + i\nu_z\frac{1}{r}\left(l - \frac{\rho_z+\nu_z}{2}\right)\right] - \mu\rho_z - \Delta_0(r)\rho_x \\ &\quad + \rho_z\nu_z\left[m + \epsilon\left(\frac{1}{r}\partial_r r\partial_r - \frac{1}{r^2}\left(l - \frac{\rho_z+\nu_z}{2}\right)^2\right)\right]. \end{aligned} \tag{3.40}$$

Here $\nu$ Pauli-matrices represent a spin-orbital coupled space. Noticing that

$$a_l = \left(\partial_r + \frac{l}{r}\right) \tag{3.41}$$

$$a^{\dagger}_l = -\left(\partial_r - \frac{l-1}{r}\right) \tag{3.42}$$

act as operators which lower and raise the level of Bessel functions (and $a^{\dagger}_l a_l$ gives the Bessel differential operator itself), it is easy to find a proper basis to expand the states. If $\Delta_0 = 0$, we recover a pair of topological insulator Hamiltonians with spectra given by $E^{\pm\pm}_k = \pm\mu \pm \sqrt{k^2 + m_k^2}$, with $m_k = m - \epsilon k^2$ and $k$ a "radial linear momentum" quantum number. In the weak pairing approximation, since we are interested only in the lowest energy modes, we solve for the eigenstates of the topological insulator Hamiltonian using the ladder operators above and project out the bands from $E^{++}_k$ and $E^{--}_k$. Thus Fourier Bessel expanding the radial wavefunctions as

$$\phi^{+}_{l,n} \approx \int dk \begin{pmatrix} c^n_{l,k} f_{l,k}(r) \\ d^n_{l,k} g_{l,k}(r) \end{pmatrix}, \tag{3.43}$$

where

$$f_{l,k}(r) = \frac{1}{\sqrt{\mathcal{N}_{k,l}^{+}}}\begin{pmatrix} kJ_{l-1}(kr) \\ \left(m_k - \sqrt{m_k^2+k^2}\right)J_l(kr) \end{pmatrix} \tag{3.44}$$

$$g_{l,k}(r) = \frac{1}{\sqrt{\mathcal{N}_{k,l}^{-}}}\begin{pmatrix} \left(m_k + \sqrt{m_k^2+k^2}\right)J_l(kr) \\ -kJ_{l+1}(kr) \end{pmatrix} \tag{3.45}$$

and $\mathcal{N}_{k,l}^{\pm}$ are normalization constants given by $\mathcal{N}_k^{\pm} = 2\left(k^2+m_k^2 \mp m_k\sqrt{m_k^2+k^2}\right)\int_0^\infty rdrJ_l(kr)J_l(kr)$ .The Schrodinger's equation reduces to

$$\begin{pmatrix} T^{-} & \Delta^{+-} \\ \Delta^{+-T} & T^{+} \end{pmatrix}\Phi_{ln}^{+} = E_{l,n}^{+}(\mu)\Phi_{ln}^{+} \tag{3.46}$$

where

$$T_{k,k'}^{\mp} = \left(\mp\mu \pm \sqrt{k^2+m_k^2}\right)\delta\left(k-k'\right), \tag{3.47}$$

with respective signs,

$$\Delta_{l,k,k'}^{+-} = \int rdrf_{l,k}^{T}(r)\begin{pmatrix} \Delta_0(r) & 0 \\ 0 & \Delta_0(r) \end{pmatrix}g_{l,k'}(r) \tag{3.48}$$

and the spinor is $\Phi_{ln}^{+} = \left(\{c_{lk}^n\},\{d_{lk}^n\}\right)^T$ .

In terms of our original variables, the wavefunctions are then written

$$\chi_{ln}^{+}(\mathbf{r}) = \begin{pmatrix} \mathbf{u}_{ln}^{+}(\mathbf{r}) \\ \mathbf{v}_{ln}^{+}(\mathbf{r}) \end{pmatrix}, \tag{3.49}$$

where

$$\mathbf{u}_{ln}^{+}(\mathbf{r}) = \int dk\frac{c_{lk}^n}{\sqrt{2\pi\mathcal{N}_k^{+}}}\begin{pmatrix} e^{-i(l-1)\theta}kJ_{l-1}(kr) \\ 0 \\ 0 \\ e^{-il\theta}\left(m_k - \sqrt{m_k^2+k^2}\right)J_l(kr) \end{pmatrix} \tag{3.50}$$

$$\mathbf{v}_{ln}^{+}(\mathbf{r}) = \int dk\frac{d_{lk}^n}{\sqrt{2\pi\mathcal{N}_k^{-}}}\begin{pmatrix} e^{-il\theta}\left(m_k + \sqrt{m_k^2+k^2}\right)J_l(kr) \\ 0 \\ 0 \\ ke^{-i(l+1)\theta}J_{l+1}(kr) \end{pmatrix} \tag{3.51}$$

and the mirror (particle-hole) partners are built from $\chi_{ln}^{-}(\mathbf{r}) = \mathcal{C}\chi_{-ln}^{+}(\mathbf{r})$.

We fix a finite radius $R$ for the cylinder size which forces us to discretize $k \to \alpha_{l,j}/R$ where $\alpha_{l,j}$ are the $j$-th Bessel zeroes at each $l$ subspace (Dirichlet boundary conditions.) We fix a UV cutoff at some (large) $N_0$-th Bessel zero. Diagonalizing the resulting Hamiltonian leads to the spectrum shown in 3.3 with parameters defined therein. One sees two branches of in-gap modes, one corresponding to an outer-edge localized set of modes, which we neglect, while the other corresponds to our desired vortex localized ones, as can be checked by plotting their respective probability densities.

For the low energy states, $n \equiv n_{CdG}$ (a label which we drop from now on), one may plot the energies for different values of the angular momentum $l$ and check that the spectrum follows

$$E_l^{\pm} = \frac{\Delta^2}{E_F}\left(l \mp \frac{1}{2} \pm \frac{\phi(\mu)}{2\pi}\right) \tag{3.52}$$

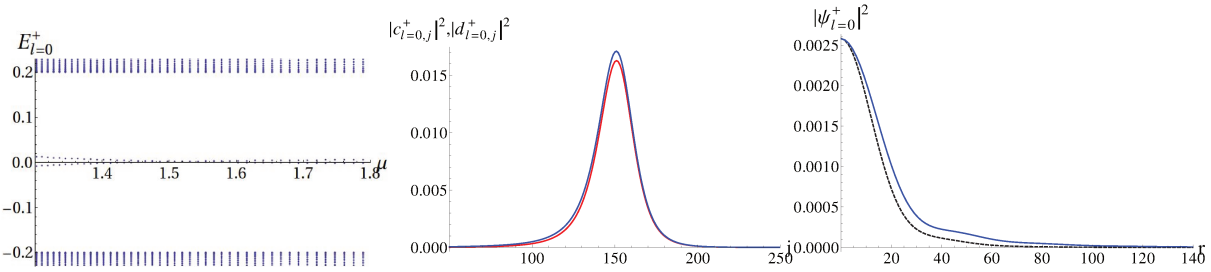


Figure 3.3: Numerical results for the lowest CdG mode spectrum, $l = 0$, in the + sector of $\mathcal{M}$ eigenstates. Fixing the parameters demands some care as one needs to consider a large enough region of k-space as to capture the TI band inversion while considering Fermi energies large to guarantee $k_F\xi > 1$ and at the same time close to the critical value $\mu_C \sim v_D\sqrt{m/\epsilon}$. For all figures we use (disk size)$R = 5000$, (number of modes) $N_0 = 300$, $m = 1$, $\epsilon = 120$, $\Delta_0 = 0.2$, and use units with Dirac velocity $v_D = 15$. Thus $\xi = v_D/\pi\Delta_0 \sim 23$, and the expected critical potential is $\mu_C \sim 1.37$. (left) Energy spectrum as function of the chemical potential. A clear superconducting gap is seen at $E^{+}_{l=0,n} = \Delta_0 = 0.2$ with in gap modes. The two modes correspond to a vortex bound mode, with positive slope, and a gapless edge mode, as can be checked plotting the probability density in real space. (middle) Momentum space distribution of the positive slope in-gap mode at chemical potential close to the critical. The red and blue curves are associated with $|c_{l=0,j}|^2$ and $|d_{l=0,j}|^2$ at discrete momenta $j \leftrightarrow k_j = \alpha_{l.j}/R$, respectively. (right) Probability density in radial direction. The blue solid curve corresponds to (3.49) while the dashed line corresponds to (3.53), demonstrating that our ansatz is indeed a good approximation for the CdG modes wavefunctions.

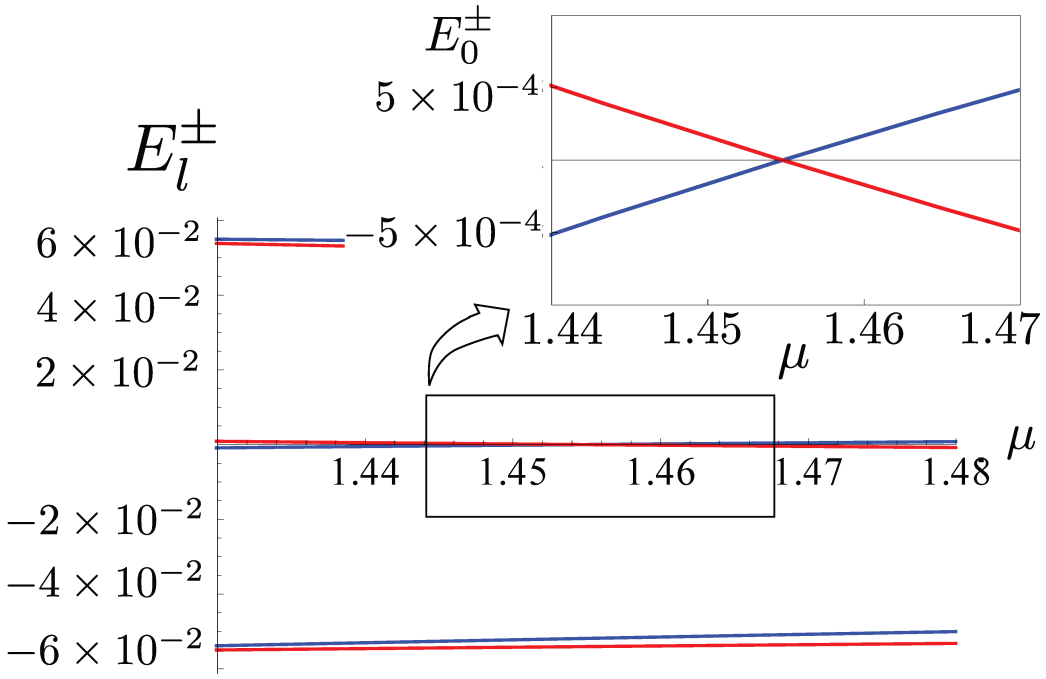


Figure 3.4: CdG vortex modes spectrum of the model 3.22. The parameters used in the calculation are described in Figure 3.3 . We show the energies $E^{+}_{l}(\mu)$ (blue) and $E^{-}_{l}(\mu)$ (red) for $l = 0, \pm 1$ at chemical potentials close to $\mu_c \approx 1.455$. The inset displays the details for $l = 0$.

where $\phi(\mu)$ is a chemical potential dependent function.

In the analytic computation of this energy spectrum, one sees that $\phi(\mu)$ actually corresponds to a Berry phase computed with the eigenstates of the topological-insulator doped Hamiltonian along a closed surface with $k_z = 0$ at the Fermi energy [25]. It grows monotonically from 0 to $2\pi$ with the chemical potential and at the critical value $\phi(\mu_C) = \pi$. Noticing that the values of the momentum in $k$-space are strongly localized at its Fermi value $k_F$ (see Fig.3.3), as one might expect, it is easy to guess an analytic approximation for the

wavefunctions which satisfies their desired asymptotic behaviors. We have

$$\chi^{+} = \mathcal{C} e^{-\frac{2}{v_F}\int_0^r dr' \Delta\left(r'\right)} \begin{pmatrix} f\left(\theta, r\right) \\ g\left(\theta, r\right) \end{pmatrix}, \tag{3.53}$$

where

$$f\left(\theta, r\right) = \frac{1}{\sqrt{2\pi N^{+}_{k_F}}} \begin{pmatrix} e^{-i(l-1)\theta} k_F J_{l-1}\left(k_F r\right) \\ 0 \\ 0 \\ e^{-il\theta}\left(m_{k_F} - \sqrt{m^2_{k_F} + k^2_F}\right) J_l\left(k_F r\right) \end{pmatrix} \tag{3.54}$$

$$g\left(\theta, r\right) = \frac{1}{\sqrt{2\pi N^{-}_{k_F}}} \begin{pmatrix} e^{-il\theta}\left(m_{k_F} + \sqrt{m^2_{k_F} + k^2_F}\right) J_l\left(k_F r\right) \\ 0 \\ 0 \\ e^{-i(l+1)\theta} k_F J_{l+1}\left(k_F r\right) \end{pmatrix} \tag{3.55}$$

and the new normalization factors read

$$N^{\pm}_{k_F} = 2\left(k^2_F + m^2_{k_F} \mp m_{k_F}\sqrt{m^2_{k_F} + k^2_F}\right). \tag{3.56}$$

Here, $\mathcal{C}$ is a normalization constant of order $\left(k_F/\xi\right)^{1/2}$.

The CdG modes spectrum (3.52) is the main result of this sub-section. We have successfully demonstrated a novel numerical approach to computing it in a continuum framework. We have also been able to demonstrate a convenient approximation for the vortex modes eigenfunctions, namely (3.53), which captures with clarity all the physical scales involved, set basically by $k_F$ and $\xi$ (inside $\Delta\left(r\right)$evaluated calculated around the doped topological insulator Fermi surface (they do not provide an explicit expression either, though.)

For the rest of this chapter, we will make extensive use of the results found here to (i) obtain insight in the topological phase transition of the vortex bound modes, in particular showing that they are equivalent to a Kitaev chain, and (ii) obtain insight on physical signatures of the topological phase transition.

**Kitaev wires and CdG vortex modes** Now that we can compute the wavefunctions and energies of the radially bound vortex modes, we can study the dispersive physics along the vortex. We will do this perturbatively. So, we start by restoring the $k_z$ dispersion in the Hamiltonian and write

$$H^0_{BdG} = v_D \mathbf{\Gamma}\cdot\mathbf{P}_{\perp} - \mu\Sigma + \Gamma_0\left(m - \epsilon P^2_{\perp}\right) - \mathbf{\Lambda}\cdot\mathbf{\Delta}\left(\mathbf{r}\right) + \Gamma_z P_z - \Gamma_0 \epsilon P^2_z \tag{3.57}$$

$$\equiv H^0_{BdG,\perp} + H^0_{BdG,z}, \tag{3.58}$$

where the $\perp$ labels imply that only the $r, \theta$ component terms are taken.

We are going to project this into the energy eigenfunctions $\chi_{ln}^{\pm}(\mathbf{r})$. Explicitly,

$$\chi_{ln}^{+}(\mathbf{r}) = \frac{1}{\sqrt{2\pi}}\int dk \begin{pmatrix} \frac{c_{lk}^{n}}{\sqrt{\mathcal{N}_k^{+}}} \begin{pmatrix} e^{-i(l-1)\theta}kJ_{l-1}(kr) \\ 0 \\ 0 \\ e^{-il\theta}\left(m_k - \sqrt{m_k^2+k^2}\right)J_l(kr) \end{pmatrix} \\ \frac{d_{lk}^{n}}{\sqrt{\mathcal{N}_k^{-}}} \begin{pmatrix} e^{-il\theta}\left(m_k + \sqrt{m_k^2+k^2}\right)J_l(kr) \\ 0 \\ 0 \\ ke^{-i(l+1)\theta}J_{l+1}(kr) \end{pmatrix} \end{pmatrix} = \begin{pmatrix} \mathbf{u}_{ln}^{+}(\mathbf{r}) \\ \mathbf{v}_{ln}^{+}(\mathbf{r}) \end{pmatrix} \tag{3.59}$$

$$\chi_{ln}^{-}(\mathbf{r}) = \frac{1}{\sqrt{2\pi}}\int dk \begin{pmatrix} \frac{\bar{c}_{lk}^{n}}{\sqrt{\mathcal{N}_k^{-}}} \begin{pmatrix} 0 \\ e^{-il\theta}\left(m_k + \sqrt{m_k^2+k^2}\right)J_l(kr) \\ e^{-i(l-1)\theta}kJ_{l-1}(kr) \\ 0 \end{pmatrix} \\ \frac{\bar{d}_{lk}^{n}}{\sqrt{\mathcal{N}_k^{+}}} \begin{pmatrix} 0 \\ e^{-i(l+1)\theta}kJ_{l+1}(kr) \\ e^{-il\theta}\left(m_k - \sqrt{m_k^2+k^2}\right)J_l(kr) \\ 0 \end{pmatrix} \end{pmatrix} = \begin{pmatrix} \mathbf{u}_{ln}^{-}(\mathbf{r}) \\ \mathbf{v}_{ln}^{-}(\mathbf{r}) \end{pmatrix}. \tag{3.60}$$

At finite z and low energies, we have $\chi_{ln}^{\pm}(\mathbf{r}) \to \chi_{ln_{CdG}}^{\pm}(\mathbf{r}) f_l^{\pm}(z)$ choosing the CdG states with $n = n_{CdG}$. We will project the radial part the Hamiltonian to find out what Hamiltonian gives the equations of motion for $f_l^{\pm}$. Considering the $\pm$ sectors then we have

$$\tilde{H}_{ll'} = Proj\left[H_{BdG}\right]_{ll'} \tag{3.61}$$

$$= \begin{pmatrix} E_l^{+} & 0 \\ 0 & E_l^{-} \end{pmatrix}\delta_{ll'} \tag{3.62}$$

$$+ \begin{pmatrix} H_{zll'}^{++} & H_{zll'}^{+-} \\ H_{zll'}^{-+} & H_{zll'}^{--} \end{pmatrix}. \tag{3.63}$$

To keep the notation short, we introduce $4\times 4$ Dirac matrices $\boldsymbol{\alpha} = \tau_x\boldsymbol{\sigma}$ and $\beta = \tau_z\sigma_0$ . It is easy to see that terms linear in $P_z$ contribute to the off-diagonals in the $\pm$ sectors while terms quadratic with $P_z^2$ contribute only to the diagonal elements. For these diagonal terms, we develop couplings

$$\epsilon \to \begin{cases} \epsilon_l^{+} = \epsilon\int d^2r\left[\mathbf{u}_l^{+}(\mathbf{r})\right]^{*}\beta\mathbf{u}_l^{+}(\mathbf{r}) - \left[\mathbf{v}_l^{+}(\mathbf{r})\right]^{*}\beta\mathbf{v}_l^{+}(\mathbf{r}) \\ \epsilon_l^{-} = \epsilon\int d^2r\left[\mathbf{u}_l^{-}(\mathbf{r})\right]^{*}\beta\mathbf{u}_l^{-}(\mathbf{r}) - \left[\mathbf{v}_l^{-}(\mathbf{r})\right]^{*}\beta\mathbf{v}_l^{-}(\mathbf{r}) \end{cases} \tag{3.64}$$

Importantly, the sign of these couplings is the same and the angular integration enforces $l = l^{'}$. For the off-diagonal terms we develop the couplings

$$\tilde{\Delta}_l = \int d^2r\left[\mathbf{u}_l^{+}(\mathbf{r})\right]^{*}\alpha^z\mathbf{u}_l^{-}(\mathbf{r}) - \left[\mathbf{v}_l^{+}(\mathbf{r})\right]^{*}\alpha^z\mathbf{v}_l^{-}(\mathbf{r}) \tag{3.65}$$

Adding up the matrix elements above gives the projected Hamiltonian

$$\tilde{H}_{ll'} = \begin{pmatrix} E_l^{+} - \epsilon_l^{+}\partial_z^2 & -i\tilde{\Delta}_l\partial_z \\ -i\tilde{\Delta}_l\partial_z & E_l^{-} + \epsilon_l^{-}\partial_z^2 \end{pmatrix}\delta_{ll'}. \tag{3.66}$$

For the diagonal terms we may still use $E_{-l}^{-} = -E_{l}^{+}$ to write

$$\begin{pmatrix} E_l^+ - \epsilon_l^+ \partial_z^2 & -i\tilde{\Delta}_l \partial_z \\ -i\tilde{\Delta}_l \partial_z & E_l^- + \epsilon_l^- \partial_z^2 \end{pmatrix} \tag{3.67}$$

$$= \begin{pmatrix} E_l^+ - \epsilon_l^+ \partial_z^2 & -i\tilde{\Delta}_l \partial_z \\ -i\tilde{\Delta}_l \partial_z & -\left(E_{-l}^+ - \epsilon_l^- \partial_z^2\right) \end{pmatrix}. \tag{3.68}$$

As the signs of $\epsilon_l^{\pm}$ are the same, one can easily see that the $l = 0$ Hamiltonian is essentially the same as a Kitaev chain. For $l \neq 0$, on the other hand, the Hamiltonian does not describe a Kitaev chain. The PH symmetry is only present when both $\pm l$, besides the $\pm$ sectors of $\mathcal{M}$, are taken into account. In this 1D projection, the contributions of the states in the whole radial direction are taken into account. These considerations are more clearly seen by writing

$$\begin{pmatrix} E_l^+ - \epsilon_l^+ \partial_z^2 & -i\tilde{\Delta}_l \partial_z \\ -i\tilde{\Delta}_l \partial_z & E_l^- + \epsilon_l^- \partial_z^2 \end{pmatrix} \tag{3.69}$$

$$\approx \begin{pmatrix} E_l^+ - \epsilon_l \partial_z^2 & -i\tilde{\Delta}_l \partial_z \\ -i\tilde{\Delta}_l \partial_z & -\left(E_{-l}^+ - \epsilon_l \partial_z^2\right) \end{pmatrix} \tag{3.70}$$

which leads to the main result of this sub-section,

$$\tilde{H}_l = \frac{E_l^+ - E_{-l}^+}{2}\rho_0 + \rho_z \left(\frac{E_l^+ + E_{-l}^+}{2} - \epsilon_l \partial_z^2\right) + \rho_x \left(-i\tilde{\Delta}_l \partial_z\right). \tag{3.71}$$

The $\rho_0$ term does not vanish here (unless $l = 0$), as usually happens in a regular superconducting BdG Hamiltonian (k-independent identity terms do not respect the Nambu constraint). To see that indeed the system is PH symmetric, one has to take into account the full second quantized Hamiltonian with all $\pm l$ pairs. In particular, compare,

$$\tilde{H}_0 = \rho_z \left(E_0^+ - \epsilon_0 \partial_z^2\right) + \rho_x \left(-i\tilde{\Delta}_0 \partial_z\right) \tag{3.72}$$

with equation (2.10), in $k_z$-space. This is nothing but a Kitaev Hamiltonian with $E_0^+$ ($\mu$) playing the role of the chemical potential itself.

This projected Hamiltonian is then equivalent to a p-wave wire network. This is a very unusual network as PH symmetry actually connects different wires while each wire has PH symmetry actually broken. Interestingly, as commented, the channel with $l = 0$ represents our desired p-wave superconducting chain, showing that the vortex in a superconducting doped topological insulator indeed corresponds to a Kitaev 1D topological superconductor.

We have now finished our analysis of the CdG modes of superconducting doped topological insulators. We have made an extensive study of all aspects of these modes in here, focusing on the chemical potential dependence of their spectrum, showing that there are two sets of gapped modes which develop zero energy states as function of the chemical potential. We have also shown that, including dispersion along the vortex, the Hamiltonian obeyed is in fact a topological superconductor Hamiltonian in 1D. With these insights into the existence of a topological phase transition along the vortex line, we now move towards studying physical signatures of such a phase transition.

## 3.5 Probing the vortex topological phase transition

Knowledge of the vortex topological phase transition motivates one to try to measure it. Measuring the presence/absence of Majorana zero-modes at surfaces has proven to be a great challenge for the already discussed reasons regarding the identification of the zero energy peak signatures as originating necessarily from Majorana fermion physics. Also, we have understood now that a bulk criterion is available to identify the topological

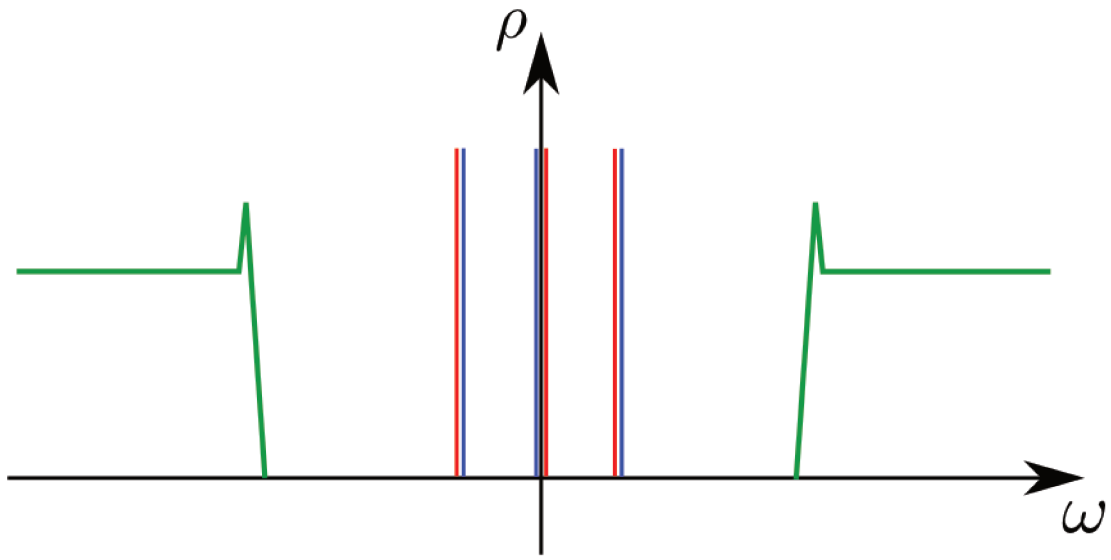


Figure 3.5: Schematic density of states for the doped topological insulator with a single vortex solution. The green curves represent the superconducting gap while the internal blue and red peaks correspond to the two CdG mode sectors. The spacing between the internal pairs of peaks correspond to the the CdG gap. The modes are represented close to the critical point. The CdG gap cannot be really resolved experimentally.

phase transition, that is the closing and opening of the CdG gap for the $l = 0$ modes.

In Fig.3.5 we have an scheme of the complete density of states of the superconducting system with a single vortex. Inside the large superconducting gap $\Delta_0$ in green, vortex localized states develop inside the gap. Blue and red correspond to the two sector of modes we described previously. In principle, as function of the chemical potential, one could see the central peaks getting closer and closer as one raises doping, until the peaks merge and separate again - of course, experimentally, one would never see a distinction between red and blue ones. Regarding the energy scales, however, the change of spectrum at the topological phase transition is controlled by the mini-gap energy scale $\delta \approx \Delta_0^2/E_F \approx 5 \times 10^{-3}\ K$ for the case of $Co_{0.12}Bi_2Se_3$. This is a very small energy scale.

Indeed, experimental signatures of CdG physics inside superconducting vortices typically manifest themselves, via scanning tunneling microscopy (STM) measurements, as a continuum of sub-gap peaks in the local density of states (LDOS) close to the vortex. The spectral resolution of STM is of the order of the measurement temperature ($3k_BT$)[70]. It is then clear that an important obstacle to the verification of topological phase transitions in this system by STM is the small CdG gap. This motivates one to look at how one could isolate signatures of such topological phase transition at an energy scale which may be accessible experimentally.

Let us study a simple proposal to overcome the problem above. It is clear that we need to consider physics at higher energy scales, due to the current experimental resolution. This physics must also be sensitive to the topological phase transition, that is, the closing and reopening of the gap of the CdG modes. Whatever phenomenon we consider must couple to the vortex bound modes.

A simple attempt one can imagine is a phonon-like coupling, but for the vortex position. Vortices are pinned to their given positions by impurities (or due to a lattice in the case of many vortices), but it is reasonable that these positions can fluctuate in time, with the frequency of oscillation being fixed by the strength of the pinning potential. Even more, quantum mechanics implies that even at absolute zero temperature such fluctuations cannot be stopped [66, 65].

For the physical picture of a fluctuating vortex to be reasonable, its position and cross-section structure must be well defined. Testing with some real numbers, the radial position of maximum peaks from the different CdG modes can be read from the wavefunctions we derived. One can see that the difference in the position of the peaks from different $l$ is fixed by the Fermi wavevector scale. For Copper doped $Bi_2Se_3$, for example, the maximum probability for the position of the vortex core from the states with $l = 0$ lie at $r = 0$ and are separated from the next closest mode (with $l = -1$) by the Fermi wavevector scale $r = 1/k_F \approx 10$Å, which is

well within the resolution of STM.

To test for a 'proof of principle' mechanism, we simplify imagining a sample thin enough so that only the 2D behavior of the modes is important while large enough so that the Majorana surface modes do not hybridize strongly. STM probes the local density of states (LDOS) at a given region of a sample's surface. The LDOS is defined by

$$\rho\left(\mathbf{r},\omega\right)=\sum_{m,\sigma,l}\left|\left\langle \epsilon_{m}\left|\psi_{\sigma,l}^{\dagger}\left(\mathbf{r}\right)\right|N_{0}\right\rangle \right|^{2}\delta\left(\omega-\epsilon_{m}\right), \tag{3.73}$$

where $|N_0\rangle$ is a $N_0$-particle ground-state, $|\epsilon_m\rangle$ is an $(N_0+1)$-particle excited state (with generic quantum numbers $m$) and $\psi_{\sigma,l}^{\dagger}(\mathbf{r})$ is an electronic state creation operator at level $l$ in sector $\sigma$. Using our vortex-modes eigenbasis, this can be written, taking into account the effects of the vortex fluctuations perturbatively in terms of a self-energy, as

$$\rho\left(\mathbf{r},\omega\right) = \sum_{\sigma=\pm}\rho_{\sigma}\left(\mathbf{r},\omega\right) \tag{3.74}$$

$$\rho_{\sigma}\left(\mathbf{r},\omega\right) = -\frac{1}{\pi}Im\sum_{l}\frac{\left|\mathbf{u}_{l}^{\sigma}\left(\mathbf{r}\right)\right|^{2}}{\omega-E_{l}^{\sigma}-\Sigma_{l}^{\sigma}+i\epsilon}. \tag{3.75}$$

$$= \sum_{l}\left|\mathbf{u}_{l}^{\sigma}\left(\mathbf{r}\right)\right|^{2}\delta\left(\omega-E_{l}^{\sigma}-\Sigma_{l}^{\sigma}\left(\omega\right)\right). \tag{3.76}$$

From (3.59) and (3.60), we see explicitly that, when looking at $\mathbf{r}=0$, only states with $l=0$ and $l=1$ contribute (notice only the $\mathbf{u}_l^\sigma$ part of the Nambu spinor contribute to the LDOS). The state from $l=-1$ only starts contributing away from $\mathbf{r}=0$, as well as all the other states, and at a distance which goes as $1/k_F$ due to the wavefunction dependence above. This means, also, that the LDOS spectrum at the origin must be particle-hole asymmetric in doped topological insulators. This is an unexpected signature of the unusual physics induced by spin-orbit coupled orbitals from the doped topological insulator regime.

The idea of studying the effects of vortex position fluctuations in the LDOS in the vicinity of a vortex has been considered before in the context of d-wave superconductivity. In that case, it is believed that a verified suppression of a central vortex peak in the LDOS is due to the possibility of such position quantum fluctuations. Vortex masses scale with the cross-sectional area of a vortex core, thus with the square of the coherence length $\sim\xi^2$. The small coherence lengths in cuprate superconductors imply that they are prime candidates to the verification of this physics. The anisotropy of the superconducting gap in that case, however, makes the problem much more demanding [65, 66].

For us, the simple s-wave nature of the superconducting phase, together with the larger coherence length, implies the possibility of a simple perturbative treatment of the problem, which would be a poor approximation for the d-wave case. The larger coherence length, however, also implies that the influence of the vortex motion in our system is expected to be small. We verify this, nevertheless, with a two-fold motivation: first, as a proof of principle that the topological phase transition is sensitive to such "external" fluctuations; second, as we know that the vortex physics can be mapped to a 1D chain topological system, one can envisage mapping the effects of the vortex position fluctuations into the context of 1D chains too, looking for a different realization of these phenomena. We focus on effects of quantum zero-point motion of the vortex.

### 3.5.1 Fluctuating vortex model

Superconductivity and the vortex quantum phase transition (VQPT) in doped topological insulators may be understood in the weak pairing limit ($\xi k_F \gg 1$, where $\xi$ is the SC coherence length)[25]. In this regime, a gradient expansion can be deployed to study the effects of the fluctuating vortex position in the low-energy spectrum[65]. We are, formally, treating the influence of the phase fluctuations of the superconducting order parameter on the vortex LDOS encapsulating them in a collective coordinate, the position of the vortex.

We start with an action of the form $\mathcal{S}=\mathcal{S}_{BdG}+\mathcal{S}_{eff}^{vortex}$. The first term is a Bogoliubov-de Gennes (BdG)

action for the superconducting doped TI,

$$\mathcal{S}_{BdG} = \frac{1}{2}\int d^2r d\tau \Psi^\dagger \left(\partial_\tau + H_{BdG}\right)\Psi \tag{3.77}$$

where $H_{BdG}$ corresponds to (3.22), now with a displaced position for the vortex, as

$$H_{BdG} = \begin{bmatrix} H_{TI} - \mu & \Delta\left(\mathbf{r} - \mathbf{R}\left(\tau\right)\right) \\ \Delta^\dagger\left(\mathbf{r} - \mathbf{R}\left(\tau\right)\right) & -H_{TI} + \mu \end{bmatrix}. \tag{3.78}$$

Here $\mu$ is the chemical potential and the effective low energy 3D TI Hamiltonian is given by (3.17) as before. The Nambu spinor again reads $\Psi = \left(\psi,\, is_y\psi^\dagger\right)^T$ where $\psi = (\psi_{A\uparrow},\, \psi_{A\downarrow},\, \psi_{B\uparrow},\, \psi_{B\downarrow})$. $A$, $B$ are orbital indices and $\tau_i$ and $s_i$ Pauli matrices act on orbital and spin Hilbert spaces, respectively. The superconducting pairing $\Delta\left(\mathbf{r} - \mathbf{R}\left(\tau\right)\right)$ contains a vortex profile centered at a fluctuating position $\mathbf{R}\left(\tau\right)$ whose dynamics is governed by[65]

$$\mathcal{S}_{eff}^{vortex} = \frac{m_v}{2}\int \frac{d\omega}{2\pi}\mathbf{R}^\dagger\left(i\omega\right)\begin{pmatrix} \omega^2 + \omega_0^2 & \omega_c\omega \\ -\omega_c\omega & \omega^2 + \omega_0^2 \end{pmatrix}\mathbf{R}\left(i\omega\right). \tag{3.79}$$

Physically, the action (3.79) describes a particle of mass $m_v$ oscillating in an harmonic trap of frequency $\omega_0$ which depends on the properties of the trapping potential [65]. This oscillator frequency dictates the qualitative features of the energy peak distribution of the LDOS. Finally, $\omega_c$ corresponds to a Magnus force acting on the vortex[64]. The frequency $\omega_c$ will be shown to play an essential role, introducing an energy scale for the chemical potential in which we have distinguished signatures of the VQPT in the system's LDOS.

To capture the coupling between electronic excitations and vortex fluctuations, we expand the superconducting pairing around the vortex rest position $\Delta\left(\mathbf{r} - \mathbf{R}\left(\tau\right)\right) \approx \Delta\left(\mathbf{r}\right) - \partial_{\mathbf{r}}\Delta\left(\mathbf{r}\right)\cdot\mathbf{R}\left(\tau\right)$. Again, this approximation is valid at weak-coupling [65], which is also the regime of validity of Hamiltonian (3.78). Within this formalism, the full problem is described by a perturbative action $\mathcal{S} = \mathcal{S}_0 + \mathcal{S}_{eff}^{vortex} + \mathcal{S}_{int}$. $\mathcal{S}_0$ is given by (3.77) with the BdG Hamiltonian in the stationary vortex limit, $\mathbf{R}\left(\tau\right) = 0$ (explicitly given in (3.22)). The interaction term is given by

$$\mathcal{S}_{int} = -\int d^2r d\tau \mathbf{R}\left(\tau\right)\cdot\Psi^\dagger\begin{pmatrix} 0 & \partial_{\mathbf{r}}\Delta \\ \partial_{\mathbf{r}}\Delta^\dagger & 0 \end{pmatrix}\Psi. \tag{3.80}$$

The interaction between vortex modes and the fluctuations in the vortex position leads to a self-energy correction to the energy of the CdG modes.

**Effective vortex modes interactions - self-energy** Here we derive the effective interactions among vortex modes. We further show that they can be perturbatively incorporated in the energy spectrum via a self-energy term.

Assuming a singlet intra-orbital pairing for doped topological insulators, the VQPT was found originally by an exact diagonalization of lattice toy models and a semi-classical study of the BdG mean-field Hamiltonian [25], as well as numerically solving the self-consistent BdG equations [26]. In order to study the effects of vortex fluctuations on the LDOS, it is convenient to use our basis basis (3.59) and (3.60) which diagonalizes the Hamiltonian in the limit of a static vortex.

We expand the Grassmann fields in terms of eigenvectors of the static-vortex BdG Hamiltonian $H_{BdG}^0$ as $\Psi = \sum_{q=1}^{8}\sum_{ln}\chi_{ln}^q\left(\mathbf{r}\right)\psi_{ln}^q\left(\tau\right)$. The eight arising bands obey $H_{BdG}^0\chi_{ln}^q\left(\mathbf{r}\right) = E_{ln}^q\chi_{ln}^q\left(\mathbf{r}\right)$ where $l$ and $n$ labels conserved quantum numbers. At weak coupling, we further project into the two bands which cross the doubly degenerate Fermi surface of $H_{TI}$. Labeling these states by $\sigma \equiv \pm$, we have, at low energies, $\Psi \approx \sum_{ln}\chi_{ln}^+\left(\mathbf{r}\right)\psi_{ln}^+\left(\tau\right) + \chi_{ln}^-\left(\mathbf{r}\right)\psi_{ln}^-\left(\tau\right)$ with $\chi_{ln}^\pm$ given by (3.59) and (3.60).

To study the VQPT we consider the lowest energy vortex modes. These are the CdG modes and allow fixing

the label $n \to n_{CdG}$, which we drop from now onwards. The two sectors (labeled by $\sigma = \pm$) are connected by particle-hole (PH) conjugation as $\Xi\chi_l^+ = \chi_{-l}^-$. The energies of the CdG vortex modes in this case are as before

$$E_l^{\pm} = \frac{\Delta^2}{E_F}\left(l \mp \frac{1}{2} \pm \frac{\Phi_b(\mu)}{2\pi}\right), \tag{3.81}$$

so that $E_l^+ = -E_{-l}^-$. Here $\Phi_b(\mu)$ is the Berry phase calculated around the Fermi surface on the curve with zero wavevector along the vortex [25]. As the chemical potential increases, the Fermi surface enlarges and $\Phi_b(\mu)$ varies from 0 to $2\pi$, defining a critical chemical potential such that $\Phi_b(\mu_C) = \pi$.

In terms of the CdG eigenstates, equation (3.80) is written

$$\mathcal{S}_{int} = -\sum_{l,l',\sigma}\int d\tau \bar{\psi}_l^{\sigma}(\tau)\psi_{l'}^{\sigma}(\tau)\mathbf{R}(\tau)\cdot\mathbf{M}_{l,l'}^{\sigma}, \tag{3.82}$$

where

$$\mathbf{M}_{l,l'}^{\sigma} = \int d^2r \chi_l^{\sigma}(\mathbf{r})^{\dagger}\begin{pmatrix} 0 & \partial_{\mathbf{r}}\Delta \\ \partial_{\mathbf{r}}\Delta^{\dagger} & 0 \end{pmatrix}\chi_{l'}^{\sigma}(\mathbf{r}). \tag{3.83}$$

We integrate out the vortex modes. For this, we start with the vortex action (3.79) and work at zero-temperature. Noticing that $\mathbf{R}^{\dagger}(i\omega) = \mathbf{R}(-i\omega)$, we introduce a basis $R_{\pm}(i\omega) = \frac{R_x(i\omega)\pm iR_y(i\omega)}{\sqrt{2}}$ which diagonalizes the Lagrangian density as

$$\mathcal{S}_{eff}^{vortex} = \int \frac{d\omega}{2\pi}\left(R_-^{\dagger}(i\omega), R_+^{\dagger}(i\omega)\right)\mathbb{D}_0^v(i\omega)^{-1}\begin{pmatrix} R_-(i\omega) \\ R_+(i\omega)\end{pmatrix}, \tag{3.84}$$

with

$$\mathbb{D}_0^v(i\omega) = \begin{pmatrix} D_-^{-1} & 0 \\ 0 & D_+^{-1}\end{pmatrix} \tag{3.85}$$

and the Green's functions $D_{\mp}(i\omega) = \frac{m_v}{2}\left((\omega \pm i\omega_c/2)^2 + \omega_v^2\right)$. This sets the two important energy scales dictated by the vortex fluctuations as $\omega_c$, from the Magnus force, and $\omega_v = \sqrt{\omega_0^2 + \omega_c^2/4}$, from the harmonic trap.

As discussed in the former section, the low-energy modes split into two Hilbert space sectors related by a $z$-mirror/particle-hole symmetry. Each sector is subject to an effective potential arising after the integration of the vortex 0D field theory. From equations 3.79 we may write:

$$e^{-V_{eff}^{\sigma}\left[\bar{\psi}_l^{\sigma},\psi_l^{\sigma}\right]} \propto \int \mathcal{D}[\mathbf{R}]\, e^{-S_{eff}^{vortex} + \int d\tau \sum_{l,l'}\mathbf{R}(\tau)\cdot\mathbf{M}_{l,l'}^{\sigma}\bar{\psi}_l^{\sigma}(\tau)\psi_{l'}^{\sigma}(\tau)}. \tag{3.86}$$

Rewriting the scalar products in terms of the $R_{\pm}(i\omega)$ coordinates and using(3.49) reduces the matrix elements to $M^{\alpha;\sigma} = \frac{1}{2}(M_x + \alpha i M_y)$, with $\alpha = \pm$, where

$$M_{l,l'}^{+;\sigma} = \left(M_{l',l}^{-;\sigma}\right)^* = \int d^2r\left[\mathbf{u}_l^{\sigma}(\mathbf{r})^{\dagger}\partial_{\bar{z}}\Delta\mathbf{v}_{l'}^{\sigma}(\mathbf{r}) + \mathbf{v}_l^{\sigma}(\mathbf{r})^{\dagger}\partial_{\bar{z}}\Delta^{\dagger}\mathbf{u}_{l'}^{\sigma}(\mathbf{r})\right]. \tag{3.87}$$

This allows for simple, although tedious, integration over the bosonic fields. As a result, the fermionic self-interaction mediated by the fluctuating vortex position modes arises as

$$\begin{aligned} V_{eff}^{\sigma}\left[\bar{\psi}_l^{\sigma},\psi_l^{\sigma}\right] = {} & \frac{1}{2}\sum_{l,l',n,n'}\int\frac{d\tilde{\omega}}{2\pi}\int\frac{d\tilde{\nu}}{2\pi}\int\frac{d\tilde{\nu}'}{2\pi}\times \\ & \bar{\psi}_l^{\sigma}(i\tilde{\nu}+i\tilde{\omega})\bar{\psi}_n^{\sigma}\left(i\tilde{\nu}'-i\tilde{\omega}\right)V_{l,l',n,n'}^{\sigma}(i\tilde{\omega})\psi_{l'}^{\sigma}(i\tilde{\nu})\psi_{n'}^{\sigma}\left(i\tilde{\nu}'\right) \end{aligned} \tag{3.88}$$

where

$$V^{\sigma}_{l,l',n,n'}\left(i\tilde{\omega}\right)=-\frac{1}{m_v}\sum_{\alpha=\pm}\left[\frac{\left(M^{\alpha;\sigma}_{l,l'}\right)^{\dagger}M^{\alpha;\sigma}_{n,n'}}{\left(\left(\tilde{\omega}+\alpha i\omega_c/2\right)^2+\omega_v^2\right)}\right]. \tag{3.89}$$

The interaction potential (3.89) displays a retarded interaction. Effectively, this is similar to a "screened" Coulomb interaction in frequency space. The GW approximation [76] then amounts to computing the spectral effects of the 'screened' interactions via a 1-loop self-energy

$$\begin{aligned}\Sigma^{\sigma}_{l}\left(i\tilde{\omega}\right) &= -\sum_{l'}V^{\sigma}_{l,l,l',l'}\left(0\right)\int_{\omega}G^{0\sigma}_{l}\left(i\omega\right)\\ &\quad+\sum_{l'}\int_{\omega}V^{\sigma}_{l,l',l',l}\left(i\tilde{\omega}-i\omega\right)G^{0\sigma}_{l'}\left(i\omega\right).\end{aligned} \tag{3.90}$$

The first term vanishes. The second must be considered with care as the pole structure is sensitive to the structure of the energy levels. An integration over the complex plane gives the self-energy

$$\Sigma^{\sigma}_{l}\left(i\tilde{\omega}\right)=\sum_{l'}\sum_{\alpha=\pm}\frac{A^{\alpha;\sigma}_{l;l'}}{\left(i\tilde{\omega}-\left(sgn\left(\Xi^{\alpha;\sigma}_{l'}\right)\omega_v+E^{\sigma}_{l'}\right)-\alpha\omega_c/2\right)}, \tag{3.91}$$

where $A^{\alpha;\sigma}_{l;l'}\equiv\frac{\left|M^{\alpha;\sigma}_{l,l'}\right|^2}{m_v\omega_v}$ and $\Xi^{\alpha;\sigma}_{l'}\equiv E^{\sigma}_{l'}+\alpha\omega_c/2$. The self-energy is real.

We can calculate the matrix elements analytically, making use of the Feynman-Hellman relations, adapted to our Hamiltonian and in a finite cylinder geometry. A long calculation, which we omit, making full use of Bessel function relations gives finally

$$\begin{aligned}M^{+;+}_{l,l'} &= \frac{\delta_{l',l+1}}{2}\sum_{j,j'}c_{lj}\left[\left(E^{+}_{l+1}-E^{+}_{l}\right)\mathcal{K}^{l+}_{j,j'}-\mathcal{L}^{l+}_{j,j'}\right]c_{l+1j'}\\ &\quad+\frac{1}{2}\sum_{j,j'}d_{lj}\left[\left(E^{+}_{l+1}-E^{+}_{l}\right)\mathcal{K}^{l-}_{j,j'}-\mathcal{L}^{l-}_{j,j'}\right]d_{l+1j'}\end{aligned} \tag{3.92}$$

where we remember that the $c_{lj}$, $d_{lj}$ coefficients come from the numerical diagonalization giving (3.59) and (3.60) with $n=n_{CdG}$ and with

$$\mathcal{K}^{l\pm}_{j,j'}=\mathrm{sgn}\left(l+1/2\right)\left(-1\right)^{j-j'}\frac{\alpha_{jl}\alpha_{j'l+1}}{R\left(\alpha^2_{j'l+1}-\alpha^2_{jl}\right)}\frac{\mathcal{M}^{\pm}_{jl}\mathcal{M}^{\pm}_{j'l+1}+\left(\frac{\alpha_{j'l+1}}{R}\right)^2}{\sqrt{\left(\left(\frac{\alpha_{jl}}{R}\right)^2+\mathcal{M}^{\pm}_{jl}\right)\left(\left(\frac{\alpha_{j'l+1}}{R}\right)^2+\mathcal{M}^{\pm}_{j'l+1}\right)}}, \tag{3.93}$$

and

$$\mathcal{L}^{l\pm}_{j,j'}=\mathrm{sgn}\left(l+1/2\right)\left(-1\right)^{j-j'}\frac{2\epsilon\alpha_{jl}\alpha_{j'l+1}}{R^3}\frac{\left(\frac{(l\mp1)(l+1\mp1)}{R^2}+\mathcal{M}^{\pm}_{jl}\mathcal{M}^{\pm}_{j'l'}\right)}{\sqrt{\left(\left(\frac{\alpha_{jl}}{R}\right)^2+\mathcal{M}^{\pm}_{jl}\right)\left(\left(\frac{\alpha_{j'l+1}}{R}\right)^2+\mathcal{M}^{\pm}_{j'l+1}\right)}}. \tag{3.94}$$

Here, $R$ is the finite cylinder radius, $\alpha_{jl}$ is the j-th zero of the l-th Bessel function and $\mathcal{M}^{\pm}_{jl}=m^2_{j,l}\mp m_{j,l}\sqrt{m^2_{j,l}+\left(\frac{\alpha_{jl}}{R}\right)^2}$ with $m_{j,l}=m-\epsilon\alpha_{jl}/R$. The other matrix elements may be found from

$$M^{\alpha;-}_{l,l'} = -M^{\alpha;+}_{-l',-l} \tag{3.95}$$

$$M^{-;\sigma}_{l,l'} = \left(M^{+;\sigma}_{l',l}\right)^{*}\equiv\left(M^{+;\sigma}_{l,l'}\right)^{\dagger}. \tag{3.96}$$

In sum, vortex fluctuations generate the following self-energy for CdG vortex modes which we calculate using the GW approximation[76]

$$\Sigma_l^\sigma\left(i\tilde{\omega}\right)=\sum_{l',\alpha=\pm}\frac{A_{l;l'}^{\alpha;\sigma}}{\left(i\tilde{\omega}-\left(sgn\left(\Xi_{l'}^{\alpha;\sigma}\right)\omega_v\right)-\Xi_{l'}^{\alpha;\sigma}\right)} \tag{3.97}$$

Here $A_{l;l'}^{\alpha;\sigma}\equiv\frac{\left|M_{l,l'}^{\alpha;\sigma}\right|^2}{m_v\omega_v}$ are reduced matrix elements with $M_{l,l'}^{\alpha;\sigma}=\frac{1}{2}\left(M_x+\alpha iM_y\right)_{l,l'}^{\sigma}$ and $\Xi_{l'}^{\alpha;\sigma}\equiv E_{l'}^{\sigma}+\alpha\omega_c/2$. For unit vorticity, angular momentum conservation implies that $l$ is connected only to $l^{'}=l+\alpha 1$ by such interactions. The energy scale introduced by $\omega_v\equiv\sqrt{\omega_0^2+\omega_c^2/4}$ ( and dominated by $\omega_0$ as aforementioned), represents a "magneto-plasma" frequency in an Einstein model [65].

Through the perturbative interaction, the energy density profile of CdG modes is modified with part of the spectral weight from $\omega=E_l^\sigma$ being transfered to new "satellite" peaks in the LDOS[65] localized at the solutions of

$$\omega-E_l^\sigma-\Sigma_l^\sigma\left(\omega\right)=0. \tag{3.98}$$

Both the spectrum $E_l^\sigma$ and the profile of $\mathbf{u}_l^\sigma\left(\mathbf{r}\right)$ dramatically change the phenomenology described by (3.76) when the parent metallic state of the superconductor comes from doped TIs, as compared with ordinary metals.

**Tunneling Conductance Analysis** STM experiments measure the local tunneling conductance of a system. The latter is found, at low temperatures, by computing the convolution of the LDOS (3.76) with the derivative of the Fermi distribution function as

$$G\left(\mathbf{r},\omega\right)=-\frac{G_0}{\rho_0}\int d\omega^{'}\rho\left(\mathbf{r},\omega+\omega^{'}\right)f^{'}\left(\omega^{'}\right). \tag{3.99}$$

The normalization constant assumes an STM tip with constant DOS $\rho_0=m_e/2\pi$ (for a free 2D electron gas) with the corresponding tunneling conductance $G_0$, and $f\left(\omega\right)$ is the Fermi-Dirac distribution. At very low temperatures, the tunneling conductance is essentially a measurement of the LDOS, however still smoothed by the finite temperature effects.

Given the atomic level resolution of STM, we can safely focus at the density of states at the vortex core $\mathbf{r}=0$. As seen in (3.59) and (3.60), the wavefunction components may be expanded in terms of Bessel functions. In particular, at $\mathbf{r}=0$, only Bessel functions of order zero have non-zero amplitude while all the other Bessel functions vanish. From our Fourier-Bessel expansion of the CdG modes above, only $l=0$ andd, as a result of spin-orbit coupling, $l=1$ modes have finite contributions in $\mathbf{u}_l^\sigma\left(\mathbf{r}\right)$ at the origin.

Focusing then on the contributions of $l=0$, 1, let us study what are the consequences of equations (3.97) and (3.98). From angular momentum conservation, $M_{l,l'}^{+;\sigma}=\delta_{l',l+1}M_{l,l+1}^{+;\sigma}$ and from $A_{l;l'}^{-;\sigma}=A_{l';l}^{+;\sigma}$ we can read the corresponding result for $\alpha=-$. These simplifications allow us to reduce the self-energy contributions to just a couple of relevant pieces,

$$\Sigma_0^\sigma\left(\omega\right)=\frac{A_{0;1}^{+;\sigma}}{\left(\omega-sgn\left(\Xi_1^{+;\sigma}\right)\omega_v-E_1^\sigma-\omega_c/2\right)}+\frac{A_{-1;0}^{+;\sigma}}{\left(\omega-sgn\left(\Xi_{-1}^{-;\sigma}\right)\omega_v-E_{-1}^\sigma+\omega_c/2\right)} \tag{3.100}$$

and

$$\Sigma_1^\sigma\left(\omega\right)=\frac{A_{1;2}^{+;\sigma}}{\left(\omega-sgn\left(\Xi_2^{+;\sigma}\right)\omega_v-E_2^\sigma-\omega_c/2\right)}+\frac{A_{0;1}^{+;\sigma}}{\left(\omega-sgn\left(\Xi_0^{-;\sigma}\right)\omega_v-E_0^\sigma+\omega_c/2\right)}. \tag{3.101}$$

To find the positions of the peaks, one solves (3.98). The solutions are clearly sensitive to the sign of $\Xi_{l'}^{\alpha;\sigma}\equiv E_{l'}^\sigma+\alpha\omega_c/2$. As we do not have an estimate for the actual strength of the Magnus effect, to be definite, we take $\omega_c=\eta\frac{\Delta^2}{\mu}$. It is a simple job to notice that $sgn\left(\Xi_1^{+;\sigma}\right)=sgn\left(\Xi_2^{+;\sigma}\right)=+$ and $sgn\left(\Xi_{-1}^{-;\sigma}\right)=-$, for any value of the chemical potential. The $l=0$ states have energies $E_0^\sigma=\sigma\frac{\Delta^2}{E_F}\left(-\frac{1}{2}+\frac{\phi(\mu)}{2\pi}\right)$. These energy levels may flow from negative to positive values (and vice versa) by changing the chemical potential, evolving

the Berry phase from 0 to $2\pi$. The sign of $\Xi_0^{-;\sigma}$ thus does depend on $\mu$. This allows one to define a value $\bar{\mu}_\sigma$ at which $sgn\left(\Xi_0^{-;\sigma}\right)$ changes. The structure of $\Sigma_1^\sigma(\omega)$ depends crucially on this. From the CdG spectrum (3.81), we set $\Xi_0^{-;\sigma}=0$ explicitly, finding

$$\begin{aligned} -\sigma+\left(\sigma\frac{\phi(\bar{\mu}_\sigma)}{\pi}-\eta\right) &= 0 \\ \Rightarrow \frac{\phi(\bar{\mu}_\sigma)}{\pi} &= 1+\eta\sigma, \end{aligned} \tag{3.102}$$

where $\phi(\mu)$ is the Berry phase. As this phase grows monotonically from 0 to $2\pi$, it is clear that the sector $\sigma=+$ has a sign change at values of $\mu$ larger than those of the $\sigma=-$ sector, as long as $\eta\neq 0$. In sum, this determines when each set of peaks will jump as function of $\mu$.

From this discussion we see there is a change of sign in the factors of $\omega_v$ in the self-energy given in 3.97 when $l^{'}=0$, which determines the energies of the satellite peaks. As a result, the topological phase transition manifests itself by a discontinuous change in the density of states by energies of order $\omega_v$ to energies of order $-\omega_v$. As we desired, the physics of the topological phase transition is sensitive to the vortex fluctuations, and vice-versa.

One also notes in passing that the Magnus force term associated with the vortex motion, whose amplitude is proportional to $\omega_c$, breaks the z-mirror symmetry of our 2D planar limit. This symmetry also connects the two particle-hole related sectors of the CdG modes. As a result, the discontinuous transition of energy of the CdG modes from the two $\sigma$ sectors does not happen simultaneously at the same value of doping for both sectors. The content of this claim is what equation (3.102) implies, remembering that $\eta$ controls the strength of $\omega_c$ relative to the CdG minigap. This effect is essential for the change in the LDOS to be seen in this context, as it provides an energy window over which the density of states at the energy of vortex oscillations is remarkably modified by the topological phase transition. As we see, the positions of the satellite peaks will move discontinuously, but the $\pm$ sectors compensate each other through the phase transition. The two sectors have "jumping" peaks which exchange place as they jump at the same value of the chemical potential if $\eta=0$ in (3.102). For finite $\eta$ the jumping of the peaks from each sector can be potentially seen at different values of the chemical potential.

We stress that this jumping peaks physics are a manifestation of the closing and reopening of the CdG modes gap as function of the chemical potential. It is a measurement that enforces that the CdG modes spectrum display a very specific behavior as function of doping and, knowing that the gap closes and reopens points to a signature of the topological phase transition for the non-interacting system. It is also important to note that for other CdG modes (such as the mode with $l=-1$ whose maximum amplitude is at $1/k_F\approx 10$Å away from the center of the vortex) the discontinuous changes in satellite peaks will also happen. Given the spatial resolution of STM, however, the different modes should be resolvable in the local tunneling conductance.

Figure 3.6 summarizes the main discussion above. It shows the differential conductivity at the vortex center $G(\mathbf{r}=0,\omega)$. The numerical values are the same from the previous diagonalization and were chosen to make the physics easier to discuss (they do not correspond to actual material values as we know that physically these effects are indeed weak). The large peaks closest to $\omega=0$ correspond to $\omega\approx E^\sigma_{l=0,1}$ demonstrating that the CdG LDOS spectrum at the vortex core display a particle-hole broken profile, with only peaks from $l=0$ and $l=1$ (peaks are shifted to zero and positive energies without their negative $\omega$ counterparts). The inset displays the satellite peaks. Angular momentum conservation implies that each non-interacting energy level unfolds into a set of three (faint) peaks.

We present the tunneling conductance for three ranges of chemical potential $\mu<\bar{\mu}_\pm$, in blue, and $\bar{\mu}_-<\mu<\bar{\mu}_+$, in red, and $\mu>\bar{\mu}_\pm$ in blue again, which appears to be identical to $\mu<\bar{\mu}_\pm$. This happens because the separation of the central peaks from $l=1$ is $E_1^+-E_1^+=\delta(-1/2+\phi(\mu)/2\pi)$, which cannot be resolved close to the phase transition (just as the peaks from $l=0$ cannot be resolved at this situation). Having a finite $\omega_c$ is crucial to observe all peaks and the discontinuous effects of the topological phase transition. The pattern in the LDOS should be of, for each $l$ and $\sigma$ sector, a large central peak located at $E_l^\sigma$ with two satellite partners. The partners are offset approximately by $\pm\Omega_l^\sigma$ with $\Omega_l^\sigma=\sqrt{(\omega_v+\delta+\omega_c/2)^2+2A_l^{+;\sigma}}$. In our case, a total of 12

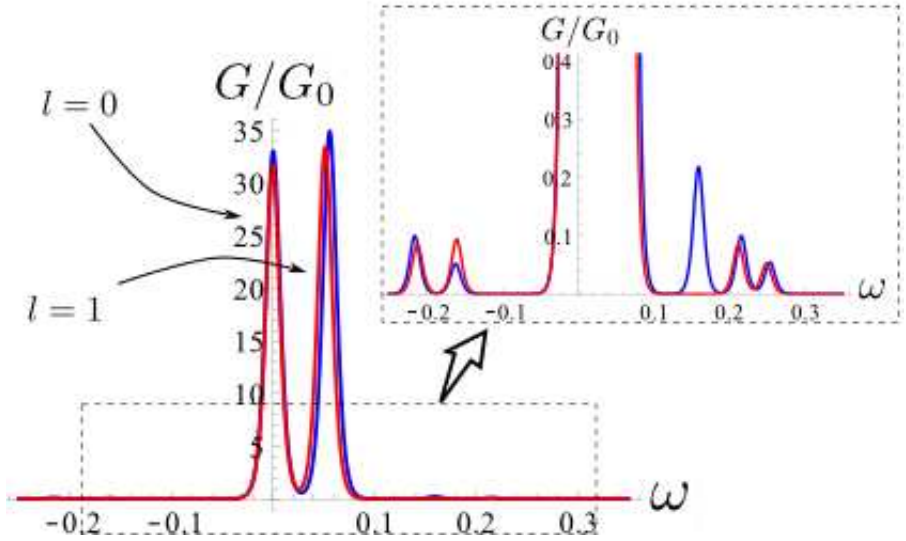


Figure 3.6: Tunneling conductance for $\mu < \bar{\mu}_\pm$, and $\mu > \bar{\mu}_\pm$ in blue, and $\bar{\mu}_- < \mu < \bar{\mu}_+$, in red. The large central peaks correspond to $\omega \approx E^\pm_{l=0}$ and $\omega \approx E^\pm_{l=1}$ (the energies of the CdG modes for stationary vortex). The inset displays the effects of vortex fluctuations.The smaller sattelite peaks appear at energies close to $\approx \pm\omega_v$. Red curves correspond to $\mu < \bar{\mu}_-$ or $\mu > \bar{\mu}_+$.

peaks are expected for each value of the chemical potential (3 from $l = 0$, another 3 from $l = 1$ and twice this due to the two sectors), not all of them being resolvable due to thermal effects. The strength of the respective satellite peaks is suppressed by a $\xi^{-5}$ factor, where $\xi$ is the coherence length [65]. This is a general consequence of our perturbative treatment and is also the reason why the satellite peaks are so faint for our system with large coherence length.

The jumping behavior develops in the $l = 1$ satellite peaks (the rightmost small peaks at both negative and positive frequencies as well as the lone blue peak.) This is evidenced by the solitary blue peak at positive $\omega$. It corresponds to the contribution coming from $\omega = E_1^- - \Omega_1^-$(right most peaks at negative energy), whose position jumps from this value by approximately $2\omega_v$ as the chemical potential pumps the negative energy state at $E_0^-$ into positive energies after crossing $\bar{\mu}_-$. Similarly, when $\mu$ moves above $\bar{\mu}_+$, the peak from $\omega = E_1^+ + \Omega_1^+$ jumps by $-2\omega_v$. In appendix A we demonstrate the approximate positions of the $l = 1$ peaks analytically.

Concerning the magnitude of the Magnus effect, if $\eta < 1$, the effects from the Magnus force are sub-dominant to the CdG energy gap and the sensibility to which one needs to tune the (zero-temperature) chemical potential may again be beyond technical realization at the current time. If $\eta > 1$, on the other hand, as the evolution of the Berry phase is from 0 to $2\pi$, the critical chemical potentials $\bar{\mu}_\sigma$ may not be captured as one tune $\mu$ and one will be always bound to the regime of $\bar{\mu}_- < \mu < \bar{\mu}_+$, which is similar to the standard s-wave case (except for the multiplicities of peaks and apparent breaking of the PH constraint.) This seems to critically constrain the actual visualization of these effects in practice.

### 3.5.2 1D wire network

As a final analysis, we will condense our findings about effective Kitaev wires in superconducting vortices and the effects of the vortex quantum motion in the vortex modes in a single scenario. We would like to use our learnings to speculate about the realization of signatures of topological phase transitions by quantum motion in truly 1D systems. We will thus use our concrete mapping between the vortex in superconducting doped topological insulators and Kitaev wires in the perturbed model of (3.80). We will clearly identify the important ingredients necessary to realize the discussed phenomena in the context of 1D topological systems.

We go back to our discussion following (3.58). Now we also keep the vortex fluctuations to first order in the

gradient of the superconducting pairing. We have

$$\begin{aligned} H_{BdG} &= H^0_{BdG,\perp} + H^0_{BdG,z} \\ &\quad -\mathbf{R}(\tau)\cdot[\mathbf{\Lambda}\cdot\partial_{\mathbf{r}}\mathbf{\Delta}(\mathbf{r})] \qquad (3.103) \\ &\equiv H^0_{BdG} + H_z + V(\mathbf{r}). \qquad (3.104) \end{aligned}$$

We are going to project this onto the lowest energy sectors $\chi^{\pm}_{ln}(\mathbf{r})$ from (3.59) and (3.60). At finite z, we have $\chi^{\pm}_{ln}(\mathbf{r}) \to \chi^{\pm}_{ln_{CdG}}(\mathbf{r}) f^{\pm}_l(z)$, choosing the CdG states with $n = n_{CdG}$. We will project the radial part the Hamiltonian to find out effective equations of motion for $f^{\pm}_l$. Considering the $\pm$ sectors then we have

$$\begin{aligned} \tilde{H}_{ll'} &= Proj\left[H_{BdG}\right]_{ll'} \qquad (3.105) \\ &= \begin{pmatrix} E^+_l & 0 \\ 0 & E^-_l \end{pmatrix}\delta_{ll'} \qquad (3.106) \\ &\quad + \begin{pmatrix} H^{++}_{zll'} & H^{+-}_{zll'} \\ H^{-+}_{zll'} & H^{--}_{zll'} \end{pmatrix} \qquad (3.107) \\ &\quad + \begin{pmatrix} V^{++}_{ll'} & 0 \\ 0 & V^{--}_{ll'} \end{pmatrix}. \qquad (3.108) \end{aligned}$$

We already know the results of projecting $H^0_{BdG,\perp} + H^0_{BdG,z}$ onto the vortex bound states basis. Now we project the vortex fluctuation terms. Notice that as $\langle\chi^+_l|\rho_x|\chi^-_l\rangle = \langle\chi^+_l|\rho_y|\chi^-_l\rangle = 0$, the fluctuating vortex potential becomes diagonal with respect to the $\pm$ sectors. This result is the same as we had found in our considerations at vanishing $k_z$ and we already know what this term looks like,

$$\begin{pmatrix} V^{++}_{ll'} & 0 \\ 0 & V^{--}_{ll'} \end{pmatrix} = \mathbf{R}(\tau)\cdot\mathbf{M}^{\sigma}_{l,l'} \qquad (3.109)$$

with

$$\begin{aligned} \mathbf{M}^{+}_{l,l'} &= \int d^2r\left[\mathbf{u}^+_l(\mathbf{r})^\dagger\,\partial_{\mathbf{r}}\Delta\mathbf{v}^+_{l'}(\mathbf{r}) + \mathbf{v}^+_l(\mathbf{r})^\dagger\,\partial_{\mathbf{r}}\Delta^\dagger\mathbf{u}^+_{l'}(\mathbf{r})\right] \qquad (3.110) \\ \mathbf{M}^{-}_{l,l'} &= \int d^2r\left[\mathbf{v}^+_l(\mathbf{r})^\dagger\,\partial_{\mathbf{r}}\Delta\mathbf{u}^+_{l'}(\mathbf{r}) + \mathbf{u}^+_l(\mathbf{r})^\dagger\,\partial_{\mathbf{r}}\Delta^\dagger\mathbf{v}^+_{l'}(\mathbf{r})\right]. \qquad (3.111) \end{aligned}$$

Due to the vortex structure in $\Delta$, we are only coupling $l$ to $l' = l \pm 1$.

Adding up the matrix elements from 3.109 to the Kitaev-chains network from 3.71 above gives the projected Hamiltonian for a set of, now hybridized, wires network

$$\begin{aligned} \tilde{H}_{ll'} &= \begin{pmatrix} E^+_l - \epsilon^+_l\partial^2_z & -i\tilde{\Delta}_l\partial_z \\ -i\tilde{\Delta}_l\partial_z & E^-_l + \epsilon^-_l\partial^2_z \end{pmatrix}\delta_{ll'} \qquad (3.112) \\ &\quad + \begin{pmatrix} \mathbf{R}(\tau)\cdot\mathbf{M}^+_{l,l'} & 0 \\ 0 & \mathbf{R}(\tau)\cdot\mathbf{M}^-_{l,l'} \end{pmatrix}. \qquad (3.113) \end{aligned}$$

For Hermiticity $\mathbf{M}^{\pm *}_{l,l'} = \mathbf{M}^{\pm}_{l',l}$. Thus, the vortex fluctuation physics gets mapped to a system of coupled 1D wires.

Likewise as above, the fluctuations may be written

$$\begin{aligned} &\begin{pmatrix} \mathbf{R}(\tau)\cdot\mathbf{M}^+_{l,l'} & 0 \\ 0 & \mathbf{R}(\tau)\cdot\mathbf{M}^-_{l,l'} \end{pmatrix} = \qquad (3.114) \\ &\mathbf{R}(\tau)\cdot\left(\frac{\mathbf{M}^+_{l,l'} + \mathbf{M}^-_{l,l'}}{2}\right)\rho_0 + \mathbf{R}(\tau)\cdot\left(\frac{\mathbf{M}^+_{l,l'} - \mathbf{M}^-_{l,l'}}{2}\right)\rho_z. \end{aligned}$$

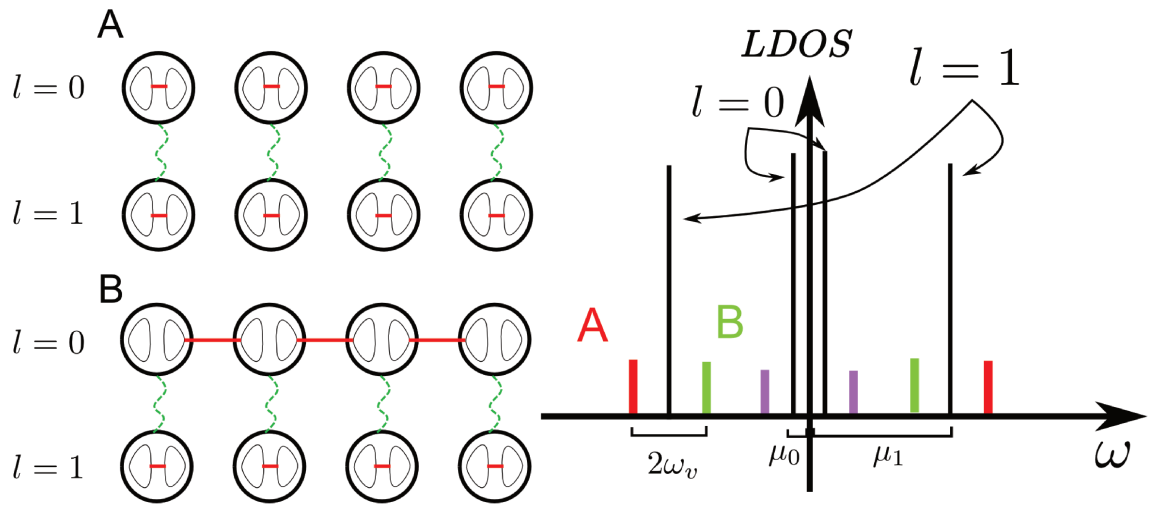


Figure 3.7: 1D chain minimal model to study topological phase transitions by quantum fluctuations. Large circles represent lattice complex fermions while the prolate circles represent the Majorana fermions inside. The $l = 0$ represents a Kitaev chain which we drive through a topological phase transition while $l = 1$ is kept at a finite gap. Situations A and B correspond to the two deep topological regimes. The chains sites couplings are represented by green wriggly lines while Majorana hoppings are represented by the red lines. On the right, we display an schematic picture of the LDOS for this system. Large black peaks correspond to the peaks at the energy gaps $\pm\mu_l$ with $k = 0$, dispersion effects are not considered. As there is a single fluctuating coupling between the chains, only a single satellite peak appears besides each $\pm\mu_l$. The purple peaks correspond to the satellite peaks of $\pm\mu_0$. The red and green peaks differ by $2\omega_v$, the fluctuation energy scale, and correspond to the two topological regimes A and B on the left figure. Even if the satellite peaks jump at the same time, since the energy gap from wire $l = 1$ is large, one may resolve the distinct situations with the satellite peaks "outside" or "inside" the peaks from $\pm\mu_1$ as in the A or B situations, respectively. Notice that PH symmetry is explicitly respected in this context.

They couple diagonally in the $\sigma = \pm$ indices and also bring up an apparently Nambu symmetry violating term $\rho_0$.

This is a very unusual network of p-wave chains, as particle-hole symmetry actually connects different wires while each wire has particle-hole symmetry actually broken. Although unusual, however, similar ideas have been considered in the literature [77]. It is remarkable, in any case, that the 3D physics we started with ends up in such an exotic 1D scenario.

From the above results, we may identify the minimal ingredients necessary to magnify the signatures of topological phase transitions in 1D systems by a mechanism analogous to the one considered in the vortex case. This minimal set of ingredients is reasonably undemanding. We list them in the context of Kitaev chains, as there seems to be a recent focus of interest in the literature concerning Kitaev wires networks (see [78], for example). We stress, however, that the same ingredients would suffice for other 1D topological systems, such as Su-Schrieffer-Heeger wires or Kitaev superconducting wires with multiple bands. In sum, one should look for at least:

1. A pair of gapped wires, one of which tunable through a TPT;

2. A diagonal fluctuating coupling between them;

With these, one may reconstruct the important features of Eqs.(3.112) and (3.114).

Notice that the broken (particle-hole) symmetry found in the projection on the vortex modes in the 3D scenario is not fundamental and is not included in our minimal list. It implies a shift of the peaks in the spectrum, like as in the large peaks from $l = 1$ in Fig. 3.6, and hence is unimportant in this context. Also, a single pair of Kitaev chains is enough (the effects from $l = 2$ and $l = -1$ in (3.100) and (3.101) are not important). This pair of wires could also be substituted by a single wire with a pair of low energy bands. The tight-binding model for this is written

$$H^l_{Kit} = -\mu_l \sum_j c^{l\dagger}_j c^l_j - \frac{1}{2}\sum_j \left( t_l c^{l\dagger}_j c^l_{j+1} + \Delta_l e^{i\phi_l} c^l_j c^l_{j+1} + H.c. \right), \tag{3.115}$$

where $\mu_l$ are the chemical potentials, $\Delta_l$ are superconducting pairings, with $\phi_l$ are the corresponding phases and $t_l$ the hopping amplitude for each wire. The index $l = 0, 1$ labels the two chains. Upon BdG doubling, it is easy to demonstrate that this reduces to (3.112) in k-space, without the $\rho_0$ term.

As for the fluctuation part of the Hamiltonian, one may have simply

$$U = \sum_j c^{0\dagger}_j \Phi(\tau)\, c^1_j + H.c., \tag{3.116}$$

for a fluctuating coupling $\Phi$. This should lead to similar self-energy corrections to the wires energies as (3.100) and (3.101), namely

$$\Sigma^\sigma_{0,k}(\omega) = \frac{A^\sigma_{0;1}}{\omega - sgn\left(E^{+;\sigma}_{1,k}\right)\omega_v - E^\sigma_{1,k}} \tag{3.117}$$

and

$$\Sigma^\sigma_{1,k}(\omega) = \frac{A^\sigma_{1;0}}{\omega - sgn\left(E^{-;\sigma}_{0,k}\right)\omega_v - E^\sigma_{0,k}}, \tag{3.118}$$

where $\sigma$ gives the two Nambu components. The fluctuation frequency $\omega_v$ of $\Phi$ determes the new large energy scale. To find the positions of the peaks, one solves again

$$\omega - E^\sigma_{l,k} - \Sigma^\sigma_{l,k}(\omega) = 0 \tag{3.119}$$

which now leads to a single satellite peak for each energy level. This situation is illustrated in Figure 3.7.

Importantly, the effects of a Magnus force analogous term are not necessary in the 1D scenario and, hence, a single fluctuating parameter is enough (for the vortex position, notice we had two, positions x and y of the vortex in the plane.) This happens because one may - by ramping up the chemical potential transversely to the wires, for example - keep a single wire well away from the phase transition with a large gap. Suppose, for example, wire $l = 1$ is kept with a large gap. In this case, the satellite peaks from the two sectors in this wire will stay always far away from each other. This way, by tuning the chemical potential from wire $l = 0$, one can verify its phase transition by probing for the jumping in the satellite peaks of wire $l = 1$.

As a final comment, out of the p-wave superconductivity context, one might work similarly with a set of Su-Schrieffer-Heeger spinless wires. In this case, the Hamiltonian will be similar to as the BdG Hamiltonian considered so far, with the caveat that the Nambu spinor now should be substituted by an ordinary spinor for a sublattice pseudo-spin degree of freedom. The gapping parameters in this case will be given by staggered hopping amplitudes and chemical potentials. Formally, the problem is the same and one may extend the results discussed so far to this situation.

## 3.6 Conclusions

Quantum fluctuations of vortex positions are ubiquitous and should manifest themselves at very low temperatures. We found out that, in the context of doped three dimensional topological insulators these fluctuations may be exploited to magnify the signatures of topological vortex quantum phase transitions. This displays, at the LDOS at the vortex core, energy peaks which discontinuously jump as function of the chemical potential. This finding also determined characteristic features of the low-energy Caroli-de Gennes-Matricon modes in this system which make them stand out as very distinct from standard s-wave Caroli-de Gennes modes, such as their spatial distribution and effects in the LDOS at the vortex core. Finally, our results also point to the possibility of capturing the effects of Magnus forces acting on the vortices, whose magnitude is directly related to the chemical potential values in which the topological phase transition induces peak position shifts.

The frequency of the position fluctuations plays an important role as it sets the scale of the peak jumps. In the context of high temperature superconductors, there are reports of this energy scale going up to meV [79]. It is important to point out that this frequency can be controlled to some extent and indeed increased depending on the properties of the vortex pinning potential. Recent developments in doping TIs with Niobium, which leads to the formation of magnetic moments in the bulk superconducting TI, can provide stronger pinning and so larger frequencies for the vortex fluctuation [80]. Measured physical values of the vortex fluctuation frequencies and Magnus force frequency in this system are not known to us at this point.

Cryogenic STM measurements are fundamental to uncover the discussed signatures. Situations with lighter and smaller vortices, whose zero-point motion effects would be stronger, could also be arranged as the vortex size is known to be strongly sensitive to temperature and magnetic field strength [81]. For vortices of too minute sizes, however, the Taylor expansion method deployed here to derive the interactions is not precise. In such cases, different approaches to the problem, such as used in [66], are necessary in order to obtain trustworthy predictions. Also, a proper account for the effects of dispersion along the vortex may need detailed attention. It is beyond the scope of this work to consider these.

Finally, we studied the local physics along the vortex core. Projecting the Hamiltonian with the Caroli-de Gennes-Matricon wavefunctions we demonstrated explicitly that the vortex line behaves as a Kitaev chain, with the corresponding topological phase transition. Further studying how the vortex position fluctuations are projected onto this system allowed us to find some key ingredients which one may use to obtain new signatures of topological phase transitions in one-dimension. A promising scenario lies in the study of the density of states upon fluctuations of the transverse coupling between a pair of neighboring gapped wires. Again, effects of dispersion along the wires still deserve proper attention.

This completes our thorough study of electronic vortex bound states in superconducting doped topological insulators.

# Chapter 4

# Vortex modes and topological superconductivity

We now move into the subject of topological superconductivity. As discussed, superconductors are gapped phases of matter and admit a topological classification of their distinct Hamiltonians at the mean-field level. Up to now we have discussed the 1D Kitaev p-wave superconducting chain as an example, as well as a manifestation of this same system in the context of doped topological insulators. We now turn to actual topological superconductivity in 3D.

We will stick to three spatial dimensions under time-reversal invariance, known as class DIII and $\mathbb{Z}$ classified (check the table at the introduction for reference). Our goal is to study the nature of the vortex bound modes in these systems, then following to a proposed effective (topological in nature) field theory description of this phase [34]. We will see that when both points of view are brought together, microscopy and field theory do not describe the same physics and a paradox arises. We offer a possible explanation for the paradox, based on the accepted notion that effective topological field theories should capture the most basic physical properties of a topological system, even in the interacting limit. Our approach, as usual, will not be general, considering the most arbitrary superconducting mean-field Hamiltonians. Instead we will introduce the important points out of a physical example and move from there.

## 4.1 Time-reversal invariant topological superconductivity

In three dimensions, under time-reversal invariance, topological superconductors consist of Hamiltonians in the so-called class DIII. These Hamiltonians are $\mathbb{Z}$ classified, the invariant counting the number of Majorana-Dirac cones on the sample 2D surfaces. Line defects - vortices - in these systems break time-reversal invariance and Hamiltonians in the presence of such defects also admit a topological classification [12]. They are then in class D, due to the broken time-reversal invariance and are again integer classified, the integer counting the number of Majorana *chiral* modes along a given vortex.

A representative Hamiltonian in class DIII is given by

$$H = \frac{1}{2}\sum_{\mathbf{k}} \left(c^\dagger_{\mathbf{k}}, c_{-\mathbf{k}}\right) \begin{pmatrix} h_{\mathbf{k}} & \Delta_{\mathbf{k}} \\ \Delta^\dagger_{\mathbf{k}} & -h^T_{-\mathbf{k}} \end{pmatrix} \begin{pmatrix} c_{\mathbf{k}} \\ c^\dagger_{-\mathbf{k}} \end{pmatrix} \tag{4.1}$$

where $h_{\mathbf{k}}$, $\Delta_{\mathbf{k}}$ are $N \times N$ matrices respecting $\mathcal{T}^\dagger h^*_{\mathbf{k}} \mathcal{T} = h_{-\mathbf{k}}$ and $\mathcal{T}^\dagger \Delta^*_{\mathbf{k}} \mathcal{T} = \Delta_{-\mathbf{k}}$ . Here $T = \mathcal{T}K$ is the time-reversal operator with $K$ being complex conjugation and $\mathcal{T}$ is the corresponding time-reversal Bloch matrix, a representation for which will be shown specifically below.

A topological invariant characterizing such Hamiltonians can be simply defined in the weak pairing limit [82]. One assumes that the pairing strength is small as compared to the kinetic energy $h_{\mathbf{k}}$. This justifies studying the low energy physics close to the different Fermi surfaces. The topological invariant characterizing

the Hamiltonian in this case may be computed as

$$N = \frac{1}{2}\sum_n C_{1n} sgn\left(\Delta_{n\mathbf{k}}\right) \tag{4.2}$$

where $C_{1n}$ are so-called the Chern numbers,

$$C_{1n} = \frac{1}{2\pi}\int_{\Sigma_n} d\Omega^{ij}\left(\partial_i a_j - \partial_j a_i\right), \tag{4.3}$$

fixed by the momentum-space Berry phase with connection $a_i = \langle n\mathbf{k}|\,\partial_{k_i}\,|n\mathbf{k}\rangle$. Most importantly,

$$\Delta_{n\mathbf{k}} = T\left(\{\langle n\mathbf{k}|\}\right)\Delta_{\mathbf{k}}\,|n\mathbf{k}\rangle\,, \tag{4.4}$$

is a projected superconducting pairing at the Fermi surface of the non-interacting Hamiltonian. The choice $T\left(\{\langle n\mathbf{k}|\}\right)$ for wavefunction at $-\mathbf{k}$ avoids the ambiguity in gauge choice of the wavefunction, making $\Delta_{n\mathbf{k}}$ a real quantity. This quantity does not change sign, on a given Fermi surface, as function of $\mathbf{k}$ in a fully gapped superconductor (notice that there is an ambiguity in defining $\mathcal{T} \to -\mathcal{T}$. This makes topological superconductors with $N$ and $-N$ equivalent physically.)

The minimal model now is given by a $2\times 2$ (in spin space) p-wave Hamiltonian

$$\begin{aligned} h_{\mathbf{k}} &= \frac{\mathbf{k}^2}{2m} - \mu + \alpha\boldsymbol{\sigma}\cdot\mathbf{k} && (4.5)\\ \Delta_{\mathbf{k}} &= i\Delta_0\sigma_y\boldsymbol{\sigma}\cdot\mathbf{k}. && (4.6)\end{aligned}$$

Here, $\alpha \neq 0$ lifts the degeneracy between the two Fermi surfaces but is not a mandatory parameter. The time-reversal Bloch matrix is implemented by $\mathcal{T} = i\sigma_y$ while Nambu particle-hole comes from $\rho_x$.

As a check for time-reversal symmetry,

$$\begin{aligned} \mathcal{T}^\dagger h^*_{\mathbf{k}}\mathcal{T} &= -i\sigma_y\left[\frac{\mathbf{k}^2}{2m} - \mu + \alpha\boldsymbol{\sigma}\cdot\mathbf{k}\right]^* i\sigma_y\\ &= \sigma_y\left[\frac{\mathbf{k}^2}{2m} - \mu + \alpha\boldsymbol{\sigma}^*\cdot\mathbf{k}\right]\sigma_y\\ &= \frac{\mathbf{k}^2}{2m} - \mu - \alpha\boldsymbol{\sigma}\cdot\mathbf{k}\\ &= h_{-\mathbf{k}}. \end{aligned} \tag{4.7}$$

Similarly,

$$\begin{aligned} \mathcal{T}^\dagger \Delta^*_{\mathbf{k}}\mathcal{T} &= -i\sigma_y\left[i\Delta_0\sigma_y\boldsymbol{\sigma}\cdot\mathbf{k}\right]^* i\sigma_y\\ &= \sigma_y\left[i\Delta_0\sigma_y\boldsymbol{\sigma}^*\cdot\mathbf{k}\right]\sigma_y\\ &= -\left[i\Delta_0\sigma_y\boldsymbol{\sigma}\cdot\mathbf{k}\right]\\ &= \Delta_{-\mathbf{k}}. \end{aligned} \tag{4.8}$$

Physically, if $\alpha = 0$, this is the Helium-3B Hamiltonian [83]. That works in the context of superfluidity. We will keep in mind a solid state realization of this Hamiltonian, for example in the context of the recently discovered Weyl semi-metallic systems [84]. For this, we may enforce the weak-pairing condition, looking for a minimal low-energy description. We may, thus, diagonalize the normal part of the BdG Hamiltonian above -

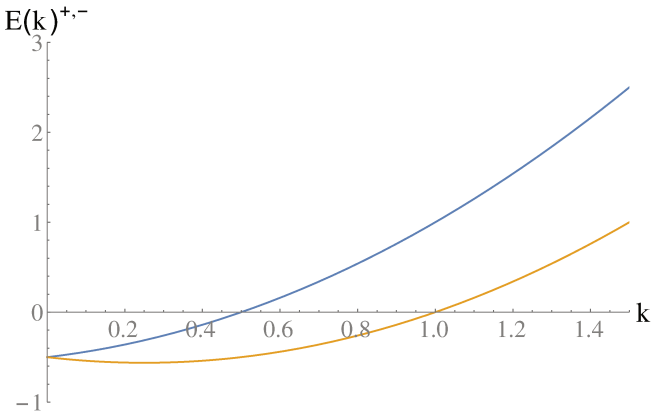


Figure 4.1: Spectrum of the metallic Hamiltonian (4.5). We use $\alpha = 0.5$ and $\mu = 0.5$. There are two spherical Fermi surfaces.

namely $h_{\mathbf{k}}$ - which has two bands,

$$E^{\pm}_{\mathbf{k}} = \frac{|\mathbf{k}|^2}{2m} - \mu \pm \alpha |\mathbf{k}| \tag{4.9}$$

$$= \frac{(|\mathbf{k}| \pm \alpha m)^2}{2m} - \frac{\alpha^2 m}{2} - \mu. \tag{4.10}$$

These bands are described at Fig.4.1 for some general parameters. Solving for $E^{\pm}_{\mathbf{k}_F} = 0$, constraining $k_F > 0$, gives us the Fermi surfaces as function of the chemical potential. Completing the squares in the energies above shows that we have two spheres of different radii,

$$k^{\pm}_F = \mp m\alpha + \sqrt{m^2\alpha^2 + 2m\mu}. \tag{4.11}$$

As the definite energy states are the eigenstates of $\boldsymbol{\sigma} \cdot \mathbf{k}$, it is easy to give a qualitative description of the topological invariant in this system. Chern numbers are defined from the winding of the Hamiltonian as one wraps the momentum space. As eigenstates of $\boldsymbol{\sigma} \cdot \mathbf{k}$ we see that the two Fermi surfaces have opposite helicities, thus with opposite Chern numbers, fixing $C_{1+} = -C_{1-} = 1$. Also, the projected pairings also have definite, and opposite, signs - still due to the chirality argument - and $sgn\left(\Delta_{+\mathbf{k}}\right) = -sgn\left(\Delta_{-\mathbf{k}}\right) \equiv sgn\left(\Delta_0\right)$. Thus,

$$N = \frac{1}{2}\left[1 - (-1)\right] \mathrm{sgn}\Delta_0 = \mathrm{sgn}\Delta_0. \tag{4.12}$$

As a check, let us now compute again the topological invariant explicitly from the formula. In the weak pairing limit, we may project the Hamiltonian around each Fermi surface. The eigenstates of the kinetic Hamiltonian (4.5) are obtained as

$$U^{\dagger} h_{\mathbf{k}} U = \begin{pmatrix} \frac{|\mathbf{k}|^2}{2m} - \mu + \alpha |\mathbf{k}| & \\ & \frac{|\mathbf{k}|^2}{2m} - \mu - \alpha |\mathbf{k}| \end{pmatrix} \tag{4.13}$$

$$\equiv \begin{pmatrix} E^{+}_{\mathbf{k}} & \\ & E^{-}_{\mathbf{k}} \end{pmatrix} \tag{4.14}$$

where

$$U = \left(|\mathbf{k}+\rangle \, |\mathbf{k}-\rangle\right) \tag{4.15}$$

$$= \frac{1}{\sqrt{2\,|\mathbf{k}|\,(|\mathbf{k}| + k_z)}} \begin{pmatrix} |\mathbf{k}| + k_z & -k_x + ik_y \\ k_x + ik_y & |\mathbf{k}| + k_z \end{pmatrix}. \tag{4.16}$$

The states then satisfy $\boldsymbol{\sigma}\cdot\mathbf{k}\,|\mathbf{k}\pm\rangle = \pm\,|\mathbf{k}|\,|\mathbf{k}\pm\rangle$. This fixes the computation of the Chern number automatically and $C_{1,\pm} = \pm 1$. As for the "time-reversal projected pairing,

$$\begin{aligned}\Delta_{\pm,\mathbf{k}} &= T\left(\{\langle\pm,\mathbf{k}|\}\right)\Delta_{\mathbf{k}}\,|\pm,\mathbf{k}\rangle \\ &= \langle\pm,-\mathbf{k}|\,(-i\sigma_y)\,i\Delta_0\sigma_y\boldsymbol{\sigma}\cdot\mathbf{k}\,|\pm,\mathbf{k}\rangle \\ &= \mp\frac{\Delta_0 k_z^2}{2\left(k_x^2+k_y^2\right)^4},\end{aligned} \tag{4.17}$$

which, as promised, has definite sign throughout the k-space, fixed by the sign of $\Delta_0$ (an extra minus sign can be absorbed in the definition of the time-reversal operator, as discussed.)

Now that we know that the weak-pairing limit of the BdG Hamiltonian generated by (4.5) and (4.6) indeed satisfies our topological criteria, we may push the description of this system at low-energy further. First we have a "regular" projection of the pairing terms (i.e. no application of time reversal operation, as in (4.4), just regular perturbation theory)

$$\begin{aligned}\Delta_{k_F^\pm} &= \left\langle\pm k_F^\pm\right|\Delta_{\mathbf{k}_F}\left|\pm k_F^\pm\right\rangle \\ &= \left\langle\pm k_F^\pm\right|i\Delta_0\sigma_y\boldsymbol{\sigma}\cdot\mathbf{k}_F\left|\pm k_F^\pm\right\rangle \\ &= \pm\Delta_0 k_F^\pm i\sigma_y.\end{aligned} \tag{4.18}$$

The metallic Hamiltonian, then projected at each band $E_{\mathbf{k}}^\pm$ close to its respective Fermi energy, $\mathbf{k} = \mathbf{k}_F^\pm + \delta\mathbf{k}$, gives to first order in the momenta

$$\begin{aligned}&\begin{pmatrix} E_{\mathbf{k}}^+ & \\ & E_{\mathbf{k}}^- \end{pmatrix} \\ \approx\ &\begin{pmatrix} (1+\alpha m)\,\frac{\mathbf{k}_F^+\cdot\delta\mathbf{k}}{m} & \\ & (1-\alpha m)\,\frac{\mathbf{k}_F^-\cdot\delta\mathbf{k}}{m} \end{pmatrix} \\ =\ &\begin{pmatrix} (1+\alpha m)\left[v_F^+ k-\mu^+\right] & \\ & (1-\alpha m)\left[v_F^- k-\mu^-\right] \end{pmatrix}\end{aligned} \tag{4.19}$$

where $\mu^\pm \equiv v_F^\pm k_F^\pm$. Linearly dispersing Fermi surfaces with non-trivial Chern numbers are equivalent to Weyl fermions ("half" a massless Dirac fermion.) The present Fermi surfaces are clear examples, with fixed spin helicity.

Renaming the two Fermi surfaces by $+\equiv R$ and $-\equiv L$, the weakly-coupled and low-energy limit of the Hamiltonians (4.5) and (4.6) is then summarized by the following Hamiltonians

$$H = \begin{pmatrix} H_R & \\ & H_L \end{pmatrix}, \tag{4.20}$$

where

$$\begin{aligned}H_R &= \sum_{\mathbf{k}}\psi_{R\mathbf{k}}^\dagger\left[v_F^R\boldsymbol{\sigma}\cdot\mathbf{k}-\mu_R\right]\psi_{R\mathbf{k}} \\ &\quad+\frac{1}{2}\sum_{\mathbf{k}}\left[\Delta_R\psi_{R-\mathbf{k}}^\dagger i\sigma_y\psi_{R\mathbf{k}}^\dagger + H.c.\right]\end{aligned} \tag{4.21}$$

$$\begin{aligned}H_L &= \sum_{\mathbf{k}}\psi_{L\mathbf{k}}^\dagger\left[-v_F^L\boldsymbol{\sigma}\cdot\mathbf{k}-\mu_L\right]\psi_{L\mathbf{k}} \\ &\quad+\frac{1}{2}\sum_{\mathbf{k}}\left[\Delta_L\psi_{L-\mathbf{k}}^\dagger i\sigma_y\psi_{L\mathbf{k}}^\dagger + H.c.\right].\end{aligned} \tag{4.22}$$

This implies that the low energy physics of time-reversal invariant topological superconductors can be captured by a pair of *Weyl fermions gapped by s-wave superconductivity*. The recent experimental observation of Weyl semi-metals, allied to the fact that s-wave superconducting pairings are the least exotic in 3D, implies that this is a convenient platform to study topological superconductivity at the present times. The caveat is that the topological regime is fixed by the relative phases of $\Delta_R$ and $\Delta_L$. For $\Delta_R \sim \Delta_L$, the system is trivial, while $\Delta_R \sim -\Delta_L$ the system is topologically non-trivial. This behavior is more exotic. This is the solid state realization of topological superconductivity that we will keep in mind.

Notice that a very unusual scenario thus arises. Superconductivity is a phase of matter whose interpretation "a la Landau" (that is, spontaneous symmetry breaking) is that of U(1) symmetry breaking. Given a set of fermionic metallic degrees of freedom, there is a single definition of electric charge, and a single U(1) symmetry which can be broken. Therefore, the phases of $\Delta_R$ and of $\Delta_L$ must be locked to each other. In principle, a constant full $\pi$ phase-shift between the two projected pairings is not prohibited throughout the system. Yet, what would happen at the interface between a topologically trivial and another topologically non-trivial superconductor in class DIII (or even the vacuum)?

A first possibility would come from the vanishing of all Chern numbers in the trivial side of the interface. This allows for a change in the topological invariant (4.2) from a given finite value, at the topological side, to zero in the trivial side. A topological phase transition for a gapped Hamiltonian, however, only happens under the closing and subsequent reopening of the bulk system's gap. Another way to think of this, is that the protection of Weyl points in semi-metals is local, not global as in insulators - that is, for insulators, topology arises from the full Brillouin zone - such that the distinction between the inside and outside of a topological semi-metal is not the same as for an insulator. The superconducting system is gapped, and at the surface, gapless modes must arise, the bulk band Weyl points having no relation to this.

The only possibility for the trivialization of the topological invariant at a surface of a topological superconductor is then if the sign of one of the superconducting pairings, say $\Delta_L$, changes as one crosses the surface's interface. The sign of the pairing projected at the other surface, say $\Delta_R$, cannot change together, as the topological invariant would then remain the same [82]. One can say that the surface of a topological superconductor "deconfines" the phases of the superconducting pairings. In particular, one can envisage using these deconfined phases to create so-called "chiral vortices", that is, superconducting vortices in which the pairing projected at only a single Fermi surface winds [34].

Our objective now is to explore this notion of deconfined phases from the projected pairings focusing on chiral vortices. This concept is exotic and its understanding and realization meets inconsistencies. We will try to solve these or analyze them, in order to realize if this scenario is possible or not, and also if they say something more profound about these states of matter.

As a final comment, let us introduce the BdG representation of our superconducting gapped Weyl modes. The Hamiltonians read, respectively

$$H^R_{BdG} = \frac{1}{2}\Psi^\dagger_R \left[v^R_F \mathbf{\Gamma}\cdot\mathbf{k} - \rho_z\mu_R + \Delta_R\Lambda_1\right]\Psi_R \tag{4.23}$$

$$H^L_{BdG} = \frac{1}{2}\Psi^\dagger_L \left[-v^L_F \mathbf{\Gamma}\cdot\mathbf{k} - \rho_z\mu_L + \Delta_L\Lambda_1\right]\Psi_L \tag{4.24}$$

where the Nambu spinors are (omitting the spin d.o.f.) $\Psi_i^T = \left(\psi_{i,\mathbf{k}}, i\sigma_y\psi^\dagger_{i,-\mathbf{k}}\right)$, $i = R, L$, and the matrix representation is given by

$$\mathbf{\Gamma} = \rho_z\boldsymbol{\sigma} \tag{4.25}$$

$$\Lambda_1 = \rho_x\sigma_0 \tag{4.26}$$

$$\Lambda_2 = \rho_y\sigma_0. \tag{4.27}$$

In this basis, TR is given by $\Theta = i\sigma_y K$ and PH is expressed by $\Xi = \rho_y \sigma_y K$. These have become what may be called "Nambu-Dirac" fermions, that is, massive Dirac Fermions (at vanishing doping) whose gap is given by a superconducting pairing. In the high-energy literature, an equivalent system is known as a "Weyl fermion with Majorana mass". Such a description may be obtained by decomposing the complex Dirac fields into Majorana operators as was done in the Kitaev chain context.

### 4.1.1 Class DIII defect bound states

Most important for the discussions to come are the bound states for the class DIII topological superconductors in (3+1)D. These appear at defect structures, regions of the space in which the superconducting pairing may vanish and arise as a realization of the bulk-boundary correspondence. We study, quite generally, the Hamiltonian of a single Fermi surface with a space-time dependent pairing term,

$$h_{BdG} = v_F \mathbf{\Gamma} \cdot \mathbf{P} - \rho_z \mu + \mathbf{\Delta}(\mathbf{X}) \cdot \mathbf{\Lambda}, \tag{4.28}$$

where $\mathbf{P}$ and $\mathbf{X}$ are the momentum and position operators. The signs of $v_F$ and overall phase of $\mathbf{\Delta}$ then fix the different chiralities/Fermi surfaces.

When the pairing is spatially homogeneous and the system is infinite, the spectrum reads

$$E^{\pm}_{\mathbf{k}} = \pm\sqrt{\left(v_F |k| - \mu\right)^2 + |\Delta|^2}. \tag{4.29}$$

This is equivalent to a topological insulator surface gapped by superconductivity, with the caveats that for a bulk Weyl semi-metal we have a pair of Dirac cones and that the momentum-space is 3D. The chemical potential is meaningless, from the topological point of view. As we show in Appendices B and C, towers of CdG vortex bound states arise in this system for any value of the chemical potential, so we drop $\mu$ generally in the present simple discussions. This, of course, is valid only for such doping values so that the band structure maintains its Weyl semi-metal spectrum.

As a warm-up, we will thus consider states bound to domain-wall structures in $\mathbf{\Delta}(\mathbf{X})$, showing the Majorana character of the surface gapless states. The most important bound states for us, however, arise at line-defects, vortices in the superconducting pairing, our already discussed Caroli-de Gennes modes, which we discuss subsequently.

#### 4.1.1.1 Domain-wall/surface bound states

To study surface states, as usual in the context of topological insulators, one studies an homogeneous and isotropic Hamiltonian in two directions, say yz, while introducing a kink in the "mass term" along the third direction. This simulates the closing and re-opening of the bulk gap across the surface. For the present case, we write (we emphasize, for a single Fermi surface)

$$\tilde{h}_{BdG} = -iv_F \Gamma_x \partial_x + \Delta \Lambda_1 e^{i\rho_z \phi}, \tag{4.30}$$

where we took a vanishing chemical potential $\mu = 0$. Here $\Delta_y/\Delta_y = \tan\phi$ gives the superconducting phase phase. A domain wall is simulated by having, for exaple $\phi(\mathbf{r}) : \pi \to 0$ as $x : -\infty \to \infty$. For simplicity, let us just consider $\phi = \pi$, if $x < 0$ and $\phi = 0$ if $x > 0$ such that

$$\Delta \to \begin{cases} \Delta & , x > 0 \\ -\Delta & , x < 0 \end{cases}. \tag{4.31}$$

Then one looks for eigenstates such that

$$\tilde{h}_{BdG} \psi(x) = \tilde{E}_n \psi(x). \tag{4.32}$$

The most interesting states are the zero-energy ones, which obey

$$\left[\partial_x - \frac{\Delta_x}{v_F}\rho_y\sigma_x\right]\psi(x) = 0. \tag{4.33}$$

This suggests two possibilities, from eigenmodes with negative eigenvalues of $\rho_y\sigma_x$,

$$\psi_1(x) = e^{-i\pi/4}\frac{e^{-\int^x dx'\frac{\Delta(x)}{v_F}}}{\sqrt{\mathcal{N}}}\begin{pmatrix}0\\ i\\ 1\\ 0\end{pmatrix}, \tag{4.34}$$

$$\psi_2(x) = e^{-i\pi/4}\frac{e^{-\int^x dx'\frac{\Delta(x)}{v_F}}}{\sqrt{\mathcal{N}}}\begin{pmatrix}1\\ 0\\ 0\\ -i\end{pmatrix}. \tag{4.35}$$

The arbitrary global phases $e^{-i\pi/4}$ were introduced by convenience, such that Particle-hole symmetry implies

$$\Xi\psi_1 = \psi_1 \tag{4.36}$$

$$\Xi\psi_2 = \psi_2. \tag{4.37}$$

Notice that, fundamentally, the full system with two Fermi surfaces should have two low energy states to generate the Majorana cone. Indeed, a domain-wall at a single Fermi surface is enough to provide with the necessary modes.The pairing of only *one* of the Fermi surfaces may be allowed to change sign across the surface( we stress again, otherwise equation (4.2) would give topologically non-trivial regimes on both sides of the gap kink.)

For completeness, let us study the second quantized operators associated with these. For an infinite system in $y, z$, we may expand

$$\begin{aligned}\Psi(\mathbf{x}) &= \sum_n \int_k \psi_n(x)\, e^{i(k_y y + k_z z)}\gamma_{n\mathbf{k}}(x)\\ &\approx \int_k \psi_1(x)\, e^{i(k_y y + k_z z)}\gamma_{1\mathbf{k}}(x) &(4.38)\\ &\quad + \int_k \psi_2(x)\, e^{i(k_y y + k_z z)}\gamma_{2\mathbf{k}}(x), &(4.39)\end{aligned}$$

keeping only the low energy sector of bound states. This implies

$$\gamma_{1\mathbf{k}}(x) = \int dydz\psi_1^\dagger(x)\,\Psi(\mathbf{x})\, e^{-i\mathbf{k}\cdot\mathbf{x}} \tag{4.40}$$

$$\gamma_{2\mathbf{k}}(x) = \int dydz\psi_2^\dagger(x)\,\Psi(\mathbf{x})\, e^{-i\mathbf{k}\cdot\mathbf{x}} \tag{4.41}$$

with $\mathbf{k} = (k_y, k_z)$ only. This means

$$\gamma_{1\mathbf{k}}(x) = e^{i\pi/4}\frac{e^{-\int_0^x dx'\frac{\Delta(x)}{v_F}}}{\sqrt{\mathcal{N}}}\left[-i\psi_{\downarrow\mathbf{k}}(x) + \psi^\dagger_{\downarrow-\mathbf{k}}(x)\right] \tag{4.42}$$

$$\gamma_{2\mathbf{k}}(x) = e^{i\pi/4}\frac{e^{-\int_0^x dx'\frac{\Delta(x)}{v_F}}}{\sqrt{\mathcal{N}}}\left[\psi_{\uparrow\mathbf{k}}(x) - i\psi^\dagger_{\uparrow-\mathbf{k}}(x)\right] \tag{4.43}$$

The Majorana character of these operators is clear. One has that

$$\gamma_{1\mathbf{k}}^{\dagger} = \gamma_{1-\mathbf{k}} \tag{4.44}$$
$$\gamma_{2\mathbf{k}}^{\dagger} = \gamma_{2-\mathbf{k}}, \tag{4.45}$$

as desired.

Expanding the field operators in this low-energy sector leads to the projected surface Hamiltonian

$$h_{surface}^{0} = v_F \left[\tau_x k_y - \tau_z k_z\right], \tag{4.46}$$

where $\tau$ Pauli matrices live in the space of the two Majorana modes. The corresponding second quantized Hamiltonian reads

$$H_{surface}^{0} = \int d^2x \Gamma_{-\mathbf{k}}^{T} v_F \left[\tau_x k_y - \tau_z k_z\right] \Gamma_{\mathbf{k}} \tag{4.47}$$

where $\Gamma_{\mathbf{k}} = (\gamma_{1\mathbf{k}}, \gamma_{2\mathbf{k}})^T$. This Hamiltonian describes "Majorana Weyl cones" at the sample surface; Weyl as there is a single chirality of Fermions, cone due to the linearly dispersion gapless spectrum and Majorana due to the Hermiticity conditions on the fermion operators.

#### 4.1.1.2 Vortices bound states: chiral-modes

Vortices develop as string-like defects in the pairing. These can only happen, in principle, for both Fermi surfaces at the same time, as there is a single U(1) symmetry for both Fermi surfaces. As we explained, however, there is a proposal to deconfine the vortex lines from the $R$ and $L$ contributions (using the interfaces of topological and trivial s-wave superconductors [34].) We will then consider what type of bound states arises in vortices for each Fermi surface separately. We start considering only the lowest energy states.

Let us focus on a single Fermi surface with a vortex along the $z$ direction and at vanishing chemical potential $\mu$, for simplicity. We will ignore the possible effects of magnetic fields inside the vortices. This can be justified in the extreme type-II superconductor limit, which is usually consider for studying Caroli-de Gennes modes. The justification is as follows. The vortex core size scales as the coherence length $\sim \xi$. Supercurrents around vortices in type II superconductors decay with the London length $\lambda$. The standard computation by Abrikosov for extreme type II SCs says that, around a vortex, the magnetic field follows a profile

$$B(r) = \frac{\Phi_0}{2\pi\lambda^2} K_0(r/\lambda), \tag{4.48}$$

where $K_0$ is a Bessel function of the second kind. For large distances compared to the coherence length, this decays as $\sqrt{\lambda/r}e^{-r/\lambda}$ [75]. For smaller distances, $\xi < r < \lambda$, this has a log-behavior which diverges as $r \to 0$. In reality, however, for $r \lesssim \xi$

$$H(0) \approx \frac{\Phi_0}{2\pi\lambda^2} \ln\kappa = const. \tag{4.49}$$

where $\kappa = \lambda/\xi$. This regime with constant field is the one of our concern for the analysis of electronic bound states inside the vortex region. One then has to compare energy scales. From dimensional grounds, electromagnetic gauge field behaves as $A \sim Hr$. Then, $A/\nabla\theta \to eA/c\hbar\nabla\theta \sim (H/\Phi_0) r^2$. For our regime $r \lesssim \xi$

$$eA/c\hbar\nabla\theta \sim (H/\Phi_0)\xi^2 \sim H/H_{c2}, \tag{4.50}$$

where $H_{c2}$ is the upper critical field. In the extreme type-II limit, $H/H_{c2} \ll 1$ and the effects of external magnetic fields can be neglected [67].

We can follow the calculation of the zero-energy bound modes without further worries. The pairing reads, in the presence of a vortex

$$\mathbf{\Delta}\cdot\mathbf{\Lambda} = |\Delta|\,\Lambda_1 e^{i\rho_z\theta}, \tag{4.51}$$

where $\theta$ is the polar angle of cylindrical coordinates and $|\Delta|$ has some tanh profile, for concreteness. The spin-orbit and superconducting phase dependencies in $\theta$ may be unwound by

$$\psi(r,\theta,z) = e^{i\left(l-\frac{\rho_z+\sigma_z}{2}\right)\theta} e^{ik_z z}\phi(r). \tag{4.52}$$

To satisfy the periodic boundary conditions $\psi(r,\theta+2\pi)=\psi(r,\theta)$, we have *integer values* $l$. Turning off $k_z$ to focus on the planar bound states, the BdG equations reduce to

$$\begin{aligned}&\left[-iv_F\rho_z\left[\sigma_x\partial_r + i\sigma_y\frac{l-(\rho_z+\sigma_z)/2}{r}\right]+|\Delta|\rho_x\right]\phi_n\\ &= E_{ln}\phi_n.\end{aligned} \tag{4.53}$$

Again, we are particularly interested in the very lowest degrees of freedom. We thus may set $l=0$. Zero-energy solutions again exist. We thus solve

$$\left[\partial_r + \frac{\rho_z\sigma_z+1}{2r} - \frac{|\Delta|}{v_F}\rho_y\sigma_x\right]\phi(r) = 0. \tag{4.54}$$

A *single* wavefunction solution exists (in contrast to the single Fermi surface analysis of domain walls)

$$\psi_0(r,\theta) = e^{-i\pi/4}\frac{e^{-\int_0^r dr'\frac{|\Delta|}{v_F}}}{\sqrt{\mathcal{N}}} e^{-i\left(\frac{\rho_z+\sigma_z}{2}\right)\theta}\begin{pmatrix}0\\ i\\ 1\\ 0\end{pmatrix} \tag{4.55}$$

$$= e^{-i\pi/4}\frac{e^{-\int_0^r dr'\frac{|\Delta|}{v_F}}}{\sqrt{\mathcal{N}}}\begin{pmatrix}0\\ i\\ 1\\ 0\end{pmatrix}. \tag{4.56}$$

Again,

$$\Xi\psi_0 = \psi_0. \tag{4.57}$$

Recovering a finite $k_z$, the second quantized operator corresponding to this state reads

$$\gamma_{k_z}(r) = \frac{e^{-\int_0^r dr'\frac{|\Delta|}{v_F}}}{\sqrt{\mathcal{N}}} e^{-i\pi/4}\left[\psi_{\downarrow k_z} + i\psi^\dagger_{\downarrow -k_z}\right], \tag{4.58}$$

with fixed $l=0$ for the angular momentum quantum number, and obeys $\gamma^\dagger_{k_z} = \gamma_{-k_z}$. The corresponding projected Hamiltonian into this low-energy sector is chiral and reads

$$h^0_{vrtx} = -iv_F\partial_z. \tag{4.59}$$

This is what happens for a winding of the superconducting pairing projected at a single Fermi surface. Our minimal model has two disconnected contributions $R$ and $L$, with opposite chirality in the kinetic terms and a possible $\pi$ phase difference between the superconducting pairings of the two Fermi surfaces. This means that the introduction of a vortex in the superconducting pairing for the other Fermi surface can be accounted for with another bound state substituting $|\Delta| \to -|\Delta|$ and $v_F \to -v_F$ in the solutions above. We see that the result for the lowest energy bound state is the same.

From the same arguments above, if the pairing in the other Fermi surface also winds, applying $v_F \to -v_F$ in (4.59) gives a counter propagating mode. This means that for vortices, the nature of the bound states can be separated in two distinct situations:

- Regular vortices

For regular vortices, the projections of the superconducting pairing at both Fermi surfaces wind together. This leads to a pair of counter propagating states with Hamiltonian

$$h_v = \int dz \begin{pmatrix} \gamma_R & \gamma_L \end{pmatrix} \begin{pmatrix} -iv_R\partial_z & M \\ M^* & +iv_L\partial_z \end{pmatrix} \begin{pmatrix} \gamma_R \\ \gamma_L \end{pmatrix}. \tag{4.60}$$

As time-reversal symmetry is broken due to the vortex, a finite backscattering probability may exist, leading to a finite mass $M$. The Majorana modes can be mixed and gapped. This is the same as saying that a regular vortex corresponds to a trivial class D system.

- Chiral vortices

For chiral vortices the situation is different from the one above. Again time-reversal symmetry is broken by vorticity, but the single chiral Majorana mode that arises is protected from back scattering (as there is no counter propagating mode to scatter into.) The Hamiltonian reads

$$h_v^i = \int dz \gamma_i \left(-iv_i\partial_z\right) \gamma_i, \tag{4.61}$$

where $v_i = v_R$ *or* $v_i = -v_L$ for a given chirality label $i$. Only a single of them will exist at a time and this corresponds to a non-trivial class D system, with a protected chiral vortex modes which cannot backscatter.

Our previous results call for an "index theorem". These are topological numbers which count the number of chiral modes for Dirac-like operators. For the states along our vortices, we may write that the total number of *chiral* modes $N_v$ are determined by

$$N_v = C_{1R}N_R + C_{1L}N_L, \tag{4.62}$$

where $C_{1,R/L}$ are the first Chern numbers from the Weyl parent metal and $N_{R/L}$ are the phase windings of the SC phase at each Fermi surface. From Nielsen-Ninomiya's theorem, we know that $C_{1R} = -C_{1L}$ and we may summarize this as

$$N_v = C_{1R}\left(N_R - N_L\right). \tag{4.63}$$

Indeed, this quantity was actually previously known in the high energy community and is called the "Weinberg index".

Actually, our analysis of regular vortices leaves some untied points. In particular, the Hamiltonian (4.60) implies that regular vortices inserted in topological superconductors in the non-trivial and trivial phases have no distinct behavior (notice that it makes no sense to talk about chiral vortices in topologically trivial and non-trivial scenarios, as they exist at the interface of both). This is a proper place for an analysis of open systems now (along the vortex direction) to try and make a distinction between these. This will be qualitative.

Vortices in real materials must terminate at a surfaces. While they are exponentially localized in the bulk due to the superconducting gap, one can imagine tracing continuations of the vortex bound states at the surface. These must exist because there will be paths along the surface through which the value of the superconducting phase will be arbitrarily close to the time-reversal invariant values of 0 and $\pi$. Interestingly, these define chiral vortices at the surfaces, as sketched in Figs. (4.2) and (4.3). On surfaces, however, the pairing phases fluctuate away from these time-reversal respecting special values and one can imagine that the lines of chiral modes are more diffuse (in the sense of having families of co-propagating modes).

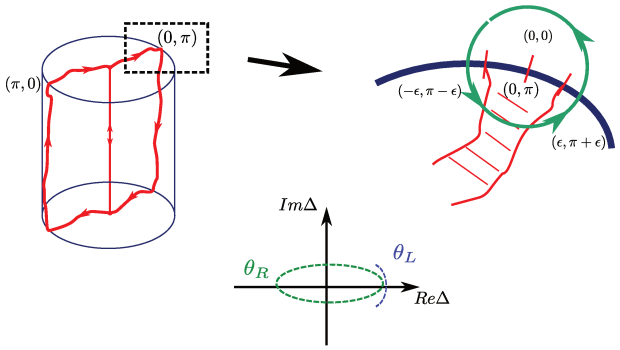


Figure 4.2: Description of surface modes for a regular vortex inserted in a class DIII superconductor in a topologically non-trivial regime. The pairs or numbers correspond to the phases of the two Fermi surfaces, $(\theta_L, \theta_R)$. As one winds through the material around the vortex, anti-podal regions of the phases are close to the time-reversal invariant values of $(0,\pi)$and $(\pi,0)$. The vortex through the bulk is exponentially localized due to the bulk gap, but at the surface, a quasi-1D region, of small width, can carry sets of quasi-chiral modes. The net effect is as described in the picture and shows that, effectively, the surface displays a chiral vortex-like structure due to the phase windings. The reasoning for topologically trivial bulks, as well as for chiral vortices are analogously explained.

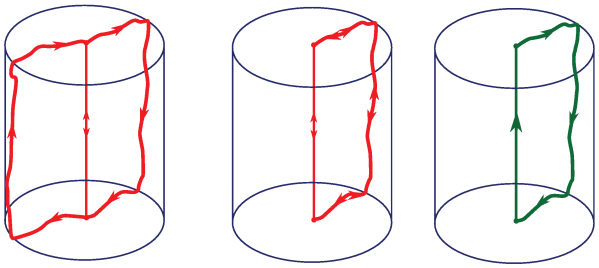

Figure 4.3: Possibilities for the surface modes and vortex modes. From left to right we have a regular vortex in a topologically non-trivial system, a regular vortex in a topologically trivial system and a bulk chiral vortex. The first case one the left describes that a regular vortex inserted in a topologically non-trivial system generates chiral modes and chiral vortices at the boundary separating in two quasi-1D regions of chiral modes. For a regular vortex, it extends into the surface with helical, not chiral modes, which can actually gap in the presence of time-reversal breaking terms. Finally, a chiral vortex in the bulk should extend as a line of chiral modes through the complete surface.

Concretely, we adopt a description of the bulk superconducting order by a bi-vector $(\theta_L, \theta_R)$ with the superconducting phases of the projected pairing at each Fermi surface. For a topologically trivial system, a regular vortex is introduced such that $\theta_R - \theta_L = 0$. For a topologically non-trivial system, the regular vortex must have a winding which maintains $\theta_R - \theta_L = \pi$. This behavior must follow through to the surface; in this case, regions close to the values $(0,\pi)$ or $(\pi,\pi)$ of the phases present also a vortex-like winding, now with respect to the topologically trivial vacuum. These allow for quasi-1D channels for chiral Fermions to move. The topological state has a regular vortex which separates into two chiral ones at the surface. The trivial state leads to a "regular" channel with helical modes (remember that helical modes can actually be gapped under time-reversal breaking conditions and really correspond to no modes.) Finally, chiral vortices extend as channels of the same chirality to the surface. Again, these possibilities are represented pictorially in Fig.4.3.

While the reasoning for this is completely qualitative, topology enforces that this is very likely the physical reality.

#### 4.1.1.3 Vortex - full spectrum

We are finally ready to discuss the full spectrum of vortex bound states in class DIII. The building block comes from the vortices in the winding of the pairing of a single Fermi surface. We show in the Appendices B and C, both analytically and numerically, that at $k_z = 0$ and with a vortex along the z direction, the spectrum for a

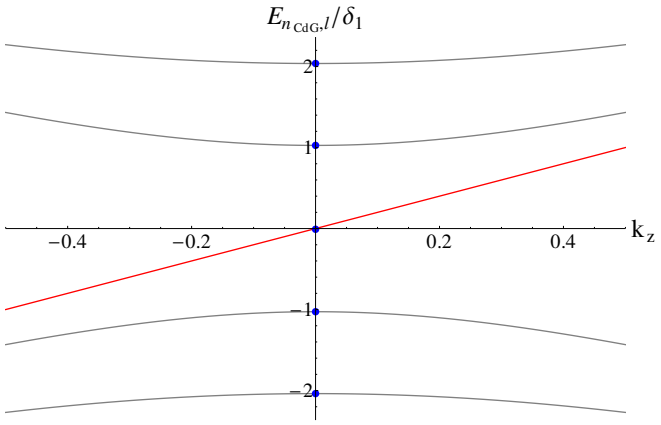


Figure 4.4: Numerically derived spectrum of the vortex-bound states as function of $k_z$, details follow in the appendix. We show the states corresponding to $l = -2, -1, 0, 1, 2$. $l = 0$ has a chiral behavior. The level spacing is set by the mini-gap $\delta_1 = \Delta_0^2/E_F$. The blue dots correspond to numerical solutions of the planar "Nambu-Dirac" Hamiltonian in the presence of a vortex, while the full lines follow from our perturbative arguments and the Hamiltonian $\tilde{h}_z$.

single Weyl cone is given by

$$E_n \approx \frac{\Delta_e}{k_F} n \equiv \frac{\Delta_e^2}{E_F} n. \tag{4.64}$$

This result is shown to be true for any value of chemical potential. In Appendix C we also demonstrate the result for finite $k_z$ (which is treated perturbatively), reading

$$\tilde{h}_z = \int dk_z \gamma_{-k_z} \gamma_{k_z} k_z \tag{4.65}$$

$$+ \sum_{n>0} \int dk_z c^\dagger_{k_z n} c_{k_z n} \sqrt{(k_z)^2 + \delta_n^2} \tag{4.66}$$

$$- \sum_{n<0} \int dk_z c^\dagger_{k_z n} c_{k_z n} \sqrt{(k_z)^2 + \delta_n^2}. \tag{4.67}$$

Here, $\delta_n = n \times \Delta_0^2/E_F$ with integer $n$ describes the Caroli-de Gennes minigap and we set, for convenience, the velocities to 1 (the correct values for the projected velocities can be found in the appendix, but are not important.) In Fig. 4.4 we plot the spectrum with dispersion along the vortex direction for a few of the tower of bound states.

From this spectrum, it is important to notice that one has a set of (mini-)gapped hyperbolic-dispersing modes. One can think of this as a set of massive Dirac fermions in 1D. Even more important is the $n = 0$ mode. This mode has two important points. First, it consists of a set of Majorana modes, $\gamma^\dagger_{k_z} = \gamma_{-k_z}$. Second, they are chiral-dispersing, with energies $\sim k_z$, along the vortex. These are the previously discussed "Majorana chiral modes".

Dirac equations in the presence of string-like defects in the mass (known as axion fields in the high-energy physics community) are known to bind chiral complex fermionic modes [85]. The superconducting Weyl modes described by (4.28) indeed correspond to a set of massive Dirac fermions. The caveat is that the particle-hole constraint from the BdG Hamiltonian cuts the number of degrees of freedom in by half, with respect to regular Dirac particles. The chiral complex fermionic modes, in this context, become real (one may neglect, say, the imaginary part of the complex fermion operators.) As such, we have the above Majorana chiral modes.

The interplay of bulk scattering states, line-defect chiral modes and electromagnetism is very rich. Such is the subject of "axion electrodynamics" and the Callan-Harvey "anomaly-inflow" mechanism [86, 85]. These, in the context of superconductivity (or Majorana-like mass for Weyl fermions) will be the subject of the next sections.

## 4.2 Electrodynamics and vortex modes

We have learned that vortices in topological superconductors bind a set of states which extend along the vortex. The winding of the superconducting phases leads to a tower of such states and dispersion along the vortex indicates that each Fermi surface contributes with a set of (mini-)gapped modes with hyperbolic dispersion, plus a chiral "real" fermionic mode. For chiral vortices, a single chiral mode exists, while, for regular vortex, the lowest energy states will have two opposite-moving branches and will be non-chiral.

Let us move into discussing the interaction between these electronic bound modes and electromagnetism. As we emphasized, the chiral modes, the lowest energy states, are described by "real" operators. The fact that their creation and annihilation operators are equivalent implies that these states are electromagnetically neutral. This can be seen by minimally coupling the Hamiltonian to the electromagnetic potentials as

$$\begin{aligned} h_{BdG} &= v_F \mathbf{\Gamma} \cdot \mathbf{P} + \mathbf{\Delta}(\mathbf{X}) \cdot \mathbf{\Lambda} && (4.68) \\ &\quad -v_F e \rho_z \mathbf{\Gamma} \cdot \mathbf{A} + e \rho_z A_0. && (4.69) \end{aligned}$$

We repeat the in-plane zero-energy state from before,

$$\psi_0(r,\theta) = e^{i\pi/4} \frac{e^{-\int_0^r dr' \frac{|\Delta|}{v_F}}}{\sqrt{\mathcal{N}}} \begin{pmatrix} 0 \\ 1 \\ -i \\ 0 \end{pmatrix}. \tag{4.70}$$

This can be used to project the Hamiltonian as

$$\tilde{h}_{z,0} = v_F k_z - v_F e \langle \rho_z \mathbf{\Gamma} \cdot \mathbf{A} \rangle + e \langle \rho_z A_0 \rangle. \tag{4.71}$$

Defining the spinor,

$$u_1 = \frac{1}{\sqrt{2}} \begin{pmatrix} 0 \\ i \\ 1 \\ 0 \end{pmatrix}, \tag{4.72}$$

however, shows that

$$\begin{aligned} u_1^\dagger \rho_z u_1 = u_2^\dagger \rho_z u_2 &= 0 && (4.73) \\ u_1^\dagger \rho_z \mathbf{\Gamma} u_1 = u_2^\dagger \rho_z \mathbf{\Gamma} u_2 &= 0. && (4.74) \end{aligned}$$

This means that the chiral modes along the vortex do not couple to electromagnetism. Indeed, a complete projection with the gapped vortex modes (see Appendix C) reads

$$\begin{aligned} \tilde{h}_z &= \sum_{k_z} k_z c_{k_z 0}^\dagger \tau_z c_{k_z 0} && (4.75) \\ &\quad + \sum_{l>0} \sum_{k_z} c_{k_z l}^\dagger \tau_0 c_{k_z l} \sqrt{\left(k_z + \tilde{A}_z\right)^2 + \delta_l^2} && (4.76) \\ &\quad - \sum_{l<0} \sum_{k_z} c_{k_z l}^\dagger \tau_0 c_{k_z l} \sqrt{\left(k_z - \tilde{A}_z\right)^2 + \delta_l^2}. && (4.77) \end{aligned}$$

Here, $\tilde{A}_z$ is the corresponding component of the vector potential averaged in the planar direction perpendicular to the vortex (assumed along z) and we absorbed the charges in the definition of the gauge field.

In what follows, we will describe a general effective field theory to describe the bulk of class DIII supercon-

ductors in the presence of electromagnetic interactions and vortices. Importantly, an "axion-electrodynamics" term ($\mathbf{E}\cdot\mathbf{B}$ action) arises, with the superconducting phase difference between the different Fermi surfaces playing the role of the axion field. We will then show that this effective theory is anomalous at chiral vortex cores. While for regular Dirac fermions such anomaly can typically be canceled by the, also anomalous, 1D chiral theory along the line-defect, in the present situation, the neutrality of the chiral modes will render the theory ill defined.

### 4.2.1 Class DIII electromagnetic response

Coupling the class DIII topological superconductor to electromagnetism allows us to study the system from an effective field theory point of view. In principle, in the presence of vortices and if the fluctuations of the superconducting density magnitude are suppressed, one may approximate the partition function of this problem, in the presence of an electromagnetic gauge field as

$$\mathcal{Z}\left[A\right] \approx \mathcal{Z}_{bulk}\left[A\right]\mathcal{Z}_{vortex}\left[A\right]. \tag{4.78}$$

This is true for weak enough electromagnetic fields; in this case, scattering between the largely gapped scattering states from the bulk and the mini-gapped bound states are not promoted. One may separate the contributions from the corresponding partition functions.

Reference [34] proposes an effective action for the bulk terms. It is given by the following expression

$$\begin{aligned} S_{eff-bulk}\left[A,\Phi\right] &= \int_x \left[\frac{\epsilon^{\sigma\mu\lambda\nu}}{2\times 8\pi^2}\partial_\sigma\left(\theta_L-\theta_R\right)A_\mu\partial_\lambda A_\nu + J\cos\left(\theta_L-\theta_R\right)\right. \\ &\left. +\frac{1}{2}\rho_L\left(\partial_\mu\theta_L-2A_\mu\right)^2+\frac{1}{2}\rho_R\left(\partial_\mu\theta_R-2A_\mu\right)^2-\frac{1}{4e^2}F_{\mu\nu}F^{\mu\nu}\right]. \end{aligned} \tag{4.79}$$

The second line contains the regular Higgs and Maxwell terms for a superconductor. The first line contains a pair of unusual contributions. The first term corresponds to the expected "axion-electrodynamics" contribution, expected from the Weyl fermions at the bulk. The second term is a Josephson like term which binds and confines the phases of the pairing projected at the two Fermi surfaces. This term would arise from studying the action at larger energy scales and considering the coupling between the two Fermi surfaces. The mass scale of the mode $\theta_L-\theta_R$ is $m^2\sim 2J/\rho$. For the action to be valid, this mass must be smaller than the pairing strengths at the two Fermi surfaces (notice that only the difference $\theta_L-\theta_R$ is massive, phases can fluctuate in separate at low energy cost, as long as they do not excite this mode.) On interfaces between topologically distinct phases, one enforces that $J$ change signs.

Two comments are in order, regarding this action. Firstly, it was derived by [34] via an indirect "dimensional-reduction" argument, that is, not through actual fermionic integration given a microscopic model in the presence of the gauge field. Second, the axion term carries an extra factor of 1/2 with respect to the typical result for, say, topological insulators.

As for $\mathcal{Z}_{vortex}\left[A\right]$, our previous discussion about the electric neutrality of the chiral modes shows that at very low energy (neglecting the mini-gapped states), the action for the vortex bound states is simply described by

$$S_{ZM}^{vrtx}=\sum_j\int d^2x\gamma_j\left[i\partial_t+iv_j\partial_z\right]\gamma_j, \tag{4.80}$$

where $j$ is summed over all the Fermi surfaces, $v_j$ has a sign which depends on the chirality of the Fermi surface and $\gamma_j$ are Majorana Fermion (real) Grassmann variables. As the Fermions are neutral, integration over the Grassman fields give no contribution to the electromagnetic action whatsoever. Notice that the other mini-gapped modes are charged and do interact with the electromagnetic fields; as they are not chiral, however, we do not expect them to contribute in any special way to the full electromagnetic action that was not included in

(4.79) .

It is worth to point out that chiral (Weyl) fermions are typically U(1) anomalous. This means that, although their Hamiltonians obey a U(1) charge conservation symmetry, quantum fluctuations (fermionic Jacobian from U(1) transformations, mathematically) generates electromagnetic gauge dependent terms. From the point of view of the continuity equation, charge conservation is broken, and charge accumulates in the system with time.

Such chiral theories, fortunately, do not arise by themselves in nature, only in defects embedded in larger systems. In such cases, the content of the so called "Callan-Harvey mechanism" is that the seemingly anomalous chiral theory is actually receiving charge from the larger bulk in which it is embedded [85]. For this to happen, the axion term from the bulk and the gauge anomalous term from the defect in (4.78) must compensate each other.

A problem arises now. For complex fermions, the charge non-conserving terms due to anomalous chiral theories and bulk axionic terms indeed cancel each other, giving a well-defined theory. In the present superconducting context, however, the bulk term $S_{axion}$ will imply charge pumped at the vortex. The vortex chiral modes, however, are neutral, and do not couple to electromagnetism, they do not see this charge build up. This is a paradox. We explain this in details in what follows.

**Full electromagnetic action - gauge paradox** Let us study once again the effects of the axion electrodynamics action proposed by [34] in this superconducting context. The equations of motion,

$$\frac{\delta S_{eff}\left[A,\Phi\right]}{\delta A_{\mu}}=0, \tag{4.81}$$

should give Maxwell's equations and matter currents. Due to the Meissner effect (Higgs modes), of the vortex cores the $F_{\mu\nu}F^{\mu\nu}$ term may be discarded. The equations of motion then imply, in the vicinities of the vortices

$$-2\rho_{L}\left(\partial_{\mu}\theta_{L}-2A_{\mu}\right)-2\rho_{R}\left(\partial_{\mu}\theta_{R}-2A_{\mu}\right) \tag{4.82}$$

$$+\frac{1}{8\pi^{2}}\epsilon^{\mu\nu\lambda\rho}\partial_{\nu}\left(\theta_{L}-\theta_{R}\right)\partial_{\lambda}A_{\rho}=0. \tag{4.83}$$

From the physics in the absence of the topological term, one may identify the electromagnetic current

$$\left\langle J_{\mu}\right\rangle =2\rho_{L}\left(\partial_{\mu}\theta_{L}-2A_{\mu}\right)+2\rho_{R}\left(\partial_{\mu}\theta_{R}-2A_{\mu}\right) \tag{4.84}$$

and the equations of motion reads

$$\left\langle J^{\mu}\right\rangle \quad=\quad\frac{1}{8\pi^{2}}\epsilon^{\mu\nu\lambda\rho}\partial_{\nu}\left(\theta_{L}-\theta_{R}\right)\partial_{\lambda}A_{\rho}. \tag{4.85}$$

Vortices or domain walls fix the behavior of the superconducting phase. We focus in the different vortex scenarios (all along the z direction):

- Regular vortex

$$\left[\partial_{x},\partial_{y}\right]\theta_{R} \quad=\quad 2\pi\delta\left(x\right)\delta\left(y\right) \tag{4.86}$$

$$\left[\partial_{x},\partial_{y}\right]\theta_{L} \quad=\quad 2\pi\delta\left(x\right)\delta\left(y\right) \tag{4.87}$$

- Chiral L vortex (similar for chiral R vortex)

$$\left[\partial_{x},\partial_{y}\right]\theta_{R} \quad=\quad 0 \tag{4.88}$$

$$\left[\partial_{x},\partial_{y}\right]\theta_{L} \quad=\quad 2\pi\delta\left(x\right)\delta\left(y\right). \tag{4.89}$$

Now we can remind ourselves of some facts of axion electrodynamics. In terms of the electromagnetic fields,

the current can be written

$$\langle J^{\mu}\rangle = \frac{1}{2}\frac{1}{8\pi^2}\epsilon^{\mu\nu\lambda\rho}\partial_{\nu}\left(\theta_L-\theta_R\right)F_{\lambda\rho}. \tag{4.90}$$

From the point of view of the continuity equation, this reads

$$\begin{aligned}\partial_{\mu}\langle J^{\mu}\rangle &= \frac{1}{2}\frac{1}{8\pi^2}\epsilon^{\mu\nu\lambda\rho}\partial_{\mu}\partial_{\nu}\left(\theta_L-\theta_R\right)F_{\lambda\rho}. &(4.91)\\ &\equiv \frac{1}{2}\frac{1}{4\pi}J_v^{\lambda\rho}F_{\lambda\rho}, &(4.92)\end{aligned}$$

where we write generally $J_v^{\lambda\rho}=\frac{1}{2\pi}\epsilon^{\mu\nu\lambda\rho}\partial_{\mu}\partial_{\nu}\left(\theta_L-\theta_R\right)$ for the vortex current. Integrating this expression out we have

$$\begin{aligned}\int d^4x\partial_{\mu}\langle J^{\mu}\rangle &= \frac{1}{2}\frac{1}{4\pi}\int d^4xJ_v^{\lambda\rho}F_{\lambda\rho}\\ \Rightarrow Q\left(t_f\right)-Q\left(t_i\right)+\int dtd\vec{S}\cdot\left\langle\vec{J}\right\rangle &= \frac{1}{2}\frac{1}{4\pi}\int d^4xJ_v^{\lambda\rho}F_{\lambda\rho}. &(4.93)\end{aligned}$$

For an infinite system, we neglect $\int dtd\vec{S}\cdot\left\langle\vec{J}\right\rangle=0$. Also, for vortices along $z$, $J_v^{z0}=-J_v^{0z}$ and $J_v^{\mu\nu}=0$ otherwise.

For *regular* vortices,

$$\frac{1}{4\pi}J_v^{\lambda\rho}F_{\lambda\rho},=\frac{1}{2\pi}\left[\delta^2\left(\mathbf{x}\right)-\delta^2\left(\mathbf{x}\right)\right]F_{0z}=0. \tag{4.94}$$

No charge is induced at the vortex by the axionic term and the total charge in the system is conserved

$$Q\left(t_f\right)=Q\left(t_i\right). \tag{4.95}$$

On the other hand, for an L *chiral* vortex, $J_v^{0z}=\delta^2\left(\mathbf{x}\right)$ and

$$\partial_{\mu}\langle J^{\mu}\rangle=\frac{1}{2}\frac{1}{2\pi}\left[\delta^2\left(\mathbf{x}\right)\right]F_{0z}. \tag{4.96}$$

Integrating, again in infinite space,

$$Q\left(t_f\right)-Q\left(t_i\right) = \frac{1}{2}\int\frac{dtdz}{2\pi}E_z\left(0,0,z,t\right). \tag{4.97}$$

Indeed, chiral vortices violate charge conservation in the presence of an electric field along the vortex line.

This is actually a known result of axion electrodynamics. Piercing an axion string with an electric field induces accumulation of charge in the system. This charge is well localized at the string position. Typically, chiral charged modes see this accumulation of charge, manifesting it in the form of an anomalous partition function. Notice that under a gauge transformation $A\to A+\partial\chi$, the axion action changes as

$$\begin{aligned}\delta S_{eff}\left[A,\theta\right] &= -\frac{1}{2}\frac{1}{4\pi}\int dzdt\chi F_{0z}\\ &\quad -\frac{1}{2}\frac{1}{8\pi^2}\lim_{\rho\to 0}\int dS_{\mu}\epsilon^{\sigma\mu\lambda\nu}\left(\chi\partial_{\sigma}\theta\partial_{\lambda}A_{\nu}\right)\\ &= -\frac{1}{2}\frac{1}{4\pi}\int dzdt\chi F_{0z}. &(4.98)\end{aligned}$$

Indeed, we verify that gauge invariance is broken at the vortex line.

Another point that we have not discussed comes from the, apparently innocuous, factor of $1/2$ present in the axion term in (4.79). The typical axion electrodynamics has a twice as large coefficient. In the original work regarding the electromagnetic response in class DIII in 3D[34], this factor of $1/2$ was said to indicate that only "half" a fermion exists in the vortex, in the form of a Majorana fermion. We have seen that, although true, this

is not a good enough justification for the validity of the action (4.79), the Callan-Harvey anomaly inflow is not at play in this situation. We will see that this factor hints to a possible solution for this paradox and a proper justification for such an effective electromagnetic action.

## 4.3 Vortex linking and $\mathbb{Z}_4$ pumps

In order to explore the paradoxical result of charge non-conservation at a chiral vortex implied by the effective electromagnetic action (4.79), let us consider a topological superconductor in class DIII in 3D with a single chiral vortex line pierced by a uniform and constant electric field. Quite generally, the Hamiltonian for the tower of vortex bound states reads

$$\tilde{h}_z = \sum_{k_z} k_z c^\dagger_{k_z 0} \tau_z c_{k_z 0} \tag{4.99}$$

$$+ \sum_{l>0} \sum_{k_z} c^\dagger_{k_z l} \tau_0 c_{k_z l} \sqrt{(k_z + Et)^2 + \delta_l^2} \tag{4.100}$$

$$- \sum_{l<0} \sum_{k_z} c^\dagger_{k_z l} \tau_0 c_{k_z l} \sqrt{(k_z - Et)^2 + \delta_l^2}, \tag{4.101}$$

where $E$ is the magnitude of the electric field along z.

The main difference between the Majorana case, versus regular complex chiral modes, is that in the latter case, the chiral part of the Hamiltonian would also have $k_z \to k_z + Et$. This is the fundamental point of anomaly inflow. On the one hand, the bulk action induces a charge current into the string defect, when in the presence of an electric field along the defect (as suggested by (4.97), remembering that in the complex case, there is one *less* factor of 1/2 in the expression). On the other hand, the 1D localized states would have their momenta shifted by the constant electric field. While the gapped hyperbolic states will move conserving the number of occupied modes, the chiral states move in a single k-direction, in such a way that the system has to build up charge (received from the bulk) to keep the same number of states occupied. This is the microscopic concept of anomaly inflow that justifies the anomalous chiral theories in 1D, when embedded in a larger (3D) system. There have been suggestions in high energy physics that, cosmologically, this could be a possible mechanism to explain baryogenesis (see [87] for recent considerations and [83] for a condensed matter point of view.)

In the present situation, the chiral modes are neutral. Their momenta do not flow with the action of a constant electric field. As we discuss now, however, the fact that the chiral modes are neutral does not mean that they are blind to the presence of the electric field through the chiral vortex.

The charge non-conservation equation reads

$$\Delta_t Q = \frac{1}{2} \int \frac{dtdz}{2\pi} E_z. \tag{4.102}$$

In a periodic system, the momenta are discretized. In fact, comparing the charge of the system at different times only makes sense if the Hilbert space is the same. This thus defines a period for time evolution of the system in the presence of an electric field, in which we have to consider the imbalance from (4.102). From the gapped vortex modes, the period for time evolution of the Hamiltonian is $T = \frac{2\pi\hbar c}{eEL}$, where $E$ is the magnitude of the electric field and $L$ is the size of the system along the vortex direction. This is the time which shifts the momenta of the gapped modes along the loop, $k_z = n2\pi/L$, by exactly one quantum, leaving the Hilbert space invariant. Plugging in $\Phi_B = \int \mathbf{B} \cdot d\mathbf{S}$ for a magnetic flux *around* the vortex, and using Faraday's law, one may rewrite the charge variation as

$$\Delta_t Q = \frac{e}{2} \frac{\Delta_t \Phi_B}{2\pi}, \tag{4.103}$$

where $hc/2e \equiv \pi$ the superconducting flux quantum. Here, the flux is considered in a surface around the loop (half a cross section of the sample.) We are, thus, exchanging the physics of a constant field along the

vortex by that of building up in time a magnetic flux around the vortex. In fact, $\Delta_t \Phi_B = ELT$. This corresponds to building a $\Delta_t \Phi_B = 2\pi \frac{\hbar c}{e} = hc/e = 2\pi$ flux around the vortex. Encircling the vortex with twice the superconducting flux quantum completes a 'pumping' cycle for the momenta of the "mini-gapped" vortex states.

In sum, following the charge build up, the lattice implies a period of time evolution which shows that, at each cycle, a total of $\Delta_T Q = e/2$ is generated. It is only reasonable to compare the charge in the system after such periodic time evolutions. So the gapped modes seem to show that half-charges are pumped into the vortex at each cycle, even though the neutral modes of the vortex do not see this. This reasoning relies, however, only on the periodic evolution defined by the (mini-)gapped modes. What can we say about the Majorana chiral modes?

The effect of piercing a loop of chiral Majorana fermions by a unit of the superconducting magnetic flux quantum is known to induce a change in the periodicity of the fermionic functions, from anti-periodic to periodic [30]. Thus, the introduction of a pair of fluxes seems to also create a cycle in which anti-periodic boundary conditions change into periodic ones (which allows for a $k_z = 0$ mode) and back to its original anti-periodic value. The question would then be, is the new ground state the same as the original one? In fact, Majorana fermions must always exist in pairs (in our geometry, an anti-vortex is assumed at radial infinity.) Such an evolution between different boundary conditions changes the parity of the ground state. This effect is very similar to the discussion of Majorana modes bound to weak links in Josephson junctions, which define $4\pi$ periodic Josephson effects. This comes from the fact that the existence of Majorana zero-mode pairs define non-locally a pair of degenerate ground states (indexed by the, conserved, system's parity). In this case, it could be expected that the true period for time evolution of our system, due to the Majorana chiral mode, would be twice as large, such that

$$\Delta_T Q = e. \tag{4.104}$$

As regular superconducting vortices carry $\pi$ fluxes, we can think of a vortex linking picture. A single linking of the vortices correspond to a time evolution over $T/2$ and implies a change in the Majorana fermions boundary conditions. A double linking (link and unlink) would correspond to a time evolution over a time equals to $T$ above. This means that a 4-fold linking (corresponding to a $4\pi$ flux or $2T$ time-period) is necessary to return the ground state to its original profile.

This hints at a promising idea to solve the paradox. Effective topological actions are known to describe the true quasi-particle structure of topological phases, even in the presence of interactions. All of our discussions up to now where in the non-interacting limit. If there exists any constraint in the ground state of this problem which defines a true $4T$ periodicity in the time evolution, a total of $2e$ charge can be pumped through the system. Indeed, such a charge can be absorbed by the superconducting condensate, and corresponds to a "no pump" effect. This could solve the apparent ill definition of (4.79). In other words, if the Hilbert space structure defines that pumped charges can only be compared at each cycle of $8\pi$ flux quanta, we see that the effective action (4.79) is actually well defined, as it implies pumps of Cooper pairs, which can be absorbed in the superconducting condensate.

To be able to look for such physics, we need to define a "parity pump", which requires another set of Majorana modes, to realize a two-level system. The encircling magnetic field picture for the constant electric field scenario supplies for this second set of modes (technically a regular magnetic flux carries non-chiral fermions, but the two chiralities have disjoint Hilbert spaces only 'half 'of the regular vortex modes overlap with the original chiral vortex fermions.)

The linking of a pair of chiral Majorana fermions is known to be equivalent to the $\pi$ flux piercing and lead to a change in the boundary conditions along the loop [88, 30]. Dynamically, the boundary conditions change from periodic to anti-periodic and vice-versa, upon linking, due to the tunneling of zero-modes from one loop into the other. This means that upon linking, modes with $k_z = 0$ (truly Majorana zero-modes) can be generated and destroyed, which leads to the enlarged periodicity, just as in the Josephson junction scenario. Figure 4.5 describes the problem as we see it.

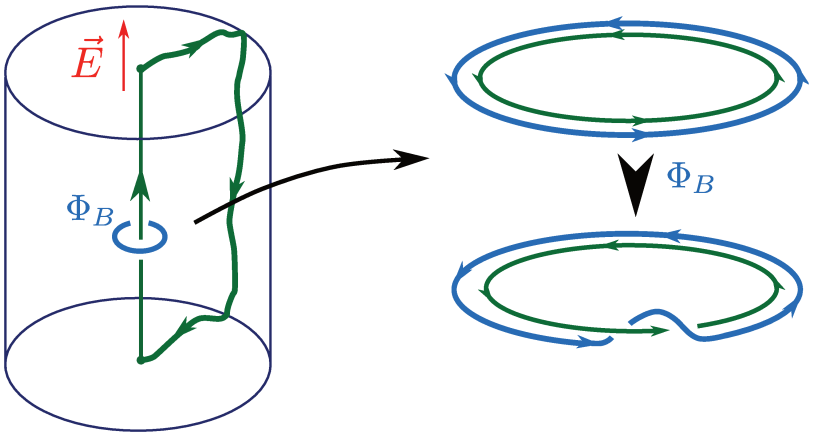


Figure 4.5: Mapping of chiral vortex with a parallel electric field electric field into the problem of linking Majorana fermion loops. Doubly linking the vortices on the right corresponds to a $2\pi$ flux insertion on the left.

In what follows, we will show in detail the known result that linking Majorana fermions leads to a change in the boundary conditions along a loop. We will then create a two-loop model to describe this problem. This two-loop problem will then be mapped into a particular problem of Josephson junctions at the edges of quantum spin-Hall insulators (time-reversal invariant topological insulators in 2D). Recent advances show that such Josephson junctions, in the presence of interactions display an "even more anomalous" Josephson effect, from $4\pi$ periodicity to $8\pi$ periodicity [35]. This will give us the $\mathbb{Z}_4$ periodic structure of cycles necessary to justify a pump of a full $2e$ Cooper pair, then possibly solving the paradox.

### 4.3.1 Majorana loop linking

To build up knowledge and comfort with the physical properties for Majorana fermion loops, we will start by showing that the linking of Majorana loops leads to a dyamical change in the periodicity boundary conditions. A regular Majorana loop has anti-periodic boundary conditions (due to fermion $2\pi$ rotation upon encircling the loop). We will see that the linking process allows the tunneling of a zero-energy mode from one loop into the other. This tunneling will dynamically change the boundary conditions periodicity. From the point of view of magnetic fluxes inside a loop, this means an *even* number of vortices inside the loop should imply anti-periodic boundary conditions, while an *odd* number should turn them periodic.

To demonstrate this, we will adopt a "squashed loop" geometry and follow Fendley and coworkers [88], later generalizing their procedures to our system. We start by writing, generally, the theory at a circular edge, assuming a $2L$ circumference,

$$H = \frac{v}{2L}\int_0^{2\pi} d\theta \Gamma(\theta)\left[-i\partial_\theta\right]\Gamma(\theta), \tag{4.105}$$

with $\Gamma(\theta)$ a Majorana field on the loop. Then, conformal invariance allows one to squash this loop into a line of length $L$ with modes going both ways

$$S_0 = \int dt \int_0^L dx \left[i\psi_R\left[\partial_t + v\partial_x\right]\psi_R + i\psi_L\left[\partial_t - v\partial_x\right]\psi_L\right]. \tag{4.106}$$

with $\psi_{R,L}$ fermions on the squashed loop. So we have non-chiral Majorana modes on a line segment. The issue now is what is the boundary condition to be applied at 0 and $L$ in order to recover the loop physics. To map the line problem back into the circular one, one has to reflect left moving modes into right moving ones and vice-versa. Instead of applying these boundary conditions by hand, we add boundary terms to the Lagrangian.

The boundary conditions are then imposed by the equations of motion. We so write

$$\begin{aligned} S &= S_0 + \int dt L_b && (4.107)\\ L_b &= -iav\psi_L(0)\psi_R(0) + ibv\psi_L(L)\psi_R(L). && (4.108) \end{aligned}$$

The equations of motion read, by varying $\psi_R$,

$$\begin{aligned} i(\partial_t + v\partial_x)\psi_R &= iv[\psi_R - \psi_L b]\delta(x-L) \\ &\quad + iv[\psi_L a - \psi_R]\delta(x). && (4.109) \end{aligned}$$

These imply, at the edges

$$\psi_R(0) = a\psi_L(0),\ \psi_R(L) = b\psi_L(L), \quad (4.110)$$

as desired. The equations of motion for $\psi_L$ give the same equations with $R$ and $L$ reversed and, as such, consistency demands that $a^2 = 1$ and $b^2 = 1$.

We expect that if we have an *even* number of vortices inside the loop, $ab = -1$ and, if we have an *odd* number, $ab = 1$. The introduction of a vortex in an initial situation with an odd number of vortices amounts to the introduction of a branch cut along the Majorana loop. It is convenient to introduce in the squashed picture the branch cut through one of the edges. The situations with $a = -b = 1$ and $-a = b = 1$ are equivalent (with the latter being preferred due to CFT conventions). Then, going into $a = b = 1$or $a = b = -1$ depends on which end the vortex is being introduced.

Let us start assuming a single vortex inside the loop. Assume that it carries a zero-mode $\psi_0$. We then bring this zero-mode close to the boundary of the loop, for definiteness at the point that corresponds to $x = 0$ in the squashed geometry. We start with $a = b = 1$ and the goal is to show that tunneling will change this to $a = -b = 1$. The Lagrangian with the tunneling term between the zero-mode and the loop reads

$$\begin{aligned} S &= S_0 + \int dt L_b + \int dt L_h && (4.111)\\ L_h &= i\psi_0\partial_t\psi_0 + ih\psi_0[\psi_R(0) + \psi_L(0)], && (4.112) \end{aligned}$$

where $h$ is the amplitude for the tunneling. The relative sign in the terms in square-brackets is fixed by the boundary condition ($a = 1$ when $h = 0$). The magnitude of $h$ is fixed by the distance between the vortex and edge; at large distances $r$, one has $h \sim e^{-\Delta r/v}$, where $\Delta$ is the bulk energy gap. The action is quadratic and equations of motion give the full quantum solution. The equations of motion at $x = 0$ reduce to

$$\begin{aligned} 2\partial_t\psi_0 &= h[\psi_R(0) + \psi_L(0)] && (4.113)\\ v\psi_R(0) &= v\psi_L(0) + h\psi_0 && (4.114)\\ v\psi_L(0) &= v\psi_R(0) - h\psi_0. && (4.115) \end{aligned}$$

Going into frequency space

$$\begin{aligned} i\omega\psi_0 &= \frac{h}{2}[\psi_R(0) + \psi_L(0)] && (4.116)\\ \psi_0 &= \frac{v}{h}(\psi_R(0) - \psi_L(0)). && (4.117) \end{aligned}$$

The last two equations are actually the same. Defining $\omega_0 = h^2/2v$ leads to

$$\psi_R(0,\omega) = \frac{\omega + i\omega_0}{\omega - i\omega_0}\psi_L(0,\omega). \quad (4.118)$$

If the vortex is very distant from the edge, $h \sim 0$ and $\omega_0 \sim 0$, such that the boundary conditions are as in the beginning, with $a = 1$. As the vortex approaches, $h$ grows and with it $\omega_0$, such that $a \to -1$. The latter

strongly coupling, $\omega_0 \to \infty$, limit is the DC limit.

There are some time scales to be considered. At $t = 0$ the vortex close to the edge is strongly scattered by the edge modes. At short times $t \ll \omega_0^{-1}$, there are little effects on the edge modes, but for $t \gg \omega_0^{-1}$, a $\pi$ phase-shift is induced in the Majorana field at the boundary. The other important time scale is set by the system size, $t_L = L/v$, which is the time it takes for an edge disturbance to circumnavigate the loop. For $t \ll t_L$, the phase shift is "local" an has no influence at the boundary at $x = L$. In the DC limit, $t \to \infty$ (before the thermodynamic limit $t_L \to \infty$), the net effect of the crossover induced by the the coupling between the vortex and edge is a global change in boundary conditions upon the circumnavigation from periodic to anti-periodic. In this DC limit, the point at which the fermion changes sign can be placed wherever one prefers (by a static gauge transformation); $x = 0$ is the most convenient choice in the squashed geometry as we used it. It is important to notice that the phase-shift in the DC limit is independent of the impurity strength $h$. This is contrasted with the case of a Dirac fermion scattering from an impurity. In this case, it is only when the energy of the impurity is fine-tuned to zero that the phase shift is also equals $\pi$. As $\psi_0^2 = 1$, a chiral Majorana fermion is always on-resonance, and no fine tuning is required.

We have thus seen that the linking between a pair of loops carrying Majorana *zero modes* leads to a change in the boundary conditions, from periodic to anti-periodic. This destroys the zero-modes in both loops. It is important to emphasize that the zero-modes now are with respect to the momenta along the loops. Effectively, the change of boundary conditions implies that solutions with $k_z = 2n\pi/L$ (for integer $n$ and a vortex along the z-axis under periodic boundary conditions) change into $k_z = (2n+1)\,\pi/L$. In the first case one can have $k_z = 0$, in the second not. This process enforces the change of parity in the double loop ground state. We will now see that the double Majorana loop linking problem can be interpreted as a Josephson junction problem. The Majorana zero-mode disappearance and reappearance under double-linking is a manifestation of the $4\pi$ periodic anomalous Josephson effect. We will then see that, under interactions, this anomalous effect actually becomes $8\pi$ periodic.

### 4.3.2 Quantum spin Hall effect, Josephson junctions, Majorana loop linking

We now study the double Majorana loop problem itself. We will show how linking such loops is equivalent to a superconducting phase slip in a Josephson junction mediated at the edge of a quantum spin-Hall insulator. The double Majorana fermion loops have a Hamiltonian

$$H_{links} = \frac{v}{2\pi R}\int_0^{2\pi} d\theta\,(\Gamma_1,\Gamma_2)\begin{pmatrix} -i\partial_\theta & \\ & -i\partial_\theta \end{pmatrix}\begin{pmatrix} \Gamma_1 \\ \Gamma_2 \end{pmatrix} \tag{4.119}$$

$$= \frac{v}{R}\sum_l (\Gamma_{1,-l},\Gamma_{2,-l})\begin{pmatrix} l & \\ & l \end{pmatrix}\begin{pmatrix} \Gamma_{1l} \\ \Gamma_{2l} \end{pmatrix}, \tag{4.120}$$

where $\Gamma_i^\dagger = \Gamma_i$, $R$ is the radius of the loop and $v$ the velocity of the Fermions. We have assumed that the loops are of the same size and that the modes are co-propagating. These points are not important and one looses no generality by this choice (at the end this will be a matter of gauge choice).

Following the single loop plus zero-mode problem from the past section, we can squash the loops and write the corresponding action,

$$S_0 = v\int d^2x\,[i\gamma_{1R}\partial_+\gamma_{1R} + i\gamma_{1L}\partial_-\gamma_{1L}] \tag{4.121}$$

$$+v\int d^2x\,[i\gamma_{2R}\partial_+\gamma_{2R} + i\gamma_{2L}\partial_-\gamma_{2L}] \tag{4.122}$$

where $x : 0 \to L = \pi R$ and $\partial_\pm = v^{-1}\partial_t \pm \partial_x$.

Boundary conditions are implemented by augmenting the action with boundary terms as

$$\begin{aligned} S &= S_0 + \int dt L_b && (4.123)\\ L_b &= -iav\gamma_{1L}(0)\gamma_{1R}(0) + ibv\gamma_{1L}(L)\gamma_{1R}(L) && (4.124)\\ &\quad -iav\gamma_{2L}(0)\gamma_{2R}(0) + ibv\gamma_{2L}(L)\gamma_{2R}(L). && (4.125)\end{aligned}$$

Notice that the factors $a = \pm 1$ and $b = \pm 1$ fix the periodic and anti-periodic boundary conditions for each loop, and are the same for both loops, as follows from fermion parity conservation.

Remarkably, the boundary action $L_b$ introduced previously is not the most general possible. To simulate the possibility of linking the loops, we can relax the boundary tunneling terms allowing, for example, for terms like $\gamma_{1L}(0)\gamma_{2R}(0)$, etc.

To be general, we then rewrite the boundary Lagrangian as

$$L_b = -iv\delta(x)a^{ij}\gamma_{iL}\gamma_{jR} + iv\delta(x-L)b^{ij}\gamma_{iL}\gamma_{jR}. \quad (4.126)$$

Applying the equations of motion and fixing the problem at $x = 0$ leads to

$$\boldsymbol{\gamma}(0) = A\boldsymbol{\gamma}(0) \quad (4.127)$$

where

$$A = \begin{pmatrix} & & a^{11} & a^{21} \\ & & a^{12} & a^{22} \\ a^{11} & a^{12} & & \\ a^{21} & a^{22} & & \end{pmatrix} \quad (4.128)$$

and $\boldsymbol{\gamma} = (\gamma_{1R}, \gamma_{2R}, \gamma_{1L}, \gamma_{2L})^T$. A similar result can be found for $b^{ij}$ at $x = L$. We have to fix the most general possibility for the entries in this $A$ matrix. From $\gamma = A\gamma$, one imposes the condition

$$A^2 = \mathbf{I}_{4\times 4}. \quad (4.129)$$

This suggests the parametrization

$$\begin{aligned} a_{11} &= \cos\varphi \\ a_{22} &= \pm\cos\varphi \\ a_{12} &= -\sin\varphi \\ a_{21} &= \pm\sin\varphi. && (4.130)\end{aligned}$$

The relative signs in $a_{22}$ and $a_{21}$ can be fixed by remembering that, at $\varphi = 0$, we have our original boundary conditions for the two unlinked loops. As fermion parity conservation fixes that boundary conditions are either simultaneously periodic or anti-periodic in both loops, we fix

$$\begin{aligned} a_{11} &= \cos\varphi \\ a_{22} &= \cos\varphi \\ a_{12} &= -\sin\varphi \\ a_{21} &= \sin\varphi. && (4.131)\end{aligned}$$

Since we would like to understand the linking between the two vortices, it is enough to consider constricting the problem at a single point, which we chose as $x = 0$, thus keeping the boundary condition at $x = L$ fixed,

say simply take $b = 1$ in (4.125). The most general boundary term thus reads

$$\begin{aligned} L_b &= -iv\left[\cos\varphi\left(\gamma_{1L}\gamma_{1R}+\gamma_{2L}\gamma_{2R}\right)-\sin\varphi\left(\gamma_{1L}\gamma_{2R}-\gamma_{2L}\gamma_{1R}\right)\right]\delta\left(x\right) && (4.132)\\ &\quad +iv\left[\gamma_{1L}\gamma_{1R}+\gamma_{2L}\gamma_{2R}\right]\delta\left(x-L\right). && (4.133)\end{aligned}$$

Clearly, $\varphi$ parametrizes the double loop linking. The boundary conditions at $x = 0$ then read, explicitly,

$$\begin{aligned} \gamma_{1R} &= \cos\varphi\gamma_{1L}+\sin\varphi\gamma_{2L} && (4.134)\\ \gamma_{2R} &= -\sin\varphi\gamma_{1L}+\cos\varphi\gamma_{2L}. && (4.135)\end{aligned}$$

At $\varphi = 0$,we have

$$\begin{aligned} \gamma_{1R} &= \gamma_{1L} && (4.136)\\ \gamma_{2R} &= \gamma_{2L}. && (4.137)\end{aligned}$$

This means that both loops are uncoupled and have periodic boundary conditions, and thus a pair of zero modes. At $\varphi = \pi$

$$\begin{aligned} \gamma_{1R} &= -\gamma_{1L} && (4.138)\\ \gamma_{2R} &= -\gamma_{2L}. && (4.139)\end{aligned}$$

Now we have anti-periodic boundary conditions and no zero modes.

At $\varphi = \pi/2$,

$$\begin{aligned} \gamma_{1R} &= \gamma_{2L} && (4.140)\\ \gamma_{2R} &= -\gamma_{1L}. && (4.141)\end{aligned}$$

Here the modes from the two wires are exactly exchanged. The boundary conditions at $x = L$ is fixed at $\gamma_{1,2R} = \gamma_{1,2L}$ overall.

In sum, at $\varphi = 0$, we have fixed periodic boundary conditions in both loops, corresponding to the situation in which each loop carries a Majorana zero mode. This is the linked loops limit. At $\varphi = \pi/2$, boundary conditions determine complete scattering at the line edges from one loop into the other. We have a system which is equivalent to a single doubly long loop winding around itself. Finally, at $\varphi = \pi$, boundary conditions are anti-periodic. We have a mapping:

**Complex fermion representation**

Interestingly, the squashed loops picture deforms the two Majorana chiral modes into four Majorana non-chiral modes under appropriate boundary conditions. We can combine such Majorana fermions in a convenient way, forming complex Dirac fermions. We write

$$\psi_R = \frac{\gamma_{1R}+i\gamma_{2R}}{\sqrt{2}},\ \psi_R^\dagger = \frac{\gamma_{1R}-i\gamma_{2R}}{\sqrt{2}} \quad (4.142)$$

$$\psi_L = \frac{i\gamma_{1L}+\gamma_{2L}}{\sqrt{2}},\ \psi_L^\dagger = \frac{-i\gamma_{1L}+\gamma_{2L}}{\sqrt{2}} \quad (4.143)$$

where $\{\gamma_i, \gamma_j\} = 2\delta_{ij}$ and $\left\{\psi_i, \psi_j^\dagger\right\} = \delta_{ij}$.

The kinetic part then becomes

$$S_0 = v\int d^2xi\left[\psi_R^\dagger\partial_+\psi_R+\psi_R\partial_+\psi_R^\dagger\right] \tag{4.144}$$

$$+v\int d^2xi\left[\psi_L^\dagger\partial_-\psi_L+\psi_L\partial_-\psi_L^\dagger\right]. \tag{4.145}$$

Even more remarkably, the boundary terms now read

$$L_b = 2\left[\psi_L\psi_R\Delta\left(x\right)-\psi_L^\dagger\psi_R^\dagger\Delta\left(x\right)^*\right], \tag{4.146}$$

where

$$\Delta\left(x\right)=\frac{v}{2}\left[b\delta\left(x-L\right)-a\delta\left(x\right)\right], \tag{4.147}$$

where $a=e^{-i\varphi_a}$ and $b=e^{-i\varphi_b}$ come from the phases introduced by the generalized, 'inter-loop', boundary conditions (we had previously set $\varphi_b=0$, as we generally will.)

Write the complex fermion in a convenient (and, by now, recurrent) Nambu spinor, $\Psi=\left(\psi_R,\psi_L,\left(\psi_R^\dagger,\psi_L^\dagger\right)i\sigma_y\right)^T=\left(\psi_R,\psi_L,\psi_L^\dagger,-\psi_R^\dagger\right)^T$ the double loop Hamiltonian, with the boundary fixing terms become

$$H_{2loop}=\int d^2x\Psi^\dagger\left[-iv\rho_z\tau_z\partial_x+\rho_x\Delta_1+\rho_y\Delta_2\right]\Psi. \tag{4.148}$$

where

$$\Delta\left(x\right) = \Delta_1+i\Delta_2 \tag{4.149}$$

$$= \frac{v}{2}\left[b\delta\left(x-L\right)-a\delta\left(x\right)\right] \tag{4.150}$$

and $a$ and $b$ are the previous complex numbers of unit modulus. also, $\vec{\tau}$ and $\vec{\rho}$ are Pauli matrices in the $L,R$ and Nambu spaces, respectively.

This Hamiltonian has been considered previously. It corresponds to a Josephson junction created by adding a pair of superconductors to the 1D edge of a 2D topological insulator (known as a quantum spin Hall insulator.) Such insulators, in their topologically non-trivial phases, have helical edge modes, that is, counter propagating metallic edge states which are time-reversal invariant from one another. Indeed, in the absence of imaginary terms in the superconducting pairing, the Hamiltonian $H_{2loop}$ respects time-reversal symmetry under

$$\Theta=i\tau_yK. \tag{4.151}$$

In the present model, the superconductors at the edges have zero length, while the loop consists of the Josephson weak-link. We have topologically deformed the problem of Majorana loop linking to a problem of Josephson junction in helical metals. In fact, we have

$$\pi \text{ flux insertion in loop} = 1 \text{ loop link} = \pi \text{ phase slip across junction.} \tag{4.152}$$

Figure 4.6 summarizes this idea.

### $\mathbb{Z}_4$ Josephson effect - interactions in topological Josephson junctions

Our final discussion will regard the so called $\mathbb{Z}_4$ Josephson effect. We have seen in Chapter 1 that Josephson junctions in the presence of Majorana fermions are $4\pi$ periodic with respect to the phase difference across the junction. It has been recently claimed that, in fact, the presence of interactions could enforce a further enlargement to $8\pi$ on the periodicity of the problem on the superconducting phase difference, due to many-body effects [35]. We will have a brief discussion about this in our system.

We start by studying the many-body spectrum of (4.148). In the bulk, the problem is solved trivially. By

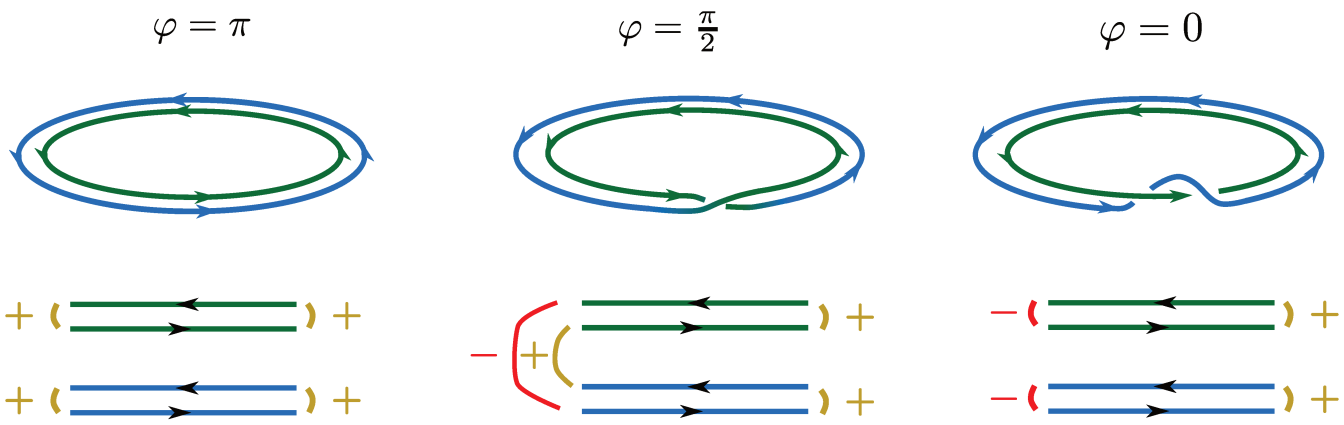


Figure 4.6: The different phases $\varphi$ parametrizing the loop linking picture. The special values $\varphi = \pi, \pi/2, 0$ correspond to a pair of unlinked loops, a single crossing over between the loops, generating a single large loop, and finally to a pair of linked loops. In the lowest part we describe the corresponding 1D squashed loop regimes. In green we have the $\gamma_{1,R/L}$ modes and in blue the $\gamma_{2,R/L}$ ones. The signs and arcs at the ends correspond to the signs of the different couplings that arise in equations (4.134) and (4.135).

writing the first quantized spinor $(u_R, u_L, v_L, v_R)^T$, equations of motion imply

$$\phi = \begin{pmatrix} u_R \\ u_L \\ v_L \\ v_R \end{pmatrix} = \begin{pmatrix} A_R e^{iEx/v} \\ A_L e^{-iEx/v} \\ B_L e^{-iEx/v} \\ B_R e^{iEx/v} \end{pmatrix}. \tag{4.153}$$

Now we apply the boundary conditions. They read

$$\psi_R(0) = a^* \psi_L^\dagger(0) \tag{4.154}$$
$$\psi_R(L) = b^* \psi_L^\dagger(L). \tag{4.155}$$

We fix here $a = e^{i\varphi}$ and $b = 1$, for concreteness.In first quantized language, we have

$$u_R(0) = e^{-i\varphi} v_L(0), \qquad u_R(L) = v_L(L) \tag{4.156}$$
$$v_R(0) = -e^{i\varphi} u_L(0), \qquad v_R(L) = -u_L(L) \tag{4.157}$$

In sum, this implies a pair of states

$$\phi_{n+} = \frac{1}{\sqrt{2L}} \begin{pmatrix} e^{iE_{n+}x/v} \\ 0 \\ e^{i\varphi} e^{-iE_{n+}x/v} \\ 0 \end{pmatrix} \tag{4.158}$$

$$\phi_{n-} = \frac{1}{\sqrt{2L}} \begin{pmatrix} 0 \\ e^{-iE_{n-}x/v} \\ 0 \\ -e^{i\varphi} e^{iE_{n-}x/v} \end{pmatrix} \tag{4.159}$$

with energies

$$E_{n\sigma} = \frac{v}{2L}(2\pi n + \sigma\varphi). \tag{4.160}$$

Notice that, as $L = \pi R$, this recovers the original loop spectrum, at $\varphi = 0$ or $\varphi = \pi$. The continuous variable

$\varphi$ allows for a gradual interpolation between the linked and unlinked regimes.

Now we want to write the second quantized problem. We need to use the time-reversal and particle-hole operations

$$\Theta = i\tau_y K,\ \Xi = \rho_y \tau_y K \tag{4.161}$$

to constrain the spinors and fields. This reads, in first and second quantized languages,

$$\begin{aligned} \Psi &= \begin{pmatrix} \psi_R \\ \psi_L \\ \psi_L^\dagger \\ -\psi_R^\dagger \end{pmatrix} \Rightarrow \left(\Psi^\dagger\right)^T = \rho_y \tau_y \Psi & (4.162) \\ \Xi\phi_{n,\sigma} &= \phi_{-n,-\sigma} \Rightarrow \rho_y \tau_y \phi_{n,\sigma} = \phi^*_{-n,-\sigma}. & (4.163) \end{aligned}$$

Now we expand

$$\begin{aligned} \Psi &= \sum_{n\sigma} \phi_{n,\sigma} c_{n,\sigma} \\ \Rightarrow c_{n,\sigma} &= \int dx \phi^\dagger_{n,\sigma} \Psi. \end{aligned} \tag{4.164}$$

This implies

$$c_{-n,-\sigma} = e^{-i\varphi} c^\dagger_{n,\sigma}. \tag{4.165}$$

This is the Nambu constraint which gets rid of the BdG degeneracy. We can now write

$$\begin{aligned} \Psi &= \sum_{n\sigma} \phi_{n,\sigma} c_{n,\sigma} \\ &= \sum_{\sigma} \phi_{0,\sigma} c_{0,\sigma} + \sum_{n>0,\sigma} \left( \phi_{n,\sigma} c_{n,\sigma} + \phi_{-n,\sigma} c^\dagger_{n,-\sigma} \right). \end{aligned} \tag{4.166}$$

In particular,

$$\psi_R = u_{0,+} c_{0,+} + \sum_{n>0} \left( u_{n,+} c_{n,+} - e^{i\varphi} v^*_{n,-} c^\dagger_{n,-} \right) \tag{4.167}$$

$$\psi_L = u_{0,-} c_{0,-} + \sum_{n>0} \left( u_{n,-} c_{n,-} + e^{i\varphi} v^*_{n,+} c^\dagger_{n,+} \right). \tag{4.168}$$

Now we can expand the Hamiltonian in the new basis. We find

$$\begin{aligned} H &= \sum_\sigma \left[ E_{0,\sigma}(\varphi) c^\dagger_{0,\sigma} c_{0,\sigma} + \sum_{n>0} \left( E_{n,\sigma}(\varphi) c^\dagger_{n,\sigma} c_{n,\sigma} + E_{-n,\sigma}(\varphi) c_{n,-\sigma} c^\dagger_{n,-\sigma} \right) \right] \\ &= \sum_\sigma \left[ E_{0,\sigma}(\varphi) c^\dagger_{0,\sigma} c_{0,\sigma} + \sum_{n>0} \left( E_{n,\sigma}(\varphi) c^\dagger_{n,\sigma} c_{n,\sigma} + E_{-n,\sigma}(\varphi) c^\dagger_{-n,\sigma} c_{-n,\sigma} \right) \right]. \end{aligned} \tag{4.169}$$

To remove the Nambu doubled states, the ground state consists of all the negative energy modes occupied. This means

$$|0\rangle = c^\dagger_{0,-} \prod_{n<0} c^\dagger_{n,\sigma} \left|\tilde{0}\right\rangle, \tag{4.170}$$

where $\left|\tilde{0}\right\rangle$ is the empty state. Thus, normal ordering removes the negative $n$ part of the Hamiltonian, as well

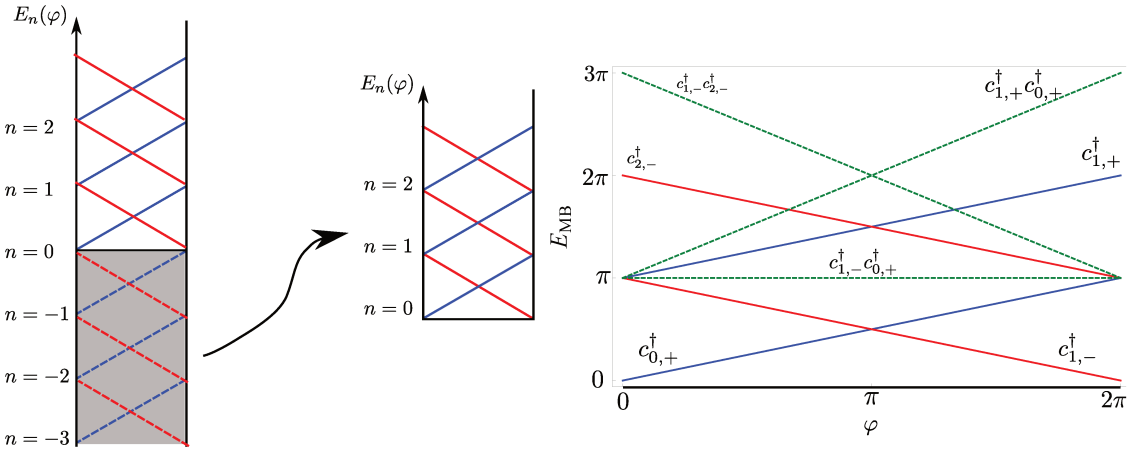


Figure 4.7: Spectrum analysis, we use $v = L = 1$ so energies are measured in units of $\pi$. On the left, the negative energy states are artificial from BdG doubling. We consider a filled sea of them, normal ordering the Hamiltonian. Red and blue correspond to $\sigma = \pm$, respectively. Notice that for $n = 0$, only $\sigma = +$ is physical. On the right, we add to the plot the two-body states (dashed green) degenerate at $\varphi = 0$. The four degenerate states are identified by the creation operators applied to the vacuum. The solid black horizontal line corresponds to the vacuum state.

as one of the zero-modes, implying

$$\begin{aligned} :H: &= H - \langle 0|H|0\rangle \\ &= E_{0,+}(\varphi)\, c^\dagger_{0,+}c_{0,+} + \sum_{n>0,\sigma} E_{n,\sigma}(\varphi)\, c^\dagger_{n,\sigma}c_{n,\sigma}. \end{aligned} \tag{4.171}$$

This allows for us to build explicitly the many-body states; the one-particle ones are

$$|1;n,\sigma\rangle = c^\dagger_{n,\sigma}|0\rangle, \tag{4.172}$$

while the two-particle states are

$$\left|2;n'\sigma',n\sigma\right\rangle = c^\dagger_{n',\sigma'}c^\dagger_{n,\sigma}|0\rangle, \tag{4.173}$$

and so on.

Some many-body energies then are:

$$\text{ground state} \qquad E_0 = 0 \tag{4.174}$$

$$\text{simple occupancy states} \qquad \begin{cases} E_{1;0+} = \frac{v}{L}(\varphi) \\ E_{1;1-} = \frac{v}{L}(2\pi-\varphi) \\ E_{1;1+} = \frac{v}{L}(2\pi+\varphi) \\ E_{1;2-} = \frac{v}{L}(4\pi-\varphi) \end{cases} \tag{4.175}$$

$$\text{double occupancy states} \qquad \begin{cases} E_{2;0+,1-} = \frac{v}{L}(2\pi) \\ E_{2;0+,1+} = \frac{v}{L}(2\pi+2\varphi) \\ E_{2;1-,0+} = \frac{v}{L}(3\pi-2\varphi) \\ E_{2;1-,2-} = \frac{v}{L}(4\pi-\varphi) \end{cases} \tag{4.176}$$

Figure 4.7 summarizes some important energy modes.

Notice that the excited states $E_{1;1\pm}$ and $E_{2;0+,1\pm}$ written above are fourfold degenerate at $\varphi = 0$ . They

correspond to a pair of one-body occupied states and another pair of two-body occupied states. The two-body states contain a filled $n = 0$ mode $c^{\dagger}_{0,+}$, which adds nothing to the energy at this phase. We may write

$$|\mu = 1\rangle = c^{\dagger}_{0,+} |0\rangle \tag{4.177}$$

while

$$|\mu = 0\rangle = |0\rangle . \tag{4.178}$$

These correspond to two degenerate ground states at $\varphi = 0$, fixed by the fermionic parity $(-1)^{c^{\dagger}_{0,+}c_{0,+}} = \mu$. We define the first excited states at $\varphi = 0$ as

$$|\sigma\mu\rangle = c^{\dagger}_{1\sigma} |\mu\rangle . \tag{4.179}$$

Here, $\sigma$ fixes Kramers degenerate modes. The gapping of this fourfold degenerate point is our final card. One notices that we can compare the ground state with itself after $2\pi$ evolutions of the phase across the junction. We write

$$|0, 0 < \varphi < 2\pi\rangle = c^{\dagger}_{0,-}(\varphi) \prod_{\sigma,n<0} c^{\dagger}_{n,\sigma}(\varphi) \left|\tilde{0}\right\rangle , \tag{4.180}$$

such that

$$\begin{aligned} |0, 2\pi < \varphi < 4\pi\rangle &= c^{\dagger}_{0,-}(2\pi < \varphi < 4\pi) \prod_{\sigma,n<0} c^{\dagger}_{n,\sigma}(2\pi < \varphi < 4\pi) \left|\tilde{0}\right\rangle \\ &= c^{\dagger}_{-1,-}(0 < \varphi < 2\pi) \prod_{n<0} c^{\dagger}_{n+1,+}(0 < \varphi < 2\pi) \prod_{n<0} c^{\dagger}_{n-1,-}(0 < \varphi < 2\pi) \left|\tilde{0}\right\rangle \\ &\propto c_{0,-}(\varphi)\, c^{\dagger}_{0,+}(\varphi) |0, 0 < \varphi < 2\pi\rangle , \end{aligned} \tag{4.181}$$

with meaningless a proportion constant equals to plus or minus 1. The general rule then states

$$|0, 2\pi < \varphi < 4\pi\rangle \propto c_{0,-}(\varphi)\, c^{\dagger}_{0,+}(\varphi) |0, 0 < \varphi < 2\pi\rangle . \tag{4.182}$$

Notice that although we evolve the phase continuously, the ground state acquires a $c^{\dagger}_{0+}$ filling. We then have three features upon such $2\pi$ evolution:

1. The filling of $c^{\dagger}_{0}$ changes, such that the parity $(-1)^{c^{\dagger}_{0+}c_{0+}}$ flips;
2. The total ground state energy is fixed;
3. The total charge is fixed;

This shows that $2\pi$ evolutions of the phase across the junction do not lead the ground state back to its original value, implying at least a $4\pi$ periodicity in phase slips. The introduction of interactions, however, may gap this four-fold degeneracy. We will not enter into this subject in detail, but in fact, it was shown in [35] ( in a more well behaved Josephson junction than our infinitely long link scenario) that interactions which preserve time-reversal invariance may lead to a $\mathbb{Z}_4$ periodic junction.

Bosonization techniques may be applied to study this problem which corroborates to this conclusion. In these systems, interactions lead to the possibility of the existence of e/2 charged quasi-particles tunneling across the junction (as opposed to Cooper pairs in the regular Josephson effect and electrons in the $\mathbb{Z}_2$ fractional Josephson effect.) The present work is in its final stages of development, but the arguments given up to now should be enough to convince the reader that this is a concrete possible way out of the paradox introduced by the action (4.79).

## 4.4 Conclusions

We studied vortices in class DIII topological superconductors in 3D. We have thoroughly analyzed the physical properties of the vortex bound states in all the different vortex regimes and regarding the full spectrum and its electromagnetic properties. The effective action for such a phase in the presence of the exotic chiral vortices is seen to lead to an unusual axion-electrodynamics problem, in which the charge pumped into the axion string (in the presence of an electric field along the line-defect) is finite and given naively in units of $e/2$, while the chiral modes along the string are neutral and do not see this charge pumping. In order to solve this paradox, we assume that, possibly, charges are pumped in units of $2e$, the charge of a Cooper pair which can condense. The constant electric field along the vortex line can be thought of as being generated by a time-evolving magnetic flux around the chiral vortex, which leads to a vortex linking picture.We demonstrate that periodic boundary conditions along the vortex direction, corresponding to this problem of Majorana chiral loop linking, is equivalent to the problem of Josephson junctions at the edges of quantum spin Hall systems in 2D. These problems demonstrate a $\mathbb{Z}_4$ periodic Josephson effect, under the effects of interactions.

Our findings have several important aspects. While helping in understanding the finer details of topological superconductivity, and pointing to unconventional aspects of the idea of such a phase, our results demonstrates that the "topological" axion term in the effective electromagnetic response of this system carries, within it, details of the effects of interactions. Such is the nature of topological field theories: even if derived in the non-interacting limit, they are known to describe the deeper subtleties of the quasi-particle structure of topological phases. Under interactions, the classification of bulk class DIII topological superconductors is known to break from $\mathbb{Z}$ to $\mathbb{Z}_{16}$. It is our belief that our findings in the context of chiral vortices in class DIII are related to this issue, but these are points which we have not finished investigating

As a final point, we emphasize that our results here were developed under the assumption that the action (4.79) proposed by [34] is indeed correct. As mentioned, their derivation of their effective action did not rely on a bona fide fermionic integration of the underlying microscopic theory. This opens the question: are their arguments correct?

In appendix D, we perform the fermionic integration for the bulk Weyl fermions coupled to the electromagnetic gauge field and in the presence of a superconducting mass with an attached vortex, explicitly computing the effective partition function. Interestingly, this calculation relies on a 1-loop Feynman diagram, the anomalous "triangle diagram". There are two such diagrams which display anomalous behavior, the so called AVV and AAA diagrams. This nomenclature is used to fix the vertices, which contain axial (A) or vector (V) fields. The regular anomaly of a topological insulator comes from an AVV type of graph. This gives the famous "theta-term" with a quantized axion field $\theta = 0, \pi$. Interestingly, we show that the BdG doubled Weyl fermions turn the AVV diagram, effectively, in a AAA type of loop. Such diagrams are known to evaluate to 1/3 of the value of the AVV case; this implies that the correct factor in front of the axial terms in (4.79) should get another factor of 1/3, as we demonstrate in the mentioned appendix.

Whether or not the results of [34] are correct remain an open question, whose answer we are still pursuing.

# Chapter 5

# Conclusions

These are our concluding remarks and final words. As of the beginning of the development of this Ph.D. thesis, we had in mind exploring different properties of emergent relativistic physics in condensed matter. In fact, our studies started in photon wavefunctions - trying to study decoherence in turbulent media - then moving to transport in graphene physics [89], finally moving into topological matter and, in particular, superconductivity in topological matter. In this last term, we focused in studying different aspects of defect bound states and Majorana fermion physics[90, 28]. With the benefit of hindsight, it is clear that vortex bound matter was the unifying point of our studies, and this body of work was written with this idea in mind.

As our main achievements, we developed different techniques to explore in full detail the local physics of electronic vortex bound states, both analytically and numerically. With these tools, we explored the physics for a pair of different scenarios: that of quantum motion of vortices in doped topological insulators, in which our goal was to verify physical signatures of vortex topological phase transitions, and that of axion electrodynamics in time-reversal invariant topological superconductors in 3D. The effective 1D physics along the vortex lines kept our ideas always close to that of Kitaev p-wave wires, in which we had a contribution in the study of the fractional Josephson effect via macroscopic quantum tunneling [37].

As of the end of this writing, a few of our works remain unpublished , some related to the matter treated in this thesis and some, mostly, unrelated. Yet, we believe that our already published works settle down our contributions in the area of topological matter, which is likely to remain as the center of our interests in the years to come.

# Appendix A

# Peak analysis

Here we describe in some detail the determination of the relative sizes and positions of the tunneling conductance peaks. We start rewriting,

$$\rho(\mathbf{r},\omega) = \sum_{\sigma=\pm}\rho_\sigma(\mathbf{r},\omega) \tag{A.1}$$

$$\rho_\sigma(\mathbf{r},\omega) = -\frac{1}{\pi}Im\sum_l \frac{|\mathbf{u}_l^\sigma(\mathbf{r})|^2}{\omega - E_l^\sigma - \Sigma_l^\sigma + i\epsilon}, \tag{A.2}$$

using the vortex-modes eigenbasis. STM measurements probe the tunneling conductance

$$G(\mathbf{r},\omega) = -\frac{G_0}{\rho_0}\int d\omega' \rho\left(\mathbf{r},\omega+\omega'\right) f'\left(\omega'\right), \tag{A.3}$$

where $f(\omega)$is the Fermi distribution.

At zero-temperature this reduces simply to the LDOS, up to a constant. At finite small temperatures we may write

$$G(\mathbf{r},\omega)/G_0 = -\frac{1}{\rho_0}\sum_{l,\sigma=\pm}\sum_i \frac{|u_l^\sigma(\mathbf{r})|^2}{\left|1-\frac{\partial\Sigma_l^\sigma\left(\omega_{l,\sigma,0}^i\right)}{\partial\omega}\right|} \tag{A.4}$$

$$\times f'\left(\omega_{l,\sigma,0}^i - \omega\right), \tag{A.5}$$

where $\omega_{l,\sigma,0}^i$ is the $i$-th solution to

$$\omega - E_l^\sigma - \Sigma_l^\sigma(\omega) = 0. \tag{A.6}$$

This represents a cubic equation. For our parameters, three solutions always exist. While (A.6) determines where are the relative positions of the peaks in energy space, the derivatives $\frac{\partial\Sigma_l^\sigma\left(\omega_{l,\sigma,0}^i\right)}{\partial\omega}$ will fix the peaks relative sizes.

We focus most of our analysis at $|\mathbf{r}| = 0$, which, from (3.49), means that only the states with $l = 0, 1$ give non-vanishing contributions. The relevant self-energy contributions were considered in the main text in equations (3.100) and (3.101). To determine the relative sizes and positions of the peaks, we examine the derivatives of the self-energy, as well as equation (A.6) explicitly.

### Peak sizes

The derivatives of the self-energies read, after some simplification

$$\frac{d\Sigma_1^\sigma(\omega)}{d\omega} = -\frac{A_{1;2}^{+;\sigma}}{\left(\Delta\omega_1^\sigma - \delta - \omega_c/2 - \omega_v\right)^2} - \frac{A_{0;1}^{+;\sigma}}{\left(\Delta\omega_1^\sigma + \delta + \omega_c/2 - \sigma sgn\left(\mu - \bar{\mu}_\sigma\right)\omega_v\right)^2} \tag{A.7}$$

$$\frac{d\Sigma_0^\sigma(\omega)}{d\omega} = -\frac{A_{0;1}^{+;\sigma}}{\left(\Delta\omega_0^\sigma - \delta - \omega_c/2 - \omega_v\right)^2} - \frac{A_{-1;0}^{+;\sigma}}{\left(\Delta\omega_0^\sigma + \delta + \omega_c/2 + \omega_v\right)^2}, \tag{A.8}$$

where $\Delta\omega_l^\sigma = \omega - E_l^\sigma$ and $\delta$ is the mini-gap.

The matrix elements are much smaller than the other physical quantities. Dimensional analysis and explicit manipulation of (3.87) shows that, at constant $\omega_v/\Delta_0$, these overlaps sizes depend on the coherence length as $\xi^{-5}$[65]. The peak sizes, nevertheless, are going to be sensitive to $A_{l;l'}^{\alpha;\sigma}$. As will be seen in the next subsection, the satellite peaks positions are dominated by the vortex oscillation frequency $\omega_v$. Plugging $\Delta\omega_l^\sigma \approx 0$ or $\Delta\omega_l^\sigma \approx \pm\omega_v$ one sees that $d\Sigma_l^\sigma(\omega)/d\omega$ is small (concretely it is$\propto A_{l,l'}^{+;\sigma}/\omega_v^2 \ll 1$) at $\Delta\omega_0^+ \approx 0$ while it may be larger at $\Delta\omega_0^\sigma \approx \pm\omega_v$, going as $\sim -A_{0;1}^{+;+}\left[\frac{1}{s^2}\right]$, where $s = \frac{\delta+\omega_c/2}{2\omega_v}$. The latter case reduces greatly the size of the satellite peaks from $l = 0$, similarly as pointed by Bartosch et al.[65].

## peak positions

Our last goal is to explain the positions of the peaks as function of the chemical potential, demonstrating that they are much less sensitive to the matrix elements than the peak sizes and that they are mainly fixed by the vortex fluctuation frequency, which might be much larger than the other energy scales of the problem.

Simplifying the self-energy and plugging into (A.6), shows that independent of chemical potential, for $l = 0$ we have

$$\begin{aligned}\Delta\omega_0^\sigma\left[\left(\Delta\omega_0^\sigma\right)^2 - \left(\delta + \omega_c/2 + \omega_v\right)^2 + \left(A_{0;1}^{\sigma;+} + A_{-1;0}^{\sigma;+}\right)\right] \\ + \left(\omega_v + \delta + \omega_c/2\right)\left(A_{0;1}^{\sigma;+} - A_{-1;0}^{\sigma;+}\right) = 0.\end{aligned} \tag{A.9}$$

Using $A_{0;1}^{\sigma;+} \approx A_{-1;0}^{\sigma;+}$ we get results similar to reference [65] for ordinary $s$-wave superconductor. Since the matrix elements are much smaller than the other parameters, we can neglect them in above equation. We then get

$$\Delta\omega_0^\sigma\left[\left(\Delta\omega_0^\sigma\right)^2 - \left(\delta + \omega_c/2 + \omega_v\right)^2\right] = 0, \tag{A.10}$$

for any $\mu$. This gives a central and two satellite peaks at, respectively

$$\Delta\omega_0^\sigma = 0 \tag{A.11}$$

$$\Delta\omega_0^\sigma = \left(\omega_v + \delta + \omega_c/2\right) \tag{A.12}$$

$$\Delta\omega_0^\sigma = -\left(\omega_v + \delta + \omega_c/2\right). \tag{A.13}$$

For $l = 1$, we may as well neglect the contributions from the matrix elements. For $\mu < \bar{\mu}_-$,

$$\Delta\omega_1^-\left[\left(\Delta\omega_1^- - \omega_v\right)^2 - \left(\delta + \omega_c/2\right)^2\right] = 0 \tag{A.14}$$

$$\Delta\omega_1^+\left[\left(\Delta\omega_1^+\right)^2 - \left(\omega_v + \delta + \omega_c/2\right)^2\right] = 0. \tag{A.15}$$

So we have peaks at

$$\Delta\omega_1^- = 0 \tag{A.16}$$
$$\Delta\omega_1^- = \omega_v + (\delta + \omega_c/2) \tag{A.17}$$
$$\Delta\omega_1^- = \omega_v - (\delta + \omega_c/2) \tag{A.18}$$

and

$$\Delta\omega_1^+ = 0 \tag{A.19}$$
$$\Delta\omega_1^+ = (\omega_v + \delta + \omega_c/2) \tag{A.20}$$
$$\Delta\omega_1^+ = -(\omega_v + \delta + \omega_c/2)\,. \tag{A.21}$$

For $\mu > \bar{\mu}_+$ the role of $+$ and $-$ in above equations are exchanged. Since the total density is the sum of contributions form both $\sigma = \pm$ sectors, and the gap between $E_1^+$ and $E_1^-$ goes as $\delta(1/2 - \phi/2\pi)$, the LDOS in the two regimes of $\mu < \bar{\mu}_-$ and $\mu > \bar{\mu}_+$ look the same.

We now get to the most important regime of $\bar{\mu}_- < \mu < \bar{\mu}_+$. The position of the peaks for both $\sigma = \pm$ sectors are at

$$\Delta\omega_1^\sigma = 0 \tag{A.22}$$
$$\Delta\omega_1^\sigma = (\omega_v + \delta + \omega_c/2) \tag{A.23}$$
$$\Delta\omega_1^\sigma = -(\omega_v + \delta + \omega_c/2)\,. \tag{A.24}$$

Clearly, as $\mu$ crossed $\bar{\mu}_-$ the third peak for $\sigma = -$ sector is shifted by $-2\omega_v$ and this leads to a clear modification of LDOS which persists up the $\mu = \bar{\mu}_+$ at which the peak form the $\sigma = +$ sector moves by $2\omega_v$ and recovers the original LDOS.

The "creation" of a satellite peak at positive energy should not happen without an accompanying compensation of a positive energy peak jumping into negative energies. Indeed, such a compensation does occur for the contribution of $l = -1$ (which exchanging angular momentum with the vortex motion is connected to $l = -2$ and $l = 0$, the latter giving the jump.) It just turns out that, since the spatial dependence of the LDOS is determined by $u_l^\sigma(\mathbf{r})$, as can be seen from (A.4), the peaks from $l = -1$ do not contribute to the LDOS at the center of the vortex, $r = 0$. The peaks from $l = -1$ should contribute to the LDOS at a distance $\sim k_F^{-1}$ from the vortex center, which should be of the order of ten Angstroms in a superconducting TI. This can be resolved with the current STM technology.

# Appendix B

# Caroli-de Gennes modes in class DIII: analytic full spectrum

We demonstrate explicitly that a set of vortex bound modes exists, for any value of the chemical potential, and that they are gapped by $\Delta_0^2/E_F$, as usually for Caroli-de Gennes states. We are able to compute the modes beyond the zero-energy one. We introduce a simple model for the pairing with a vortex along the $z$ direction follows as $\Delta(\mathbf{r}) = \frac{\Delta_0}{\xi}(x - iy)$. This will be valid for wavefunctions $\psi(\mathbf{k})$ smooth on the scale $\xi^{-1}$ of the coherence length. The first quantized Hamiltonian then reads

$$H_0 = \begin{bmatrix} H - \mu & \frac{\Delta_0}{\xi}(x - iy) \\ \frac{\Delta_0}{\xi}(x + iy) & -H + \mu \end{bmatrix}. \tag{B.1}$$

In k-space it reads

$$H_0 = \begin{bmatrix} H_{\mathbf{k}} - \mu & i\frac{\Delta_0}{\xi}\left(\partial_{k_x} - i\partial_{k_y}\right) \\ i\frac{\Delta_0}{\xi}\left(\partial_{k_x} + i\partial_{k_y}\right) & -H_{\mathbf{k}} + \mu \end{bmatrix}. \tag{B.2}$$

Let us first diagonalize $H_{\mathbf{k}}$. It reads

$$H_{\mathbf{k}} = \boldsymbol{\sigma} \cdot \mathbf{k}. \tag{B.3}$$

We separate the contributions from $k_z$ from the others and from now on $\mathbf{k} = (k_x, k_y)$. We then write

$$\mathcal{H}_0 = \mathcal{H}_{0\perp} + \mathcal{H}_{0z} \tag{B.4}$$

with the first quantized Hamiltonians

$$H_{0\perp} = \begin{bmatrix} \boldsymbol{\sigma} \cdot \mathbf{k} - \mu & i\frac{\Delta_0}{\xi}\left(\partial_{k_x} - i\partial_{k_y}\right) \\ i\frac{\Delta_0}{\xi}\left(\partial_{k_x} + i\partial_{k_y}\right) & -\boldsymbol{\sigma} \cdot \mathbf{k} + \mu \end{bmatrix} \tag{B.5}$$

$$H_{0z} = \begin{bmatrix} k_z\sigma_z & 0 \\ 0 & -k_z\sigma_z \end{bmatrix}. \tag{B.6}$$

Let us neglect, as usual $H_{0z}$; we recover its contributions later. The perpendicular part of the metallic Hamiltonian has a single pair of eigenvalues $E^{\pm}_{\perp\mathbf{k}} = \pm k = \pm\sqrt{k_x^2 + k_y^2}$ with corresponding eigenstates

$$\left|\varphi^{\pm}_{k_x k_y}\right\rangle = \frac{1}{\sqrt{2}} \begin{pmatrix} 1 \\ \pm e^{i\theta} \end{pmatrix} \tag{B.7}$$

$\left[\left|\varphi^{\pm}_{k_xk_y}\right\rangle = \frac{1}{\sqrt{2}}\begin{pmatrix}\mp e^{-i\theta}\\ -1\end{pmatrix} \text{ for the PH sector}\right]$ where $\tan\theta = k_y/k_x$. As the chemical potential crosses a single band of the metallic Hamiltonian, we may project into the states with $E^{\pm}_{\mathbf{k}} \sim \mu$. Taking, for concreteness, a positive chemical potential, this means we may project into the $\left|\varphi^{+}_{k_xk_y}\right\rangle$ subspace. The wavefunctions are

$$\psi \to \frac{1}{\sqrt{2}}\begin{pmatrix}\begin{pmatrix}1\\ \pm e^{i\theta}\end{pmatrix}\psi_1\\ \begin{pmatrix}\mp e^{-i\theta}\\ -1\end{pmatrix}\psi_2\end{pmatrix} \tag{B.8}$$

We are then left with a Hamiltonian for $(\psi_1\,\psi_2)^T$,

$$H^{+}_{0\perp} \approx \begin{bmatrix} k-\mu & \Delta_e\begin{pmatrix} i\left(\partial_{k_x} - i\partial_{k_y}\right)\\ +A^{+}_x - iA^{+}_y\end{pmatrix}\\ \Delta_e\begin{pmatrix} i\left(\partial_{k_x} + i\partial_{k_y}\right)\\ +A^{+}_x + iA^{+}_y\end{pmatrix} & -k+\mu\end{bmatrix}, \tag{B.9}$$

where we defined $\Delta_e = \frac{\Delta_0}{\xi}$ and a U(1) Berry connection $\mathbf{A}^{+} = \left\langle\varphi^{+}_{\mathbf{k}}\left|i\nabla_{\mathbf{k}}\right|\varphi^{+}_{\mathbf{k}}\right\rangle$.

The Hamiltonian may be written

$$H^{+}_{0\perp} \approx \begin{bmatrix} E_{\mathbf{k}}-\mu & \Delta_e\left(i\left(\mathcal{D}_{k_x} - i\mathcal{D}_{k_y}\right)\right)\\ \Delta_e\left(i\left(\mathcal{D}_{k_x} + i\mathcal{D}_{k_y}\right)\right) & -E_{\mathbf{k}}+\mu\end{bmatrix}, \tag{B.10}$$

where we introduced the covariant derivative $\mathcal{D} = \partial - iA$. So if we look at $\mathbf{k}$ as a position operator, this is like a particle in real space in the presence of a gauge field. The Berry curvature reads, by definition

$$\mathcal{F} = d\mathcal{A} \tag{B.11}$$

or, in components

$$F_z \equiv F_{xy} = \partial_x A_y - \partial_y A_x. \tag{B.12}$$

Exchanging $\mathbf{x}$ with $\mathbf{k}$, this is effectively a quantum Hall problem and we may expect a similar spectrum.

For our single Fermi surface at $\mu = |\mathbf{k}| = k_F$ with rotational symmetry,

$$\begin{aligned} k_x + ik_y &= ke^{i\theta} && \text{(B.13)}\\ \partial_{k_x} - i\partial_{k_y} &= e^{-i\theta}\left(\partial_k - \frac{1}{k}\partial_\theta\right) && \text{(B.14)}\\ A_x - iA_y &= e^{-i\theta}\left(A_k - iA_\theta\right). && \text{(B.15)}\end{aligned}$$

(Notice that the vector field components are with lower indices as they are summed with the gradients, and transform like so. Also notice that $A_\theta$ is has dimension of $1/k$ and we are writing, $\mathbf{A} = A_k\hat{k} + A_\theta\hat{\theta}$, incorporating the $1/k$ from $\hat{\theta}$ in $A_\theta$.)

Since only $F_z \neq 0$, one may choose a gauge with $A_k = 0$ and $A_\theta = A_\theta(k)$. The curl in polar coordinates then gives

$$\begin{aligned} \frac{1}{k}\partial_k\left(kA_\theta\right) - \frac{1}{k}\partial_\theta A_k &= F_z\\ \Rightarrow \partial_k\left(kA_\theta\right) &= kF_z\\ \Rightarrow kA_\theta &= \int_0^k dk'\,k'\,F_z\left(k'\right) && \text{(B.16)}\end{aligned}$$

or

$$\Rightarrow 2\pi kA_\theta = 2\pi\int_0^k dk'\,k'\,F_3\left(k'\right). \tag{B.17}$$

We identify the left-hand-side. with the Berry connection line-integrated over a circle of radius $2\pi k$, that is, the Berry phase along this circle. For an insulating system, this value is dependent on the chemical potential. For the present system, however, we know we have metallic bands with well defined chirality, as

$$\begin{aligned} A_\theta &= i\frac{1}{k}\left\langle \varphi^+_{\mathbf{k}} \left| \partial_\theta \right| \varphi^+_{\mathbf{k}} \right\rangle \\ &= i\frac{1}{k}\frac{1}{2}\left(1\ e^{-i\theta}\right)\begin{pmatrix} 0 \\ ie^{i\theta} \end{pmatrix} \\ &= -\frac{1}{2k} \end{aligned} \tag{B.18}$$

and, hence,

$$2\pi k A_\theta = -1 \times \pi, \tag{B.19}$$

as expected. This is independent of the chemical potential.

The first quantized Hamiltonian becomes,

$$H_{0\perp} = \begin{bmatrix} E_k - \mu & i\Delta_e e^{-i\theta}\left(\partial_k - \left(\frac{i}{k}\partial_\theta + A_\theta\right)\right) \\ i\Delta_e e^{i\theta}\left(\partial_k + \left(\frac{i}{k}\partial_\theta + A_\theta\right)\right) & -E_k + \mu \end{bmatrix}. \tag{B.20}$$

We now unwind the $\theta$ phase with

$$W = \begin{bmatrix} e^{i\theta/2} & \\ & e^{-i\theta/2} \end{bmatrix}, \tag{B.21}$$

such that

$$\tilde{H}_{0\perp} = W^{-1}H_{0\perp}W \tag{B.22}$$

$$\begin{aligned} &= (E_k - \mu)\rho_z \\ &\quad +\Delta_e\left(\rho_x i\partial_k - \rho_y\left(\frac{1}{k}\left(-i\partial_\theta - \rho_z\frac{1}{2}\right) - A_\theta\right)\right). \end{aligned} \tag{B.23}$$

This new Hamiltonian clearly commutes with $-i\partial_\theta$, such that the original one obeys

$$\left[H_{0\perp}, \tilde{L}_z\right] = 0, \tag{B.24}$$

with $\tilde{L}_z = -i\partial_\theta - \frac{1}{2}\rho_z$. So we finish unwinding by writing

$$\begin{aligned} \psi &= W^{-1}\tilde{\psi} \\ \tilde{\psi} &= e^{in\theta}\phi. \end{aligned} \tag{B.25}$$

Then

$$\psi = \begin{pmatrix} e^{i(n-1/2)\theta}\phi_1(k) \\ e^{i(n+1/2)\theta}\phi_2(k) \end{pmatrix}. \tag{B.26}$$

The wavefunctions $\psi$ must obey periodic boundary conditions around $\theta$, so $n$ is a half-integer here. We thus want to solve

$$\left[(E_k - \mu)\rho_z + \Delta_e\left(\rho_x i\partial_k - \rho_y\left(\frac{1}{k}\left(n - \rho_z\frac{1}{2}\right) - A_\theta\right)\right)\right]\phi_n = E_n\phi_n. \tag{B.27}$$

We may play with this unitary transformation to find more convenient forms of the Hamiltonian. The

normalization condition,

$$\begin{aligned}\int_0^{2\pi} d\theta \int_0^{\infty} kdk\,|\psi|^2 &= 1 \\ \Rightarrow \int_0^{\infty} kdk\,|\phi|^2 &= \frac{1}{2\pi},\end{aligned} \tag{B.28}$$

for example, suggests the introduction of factors of $\sqrt{k}$ which compensate the shifts $\rho_z/2$. In general, the two most convenient transformation reads

$$W_{ph} = \frac{1}{\sqrt{k}} \begin{bmatrix} e^{i(n-1)\theta} & \\ & ie^{in\theta} \end{bmatrix}, \tag{B.29}$$

which lead us to

$$H_{0\perp} = \begin{bmatrix} E_k - \mu & \Delta_e \left(\partial_k + \frac{n-\frac{1}{2}}{k} - A_\theta\right) \\ \Delta_e \left(-\partial_k + \frac{n-\frac{1}{2}}{k} - A_\theta\right) & -E_k + \mu \end{bmatrix}, \tag{B.30}$$

now with $n$ an integer. We stick to the latter case.

The wavefunction reads, generally,

$$\psi = W_{ph} \begin{pmatrix} u(k) \\ v(k) \end{pmatrix}. \tag{B.31}$$

From our previous considerations, $A_\theta = -1/2k$. Then,

$$H_{0\perp} = \rho_z (E_k - \mu) + \rho_x \frac{\Delta_e}{k} n + \rho_y \Delta_e i\partial_k. \tag{B.32}$$

The functions $u(k)$ and $v(k)$ are centered around $k_F$. We may thus approximate this as

$$H_{0\perp} \approx \rho_z (E_k - \mu) + \rho_x \frac{\Delta_e}{k_F} n + \rho_y \Delta_e i\partial_k. \tag{B.33}$$

This is equivalent to the Jackiw-Rebbi model in k-space. Kinks in the "soliton field", whose role here is played by $E_k - \mu \equiv k - k_F$, gives mid-gap states (bound to the kink). For whatever value of the chemical potential, such kink always exists. The energies are

$$E_n \approx \frac{\Delta_e}{k_F} n \tag{B.34}$$

For $n = 0$, we always have a zero-energy eigenstate, as promised.

Normalization demands that ZMs appear alone. The general form is

$$u(k) = e^{\int^k \frac{\mu - E_{k'}}{\Delta_e} dk'} \tag{B.35}$$

$$v(k) = u(k), \tag{B.36}$$

with the energy a monotonically increasing function of $k$. Notice that if $E_k$ is close to the Fermi energy we may approximate $\mu - E_{k'} \approx \hbar v_F k$ and $u(k)$ will be a Gaussian with width $\sqrt{\Delta_e/(\hbar v_F)} \approx \sqrt{\Delta_0/(\hbar v_F \xi)}$.

Quite generally then

$$\psi_n = e^{in\theta} \frac{e^{\int^k \frac{\mu - E_{k'}}{\Delta_e} dk'}}{\sqrt{2\pi k}} \begin{pmatrix} e^{-i\theta} \\ i \end{pmatrix}. \tag{B.37}$$

Now, $\psi_0$ corresponds to the zero-energy eigenstate. A feature to notice here is that the spinor is an eigenstate of $\mathbf{t} \cdot \boldsymbol{\rho}$ with $\mathbf{t}$ a vector which is tangent to the FS at $(k_F, \theta)$ this pseudo-spin locking to the momentum gives the $\pi$ phase around the Fermi surface and allows generalization for more complicated Fermi surfaces.

# Appendix C

# Caroli-de Gennes spectrum in class DIII: numerics and dispersion

We may use the same method considered in the case of vortex modes of doped topological insulators to numerically compute the full spectrum at arbitrary $\mu$ for vortex modes in class DIII topological superconductors. We will also treat the $k_z$ dispersion perturbatively. Back to the Hamiltonian, after Fourier transforming in the $z$ direction and rotating out the angular dependence, the wave functions read

$$\psi_l(r,\theta) = e^{i\left(l-\frac{\rho_z+\sigma_z}{2}\right)\theta}\phi(r), \tag{C.1}$$

where $\phi(r)$ satisfies

$$\begin{aligned}
\left[-iv_F\rho_z\left[\sigma_x\partial_r + i\sigma_y\frac{l-(\rho_z+\sigma_z)/2}{r}\right] + v_F\rho_z\sigma_z k_z - \rho_z\mu + |\Delta|\rho_x\right]\phi(r) &= E_l\phi(r) \\
\Rightarrow \begin{pmatrix}
v_Fk_z-\mu & -iv_F\left[\partial_r+\frac{l}{r}\right] & |\Delta| & \\
-iv_F\left[\partial_r-\frac{(l-1)}{r}\right] & -v_Fk_z-\mu & & |\Delta| \\
|\Delta| & & -v_Fk_z+\mu & iv_F\left[\partial_r+\frac{(l+1)}{r}\right] \\
& |\Delta| & iv_F\left[\partial_r-\frac{l}{r}\right] & v_Fk_z+\mu
\end{pmatrix}\phi_{nl}(r) &= E_{nl}\phi_{nl}(r).
\end{aligned} \tag{C.2}$$

For each given value of $l$, we may have many (labeled by $n$) eigenstates. Let us start by making $k_z = 0$. We thus have

$$\begin{pmatrix}
-\mu & -iv_F\left[\partial_r+\frac{l}{r}\right] & |\Delta| & \\
-iv_F\left[\partial_r-\frac{(l-1)}{r}\right] & -\mu & & |\Delta| \\
|\Delta| & & \mu & iv_F\left[\partial_r+\frac{(l+1)}{r}\right] \\
& |\Delta| & iv_F\left[\partial_r-\frac{l}{r}\right] & \mu
\end{pmatrix}\phi_{nl}(r) = E_{nl}\phi_{nl}(r). \tag{C.3}$$

Let us rescale the energies by the gap strength $\Delta_0$ and lengths by the coherence length $v_F/\Delta_0$. Then, labeling the dimensionless variables by bars,

$$\begin{pmatrix}
-\bar{\mu} & -i\left[\partial_{\bar{r}}+\frac{l}{\bar{r}}\right] & |\bar{\Delta}| & \\
-i\left[\partial_{\bar{r}}-\frac{(l-1)}{\bar{r}}\right] & -\bar{\mu} & & |\bar{\Delta}| \\
|\bar{\Delta}| & & \bar{\mu} & i\left[\partial_{\bar{r}}+\frac{(l+1)}{\bar{r}}\right] \\
& |\bar{\Delta}| & i\left[\partial_{\bar{r}}-\frac{l}{\bar{r}}\right] & \bar{\mu}
\end{pmatrix}\phi_{nl}(\bar{r}) = E_{nl}\phi_{nl}(\bar{r}). \tag{C.4}$$

In what follows we omit the bars to avoid cluttering.

Define the kinetic Hamiltonian

$$K_l \equiv \begin{pmatrix} -\mu & -i\left[\partial_r + \frac{l}{r}\right] \\ -i\left[\partial_r - \frac{(l-1)}{r}\right] & -\mu \end{pmatrix}. \tag{C.5}$$

We expand the wavefunctions in terms of Bessel functions. Noticing the following recurrence relations

$$\left(\partial_r + \frac{l}{r}\right) J_l(kr) = kJ_{l-1}(kr), \tag{C.6}$$

$$\left(\partial_r - \frac{l}{r}\right) J_l(kr) = -kJ_{l+1}(kr), \tag{C.7}$$

we may define the raising and lowering operators

$$a_l = \left(\partial_r + \frac{l}{r}\right) \tag{C.8}$$

$$a_l^\dagger = -\left(\partial_r - \frac{l-1}{r}\right). \tag{C.9}$$

They naturally act as

$$a_l J_l(kr) = kJ_{l-1}(kr) \tag{C.10}$$

$$a_l^\dagger J_{l-1}(kr) = kJ_l(kr). \tag{C.11}$$

This allows writing the Bessel equation naturally as

$$a_l^\dagger a_l J_l(kr) = k^2 J_l(kr). \tag{C.12}$$

The kinetic Hamiltonian reads

$$K_l \equiv \begin{pmatrix} -\mu & -ia_l \\ ia_l^\dagger & -\mu \end{pmatrix}. \tag{C.13}$$

With this we may guess eigenstates of the kinetic part of the Hamiltonian

$$\begin{aligned} & K_l \begin{pmatrix} \alpha J_{l-1}(kr) \\ \beta J_l(kr) \end{pmatrix} \\ = & \begin{pmatrix} -\mu\alpha - ik\beta & 0 \\ 0 & ik\alpha - \mu\beta \end{pmatrix} \begin{pmatrix} J_{l-1}(kr) \\ J_l(kr) \end{pmatrix} \qquad \text{(C.14)} \\ = & \lambda \begin{pmatrix} \alpha J_{l-1}(kr) \\ \beta J_l(kr) \end{pmatrix}. \qquad \text{(C.15)} \end{aligned}$$

This implies

$$\begin{pmatrix} -\mu - \lambda & -ik \\ ik & -\mu - \lambda \end{pmatrix} \begin{pmatrix} \alpha \\ \beta \end{pmatrix} = 0 \tag{C.16}$$

Solutions give energies $\lambda_l^\pm(k) = -\mu \pm k$. The corresponding coefficients are

$$\begin{pmatrix} \alpha^\pm \\ \beta^\pm \end{pmatrix} = \frac{1}{\sqrt{2}} \begin{pmatrix} 1 \\ \pm i \end{pmatrix}. \tag{C.17}$$

We thus write

$$\chi_{kl}^\pm = \frac{1}{\sqrt{\mathcal{N}_k}} \begin{pmatrix} J_{l-1}(kr) \\ \pm iJ_l(kr) \end{pmatrix}. \tag{C.18}$$

The normalization factor reads

$$\mathcal{N}_k = \int_0^\infty r dr J_l\left(kr\right) J_l\left(kr\right). \tag{C.19}$$

Notice that in this continuum limit

$$\begin{aligned} & \int_0^\infty r dr J_l\left(kr\right) J_l\left(k^{'} r\right) && \text{(C.20)} \\ = & \int_0^\infty r dr J_{l+1}\left(kr\right) J_{l+1}\left(k^{'} r\right) && \text{(C.21)} \\ = & \frac{\delta\left(k-k^{'}\right)}{k}. && \text{(C.22)} \end{aligned}$$

These normalization factors will be regularized in the case of having a finite cylinder.

The Nambu partners are solved similarly by diagonalizing $-K_{l+1}$. The states read

$$\tilde{\chi}_{kl}^{\pm} = \frac{1}{\sqrt{\tilde{\mathcal{N}}_k^{\pm}}} \begin{pmatrix} J_l\left(kr\right) \\ \pm i J_{l+1}\left(kr\right) \end{pmatrix} \tag{C.23}$$

with energies $\tilde{\lambda}_l^{\pm}\left(k\right) = \mu \pm k$. Notice $\tilde{\lambda}_l^{\pm} = -\lambda_l^{\pm}$. We take the same label $l$ in the eigenvalues $\lambda$ for both Nambu sectors as we will sum over the same values of $k$ (even in the finite radius.)

The eigenstates of the vortex BdG Hamiltonian are thus

$$\psi_{nl}\left(r,\theta\right) = e^{i\left(l-\frac{\rho_z+\sigma_z}{2}\right)\theta} \phi_{nl}\left(r\right), \tag{C.24}$$

where

$$\phi_{nl}\left(r\right) = \begin{pmatrix} \int dk \left[c_{lk}^{n+} \chi_{kl}^{+} + c_{lk}^{n-} \chi_{kl}^{-}\right] \\ \int dk \left[d_{lk}^{n+} \tilde{\chi}_{kl}^{+} + d_{lk}^{n-} \tilde{\chi}_{kl}^{-}\right] \end{pmatrix}. \tag{C.25}$$

The radial BdG equation will read

$$\begin{aligned} & \begin{pmatrix} K_l & |\Delta| \\ |\Delta| & -K_{l+1} \end{pmatrix} \begin{pmatrix} \int_k \left[c_{lk}^{n+} \chi_{kl}^{+} + c_{lk}^{n-} \chi_{kl}^{-}\right] \\ \int_k \left[d_{lk}^{n+} \tilde{\chi}_{kl}^{+} + d_{lk}^{n-} \tilde{\chi}_{kl}^{-}\right] \end{pmatrix} && \text{(C.26)} \\ = & E_{nl} \begin{pmatrix} \int_k \left[c_{lk}^{n+} \chi_{kl}^{+} + c_{lk}^{n-} \chi_{kl}^{-}\right] \\ \int_k \left[d_{lk}^{n+} \tilde{\chi}_{kl}^{+} + d_{lk}^{n-} \tilde{\chi}_{kl}^{-}\right] \end{pmatrix}. && \text{(C.27)} \end{aligned}$$

Taking the scalar product with $\phi_{nl}$ with a $\int rdr$ measure, we have

$$\begin{aligned}
&\left\langle nl\left|\begin{pmatrix} K_l & |\Delta| \\ |\Delta| & -K_{l+1}\end{pmatrix}\right|nl\right\rangle \\
&= \int_0^\infty rdr\phi_{nl}^{+}(r)^\dagger \begin{pmatrix} K_l & |\Delta| \\ |\Delta| & -K_{l+1}\end{pmatrix}\phi_{nl}^{+}(r) \qquad \text{(C.28)}\\
&= \int_k \left[c_{lk}^{n+*}c_{lk}^{n+}\lambda_{lk}^{+}+c_{lk}^{n-*}c_{lk}^{n-}\lambda_{lk}^{-}\right] \\
&\quad+\int_k \left[d_{lk}^{n+*}d_{lk}^{n+}\tilde{\lambda}_{l+1k}^{+}+d_{lk}^{n-*}d_{lk}^{n-}\tilde{\lambda}_{l+1k}^{-}\right] \\
&\quad+\int_{k'}\int_k\int_0^\infty rdr\,|\Delta|\left[c_{lk'}^{n+*}d_{lk}^{n+}\chi_{k'l}^{+\dagger}\tilde{\chi}_{kl}^{+}+c_{lk'}^{n-*}d_{lk}^{n+}\chi_{k'l}^{-\dagger}\tilde{\chi}_{kl}^{+}\right] \\
&\quad+\int_{k'}\int_k\int_0^\infty rdr\,|\Delta|\left[c_{lk'}^{n+*}d_{lk}^{n-}\chi_{k'l}^{+\dagger}\tilde{\chi}_{kl}^{-}+c_{lk'}^{n-*}d_{lk}^{n-}\chi_{k'l}^{-\dagger}\tilde{\chi}_{kl}^{-}\right]+h.c. \\
&= \int_{k,k'}\begin{pmatrix} c_{lk}^{n+} & c_{lk}^{n-} & d_{lk}^{n+} & d_{lk}^{n-}\end{pmatrix}^*\begin{pmatrix} \lambda_{lk}^{+}\delta_{kk'} & & |\Delta|_{l,kk'}^{++} & |\Delta|_{l,kk'}^{+-} \\ & \lambda_{lk}^{-}\delta_{kk'} & |\Delta|_{l,kk'}^{-+} & |\Delta|_{l,kk'}^{--} \\ |\Delta|_{l,kk'}^{++} & |\Delta|_{l,kk'}^{-+} & -\lambda_{lk}^{+}\delta_{kk'} & \\ |\Delta|_{l,kk'}^{+-} & |\Delta|_{l,kk'}^{--} & & -\lambda_{lk}^{-}\delta_{kk'}\end{pmatrix}\begin{pmatrix} c_{lk'}^{n+} \\ c_{lk'}^{n-} \\ d_{lk'}^{n+} \\ d_{lk'}^{n-}\end{pmatrix} \qquad \text{(C.29)}
\end{aligned}$$

where we used

$$\begin{aligned}
\int_0^\infty rdr\tilde{\chi}_{k'l}^{\sigma'\dagger}\tilde{\chi}_{kl}^{\sigma} &= \delta_{\sigma\sigma'}\delta\left(k-k'\right) \qquad \text{(C.30)}\\
\int_0^\infty rdr\chi_{k'l}^{\sigma'\dagger}|\Delta|\tilde{\chi}_{kl}^{\sigma} &= \frac{1}{\sqrt{\mathcal{N}^\sigma\tilde{\mathcal{N}}^{\sigma'}}}\int_0^\infty rdr\,|\Delta|\left[J_{l-1}\left(k'r\right)J_l(kr)\right. \\
&\quad\left.+\sigma\sigma' J_l\left(k'r\right)J_{l+1}(kr)\right] \\
&\equiv |\Delta|_{l,kk'}^{\sigma\sigma'}. \qquad \text{(C.31)}
\end{aligned}$$

We end at the problem

$$\int_{k,k'}\begin{pmatrix} c_{lk}^{n+} \\ c_{lk}^{n-} \\ d_{lk}^{n+} \\ d_{lk}^{n-}\end{pmatrix}^\dagger\begin{pmatrix} \left(\lambda_{lk}^{+}-E_{nl}\right)\delta_{kk'} & & |\Delta|_{l,kk'}^{++} & |\Delta|_{l,kk'}^{+-} \\ & \left(\lambda_{lk}^{-}-E_{nl}\right)\delta_{kk'} & |\Delta|_{l,kk'}^{-+} & |\Delta|_{l,kk'}^{--} \\ |\Delta|_{l,k'k}^{++} & |\Delta|_{l,k'k}^{-+} & \left(-\lambda_{lk}^{+}-E_{nl}\right)\delta_{kk'} & \\ |\Delta|_{l,k'k}^{+-} & |\Delta|_{l,k'k}^{--} & & \left(-\lambda_{lk}^{-}-E_{nl}\right)\delta_{kk'}\end{pmatrix}\begin{pmatrix} c_{lk'}^{n+} \\ c_{lk'}^{n-} \\ d_{lk'}^{n+} \\ d_{lk'}^{n-}\end{pmatrix}=0. \qquad \text{(C.32)}$$

Take a positive value for the chemical potential $\mu$. The states with $\lambda^-$ above are then high energy and do not cross the Fermi energy for any value of $k$. They are not relevant for the low energy excitations. One may then neglect the unnecessary coefficients, arriving at

$$\phi_{nl}(r)=\begin{pmatrix}\int dk\left[c_{lk}^{n+}\chi_{kl}^{+}\right] \\ \int dk\left[d_{lk}^{n+}\tilde{\chi}_{kl}^{+}\right]\end{pmatrix} \qquad \text{(C.33)}$$

in which case the eigenvalue problem simplifies to

$$\int_{k,k'}\begin{pmatrix} c_{lk}^{n+} & d_{lk}^{n-}\end{pmatrix}\begin{pmatrix}\left(\lambda_{lk}^{+}-E_{nl}\right)\delta_{kk'} & |\Delta|_{l,kk'}^{++} \\ |\Delta|_{l,k'k}^{++} & \left(-\lambda_{lk}^{+}-E_{nl}\right)\delta_{kk'}\end{pmatrix}\begin{pmatrix} c_{lk'}^{n+} \\ d_{lk'}^{n+}\end{pmatrix}=0. \qquad \text{(C.34)}$$

We know that the solution consists of $E_{nl}\sim\Delta_0$, which correspond to scattering states and $E_{n_{CdG}l}=$

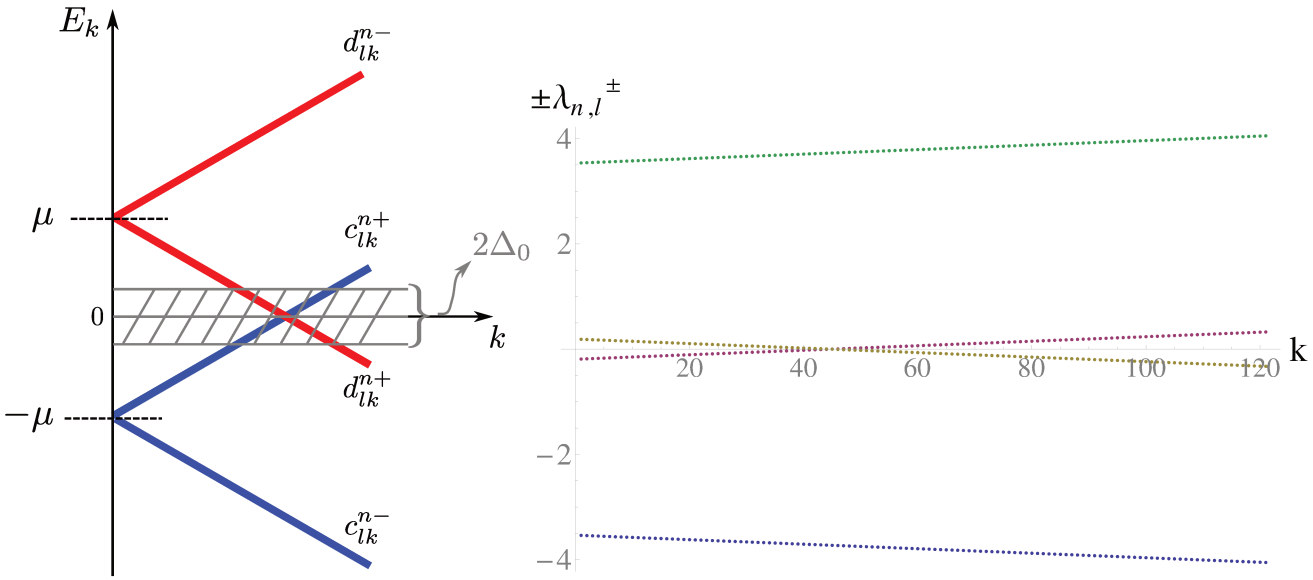


Figure C.1: (left) Schematics of the energy bands and coupling by SC. Only the bands $\lambda^+_{lk}$ and $-\lambda^+_{l+1k}$ match in energy at the Fermi momentum. To compute the low-energy vortex bound-states spectrum numerically, it is enough to consider only these. (right) Actual bands used for the numerics. In a finite system with radius $R$, $k \to \alpha_{lj}/R$. We focus in values of $j$ around the lowest energy-bands crossing. Details of the parameters used follow below in the text.

$\Delta_0^2/E_F \times l$. We may then simply write

$$\psi_{nl}(r,\theta) = \int dk e^{i\left(l-\frac{\rho_z+\sigma_z}{2}\right)\theta} \begin{pmatrix} \frac{c^{n+}_{lk}}{\sqrt{\mathcal{N}^+_k}} \begin{pmatrix} J_{l-1}(kr) \\ iJ_l(kr) \end{pmatrix} \\ \frac{d^{n+}_{lk}}{\sqrt{\mathcal{N}^+_k}} \begin{pmatrix} J_l(kr) \\ iJ_{l+1}(kr) \end{pmatrix} \end{pmatrix} \tag{C.35}$$

$$= \int dk \begin{pmatrix} \frac{c^{n}_{lk}}{\sqrt{\mathcal{N}_k}} \begin{pmatrix} e^{i(l-1)\theta}J_{l-1}(kr) \\ ie^{il\theta}J_l(kr) \end{pmatrix} \\ \frac{d^{n}_{lk}}{\sqrt{\mathcal{N}_k}} \begin{pmatrix} e^{il\theta}J_l(kr) \\ ie^{i(l+1)\theta}J_{l+1}(kr) \end{pmatrix} \end{pmatrix} \tag{C.36}$$

$$\equiv \begin{pmatrix} \mathbf{u}_{ln}(r,\theta) \\ \mathbf{v}_{ln}(r,\theta) \end{pmatrix}, \tag{C.37}$$

and focus on the values of $n$ corresponding to the CdG modes. We notice that $\mathcal{N}^+_k = \tilde{\mathcal{N}}^-_k \equiv \mathcal{N}_k$ and that we may discard the + labels.

## Hamiltonian in the "vortex basis"

Let us make use of the states we computed above to rewrite the SC Hamiltonian in a way in which we can capture the effects of the gap in the energies of the in-plane vortex modes into a $k_z$ parametrized Hamiltonian.

For a given Fermi surface, the full second quantized Hamiltonian, in the presence of a vortex and a background EM field, reads

$$H = \int d^3x \Psi^\dagger h_{BdG} \Psi, \tag{C.38}$$

where

$$
\begin{aligned}
h_{BdG} &= v_F \mathbf{\Gamma} \cdot (-i\nabla) + \Lambda_x \Delta_0 (r) e^{i\rho_z \theta} && \text{(C.39)}\\
&\quad -v_F \rho_z \mathbf{\Gamma} \cdot \mathbf{A} + \rho_z A_0 && \text{(C.40)}\\
&= v_F \mathbf{\Gamma} \cdot (-i\nabla)_\perp + \Lambda_x \Delta_0 (r) e^{i\rho_z \theta} && \text{(C.41)}\\
&\quad +v_F \Gamma_z (-i\partial_z) && \text{(C.42)}\\
&\quad -v_F \rho_z \mathbf{\Gamma} \cdot \mathbf{A} + \rho_z A_0 && \text{(C.43)}\\
&\equiv h_\perp + h_z + h_{EM}. && \text{(C.44)}
\end{aligned}
$$

We will consider $\mathbf{A} = (0, 0, Et)$, which is the main case of interest. As this is independent of $z$, $k_z$ stays a good quantum number in this situation.

We now expand,

$$
\Psi = \sum_{k_z, n, l} e^{ik_z z} \phi_{nl} (r, \theta) f_{k_z nl}. \tag{C.45}
$$

We have

$$
\begin{aligned}
\phi_{nl} (r) &= \begin{pmatrix} \int dk \left[ c_{lk}^{n+} \chi_{kl}^{+} + c_{lk}^{n-} \chi_{kl}^{-} \right] \\ \int dk \left[ d_{lk}^{n+} \tilde{\chi}_{kl}^{+} + d_{lk}^{n-} \tilde{\chi}_{kl}^{-} \right] \end{pmatrix} && \text{(C.46)}\\
&\equiv \begin{pmatrix} \mathbf{u}_{ln}^{+} (r, \theta) + \mathbf{u}_{ln}^{-} (r, \theta) \\ \mathbf{v}_{ln}^{+} (r, \theta) + \mathbf{v}_{ln}^{-} (r, \theta) \end{pmatrix}. && \text{(C.47)}
\end{aligned}
$$

From our previous arguments, one might expect that $\mathbf{u}^- \approx \mathbf{v}^- \approx 0$. The complete basis for expansion, however is this one, and might prove necessary for the complete expansion of the fermionic operator.

Taking each contribution $h_\perp + h_z + h_{EM}$ separately,

$$
\begin{aligned}
H &= \int d^3 x \Psi^\dagger h_{BdG} \Psi\\
&= \sum_{k_z, n, l} \sum_{k_z', n', l'} \int d^3 x f_{k_z' n' l'}^\dagger e^{-ik_z' z} \phi_{n' l'}^\dagger (r, \theta) h_{BdG} e^{ik_z z} \phi_{nl} (r, \theta) f_{k_z nl}\\
&= \sum_{k_z, n, l} \sum_{k_z', n', l'} \int d^3 x f_{k_z' n' l'}^\dagger e^{-ik_z' z} \phi_{n' l'}^\dagger (r, \theta) h_\perp e^{ik_z z} \phi_{nl} (r, \theta) f_{k_z nl}\\
&\quad + \sum_{k_z, n, l} \sum_{k_z', n', l'} \int d^3 x f_{k_z' n' l'}^\dagger e^{-ik_z' z} \phi_{n' l'}^\dagger (r, \theta) h_z e^{ik_z z} \phi_{nl} (r, \theta) f_{k_z nl}\\
&\quad + \sum_{k_z, n, l} \sum_{k_z', n', l'} \int d^3 x f_{k_z' n' l'}^\dagger e^{-ik_z' z} \phi_{n' l'}^\dagger (r, \theta) h_{EM} e^{ik_z z} \phi_{nl} (r, \theta) f_{k_z nl}\\
&= \sum_{k_z, n, l} f_{k_z nl}^\dagger f_{k_z nl} E_{nl} && \text{(C.48)}\\
&\quad + \sum_{k_z, n, l} \sum_{n', l'} f_{k_z n' l'}^\dagger \tilde{h}_z^{n' l', nl} f_{k_z nl} && \text{(C.49)}\\
&\quad + \sum_{k_z, n, l} \sum_{n', l'} f_{k_z n' l'}^\dagger \tilde{h}_{EM}^{n' l', nl} f_{k_z nl}, && \text{(C.50)}
\end{aligned}
$$

where

$$
\begin{aligned}
\tilde{h}_z^{n' l', nl} &= v_F k_z \int d^2 r \phi_{n' l'}^\dagger (r, \theta) \Gamma_z \phi_{nl} (r, \theta) && \text{(C.51)}\\
\tilde{h}_{EM}^{n' l', nl} &= -v_F A_z \int d^2 r \phi_{n' l'}^\dagger (r, \theta) \rho_z \Gamma_z \phi_{nl} (r, \theta). && \text{(C.52)}
\end{aligned}
$$

Let us compute these explicitly. First, notice that

$$\phi_{nl}(r,\theta)=\int dke^{i\left(l-\frac{\rho_z+\sigma_z}{2}\right)\theta}\begin{pmatrix}\frac{c_{lk}^{n+}}{\sqrt{\mathcal{N}_k}}\begin{pmatrix}J_{l-1}(kr)\\ iJ_l(kr)\end{pmatrix}+\frac{c_{lk}^{n-}}{\sqrt{\mathcal{N}_k}}\begin{pmatrix}J_{l-1}(kr)\\ -iJ_l(kr)\end{pmatrix}\\ \frac{d_{lk}^{n+}}{\sqrt{\mathcal{N}_k}}\begin{pmatrix}J_l(kr)\\ iJ_{l+1}(kr)\end{pmatrix}+\frac{d_{lk}^{n-}}{\sqrt{\mathcal{N}_k}}\begin{pmatrix}J_l(kr)\\ -iJ_{l+1}(kr)\end{pmatrix}\end{pmatrix}, \tag{C.53}$$

and that the exponential factor $e^{i\left(l-\frac{\rho_z+\sigma_z}{2}\right)\theta}$ commutes with both $\Gamma_z$ and $\rho_z\Gamma_z$. We safely write then

$$\phi_{nl}(r,\theta)=e^{i\left(l-\frac{\rho_z+\sigma_z}{2}\right)\theta}\tilde{\phi}_{nl}(r) \tag{C.54}$$

and notice that

$$\left\langle nl|\Gamma_z|n^{'}l^{'}\right\rangle=\delta_{ll'}\int rdr\tilde{\phi}_{n^{'}l}^{\dagger}(r)\,\Gamma_z\tilde{\phi}_{nl}(r) \tag{C.55}$$

and similarly for $\rho_z\Gamma_z$. Variables with tilde will be taken for when neglecting the $\theta$ contributions. Now

$$\begin{aligned}&\int rdr\tilde{\phi}_{n^{'}l}^{\dagger}(r)\,\Gamma_z\tilde{\phi}_{nl}(r)\\ =&\sum_{\sigma,\sigma^{'}=\pm}\int rdr\left(\tilde{\mathbf{u}}_{ln^{'}}^{\sigma^{'}}\right)^{\dagger}\sigma_z\tilde{\mathbf{u}}_{ln}^{\sigma}\\ &-\int rdr\left(\tilde{\mathbf{v}}_{ln^{'}}^{\sigma^{'}}\right)^{\dagger}\sigma_z\tilde{\mathbf{v}}_{ln}^{\sigma}.\end{aligned} \tag{C.56}$$

Now we have

$$\begin{aligned}&\int rdr\left(\tilde{\mathbf{u}}_{ln^{'}}^{\sigma^{'}}\right)^{\dagger}\sigma_z\tilde{\mathbf{u}}_{ln}^{\sigma}\\ =&\int dkdk^{'}\frac{c_{lk^{'}}^{n^{'}\sigma^{'}}c_{lk}^{n\sigma}}{\sqrt{\mathcal{N}_{k^{'}}\mathcal{N}_k}}\int rdr\left(J_{l-1}\left(k^{'}r\right)-i\sigma^{'}J_l\left(k^{'}r\right)\right)\begin{pmatrix}J_{l-1}(kr)\\ -i\sigma J_l(kr)\end{pmatrix}\\ =&\int dkdk^{'}\frac{c_{lk^{'}}^{n^{'}\sigma^{'}}c_{lk}^{n\sigma}}{\sqrt{\mathcal{N}_{k^{'}}\mathcal{N}_k}}\int rdr\left[J_{l-1}\left(k^{'}r\right)J_{l-1}(kr)-\sigma^{'}\sigma J_l\left(k^{'}r\right)J_l(kr)\right].\end{aligned} \tag{C.57}$$

Now

$$\int_0^{\infty}rdrJ_l(kr)\,J_l\left(k^{'}r\right)=\frac{\delta\left(k-k^{'}\right)}{k}. \tag{C.58}$$

Then,

$$\begin{aligned}\int rdr\left(\tilde{\mathbf{u}}_{ln^{'}}^{\sigma^{'}}\right)^{\dagger}\sigma_z\tilde{\mathbf{u}}_{ln}^{\sigma}&=\int dkdk^{'}\frac{c_{lk^{'}}^{n^{'}\sigma^{'}}c_{lk}^{n\sigma}}{\sqrt{\mathcal{N}_{k^{'}}\mathcal{N}_k}}\frac{\delta\left(k-k^{'}\right)}{k}\left[1-\sigma^{'}\sigma\right]\\ &=\left[1-\sigma^{'}\sigma\right]\int dkc_{lk}^{n^{'}\sigma^{'}}c_{lk}^{n\sigma}\\ &=(1-\delta_{\sigma\sigma^{'}})\int dkc_{lk}^{n^{'}\sigma^{'}}c_{lk}^{n\sigma}.\end{aligned} \tag{C.59}$$

Similarly,

$$\int rdr\left(\tilde{\mathbf{v}}_{ln^{'}}^{\sigma^{'}}\right)^{\dagger}\sigma_z\tilde{\mathbf{v}}_{ln}^{\sigma}=(1-\delta_{\sigma\sigma^{'}})\int dkd_{lk}^{n^{'}\sigma^{'}}d_{lk}^{n\sigma}. \tag{C.60}$$

Thus

$$\begin{aligned}
\left\langle nl|\Gamma_z|n^{'}l\right\rangle &= 2\int dk\left[c_{lk}^{n^{'}+}c_{lk}^{n-}+c_{lk}^{n^{'}-}c_{lk}^{n+}\right] \\
&\quad -2\int dk\left[d_{lk}^{n^{'}+}d_{lk}^{n-}+d_{lk}^{n^{'}-}d_{lk}^{n+}\right] &\text{(C.61)}\\
&\equiv \tilde{v}_l^{nn^{'}} &\text{(C.62)}\\
\left\langle nl|\rho_z\Gamma_z|n^{'}l\right\rangle &= 2\int dk\left[c_{lk}^{n^{'}+}c_{lk}^{n-}+c_{lk}^{n^{'}-}c_{lk}^{n+}\right] \\
&\quad +2\int dk\left[d_{lk}^{n^{'}+}d_{lk}^{n-}+d_{lk}^{n^{'}-}d_{lk}^{n+}\right] &\text{(C.63)}\\
&\equiv \tilde{q}_l^{nn^{'}}. &\text{(C.64)}
\end{aligned}$$

In this new basis we thus have

$$H=\sum_{k_z,l,n,n^{'}} f_{k_zln}^{\dagger}\left[E_{nl}\delta_{nn^{'}}+v_F\left(k_z\tilde{v}_l^{nn^{'}}-\tilde{q}_l^{nn^{'}}A_z\right)\right]f_{k_zln^{'}}. \tag{C.65}$$

## Coefficients analysis

To try and evaluate $\tilde{v}$ and $\tilde{q}$ explicitly in some cases of interest, let us try to relate the coefficients $c^{\pm}$ and $d^{\pm}$

Let us first check PH symmetry properties. The operator reads $\Xi=\rho_y\sigma_yK$. We have

$$\begin{aligned}
\Xi\psi_{nl} &= \begin{pmatrix} & & & -1\\ & & 1 & \\ & 1 & & \\ -1 & & & \end{pmatrix}\int\frac{dk}{\sqrt{\mathcal{N}_k}}\left(\begin{array}{c} c_{lk}^{n+}\begin{pmatrix} e^{i(l-1)\theta}J_{l-1}(kr)\\ ie^{il\theta}J_l(kr)\end{pmatrix}+c_{lk}^{n-}\begin{pmatrix} e^{i(l-1)\theta}J_{l-1}(kr)\\ -ie^{il\theta}J_l(kr)\end{pmatrix}\\ d_{lk}^{n+}\begin{pmatrix} e^{il\theta}J_l(kr)\\ ie^{i(l+1)\theta}J_{l+1}(kr)\end{pmatrix}+d_{lk}^{n-}\begin{pmatrix} e^{il\theta}J_l(kr)\\ -ie^{i(l+1)\theta}J_{l+1}(kr)\end{pmatrix}\end{array}\right)^* \\
&= \int dk\frac{1}{\sqrt{\mathcal{N}_k}}\left(\begin{array}{c} d_{lk}^{n+*}\begin{pmatrix} ie^{-i(l+1)\theta}J_{l+1}(kr)\\ e^{-il\theta}J_l(kr)\end{pmatrix}+d_{lk}^{n-*}\begin{pmatrix} -ie^{-i(l+1)\theta}J_{l+1}(kr)\\ e^{-il\theta}J_l(kr)\end{pmatrix}\\ c_{lk}^{n+*}\begin{pmatrix} -ie^{-il\theta}J_l(kr)\\ -e^{-i(l-1)\theta}J_{l-1}(kr)\end{pmatrix}+c_{lk}^{n-*}\begin{pmatrix} ie^{-il\theta}J_l(kr)\\ -e^{-i(l-1)\theta}J_{l-1}(kr)\end{pmatrix}\end{array}\right) &\text{(C.66)}\\
&\propto \psi_{n^{'},-l}, &\text{(C.67)}
\end{aligned}$$

as $\{L_z,\Xi\}=0$. Now,

$$\psi_{n,-l} = i\int dk\frac{(-1)^l}{\sqrt{\mathcal{N}_k}}\left(\begin{array}{c} c_{-lk}^{n+}\begin{pmatrix} ie^{-i(l+1)\theta}J_{l+1}(kr)\\ e^{-il\theta}J_l(kr)\end{pmatrix}+c_{-lk}^{n-}\begin{pmatrix} ie^{-i(l+1)\theta}J_{l+1}(kr)\\ -e^{-il\theta}J_l(kr)\end{pmatrix}\\ d_{-lk}^{n+}\begin{pmatrix} -ie^{-il\theta}J_l(kr)\\ -e^{-i(l-1)\theta}J_{l-1}(kr)\end{pmatrix}+d_{-lk}^{n-}\begin{pmatrix} -ie^{-il\theta}J_l(kr)\\ e^{-i(l-1)\theta}J_{l-1}(kr)\end{pmatrix}\end{array}\right) \tag{C.68}$$

where we used $J_{-l}=(-1)^l J_l$ for $l$ integer as is the case. As the coefficients are real, the constant of proportion is $-i$ and

$$\begin{aligned}
d_{lk}^{n^{'}+} &= c_{-lk}^{n+}(-1)^l &\text{(C.69)}\\
d_{lk}^{n^{'}-} &= -c_{-lk}^{n-}(-1)^l &\text{(C.70)}
\end{aligned}$$

with matching signs.

Interestingly, as the vortex bound modes decouple from the others, we may expect that

$$\begin{aligned}
d_{lk}^{n_{CdG}+} &= c_{-lk}^{n_{CdG}+}(-1)^l\\
d_{lk}^{n_{CdG}-} &= -c_{-lk}^{n_{CdG}-}(-1)^l
\end{aligned}$$

Then, for the CdG modes, (for these we omit the $n$ labels)

$$\psi_{n_{CdG}l}(r,\theta)=\int dk\frac{1}{\sqrt{\mathcal{N}_k}}\begin{pmatrix} c_{lk}^{+}\begin{pmatrix} e^{i(l-1)\theta}J_{l-1}(kr)\\ ie^{il\theta}J_l(kr)\end{pmatrix}+c_{lk}^{-}\begin{pmatrix} e^{i(l-1)\theta}J_{l-1}(kr)\\ -ie^{il\theta}J_l(kr)\end{pmatrix}\\ c_{-lk}^{+}(-1)^l\begin{pmatrix} e^{il\theta}J_l(kr)\\ ie^{i(l+1)\theta}J_{l+1}(kr)\end{pmatrix}-c_{-lk}^{-}(-1)^l\begin{pmatrix} e^{il\theta}J_l(kr)\\ -ie^{i(l+1)\theta}J_{l+1}(kr)\end{pmatrix}\end{pmatrix} \tag{C.71}$$

Focus in the $\psi_0$ term

$$\psi_{n_{CdG}0}(r,\theta)=\int\frac{dk}{\sqrt{\mathcal{N}_k}}\begin{pmatrix}\begin{pmatrix}\left(c_{0k}^{+}+c_{0k}^{-}\right)e^{-i\theta}J_1(kr)\\ \left(c_{0k}^{+}-c_{0k}^{-}\right)iJ_0(kr)\end{pmatrix}\\ \begin{pmatrix}\left(c_{0k}^{+}-c_{0k}^{-}\right)J_0(kr)\\ \left(c_{0k}^{+}+c_{0k}^{-}\right)ie^{i\theta}J_1(kr)\end{pmatrix}\end{pmatrix}. \tag{C.72}$$

In this case,

$$\begin{aligned}
&\int rdr\psi_{n_{CdG}0}^{\dagger}\Gamma_z\psi_{n_{CdG}0}\\
=&\int\frac{dk^{'}dk}{\sqrt{\mathcal{N}_{k'}\mathcal{N}_k}}\int rdr\left[\left(c_{0k'}^{+}+c_{0k'}^{-}\right)\left(c_{0k}^{+}+c_{0k}^{-}\right)J_1\left(k^{'}r\right)J_1(kr)-\left(c_{0k'}^{+}-c_{0k'}^{-}\right)\left(c_{0k}^{+}-c_{0k}^{-}\right)J_0\left(k^{'}r\right)J_0(kr)\right]\\
&-\int\frac{dk^{'}dk}{\sqrt{\mathcal{N}_{k'}\mathcal{N}_k}}\int rdr\left[\left(c_{0k'}^{+}-c_{0k'}^{-}\right)\left(c_{0k}^{+}-c_{0k}^{-}\right)J_0\left(k^{'}r\right)J_0(kr)-\left(c_{0k'}^{+}+c_{0k'}^{-}\right)\left(c_{0k}^{+}+c_{0k}^{-}\right)J_1\left(k^{'}r\right)J_1(kr)\right]\\
=&\int dk\left[\left(c_{0k}^{+}+c_{0k}^{-}\right)^2-\left(c_{0k}^{+}-c_{0k}^{-}\right)^2\right]-\int dk\left[\left(c_{0k}^{+}-c_{0k}^{-}\right)^2-\left(c_{0k}^{+}+c_{0k}^{-}\right)^2\right]\\
=&\ 4\int dkc_{0k}^{+}c_{0k}^{-}.
\end{aligned} \tag{C.73}$$

Similarly,

$$\begin{aligned}
&\int rdr\psi_{n_{CdG}0}^{\dagger}\rho_z\Gamma_z\psi_{n_{CdG}0}\\
=&\int dk\left[\left(c_{0k}^{+}+c_{0k}^{-}\right)^2-\left(c_{0k}^{+}-c_{0k}^{-}\right)^2\right]+\int dk\left[\left(c_{0k}^{+}-c_{0k}^{-}\right)^2-\left(c_{0k}^{+}+c_{0k}^{-}\right)^2\right]\\
=&\ 0.
\end{aligned} \tag{C.74}$$

This shows explicitly that the CdG modes from $l=0$ do not couple to the EM field.

## Numerics

To implement the numerical diagonalization, we set a finite size in the cylinder radius $R$. The wavefunction expansion then reads

$$\phi_{nl}(r)=\begin{pmatrix}\sum_j\left[c_{jl}^{n+}\chi_{jl}^{+}\right]\\ \sum_j\left[d_{jl}^{n+}\tilde{\chi}_{jl}^{+}\right]\end{pmatrix} \tag{C.75}$$

with

$$\chi_{lj}^{\pm}=\frac{1}{\sqrt{\mathcal{N}_{lj}}}\begin{pmatrix}J_{l-1}\left(\frac{\alpha_{lj}r}{R}\right)\\ \pm iJ_l\left(\frac{\alpha_{lj}r}{R}\right)\end{pmatrix} \tag{C.76}$$

and

$$\tilde{\chi}_{lj}^{\pm}=\frac{1}{\sqrt{\mathcal{N}_{lj}}}\begin{pmatrix}J_{l}\left(\frac{\alpha_{lj}r}{R}\right)\\ \pm iJ_{l+1}\left(\frac{\alpha_{lj}r}{R}\right)\end{pmatrix}. \tag{C.77}$$

Now we normalize. We need

$$\begin{aligned}\int_0^c rdrJ_l(ar)J_l(br) &= \frac{c}{a^2-b^2}\left[J_l(ar)\partial_r J_l(br)-\partial_r J_l(ar)J_l(br)\right]_{r=c}\\ &= \frac{c}{a^2-b^2}\left[bJ_l(ac)J_l^{'}(bc)-aJ_l^{'}(ac)J_l(bc)\right],\ a\neq b \end{aligned} \tag{C.78}$$

and

$$\int_0^c rdrJ_l(ar)^2 = \frac{c^2}{2}\left[J_l(ac)^2 - J_{l-1}(ac)J_{l+1}(ac)\right]. \tag{C.79}$$

Notice that

$$J_l^{'}(x) = \frac{n}{x}J_l(x) - J_{l+1}(x). \tag{C.80}$$

Then

$$\begin{aligned}\int_0^R rdrJ_l(ar)J_l(br) &= \frac{R}{a^2-b^2}\left[bJ_l(aR)J_l^{'}(bR)-aJ_l^{'}(aR)J_l(bR)\right]\\ &= \frac{R}{a^2-b^2}\left[bJ_l(aR)\left(\frac{n}{bR}J_l(bR)-J_{l+1}(bR)\right)-a\left(\frac{l}{aR}J_l(aR)-J_{l+1}(aR)\right)J_l(bR)\right]\\ &= \frac{1}{a^2-b^2}\left[(aR)J_{l+1}(aR)J_l(bR)-(bR)J_l(aR)J_{l+1}(bR)\right] \quad (C.81)\\ &\quad +\frac{l}{a^2-b^2}\left[J_l(aR)J_l(bR)-J_l(aR)J_l(bR)\right] \quad (C.82)\\ &= \frac{1}{a^2-b^2}\left[(aR)J_{l+1}(aR)J_l(bR)-(bR)J_l(aR)J_{l+1}(bR)\right] \quad (C.83)\end{aligned}$$

So we have,

$$\begin{aligned}&\int_0^R rdr\chi_{j'l}^{+\dagger}\chi_{jl}^{+}\\ &= \frac{R^2}{\sqrt{\mathcal{N}_{lj}\mathcal{N}_{lj'}}}\int_0^1 xdx\left[J_{l-1}(\alpha_{lj}x)J_{l-1}\left(\alpha_{lj'}x\right)+J_l(\alpha_{lj}x)J_l\left(\alpha_{lj'}x\right)\right]\\ &= \frac{1}{\sqrt{\mathcal{N}_{lj}\mathcal{N}_{lj'}}}\left[\int_0^1 xdxJ_{l-1}(\alpha_{lj}x)J_{l-1}\left(\alpha_{lj'}x\right)+\frac{1}{2}\delta_{jj'}J_{l+1}(\alpha_{lj})^2\right].\end{aligned} \tag{C.84}$$

One still needs to evaluate

$$\begin{aligned}\int_0^1 xdxJ_{l-1}(\alpha_{lj}x)J_{l-1}\left(\alpha_{lj'}x\right) &= \frac{1}{\alpha_{lj}^2-\alpha_{lj'}^2}\left[\alpha_{lj}J_l(\alpha_{lj})J_{l-1}\left(\alpha_{lj'}\right)-\alpha_{lj'}J_{l-1}(\alpha_{lj})J_l\left(\alpha_{lj'}\right)\right]\\ &= 0\end{aligned} \tag{C.85}$$

(in this limit one should actually be careful about the neglected terms) and

$$\begin{aligned}\int_0^1 rdrJ_{l-1}(\alpha_{lj}r)^2 &= \frac{1}{2}\left[J_{l-1}(\alpha_{lj})^2 - J_{l-2}(\alpha_{lj})J_l(\alpha_{lj})\right] \quad (C.86)\\ &\quad \frac{1}{2}\left[J_{l-1}(\alpha_{lj})^2\right]. \quad (C.87)\end{aligned}$$

So we have

$$\int_0^1 xdxJ_l\left(\alpha_{lj}x\right)J_l\left(\alpha_{lj'}x\right) = \frac{1}{2}\delta_{jj'}J_{l+1}\left(\alpha_{lj}\right)^2 \tag{C.88}$$

$$\int_0^1 xdxJ_{l-1}\left(\alpha_{lj}x\right)J_{l-1}\left(\alpha_{lj'}x\right) = \frac{1}{2}\delta_{jj'}J_{l-1}\left(\alpha_{lj}\right)^2 \tag{C.89}$$

Using that

$$J_{l+1}\left(\alpha_{lj}\right) = \frac{2l}{\alpha_{lj}}J_l\left(\alpha_{lj}\right) - J_{l-1}\left(\alpha_{lj}\right) \tag{C.90}$$

$$= -J_{l-1}\left(\alpha_{lj}\right), \tag{C.91}$$

the normalization factors reads

$$\mathcal{N}_{lj} = \frac{R^2}{2}\left[J_{l-1}\left(\alpha_{lj}\right)^2 + J_{l+1}\left(\alpha_{lj}\right)^2\right]$$

$$= R^2J_{l+1}\left(\alpha_{lj}\right)^2. \tag{C.92}$$

Then we have, finally,

$$\mathcal{N}_{lj} = \left|RJ_{l+1}\left(\alpha_{lj}\right)\right|^2 \tag{C.93}$$

The index $j$ is an integer and is summed from $-N_0/2$ up to $N_0/2$ fixed at a starting value $N_i$ which fixes $\alpha_{lN_i}/R \sim k_F$. Similar considerations may be applied to the $\tilde{\chi}$ spinors, the normalization factor is easily seen to be the same.

The matrix elements now read approximately

$$\int_0^R rdr\chi^{+\dagger}_{j'l}\chi^{+}_{jl} = \int_0^R rdr\tilde{\chi}^{+\dagger}_{j'l}\tilde{\chi}^{+}_{jl}$$

$$= \delta_{jj'} \tag{C.94}$$

$$\int_0^R rdr\chi^{\sigma'\dagger}_{k'l}\left|\Delta\right|\tilde{\chi}^{\sigma}_{kl}$$

$$= \frac{\int_0^1 xdx\left|\Delta\left(xR\right)\right|}{\sqrt{J_{l+1}\left(\alpha_{lj}\right)^2J_{l+1}\left(\alpha_{lj'}\right)^2}}$$

$$\left[J_{l-1}\left(\alpha_{lj'}x\right)J_l\left(\alpha_{lj}x\right)\right. \tag{C.95}$$

$$\left.+\sigma\sigma'J_l\left(\alpha_{lj'}r\right)J_{l+1}\left(\alpha_{lj}r\right)\right]$$

$$\equiv \left|\Delta\right|^{\sigma\sigma'}_{l,jj'}. \tag{C.96}$$

and

$$\left|\Delta\left(r\right)\right| = \Delta_0\tanh\left(\frac{r}{\xi}\right) \tag{C.97}$$

$$\Rightarrow \left|\Delta\left(xR\right)\right| = \Delta_0\tanh\left(x\frac{R}{\xi}\right) \tag{C.98}$$

where $\xi = v_F\pi/\Delta_0$ is the SC coherence length and $\Delta_0$ is the magnitude of the SC pairing.

Thus, defining

$$\Phi_{ln} = \left(c^{n+}_{1l}...c^{n+}_{N_0l}, d^{n+}_{1l}...d^{n+}_{N_0l}\right), \tag{C.99}$$

where

$$\Phi_{ln}^{\dagger}\Phi_{ln'} = \delta_{nn'}, \tag{C.100}$$

the eigenvalue problem becomes completely algebraic

$$\begin{pmatrix} T_l & \Delta_l \\ \Delta_l^T & -T_l \end{pmatrix} \Phi_{ln} = E_{l,n}\Phi_{ln} \tag{C.101}$$

where

$$T_l = \begin{pmatrix} \lambda_{l1}^{+} & & \\ & \ddots & \\ & & \lambda_{lN_0}^{+} \end{pmatrix} \tag{C.102}$$

and

$$\Delta_l = \begin{pmatrix} |\Delta|_{l,11}^{++} & & |\Delta|_{l,1N_0}^{++} \\ & \ddots & \\ |\Delta|_{l,N_01}^{++} & & |\Delta|_{l,N_0N_0}^{++} \end{pmatrix}. \tag{C.103}$$

So all we have to do is to compute the following integrals,

$$I_{jj'}^{1} = \int_0^1 xdx\,|\Delta(xR)|\left[J_{l-1}\left(\alpha_{lj'}x\right)J_l\left(\alpha_{lj}x\right)\right] \tag{C.104}$$

$$I_{jj'}^{2} = \int_0^1 xdx\,|\Delta(xR)|\left[J_{l}\left(\alpha_{lj'}x\right)J_{l+1}\left(\alpha_{lj}x\right)\right] \tag{C.105}$$

such that

$$|\Delta|_{l,jj'}^{++} = \frac{\left[I_{jj'}^{1} + I_{jj'}^{2}\right]}{\sqrt{\mathcal{N}_j\mathcal{N}_{j'}}}. \tag{C.106}$$

We fix

$$R = 1000 \tag{C.107}$$

$$N_i = 450 \tag{C.108}$$

$$N_0 = 120 \tag{C.109}$$

$$\alpha = 0.05 \tag{C.110}$$

$$\mu = 1 \tag{C.111}$$

$$m = 1 \tag{C.112}$$

$$\Delta_0 = 0.05 \tag{C.113}$$

The spectrum follows

The projection coefficients may be found exactly in the same way as we did for the infinite radius case, and reads

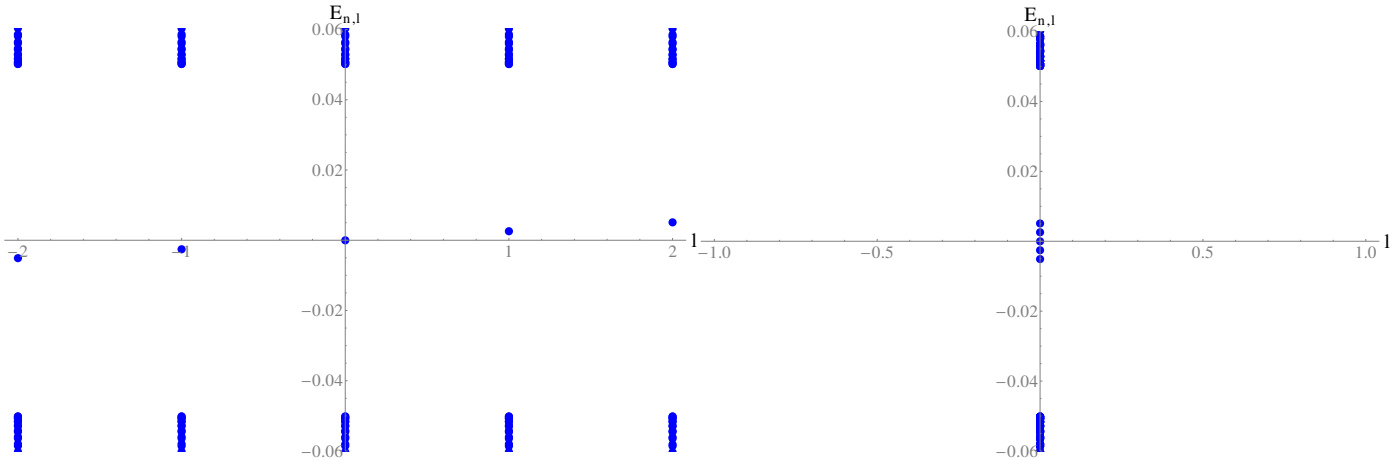


Figure C.2: Energy levels in the 2D plane. On the left we have the separate energies for $l = -2, ..., 2$ while on the right we have the same energies collapsed at a single line for illustration. Our approximation $E_l = \frac{\Delta_0^2}{E_F} l$ is reasonably decent. A tendency for increasing values of the minigap is seen on the right figure. This might be a finite size effect or our approximation was not exact.

$$\begin{aligned} \tilde{v}_l^{nn'} &= 2\sum_j \left[ c_{lj}^{n'+} c_{lj}^{n-} + c_{lj}^{n'-} c_{lj}^{n+} \right] \\ &\quad -2\sum_j \left[ d_{lj}^{n'+} d_{lj}^{n-} + d_{lj}^{n'-} d_{lj}^{n+} \right] \qquad \text{(C.114)} \\ \tilde{q}_l^{nn'} &= 2\sum_j \left[ c_{lj}^{n'+} c_{lj}^{n-} + c_{lj}^{n'-} c_{lj}^{n+} \right] \\ &\quad +2\sum_j \left[ d_{lj}^{n'+} d_{lj}^{n-} + d_{lj}^{n'-} d_{lj}^{n+} \right] \qquad \text{(C.115)} \end{aligned}$$

Reminding ourselves again that, for the CdG modes

$$\begin{aligned} d_{lk}^{n_{CdG}+} &= c_{-lk}^{n_{CdG}+} (-1)^l \\ d_{lk}^{n_{CdG}-} &= -c_{-lk}^{n_{CdG}-} (-1)^l \end{aligned}$$

and that their subspace is separated from the rest of the gapped modes for $n \neq n_{CdG}$,

$$\begin{aligned} \tilde{v}_l^{n_{CdG}} &= 2\sum_j \left[ c_{lj}^{n_{CdG}+} c_{lj}^{n_{CdG}-} + c_{lj}^{n_{CdG}-} c_{lj}^{n_{CdG}+} \right] \\ &\quad -2\sum_j \left[ d_{lj}^{n_{CdG}+} d_{lj}^{n_{CdG}-} + d_{lj}^{n_{CdG}-} d_{lj}^{n_{CdG}+} \right] \qquad \text{(C.116)} \\ \tilde{q}_l^{n_{CdG}} &= 2\sum_j \left[ c_{lj}^{n_{CdG}+} c_{lj}^{n_{CdG}-} + c_{lj}^{n_{CdG}-} c_{lj}^{n_{CdG}+} \right] \\ &\quad +2\sum_j \left[ d_{lj}^{n_{CdG}+} d_{lj}^{n_{CdG}-} + d_{lj}^{n_{CdG}-} d_{lj}^{n_{CdG}+} \right] \qquad \text{(C.117)} \end{aligned}$$

and

$$\begin{aligned}\tilde{v}_l^{n_{CdG}} &= 4\sum_j \left[c_{lj}^{n_{CdG}+} c_{lj}^{n_{CdG}-}\right] \\ &\quad +4\sum_j \left[c_{-lj}^{n_{CdG}+} c_{-lj}^{n_{CdG}-}\right] \qquad \text{(C.118)}\\ \tilde{q}_l^{n_{CdG}} &= 4\sum_j \left[c_{lj}^{n_{CdG}+} c_{lj}^{n_{CdG}-}\right] \\ &\quad -4\sum_j \left[c_{-lj}^{n_{CdG}+} c_{-lj}^{n_{CdG}-}\right] \qquad \text{(C.119)}\end{aligned}$$

which implies $\tilde{q}_{l=0}^{n_{CdG}} = 0$.

## Vortex bound states and perturbation theory

We have found that the original Hamiltonian for a cylindrical DIII TSC in 3D in the presence of a chiral vortex may be written

$$H = \sum_{k_z,l,n,n'} f_{k_z ln}^\dagger \left[E_{nl}\delta_{nn'} + v_F\left(k_z \tilde{v}_l^{nn'} - \tilde{q}_l^{nn'} A_z\right)\right] f_{k_z ln'}, \qquad \text{(C.120)}$$

for one Fermi surface. (the other Fermi surface contains only contributions of states gapped by the SC gap)

Let us neglect the effects of the vector potential for now, and analyze how is the spectrum of this system as function of $k_z$. We have then,

$$H = \sum_{k_z,l,n,n'} f_{k_z ln}^\dagger \left[E_{nl}\delta_{nn'} + v_F \tilde{v}_{nn'}^l k_z\right] f_{k_z ln'} \qquad \text{(C.121)}$$

where (I modified the notation slightly)

$$\begin{aligned}\tilde{v}_{n'n}^l &= 2\sum_j \left[c_{lj}^{n'+} c_{lj}^{n-} + c_{lj}^{n'-} c_{lj}^{n+}\right] \\ &\quad -2\sum_j \left[d_{lj}^{n'+} d_{lj}^{n-} + d_{lj}^{n'-} d_{lj}^{n+}\right] \qquad \text{(C.122)}\\ \tilde{q}_{n'n}^l &= 2\sum_j \left[c_{lj}^{n'+} c_{lj}^{n-} + c_{lj}^{n'-} c_{lj}^{n+}\right] \\ &\quad +2\sum_j \left[d_{lj}^{n'+} d_{lj}^{n-} + d_{lj}^{n'-} d_{lj}^{n+}\right] \qquad \text{(C.123)}\end{aligned}$$

and $c_{lj}^{n\pm}$ and $d_{lj}^{n\pm}$ are the coefficients of the wavefunctions

$$\phi_{nl}(r,\theta) = \sum_k \frac{1}{\sqrt{\mathcal{N}_j}} \begin{pmatrix} c_{lj}^{n+}\begin{pmatrix} e^{i(l-1)\theta} J_{l-1}\left(\frac{\alpha_{lj}}{R} r\right) \\ i e^{il\theta} J_l\left(\frac{\alpha_{lj}}{R} r\right)\end{pmatrix} + c_{lj}^{n-}\begin{pmatrix} e^{i(l-1)\theta} J_{l-1}\left(\frac{\alpha_{lj}}{R} r\right) \\ -i e^{il\theta} J_l\left(\frac{\alpha_{lj}}{R} r\right)\end{pmatrix} \\ d_{lj}^{n+}\begin{pmatrix} e^{il\theta} J_l\left(\frac{\alpha_{lj}}{R} r\right) \\ i e^{i(l+1)\theta} J_{l+1}\left(\frac{\alpha_{lj}}{R} r\right)\end{pmatrix} + d_{lj}^{n-}\begin{pmatrix} e^{il\theta} J_l\left(\frac{\alpha_{lj}}{R} r\right) \\ -i e^{i(l+1)\theta} J_{l+1}\left(\frac{\alpha_{lj}}{R} r\right)\end{pmatrix} \end{pmatrix} \qquad \text{(C.124)}$$

that diagonalize the planar part of the Hamiltonian in a finite radius $R$ with energies $E_{nl}$. The coefficients $c_{lj}^{n-}$ and $d_{lj}^{n-}$are expected to be small, in the limit of weak pairing, in comparison with $c_{lj}^{n+}$ and $d_{lj}^{n+}$.

So we have the first quantized Hamiltonian

$$h_l(k_z) = E_{nl}\delta_{nn'} + v_F \tilde{v}_{nn'}^l k_z. \qquad \text{(C.125)}$$

Now it makes sense to compute the effects of $k_z$ in the energy at fixed $n = n_{CdG}$ and given $l$ in perturbation

theory.

We start focusing in the subspace of CdG modes

$$h_l^0 = E_{n_{CdG}l} = l \times \frac{\Delta_0^2}{E_F} \equiv \delta_l. \tag{C.126}$$

These states are non-degenerate in $l$ and perturbation theory is computed easily. The first order corrections in $k_z$ read

$$h^0_{n_{CdG}l} = v_F \tilde{v}^l_{n_{CdG}n_{CdG}} k_z, \tag{C.127}$$

where

$$\begin{aligned} \tilde{v}^l_{n_{CdG}n_{CdG}} &= 4\sum_j \left[ c_{lj}^{n_{CdG}+} c_{lj}^{n_{CdG}-} - d_{lj}^{n_{CdG}+} d_{lj}^{n_{CdG}-} \right] && \text{(C.128)} \\ &= 4\sum_j \left[ c_{lj}^{n_{CdG}+} c_{lj}^{n_{CdG}-} + c_{-lj}^{n_{CdG}+} c_{-lj}^{n_{CdG}-} \right]. && \text{(C.129)} \end{aligned}$$

Now, to second order, we have

$$h^0_{n_{CdG}l} = (v_F k_z)^2 \sum_{n \neq n_{CdG}} \frac{\tilde{v}^l_{n_{CdG}n} \tilde{v}^l_{nn_{CdG}}}{E_{n_{CdG}l} - E_{nl}}. \tag{C.130}$$

For a fixed angular momentum $l$, the states labeled by $n \neq n_{CdG}$ separate in states of positive energy and states of negative energy, which we label as $n_\pm$, respectively. These states have energies of the order of the SC gap $\Delta_0$. We may then write

$$\begin{aligned} \frac{1}{\tilde{m}_l} &\equiv \sum_{n \neq n_{CdG}} \frac{\tilde{v}^l_{n_{CdG}n} \tilde{v}^l_{nn_{CdG}}}{E_{n_{CdG}l} - E_{nl}} \\ &= \sum_{n_+} \frac{\tilde{v}^l_{n_{CdG}n_+} \tilde{v}^l_{n_+n_{CdG}}}{E_{n_{CdG}l} - E_{n_+l}} \\ &\quad + \sum_{n_-} \frac{\tilde{v}^l_{n_{CdG}n_-} \tilde{v}^l_{n_-n_{CdG}}}{E_{n_{CdG}l} - E_{n_-l}}. \end{aligned} \tag{C.131}$$

Let us focus shortly at $\tilde{m}_0$. In this case, since particle-hole symmetry sends $l = 0 \to 0$, we can safely say that$E_{n_-l} = -E_{n_+l}$ and $\tilde{v}^l_{n_+n_{CdG}} = \tilde{v}^l_{n_-n_{CdG}}$ (up to a sign factor which cancels in the multiplication by the conjugation transpose.) Then

$$\begin{aligned} \frac{1}{\tilde{m}_0} &= -\sum_{n_+} \frac{\tilde{v}^l_{n_{CdG}n_+} \tilde{v}^l_{n_+n_{CdG}}}{E_{n_+l}} \\ &\quad - \sum_{n_-} \frac{\tilde{v}^l_{n_{CdG}n_-} \tilde{v}^l_{n_-n_{CdG}}}{E_{n_-l}} \\ &= -\sum_{n_+} \frac{\tilde{v}^l_{n_{CdG}n_+} \tilde{v}^l_{n_+n_{CdG}}}{E_{n_+l}} \\ &\quad + \sum_{n_-} \frac{\tilde{v}^l_{n_{CdG}n_+} \tilde{v}^l_{n_+n_{CdG}}}{E_{n_+l}} = 0. \end{aligned} \tag{C.132}$$

The $l = 0$ states receive no contribution to second order in perturbation theory.

Let us make also a crude analysis of the energy denominator. We may write the contributions approximately as

$$\frac{1}{\epsilon - \Delta_0} + \frac{1}{\epsilon + \Delta_0} \approx \frac{2\epsilon}{\Delta_0^2}, \tag{C.133}$$

where $\epsilon$ represents the mini-gap energies of the CdG modes and$\Delta_0$ represents the energies of the gapped higher energy modes. We clearly see that the sign of $m_l$ depends on the sign of the CdG mode energies. Thus an

analysis of the energy denominator also suggests that if $l > 0$ then $m_l > 0$ and if $l < 0$ then $m_l < 0$.

Notice that for the charge elements $\tilde{q}_l$, the arguments above follow much in the same way. So we may write

$$E_{n_{CdG}l} \approx \delta_l + \tilde{v}^l_{n_{CdG}n_{CdG}} [v_F k_z] + \frac{[v_F k_z]^2}{\tilde{m}_l}. \tag{C.134}$$

We may extrapolate this perturbative expression of powers of the momentum as an expansion of a hyperbola. Taking into account the signs of masses and charges and the zero mode. A very likely Hamiltonian describing the physics at the vortex is given by

$$\tilde{h}_z = \int dk_z k_z \gamma_{-k_z 0} \gamma_{k_z 0} \tag{C.135}$$

$$+ \sum_{l>0} \int dk_z c^\dagger_{k_z l} c_{k_z l} \sqrt{(k_z + Et)^2 + \delta_l^2} \tag{C.136}$$

$$- \sum_{l<0} \int dk_z c^\dagger_{k_z l} c_{k_z l} \sqrt{(k_z - Et)^2 + \delta_l^2} \tag{C.137}$$

# Appendix D

# Goldstone-Wilczek axion calculation for a class DIII system

Let us start rewriting the BdG Hamiltonian from a single Weyl fermion,

$$h_{BdG} = v_F \boldsymbol{\alpha} \cdot \mathbf{P} + \boldsymbol{\Delta}(\mathbf{X}) \cdot \boldsymbol{\Lambda}, \tag{D.1}$$

in a different language. We write $\boldsymbol{\Delta}(\mathbf{X}) = v_F(\Phi_1, \Phi_2)$. The second quantized BdG equation may be written

$$H_{BdG}/v_F = \int d^3x \Psi^\dagger \left[\boldsymbol{\alpha} \cdot \mathbf{P} + \Phi_1 \Lambda_x + \Phi_2 \Lambda_y\right] \Psi \tag{D.2}$$

where again $\Psi^T = \left(\psi, i\sigma_y \psi^\dagger\right)$. We bear in mind that we actually have two of these, one for each Fermi surface. Also bear in mind that the fermionic representation is then constrained and $\Psi^\dagger$ is not independent of $\Psi$ but rather $\Psi^\dagger = \left[i\rho_x \sigma_y \Psi\right]^T$.

Using our representation

$$\begin{aligned} \boldsymbol{\alpha} &= \rho_z \boldsymbol{\sigma} && \text{(D.3)} \\ \Lambda_1 &= \rho_x \sigma_0 && \text{(D.4)} \\ \Lambda_2 &= \rho_y \sigma_0, && \text{(D.5)} \end{aligned}$$

we then write the action in relativistic form

$$S_{BdG} = \int d^4x \bar{\Psi} \left[i\Gamma^\mu \partial_\mu - \left[\Phi_1 + i\bar{\Gamma}\Phi_2\right]\right] \Psi, \tag{D.6}$$

where we rescaled $v_F t \to x^0$ and

$$\begin{aligned} \Gamma^0 &= \rho_x \sigma_0 && \text{(D.7)} \\ \Gamma^i &= -i\rho_y \sigma_i = \Gamma^0 \alpha_i && \text{(D.8)} \\ \bar{\Gamma} &= \rho_z \sigma_0 = i\Gamma^0 \Gamma^1 \Gamma^2 \Gamma^3. && \text{(D.9)} \end{aligned}$$

We use the metric $\eta_{\mu\nu} = diag(1, -1, -1, -1)$This matches notation in [85]. The superconducting phase fluctuations are identified with what is called an "axion string". They are fixed by the phase of $\Phi = \Phi_1 + i\Phi_2$.

The partition function for the gapped part of the superconducting spectrum in the presence of an electro-

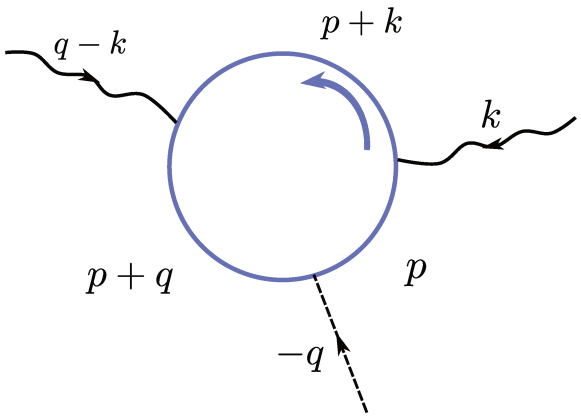


Figure D.1: Bubble diaram for the axion electrodynamics coupling in 3+1D.

magnetic field and axion string reads

$$\mathcal{Z}\left[A,\Phi\right]=\int\mathcal{D}\left[\psi^{\dagger},\psi\right]e^{iS_{BdG}\left[\psi^{\dagger},\psi,A,\Phi\right]} \tag{D.10}$$

where $\psi$ comprises the Grassmann variables for both spins and the action reads

$$S_{BdG}^{String}=\int d^{4}x\bar{\Psi}\left[i\Gamma^{\mu}\partial_{\mu}-\bar{\Gamma}\Gamma^{\mu}A_{\mu}-\left[\Phi_{1}+i\bar{\Gamma}\Phi_{2}\right]\right]\Psi, \tag{D.11}$$

where we rescaled the physical gauge fields as $eA_{\mu}^{phys}=A_{\mu}$. The ground state of $\Phi$ can be written $\left[\Phi_{1}+i\bar{\Gamma}\Phi_{2}\right]=f\left(\rho\right)e^{i\bar{\Gamma}\theta}$ where $f\left(\rho\right)$ goes from 0 at $\rho=0$ to the vacuum expectation value $\nu$ as $\rho\to\infty$, where $\rho$ is the radial coordinate and $\theta$ is the angular coordinate in cylindrical coordinates.

Fermionic integration here must be carried out with a bit of care. This is because the spinors $\Psi$ an $\bar{\Psi}$ are actually constrained here, as opposed to the ordinary situation where the Grassmann variables are independent. The result reads

$$\mathcal{Z}\left[A,\Phi\right]=\sqrt{\det\left[i\Gamma^{\mu}\partial_{\mu}-\bar{\Gamma}\Gamma^{\mu}A_{\mu}-\left[\Phi_{1}+i\bar{\Gamma}\Phi_{2}\right]\right]}. \tag{D.12}$$

A short manipulation gives

$$\mathcal{Z}\left[A,\Phi\right]=e^{\frac{1}{2}Tr\ln\left[i\Gamma^{\mu}\partial_{\mu}-\bar{\Gamma}\Gamma^{\mu}A_{\mu}-\left[\Phi_{1}+i\bar{\Gamma}\Phi_{2}\right]\right]}. \tag{D.13}$$

The 'capitalized' trace contains space-time and internal degrees of freedom.

This computation is poorly defined for massless fermions. We will consider to be away from $\rho=0$ such that $|\Phi|\sim v$ which is reasonable to impose for the bulk scattering states (which we know are fully gapped.) For this we fix $\Phi_{1}=m$ while $\Phi_{2}$ fluctuates adiabatically. We write

$$\begin{aligned}\mathcal{Z}\left[A,\Phi\right] &= e^{\frac{1}{2}Tr\ln\left[i\Gamma^{\mu}\partial_{\mu}-m-\bar{\Gamma}\Gamma^{\mu}A_{\mu}-i\bar{\Gamma}\Phi_{2}\right]} &\text{(D.14)}\\ &= \mathcal{Z}\left[0,0\right]e^{\frac{1}{2}Tr\ln\left[1-\frac{\left(\bar{\Gamma}\Gamma^{\mu}A_{\mu}+i\bar{\Gamma}\Phi_{2}\right)}{i\Gamma^{\mu}\partial_{\mu}-m}\right]} &\text{(D.15)}\\ &= \mathcal{Z}\left[0,0\right]e^{-\frac{1}{2}\sum_{n}\frac{1}{n}Tr\left[\frac{\left(\bar{\Gamma}\Gamma^{\mu}A_{\mu}+i\bar{\Gamma}\Phi_{2}\right)}{i\Gamma^{\mu}\partial_{\mu}-m}\right]^{n}}. &\text{(D.16)}\end{aligned}$$

This is the ground-state energy computation. It is a sum over bubbles.

We are particularly interested in the current induced in the axion field vacuum by the background electromagnetic field. This is known as a "Goldstone-Wilczek" calculation [91] and comes from computing the 3-legged bubble in Fig. (D.1).

This is given by

$$\begin{aligned} iS_{axion}\left[A,\Phi\right] &= -\frac{1}{2}\frac{1}{3}Tr\left[\left(G_0\left(\bar{\Gamma}\Gamma^\mu A_\mu + i\bar{\Gamma}\Phi_2\right)\right)^3\right] \\ &= -\frac{1}{2}Tr\left[G_0\left(\bar{\Gamma}\Gamma^\mu A_\mu\right)G_0\left(\bar{\Gamma}\Gamma^\mu A_\mu\right)G_0\left(i\bar{\Gamma}\Phi_2\right)\right] \end{aligned} \tag{D.17}$$

where

$$G_0\left(x-y\right) = \frac{1}{i\Gamma^\mu\partial_\mu - m}\delta\left(x-y\right). \tag{D.18}$$

In momentum space, the capital trace becomes

$$\begin{aligned} S_{axion}\left[A,\Phi\right] &= -\frac{1}{2}\int_{k,q} A_\mu\left(q-k\right)A_\nu\left(k\right)\Phi_2\left(-q\right) \\ &\quad \int_p tr\left[\bar{\Gamma}\Gamma^\mu G_0\left(p+k\right)\bar{\Gamma}\Gamma^\nu G_0\left(p\right)\bar{\Gamma}G_0\left(p+q\right)\right] \end{aligned} \tag{D.19}$$

where $\int_k \equiv \int \frac{d^4k}{(2\pi)^4}$ and $tr$ runs over the internal degrees of freedom only. This last $p$ integral and trace represents the actual "bubble" diagram. We call

$$I^{\mu\nu} = \int_p tr\left[\bar{\Gamma}\Gamma^\mu G_0\left(p+k\right)\bar{\Gamma}\Gamma^\nu G_0\left(p\right)\bar{\Gamma}G_0\left(p+q\right)\right]. \tag{D.20}$$

We deploy the gradient expansion in the "external momenta" $k$, $q$,

$$\begin{aligned} G_0\left(p+k\right) &= \frac{\Gamma^\mu\left(p_\mu+k_\mu\right)+m}{\left(p+k\right)^2-m^2} \\ &\approx G_0\left(p\right) + \frac{\Gamma^\mu k_\mu}{p^2-m^2} - \frac{2p\cdot k}{\left(p^2-m^2\right)^2}. \end{aligned} \tag{D.21}$$

Terms odd in $p$ in the numerator (such as from $p\cdot k$) vanish from the angular integrals. One has to be careful with the tracing also. We have

$$\begin{aligned} & tr\left[\bar{\Gamma}\Gamma^\mu\left(\Gamma\cdot\left(p+k\right)+m\right)\bar{\Gamma}\Gamma^\nu\left(\Gamma\cdot p+m\right)\bar{\Gamma}\left(\Gamma\cdot\left(p+q\right)+m\right)\right] \\ = \; & m\left\{tr\left[\Gamma^\mu\left(\Gamma\cdot\left(p+k\right)\right)\Gamma^\nu\left(\Gamma\cdot p\right)\bar{\Gamma}\right]\right. \\ & +tr\left[\Gamma^\mu\left(\Gamma\cdot\left(p+k\right)\right)\Gamma^\nu\bar{\Gamma}\left(\Gamma\cdot\left(p+q\right)\right)\right] \\ & \left.-tr\left[\Gamma^\mu\Gamma^\nu\left(\Gamma\cdot p\right)\bar{\Gamma}\left(\Gamma\cdot\left(p+q\right)\right)\right]\right\} \\ = \; & m\left\{tr\left[\Gamma^\mu\left(\Gamma\cdot\left(p+k\right)\right)\Gamma^\nu\left(\Gamma\cdot p\right)\bar{\Gamma}\right]\right. \\ & \left.+tr\left[\Gamma^\mu\left(\Gamma\cdot\left(2p+k\right)\right)\Gamma^\nu\bar{\Gamma}\left(\Gamma\cdot\left(p+q\right)\right)\right]\right\} \\ = \; & m\left\{\left(p_\lambda+k_\lambda\right)\left(p_\sigma\right)tr\left[\Gamma^\mu\Gamma^\lambda\Gamma^\nu\Gamma^\sigma\bar{\Gamma}\right] + \left(2p_\lambda+k_\lambda\right)\left(p_\sigma+q_\sigma\right)tr\left[\Gamma^\mu\Gamma^\lambda\Gamma^\nu\bar{\Gamma}\Gamma^\sigma\right]\right\} \\ = \; & m\left\{-\left(p_\lambda+k_\lambda\right)\left(p_\sigma\right)+\left(2p_\lambda+k_\lambda\right)\left(p_\sigma+q_\sigma\right)\right\}tr\left[\Gamma^\mu\Gamma^\nu\Gamma^\lambda\Gamma^\sigma\bar{\Gamma}\right] \\ = \; & -i4\epsilon^{\mu\nu\lambda\sigma}m\left\{2p_\lambda q_\sigma + k_\lambda q_\sigma\right\} \\ = \; & -i4m\epsilon^{\mu\nu\lambda\sigma}\left\{2p_\lambda q_\sigma + k_\lambda q_\sigma\right\}, \end{aligned} \tag{D.22}$$

where we used that

$$tr\left[\Gamma^\sigma\Gamma^\mu\Gamma^\lambda\Gamma^\nu\bar{\Gamma}\right] = -4i\epsilon^{\sigma\mu\lambda\nu}. \tag{D.23}$$

As a result

$$I^{\mu\nu} = -i4m\epsilon^{\mu\nu\lambda\sigma}k_\lambda q_\sigma \int_p \frac{1}{\left(p^2-m^2\right)^3} \tag{D.24}$$

$$+i16m\epsilon^{\mu\nu\lambda\sigma}q_\sigma \left(k+q\right)^\rho \int_p \frac{p_\lambda p_\rho}{\left(p^2-m^2\right)^4} \tag{D.25}$$

$$= -i4m\epsilon^{\mu\nu\lambda\sigma}\left[k_\lambda q_\sigma \int_p \frac{1}{\left(p^2-m^2\right)^3} - 4q_\sigma \left(k+q\right)^\rho \int_p \frac{p_\lambda p_\rho}{\left(p^2-m^2\right)^4}\right] \tag{D.26}$$

Now, upon Wick rotation $p_0 = -ip_{0E}$ and

$$\int_p \frac{1}{\left(p^2-m^2\right)^3} = -i\frac{1}{32\pi^2}\frac{1}{m^2} \tag{D.27}$$

$$\int_p \frac{p_\lambda p_\rho}{\left(p^2-m^2\right)^4} = -ig_{\lambda\rho}\frac{1}{6}\frac{1}{32\pi^2}\frac{1}{m^2} \tag{D.28}$$

Hence

$$I^{\mu\nu} = -\frac{1}{3}\frac{1}{8\pi^2}\frac{1}{m}\epsilon^{\mu\nu\lambda\sigma}k_\lambda q_\sigma. \tag{D.29}$$

Thus

$$\begin{aligned} S_{eff} &= -\frac{1}{2}\frac{1}{3}\frac{1}{8\pi^2 m}\int_{k.q}\epsilon^{\mu\nu\lambda\sigma}k_\lambda q_\sigma A_\mu\left(q-k\right)A_\nu\left(k\right)\Phi_2\left(-q\right) \\ &= \frac{1}{2}\frac{1}{3}\frac{1}{8\pi^2}\int_x \epsilon^{\sigma\mu\lambda\nu}\frac{\partial_\sigma\Phi_2}{\Phi_1}A_\mu\partial_\lambda A_\nu \end{aligned} \tag{D.30}$$

Fourier transforming to real-space and noticing $m = \Phi_1$ we have, up to surface terms,

$$S_{axion}\left[A,\Phi\right] = -\frac{1}{3}\frac{1}{2}\frac{\epsilon^{\sigma\mu\lambda\nu}}{8\pi^2}\int_x \frac{\partial_\sigma\Phi_2}{\Phi_1}A_\mu\partial_\lambda A_\nu. \tag{D.31}$$

This is not symmetric between $\Phi_1$ and $\Phi_2$ because we favored fluctuations in $\Phi_2$ in the beginning. It is easy to recover the axial symmetry, in which case we have

$$S_{axion}\left[A,\Phi\right] = -\frac{1}{3}\frac{1}{2}\frac{\epsilon^{\sigma\mu\lambda\nu}}{8\pi^2}\int_x \frac{\Phi_1\partial_\sigma\Phi_2 - \Phi_2\partial_\sigma\Phi_1}{\left|\Phi\right|^2}A_\mu\partial_\lambda A_\nu. \tag{D.32}$$

Recovering the original physical parameters ($x^0 = v_F t$, $A_\mu = eA_\mu^{phys}$, we drop the phys label and $\mathbf{\Delta}\left(\mathbf{X}\right) = v_F\left(\Phi_1,\Phi_2\right)$) and rewriting,

$$S_{axion}\left[A,\Phi\right] = -e^2\frac{1}{2}\frac{1}{3}\frac{\epsilon^{\sigma\mu\lambda\nu}}{8\pi^2}\int_x \frac{\epsilon^{ab}\Delta_a\partial_\sigma\Delta_b}{\left|\Delta\right|^2}A_\mu\partial_\lambda A_\nu. \tag{D.33}$$

To finish, one may remember that $\Delta = \left|\Delta\right|e^{i\theta}$ for a vortex. Also remembering that we have a pair of Fermi surfaces, with opposite chirality (this implies that to find the result for the other Fermi surfaces, it is enough to multiply all Green's functions by $-1$ to consider the second Fermi surface. As the vortex induced current goes as $G_0^3$, this gives an overall $-1$ factor.)

These arguments imply that the result of [34] may be off by a factor of 1/3.

# Bibliography


[1] C. Nash. Topology and physics-a historical essay. *arXiv:hep-th/9709135*, 1997.

[2] Ching-Kai Chiu, Jeffrey C.Y. Teo, Andreas P. Schnyder, and Shinsei Ryu. Classification of topological quantum matter with symmetries. *arXiv: 1505.03535*, 2015.

[3] Xiao-Liang Qi and Shou-Cheng Zhang. Topological insulators and superconductors. *Rev. Mod. Phys.*, 83:1057–1110, Oct 2011.

[4] M. Z. Hasan and C. L. Kane. *Colloquium* : Topological insulators. *Rev. Mod. Phys.*, 82:3045–3067, Nov 2010.

[5] N. D. Mermin. The topological theory of defects in ordered media. *Rev. Mod. Phys.*, 51:591–648, Jul 1979.

[6] D. J. Thouless, M. Kohmoto, M. P. Nightingale, and M. den Nijs. Quantized hall conductance in a two-dimensional periodic potential. *Phys. Rev. Lett.*, 49:405–408, Aug 1982.

[7] Xie Chen, Zheng-Cheng Gu, Zheng-Xin Liu, and Xiao-Gang Wen. Symmetry protected topological orders and the group cohomology of their symmetry group. *Phys. Rev. B*, 87:155114, Apr 2013.

[8] L. D. Landau. *Phys. Z. Sowjetunion*, 11:26, 1937.

[9] L. D. Landau and E. M. Lifschitz. *Statistical Physics - Course of Theoretical Physics Vol 5.* Pergamon, London, 1958.

[10] Alexei Kitaev. Periodic table for topological insulators and superconductors. *AIP Conference Proceedings*, 1134(1):22–30, 2009.

[11] Shinsei Ryu, Andreas P Schnyder, Akira Furusaki, and Andreas W W Ludwig. Topological insulators and superconductors: tenfold way and dimensional hierarchy. *New Journal of Physics*, 12(6):065010, 2010.

[12] Jeffrey C. Y. Teo and C. L. Kane. Topological defects and gapless modes in insulators and superconductors. *Phys. Rev. B*, 82:115120, Sep 2010.

[13] Alexander Altland and Martin R. Zirnbauer. Nonstandard symmetry classes in mesoscopic normal-superconducting hybrid structures. *Phys. Rev. B*, 55:1142–1161, Jan 1997.

[14] Andreas P. Schnyder, Shinsei Ryu, Akira Furusaki, and Andreas W. W. Ludwig. Classification of topological insulators and superconductors in three spatial dimensions. *Phys. Rev. B*, 78:195125, Nov 2008.

[15] Xiao-Yu Dong and Chao-Xing Liu. The classification of topological crystalline insulators based on representation theory. *arXiv: 1507.00241*, 2015.

[16] Chao-Xing Liu, Rui-Xing Zhang, and Brian K. VanLeeuwen. Topological nonsymmorphic crystalline insulators. *Phys. Rev. B*, 90:085304, Aug 2014.

[17] Chong Wang, Andrew C. Potter, and T. Senthil. Classification of interacting electronic topological insulators in three dimensions. *Science*, 343(6171):629–631, 2014.

[18] Max A. Metlitski, Lukasz Fidkowski, Xie Chen, and Ashvin Vishwanath. Interaction effects on 3d topological superconductors: surface topological order from vortex condensation, the 16 fold way and fermionic kramers doublets. *arXiv: 1406.3032*, 2014.

[19] Frank Pollmann, Erez Berg, Ari M. Turner, and Masaki Oshikawa. Symmetry protection of topological phases in one-dimensional quantum spin systems. *Phys. Rev. B*, 85:075125, Feb 2012.

[20] D. Hsieh, Y. Xia, D. Qian, L. Wray, J. H. Dil, F. Meier, J. Osterwalder, L. Patthey, J. G. Checkelsky, N. P. Ong, A. V. Fedorov, H. Lin, A. Bansil, D. Grauer, Y. S. Hor, R. J. Cava, and M. Z. Hasan. A tunable topological insulator in the spin helical dirac transport regim. *Nature*, 460:1101–1105, 2009.

[21] Satoshi Sasaki, M. Kriener, Kouji Segawa, Keiji Yada, Yukio Tanaka, Masatoshi Sato, and Yoichi Ando. Topological superconductivity in $cu_xbi_2se_3$. *Phys. Rev. Lett.*, 107:217001, Nov 2011.

[22] Y. S. Hor, A. J. Williams, J. G. Checkelsky, P. Roushan, J. Seo, Q. Xu, H. W. Zandbergen, A. Yazdani, N. P. Ong, and R. J. Cava. Superconductivity in $cu_xbi_2se_3$ and its implications for pairing in the undoped topological insulator. *Phys. Rev. Lett.*, 104:057001, Feb 2010.

[23] L. Andrew Wray, Su-Yang Xu, Yuqi Xia, Yew San Hor, Dong Qian, Alexei V. Fedorov, Hsin Lin, Arun Bansil, Robert J. Cava, and M. Zahid Hasan. Observation of topological order in a superconducting doped topological insulator. *Nature Physics*, 6:855, 2010.

[24] T. V. Bay, T. Naka, Y. K. Huang, H. Luigjes, M. S. Golden, and A. de Visser. Superconductivity in the doped topological insulator $cu_xbi_2se_3$ under high pressure. *Phys. Rev. Lett.*, 108:057001, Jan 2012.

[25] Pavan Hosur, Pouyan Ghaemi, Roger S. K. Mong, and Ashvin Vishwanath. Majorana modes at the ends of superconductor vortices in doped topological insulators. *Phys. Rev. Lett.*, 107:097001, Aug 2011.

[26] Hsiang-Hsuan Hung, Pouyan Ghaemi, Taylor L. Hughes, and Matthew J. Gilbert. Vortex lattices in the superconducting phases of doped topological insulators and heterostructures. *Phys. Rev. B*, 87:035401, Jan 2013.

[27] Ching-Kai Chiu, Pouyan Ghaemi, and Taylor L. Hughes. Stabilization of majorana modes in magnetic vortices in the superconducting phase of topological insulators using topologically trivial bands. *Phys. Rev. Lett.*, 109:237009, Dec 2012.

[28] Pedro L. e S. Lopes and Pouyan Ghaemi. Magnification of signatures of a topological phase transition by quantum zero point motion. *Phys. Rev. B*, 92:064518, Aug 2015.

[29] A. Yu Kitaev. Unpaired majorana fermions in quantum wires. *Physics-Uspekhi*, 44:131, 2001.

[30] Jason Alicea. New directions in the pursuit of majorana fermions in solid state systems. *Rep. Prog. Phys.*, 75:076501, 2012.

[31] Liang Fu and C. L. Kane. Josephson current and noise at a superconductor/quantum-spin-hall-insulator/superconductor junction. *Phys. Rev. B*, 79:161408, Apr 2009.

[32] P. L. S. Lopes, V. Shivamoggi, and A. O. Caldeira. Majorana fermions signatures in macroscopic quantum tunneling. *arXiv:1407.8182*, 2014.

[33] Liang Fu and C. L. Kane. Topological insulators with inversion symmetry. *Phys. Rev. B*, 76:045302, Jul 2007.

[34] Xiao-Liang Qi, Edward Witten, and Shou-Cheng Zhang. Axion topological field theory of topological superconductors. *Phys. Rev. B*, 87:134519, Apr 2013.

[35] Fan Zhang and C. L. Kane. Time-reversal-invariant $Z_4$ fractional josephson effect. *Phys. Rev. Lett.*, 113:036401, Jul 2014.

[36] Caldeira. *An Introduction to Macroscopic Quantum Phenomena and Quantum Dissipation*. Cambridge University Press, 2014.

[37] P. L. S. Lopes, V. Shivamoggi, and A. O. Caldeira. Majorana fermions signatures in macroscopic quantum tunneling. *arXiv:1407.8182*, 2014.

[38] Roman M. Lutchyn, Jay D. Sau, and S. Das Sarma. Majorana fermions and a topological phase transition in semiconductor-superconductor heterostructures. *Phys. Rev. Lett.*, 105:077001, Aug 2010.

[39] Stevan Nadj-Perge, Ilya K. Drozdov, Jian Li, Hua Chen, Sangjun Jeon, Jungpil Seo, Allan H. MacDonald, B. Andrei Bernevig, and Ali Yazdani. Observation of majorana fermions in ferromagnetic atomic chains on a superconductor. *Science*, 346(6209):602–607, 2014.

[40] W. P. Su, J. R. Schrieffer, and A. J. Heeger. Solitons in polyacetylene. *Phys. Rev. Lett.*, 42:1698–1701, Jun 1979.

[41] A. Kitaev. Fault-tolerant quantum computation by anyons. *arXiv:quant-ph/9707021v1*, 1997.

[42] C. W. J. Beenakker. Search for majorana fermions in superconductors. *Annu. Rev. Con. Mat.*, 4:113, 2013.

[43] A. D. K. Finck, D. J. Van Harlingen, P. K. Mohseni, K. Jung, and X. Li. Anomalous modulation of a zero-bias peak in a hybrid nanowire-superconductor device. *Phys. Rev. Lett.*, 110:126406, Mar 2013.

[44] C. Kurter, A.D.K. Finck, Y. S. Hor, and D. J. Van Harlingen. Evidence for an anomalous current-phase relation in topological insulator josephson junctions. *NATURE COMMUNICATIONS*, 2015.

[45] V. Mourik, K. Zuo, S. M. Frolov, S. R. Plissard, E. P. A. M. Bakkers, and L. P. Kouwenhoven. Signatures of majorana fermions in hybrid superconductor-semiconductor nanowire devices. *Science*, 336(6084):1003–1007, 2012.

[46] D. J. Thouless. Quantization of particle transport. *Phys. Rev. B*, 27:6083–6087, May 1983.

[47] Raffaele Resta. Macroscopic polarization in crystalline dielectrics: the geometric phase approach. *Rev. Mod. Phys.*, 66:899–915, Jul 1994.

[48] R. B. Laughlin. Quantized hall conductivity in two dimensions. *Phys. Rev. B*, 23:5632–5633, May 1981.

[49] Vinay Ambegaokar, Ulrich Eckern, and Gerd Schön. Quantum dynamics of tunneling between superconductors. *Phys. Rev. Lett.*, 48:1745–1748, Jun 1982.

[50] M. Tinkham. *Introduction to Superconductivity*. McGraw-Hill, 1996.

[51] A. O. Caldeira and A. J. Leggett. Quantum tunnelling in a dissipative system. *Annals of Physics*, 149:374–456, September 1983.

[52] A. O. Caldeira and A. J. Leggett. Path integral approach to quantum brownian motion. *Physica A Statistical Mechanics and its Applications*, 121:587–616, September 1983.

[53] G. Schon and A. D. Zaikin. Quantum coherent effects, phase transitions, and the dissipative dynamics of ultra small tunnel junctions. *Physics Reports*, 198:237–412, December 1990.

[54] C. W. J. Beenakker, D. I. Pikulin, T. Hyart, H. Schomerus, and J. P. Dahlhaus. Fermion-parity anomaly of the critical supercurrent in the quantum spin-hall effect. *Phys. Rev. Lett.*, 110:017003, Jan 2013.

[55] Jonathan R. Friedman, Vijay Patel, W. Chen, S. K. Tolpygo, and J. E. Lukens. Quantum superposition of distinct macroscopic states. *Nature*, 406(6791):43–46, July 2000.

[56] Curtis G. Callan and Sidney Coleman. Fate of the false vacuum. ii. first quantum corrections. *Phys. Rev. D*, 16:1762–1768, Sep 1977.

[57] Lit-Deh Chang and Sudip Chakravarty. Quantum decay in a dissipative system. *Phys. Rev. B*, 29:130–137, Jan 1984.

[58] J.S. Langer. Theory of the condensation point. *Annals of Physics*, 41:108–157, January 1967.

[59] F. Wilczek. Majorana returns. *Nature Physics*, 5:614, 2009.

[60] V. Mourik, K. Zuo, S. M. Frolov, S. R. Plissard, E. P. A. M. Bakkers, and L. P. Kouwenhoven. Signatures of majorana fermions in hybrid superconductor-semiconductor nanowire devices. *Science*, 336(6084):1003–1007, 2012.

[61] Stevan Nadj-Perge, Ilya K. Drozdov, Jian Li, Hua Chen, Sangjun Jeon, Jungpil Seo, Allan H. MacDonald, B. Andrei Bernevig, and Ali Yazdani. Observation of majorana fermions in ferromagnetic atomic chains on a superconductor. *Science*, 346(6209):602–607, 2014.

[62] B. Andrei Bernevig, Taylor L. Hughes, and Shou-Cheng Zhang. Quantum spin hall effect and topological phase transition in hgte quantum wells. *Science*, 314(5806):1757–1761, 2006.

[63] Pouyan Ghaemi, Sarang Gopalakrishnan, and Taylor L. Hughes. Designer quantum spin hall phase transition in molecular graphene. *Phys. Rev. B*, 86:201406, Nov 2012.

[64] Ping Ao and David J. Thouless. Berry's phase and the magnus force for a vortex line in a superconductor. *Phys. Rev. Lett.*, 70:2158–2161, Apr 1993.

[65] Lorenz Bartosch and Subir Sachdev. Influence of the quantum zero-point motion of a vortex on the electronic spectra of $s$-wave superconductors. *Phys. Rev. B*, 74:144515, Oct 2006.

[66] Predrag Nikolic and Subir Sachdev. Effective action for vortex dynamics in clean $d$-wave superconductors. *Phys. Rev. B*, 73:134511, Apr 2006.

[67] C. Caroli, P.G. De Gennes, and J. Matricon. Bound fermion states on a vortex line in a type ii superconductor. *Physics Letters*, 9:307, May 1964.

[68] H. F. Hess, R. B. Robinson, and J. V. Waszczak. Vortex-core structure observed with a scanning tunneling microscope. *Phys. Rev. Lett.*, 64:2711–2714, May 1990.

[69] A. Maldonado, S. Vieira, and H. Suderow. Supercurrent on a vortex core in $2h$-$nbse_2$: Current-driven scanning tunneling spectroscopy measurements. *Phys. Rev. B*, 88:064518, Aug 2013.

[70] C. Chen. *Introduction to scanning tunneling mictoscopy.* Oxford University Press, 1993.

[71] Predrag Nikolic, P., Subir Sachdev, and Lorenz Bartosch. Electronic states near a quantum fluctuating point vortex in a $d$-wave superconductor: Dirac fermion theory. *Phys. Rev. B*, 74:144516, Oct 2006.

[72] Liang Fu and Erez Berg. Odd-parity topological superconductors: Theory and application to $cu_xbi_2se_3$. *Phys. Rev. Lett.*, 105:097001, Aug 2010.

[73] Liang Fu and C. L. Kane. Superconducting proximity effect and majorana fermions at the surface of a topological insulator. *Phys. Rev. Lett.*, 100:096407, Mar 2008.

[74] Haijun Zhang, Chao-Xing Liu, Xiao-Liang Qi, Xi Dai, Zhong Fang, and Shou-Cheng Zhang. *Nature Physics*, 5:438, 2009.

[75] A.A. Abrikosov. The magnetic properties of superconducting alloys. *Journal of Physics and Chemistry of Solids*, 2(3):199 – 208, 1957.

[76] Lars Hedin. New method for calculating the one-particle green's function with application to the electron-gas problem. *Phys. Rev.*, 139:A796–A823, Aug 1965.

[77] Erikas Gaidamauskas, Jens Paaske, and Karsten Flensberg. Majorana bound states in two-channel time-reversal-symmetric nanowire systems. *Phys. Rev. Lett.*, 112:126402, Mar 2014.

[78] Ryohei Wakatsuki, Motohiko Ezawa, and Naoto Nagaosa. Majorana fermions and multiple topological phase transition in kitaev ladder topological superconductors. *Phys. Rev. B*, 89:174514, May 2014.

[79] Lorenz Bartosch, Leon Balents, and Subir Sachdev. Detecting the quantum zero-point motion of vortices in the cuprate superconductors. *Annals of Physics*, 321(7):1528 – 1546, 2006. July 2006 Special Issue.

[80] Yunsheng Qiu, Nocona K. Sandersa, Jixia Dai, Julia E. Medvedeva, Weida Wu, Pouyan Ghaemi, Thomas Vojta, and Yew San Hor. Symbiosis of ferromagnetism and supercurrent in topological insulators.

[81] Jeff E Sonier. Investigations of the core structure of magnetic vortices in type-ii superconductors using muon spin rotation. *Journal of Physics: Condensed Matter*, 16(40):S4499, 2004.

[82] Xiao-Liang Qi, Taylor L. Hughes, and Shou-Cheng Zhang. Topological invariants for the fermi surface of a time-reversal-invariant superconductor. *Phys. Rev. B*, 81:134508, Apr 2010.

[83] Grigory E. Volovik. *The Universe in a Helium Droplet*. Oxford Science Publications.

[84] Su-Yang Xu, Ilya Belopolski, Nasser Alidoust, Madhab Neupane, Guang Bian, Chenglong Zhang, Raman Sankar, Guoqing Chang, Zhujun Yuan, Chi-Cheng Lee, Shin-Ming Huang, Hao Zheng, Jie Ma, Daniel S. Sanchez, BaoKai Wang, Arun Bansil, Fangcheng Chou, Pavel P. Shibayev, Hsin Lin, Shuang Jia, and M. Zahid Hasan. Discovery of a weyl fermion semimetal and topological fermi arcs. *Science*, 349(6248):613–617, 2015.

[85] C. G. Callan and J. A. Harvey. Anomalies and fermion zero modes on strings and domain walls. *Nucl. Phys. B*, 1985.

[86] Frank Wilczek. Two applications of axion electrodynamics. *Phys. Rev. Lett.*, 58:1799–1802, May 1987.

[87] Géraldine Servant. Baryogenesis from strong *cp* violation and the qcd axion. *Phys. Rev. Lett.*, 113:171803, Oct 2014.

[88] Paul Fendley, Matthew P.A. Fisher, and Chetan Nayak. Boundary conformal field theory and tunneling of edge quasiparticles in non-abelian topological states. *Annals of Physics*, 324(7):1547 – 1572, 2009. July 2009 Special Issue.

[89] P. L. e S. Lopes, A. H. Castro Neto, and A. O. Caldeira. Chiral filtering in graphene with coupled valleys. *Phys. Rev. B*, 84:245432, Dec 2011.

[90] Pedro L. e S. Lopes, Jeffrey C. Y. Teo, and Shinsei Ryu. Effective response theory for zero-energy majorana bound states in three spatial dimensions. *Phys. Rev. B*, 91:184111, May 2015.

[91] Jeffrey Goldstone and Frank Wilczek. Fractional quantum numbers on solitons. *Phys. Rev. Lett.*, 47:986–989, Oct 1981.